POLITECNICO DI MILANO

Facoltà di Ingegneria Industriale
Dipartimento di Ingegneria Aerospaziale
Corso di Laurea Magistrale in Ingegneria Spaziale

Landing Site Selection for Rosetta Lander Philae through a Multidisciplinary Approach

Relatore: Prof. Franco BERNELLI – ZAZZERA
Correlatore: Dott. Francesco TOPPUTO

Tesi di Laurea di

Giulio PINZAN Matr. 751313

Academic Year 2011/2012

Table of Contents

List of Figures

List of Tables

Acronyms

AU: Astronomic Unit

CFF: Comet Fixed Frame

ESA: European Space Agency

EOL: End of Life

ERF: Equatorial Reference Frame

FSS: First Science Sequence

LDR: Lander Reference Frame

LILT: Low Intensity Low Temperature

LSF : Local Site Frame

LSS: Landing Site Simulator

LTS : Long Term Science

ORF: Orbital Reference Frame

SA: Solar Array

SAA: Solar Aspect Angles

SAS: Solar Array Simulator

SC: Solar Constant

Abstract

This document represents the Master in Science Thesis in Space Engineering of Giulio Pinzan from the Politecnico di Milano. The aim of the thesis is to formulate a model of the comet and an optimization strategy that permits to address the landing site selection of the Rosetta lander Philae on the comet 67P Churyumov-Gerasimenko. In this work, the main driver for the landing site selection is represented by the power produced by the solar arrays although rationales on the effects of the landing site on the thermal subsystem and other constraints are also discussed: the landing site selection aims to chose a site that guarantees the most efficient power generation during the Long Term Science phase of the mission, while respecting mission constraints.. A multidisciplinary approach is the key to obtain realistic results on the properties of a landing site, as long as application of constraints deriving from different aspects produce contrasting indications, thus landing site selection becomes a compromise choice between the optimum of the every single constraint. Results of this work permit to assess optimal Philae orientation on the comet surface for the entire mission, to evaluate the most suitable landing sites in terms of generated power and insolation. A preliminary analysis on the respect of thermal constraint is also discussed, as also the effects of variation of the comet spin axis orientation with respect to the nominal value. The most performing landing sites, that respect majority constraints, are located in groups situated in hills/humps of the Nothern Hemisphere.

Sommario

Questo sommario descrive in breve il lavoro di Tesi di Laurea Magistrale in Ingegneria Spaziale di Giulio Pinzan, presso il Politecnico di Milano. Lo scopo della tesi è di formulare un modello della cometa e una strategia di ottimizzazione per permettere la selezione del sito di atterraggio del lander Philae della missione Rosetta, sulla superficie della cometa 67P Churyumov-Gerasimenko.

La variabile di ottimizzazione principale in questo lavoro è rappresentata dalla potenza generata dai pannelli solari del lander, sono inoltre discussi gli effetti del sito di atterraggio sul sottosistema termico ed altri vincoli legati all'ambiente ed alla missione: la selezione del sito di atterraggio infatti è rivolta ad individuare i siti che permetto la più efficiente generazione di potenza, ma che permettano al contempo di rispettare tutti i vincoli di missione. La multidisciplinarità del problema è un approccio chiave per avere risultati realistici sulla bontà del sito di atterraggio selezionato, poiché l'applicazione di vincoli derivanti da aspetti diversi produce risultati discordanti e non intersecantisi, per cui la selezione del sito di atterraggio diviene una scelta di compromesso tra i vari punti di ottimo relativi ad ogni singolo vincolo.

Il lancio della Missione Rosetta è avvenuto nel maggio 2004 e dopo circa 10 anni di trasferimento interplanetario, durante il quale verranno sfruttati i fly-bys di Terra, Marte, Terra Terra, la missione

raggiungerà la cometa 67P Churyumov-Gerasimenko. La fase di avvicinamento è prevista nel maggio 2014 ad una distanza da Sole di circa 4UA. Nel settembre 2014, ad una distanza di 3.4UA, Rosetta verrà posta in un'orbita chiusa attorno alla cometa. Questa fase permetterà un'accurata determinazione delle caratteristiche cometarie, in particolare al fine della selezione del sito di atterraggio. La vita operativa della Missione Rosetta per lo studio della cometa 67P Churyumov-Gerasimenko inizia a 4UA, prosegue in tutta la fase di avvicinamento della cometa al perielio e termina nominalmente ad una distanza di 2UA dopo il passaggio al perielio. In data di completamento di questo lavoro di tesi, Rosetta si trova nell'ultima fase di trasferimento orbitale ed è in condizioni nominali di funzionamento in tutti i suoi sottosistemi.

L'atterraggio del lander Philae è previsto per l'11 novembre 2014. Philae rappresenta il segmento di missione che permetterà di produrre misurazioni in-situ sulla composizione, sulle proprietà superficiali, sulla struttura a larga scala e sull'attività della cometa durante il suo approssimarsi al perielio. Il lander ha una massa di circa 100kg e costituisce un segmento di missione completamente indipendente dal punto di vista sottosistemistico: l'unica funzione di supporto che fornisce l'orbiter Rosetta è quella di permettere la trasmissione dei dati a Terra. Philae è costituito da un box poligonale, equipaggiato con un sistema di pannelli solari su tutte le superfici laterali e superiore, ad eccezione di una superficie laterale dove è collocato il payload. Philae è fornito di un carrello di atterraggio tripodale che permette contemporaneamente di assorbire l'urto all'atterraggio e di assicurare la stabilità e l'aggancio alla superficie cometaria per l'intera missione. Il sottosistema di potenza ha come fonte primaria batterie primarie non ricaricabili con capacità di 1000Wh all'atterraggio, mentre come fonte secondaria i pannelli solari dall'estensione di $2m^{2,}$ permettono di ricaricare batterie dalla capacità di 130Wh all'atterraggio. Le celle solari di Philae, ed il suo sistema di pannelli solari in generale, sono stati progettati per condizioni di bassa intensità solare e bassa temperatura (LILT): queste sono infatti le condizioni che si verranno a trovare durante la missione. Il sottosistema termico è controllato attivamente da una serie di heaters, mentre lo scambio di calore è controllato passivamente da due assorbitori solari posti sulla faccia superiore e da delle coperte in MLI che garantiscono l'isolamento per tutto il resto della superficie del corpo principale del lander. Philae ha inoltre la capacità di ruotare il corpo principale rispetto al carrello di atterraggio di 360°, questa caratteristica permette di interagire con l'ambiente esterno in modo efficace ed inoltre di orientare efficientemente i pannelli solari. Relativamente alle fasi di missione del lander, la più critica è la fase di separazione dall'orbiter Rosetta, discesa ed atterraggio sulla cometa (SDL), a cui seguirà la fase di First Science Sequence che permetterà di utilizzare tutti gli strumenti scientifici a bordo almeno una volta. Entrambe queste fasi saranno assicurate dalle batterie primarie per una durata di circa 120 ore. In seguito è prevista una fase di Long Term Science della durata di 6 mesi, in cui verranno utilizzate le batterie secondarie ricaricate dai pannelli solari.

L'interesse verso la cometa 67P è relativo al fatto che la sua determinazione orbitale ha permesso di ricostruire la sua provenienza essere la fascia di Kuiper, una fascia situata oltre Nettuno che conserva tracce primordiali della nebulosa che ha formato il Sistema Solare. La comprensione dell'origine della cometa, oltre che della sua formazione ed evoluzione, permetterà la miglior comprensione delle comete in generale, degli oggetti situati nella fascia di Kuiper e dell'origine del Sistema Solare. Infine si ritiene che le comete possano essere il vettore che ha trasportato la vita in luoghi diversi del Sistema Solare, quindi possibilmente anche sulla Terra; lo studio di 67P permetterà di approfondire anche questa teoria.

La cometa 67P ha un diametro di circa 5km ed è costituita da ghiaccio e polvere. Le caratteristiche della cometa che interessano questo studio sono in particolare l'orbita, la forma, la direzione dell'asse di rotazione, la velocità di rotazione, la dinamica di rotazione, l'attività di sublimazione cometaria nel tempo, l'albedo, le condizioni di illuminazione presenti sulla superficie, le caratteristiche di composizione e resistenza della superficie. Tutti questi aspetti sono trattati estensivamente attraverso l'utilizzo di una bibliografia aggiornata e con riferimenti autorevoli, in particolar modo sono discusse le tecniche di osservazione, le metodologie utilizzate per la riduzione dei dati e l'indeterminazione dei parametri associata ai risultati di ogni studio.

Il fine è quello di presentare una modellazione che sia la più realistica possibile, sia relativamente all'ambiente che ai sottosistemi di Philae, per poter permettere una corretta descrizione dello scenario operativo della missione. Dunque in breve le scelte di modellazione della cometa sono sviluppate come descritto in seguito.

L'orbita è modellata attraverso l'uso dei parametri Kepleriani. La discretizzazione temporale prevede l'inizio di missione all'11 novembre 2014 e la durata è di 6 mesi terrestri, il tempo è discretizzato in frazioni di giorno cometario in modo da poter controllare direttamente l'accuratezza dei risultati. Il modello dinamico e di rotazione descrivono la cometa come un corpo in rotazione attorno al suo asse principale d'inerzia, con una velocità di rotazione costante di circa 12 ore ed un'inclinazione inerziale dell'asse di rotazione, orientato tale per cui il polo positivo di rotazione (il Polo Nord, definito dalla regola della mano destra) punta verso il semispazio negativo dell'orbita: la rotazione della cometa è retrograda. La forma della cometa è estremamente irregolare, sia latitudinalmente che longitudinalmente, ed è descritta attraverso una mesh triangolare, costituita da 512 superfici triangolari. Questa forma deriva dall'inversione delle curve di luce derivanti da osservazioni della cometa con l'utilizzo del telescopio Hubble. Si assume che i siti di atterraggio possibili siano i baricentri delle superfici triangolari, inoltre le proprietà calcolate per ogni triangolo sono valutate nel suo baricentro ed estese poi su tutta la sua superficie, ciò vale in particolare per: la direzione della normale, l'insolazione, la potenza prodotta dal lander. L'illuminazione sulla superficie della cometa è modellata come insolazione diretta da parte di una fonte puntiforme posta all'infinito, la frazione di luce riflessa dalla cometa viene trascurata poiché l'albedo è molto basso. E' necessario invece modellare l'auto adombramento della cometa, la sua forma irregolare infatti presenta avvallamenti le cui condizioni di insolazione e capacità di potenza prodotta sarebbero sovrastimate se questo aspetto fosse trascurato.

Per quel che riguarda invece la modellazione del lander Philae gli aspetti fondamentali sono la geometria, l'orientazione del lander, il sottosistema di potenza, il sottosistema termico. Il sottosistema di potenza è modellato attraverso il Solar Array Simulator sviluppato dal Politecnico di Milano, permette si stimare la potenza prodotta dal lander in ogni istante di tempo tenendo conto dell'orientazione del lander (e quindi dei singoli pannelli solari), degli effetti sull'efficienza dati dalla temperatura, delle condizioni di degradazione e della modalità di generazione di potenza (maximum peak power tracking). Il modello di cella e di pannello solare sono stati determinati sperimentalmente. Il sottosistema termico è invece modellato in modo preliminare, attraverso un modello a parametri concentrati a tempo variante, costituito da due nodi: gli assorbitori solari ed il compartimento interno del lander. Le assunzioni a riguardo portano i risultati relativi a questo modello ad essere considerabili solo come preliminari, in particolare viene modellato in modo approssimato lo scambio termico attraverso le coperte di MLI. La geometria del lander invece è ben nota.

La modellazione di tutti gli aspetti sopra descritti consente lo sviluppo di un software Matlab che permette di simulare lo scenario di missione di Philae.Sono disponibili 5 tipi di analisi.

La prima è atta a comprendere il movimento del Sole, visto da un sistema di riferimento locale associato ad ogni superficie triangolare. Permette di comprendere in modo accurato le condizioni esotiche di illuminazione che si vengono a creare per un corpo di forma irregolare, la cui direzione radiale ad ogni sito differisce tipicamente di decine di gradi rispetto alla normale alla superficie, che ruota in senso retrogrado ed ha inclinazione dell’asse di rotazione maggiore di quello terrestre per cui l’effetto di variazione stagionale risulta essere più marcato. Da quest’analisi è stato provato che nonostante la radiale locale differisca di diversi gradi rispetto alla normale locale, il Sole culmina sempre a Nord o a Sud in un’accezione molto simile a quella terrestre

La seconda analisi permette di studiare l’insolazione e la generazione di potenza del lander per tutti i siti sulla superficie cometaria senza considerare effetti di auto adombramento della cometa. Quest’analisi permette di ottenere l’orientazione ottimale del lander in termini di generazione di potenza per ogni posizione sulla superficie della cometa e per ogni istante della missione. Le operazioni di orientazione del lander sono minime, in termini generali è necessario orientare l’asse di simmetria del lander verso la direzione di proiezione della culminazione del Sole sull’orizzonte, od in opposizione ad essa. In conclusione il numero di manovre di orientazione del lander necessarie per ottenere un’esposizione ottimale è al massimo due, per tutta la durata della missione. Questo risultato è di fondamentale importanza perché permette in modo semplice di ottenere l’orientazione ottimale del lander, inoltre le manovre e le operazioni necessarie a garantirlo sono minime e consentono una ridottissima richiesta di potenza. L’analisi è sviluppata senza auto adombramento, poiché diversamente non è più possibile risolvere il problema in modo semplificato, per cui risulta che l’orientazione per le superfici triangolari soggette ad auto adombramento è solo vicina alla condizione di ottimo. Questa approssimazione ha scarse conseguenze dato che i siti più favorevoli sulla cometa sono disposti su rilievi soggetti ad auto adombramento minimo.

Il terzo tipo di analisi permette di studiare l’insolazione e la generazione di potenza del lander per tutti i siti sulla superficie considerando effetti di auto adombramento della cometa. I risultati disponibili sono sia globali per la missione che suddivisi in separatamente in 6 frazioni uguali della durata di missione. Questi risultati determinano le categorie di siti cometari che risultano avere migliori prestazioni. Ne sono state individuate tre, tutte situate su prominenze dell’emisfero Nord. La prima è costituita da siti che permettono la maggior generazione di potenza globalmente nella missione (superiore ai 9W medi), sono collocati in un ampio intervallo di latitudini, ma hanno inclinazione della normale molto simile e mostrano adombramento minimo. Questi siti tuttavia non hanno un'ottimale generazione di potenza ad inizio missione, inferiore a 5.11W, cioè la soglia minima di potenza necessaria per il Safe Mode del lander. Il fatto che siti dalle prestazioni simili siano caratterizzati da inclinazione della normale simile è un risultato generale: le caratteristiche di un sito sono legate all'orientazione della normale piuttosto che alla latitudine. La seconda categoria di siti è localizzata a latitudini molto elevate del Polo Nord, hanno generazione di potenza globalmente nella missione di 8.5W circa, mostrano la migliore regolarità di potenza per tutta la missione: in ogni giorno cometario permettono di produrre almeno 6.11W medi, ed hanno la miglior generazione di potenza ad inizio missione: 7.6W. Tuttavia la loro elevata latitudine potrebbe creare problematiche all'atterraggio. La terza ed ultima categoria generazione di potenza globalmente nella missione di 8.0W medi circa, in ogni giorno cometario permettono di produrre almeno 6.11W medi ed ad inizio missione ne producono circa 6.2W. I valori di insolazione per queste tre categorie permettono di asserire che l'attività cometaria e la conseguente erosione non dovrebbero essere vincolanti. La ragione alla base di ciò è che la condizione più favorevole per la generazione di potenza avviene per basse elevazioni del Sole sull'orizzonte, per cui l'insolazione non è elevata: 5 dei 6 pannelli solari sono disposti verticalmente rispetto alla superficie cometaria (supponendo la base del lander parallela alla superficie).

La quarta simulazione presenta i risultati preliminari dell'andamento termico del lander, tutti i siti indicati dalla simulazione precedente permettono di giungere a fine missione senza restrizioni termiche.

La quinta ed ultima analisi simula la variazione dell'asse di spin di ±10° in due direzioni angolari ortogonali. Si può notare che anche per piccole variazione della direzione dell'asse di spin gli effetti sulla produzione di potenza sono notevoli, soprattutto relativamente alla posizione dei siti più favorevoli.

Quest'ultima analisi permette di mettere in particolare evidenza l'importanza di una corretta modellazione di tutti i parametri del problema per poter ottenere risultati realistici. Nella fase di approccio alla cometa sarà dunque necessario determinare attraverso osservazione diretta tutte le caratteristiche ambientali. Sarà inoltre necessario raffinare la modellazione dei sottosistemi del lander.

Key Words

ROSETTA, PHILAE, 67P, LANDING, SITE, SELECTION

Parole Chiave

ROSETTA, PHILAE, 67P, SELEZIONE, SITO, ATTERRAGGIO

1.Introduction

This Master in Science Thesis is intended to support the selection of the landing site of the Rosetta lander Philae on the surface of comet 67P Churyumov-Gerasimenko.

Rosetta is an ESA mission whose prime objective is to determine the origin, composition and evolution of comet 67P Churyumov-Gerasimenko and of the Kuiper belt objects in general. The dedicated study of 67P Churyumov-Gerasimenko will also permit to deepen the knowledge on the Solar System evolution and possibly also to understand the origin of life on Earth. Rosetta mission was successfully launched in May 2004, at the moment of this thesis editing, the mission is approaching its goal 67P Churyumov-Gerasimenko in the last phase of its 10 year orbital transfer. Rosetta mission is constituted of Rosetta orbiter that will be placed in a closed orbit to study 67P Churyumov-Gerasimenko and the lander Philae that will perform in-situ measurements. Comet approach is forecast in May 2014 and after 5 months of data collection in order to better assess the comet features, the lander Philae will be delivered on the nuclei surface. The objective of Philae is to characterize directly the nucleus composition, morphology and activity.

This Master in Science thesis is intended to support to address the selection of the landing site of Philae using a multidisciplinary approach, thus different constraints deriving both from the environment and from the mission design will be taken into account. The prime variable of optimization of the problem is the electrical power produced during the mission by the six Low Intensity Low Temperature solar panels mounted on the body of Philae, although rationales on the effects of the landing site on the thermal subsystem and other constraints are also discussed.

This thesis is developed in the joint purpose of the Politecnico di Milano and the DLR of Köln to have a better understanding on how the subjects discussed in this work may affect Philae operative scenario and capabilities. The Politecnico di Milano has the responsibility of the Philae solar generator and all related works during the journey to the comet and the in-situ operations. The DLR of Köln is instead responsible for the overall lander project management, the operations at the Lander Control Centre and of the Lander Ground Reference Model.

The scope is to produce a model of the problem that pictures realistically Philae mission scenarios in order to produce constraints and requirements on the most favourable landing sites. The problem is approached through a multidisciplinary view, that takes into account of both the mission design and the environment. All the problem-related features are discussed together with their mutual repercussions. The study of the problem is also supported by the creation of a numerical code, the Landing Site Simulator, which is useful to deepen the understanding on the complex Philae scenario. The interest in particular is about the power production capabilities associated with different cometary sites, in order to extend and optimize Philae operative life. The work also takes into account a wide number of constraints deriving from the environment and other mission subsystems in order to produce a simulation as realistic as possible.

1.1 Approach to the Landing Site Selection Concept

Before discussing the approach to the landing site selection problem, two terms will introduced as long as they are frequently used in the dissertation.

For **LSSel Concept** (Landing Site Selection Concept) it is intended the totality of phenomena modelling, choices and analysis that are outlined and developed in order to address the landing site selection of Philae on comet 67P Churyumov-Gerasimenko. The complexity of the problem requires a vast number of assumptions and considerations that will be outlined step by step in the dissertation. For sake of simplicity the “LSSel Concept“ term will be used.

The **LSS (**Landing Site Simulator) on the other hand is the routine tool that was developed in parallel with the LSSel Concept, it strictly reflects the problem modelling assumptions of LSSel Concept and permits to produce a wide number of analysis and results. The platform used to develop the LSS is Matlab.

Philae Landing Site Selection for on-comet power optimization is a multidisciplinary problem that has to take into account of:

- different requirements and constraints deriving from the mission subsystems and the environment,
- outputs that strongly depend on the imposed constraints.

Indeed, both inputs and outputs of the problem have mutual interactions. Consequently, to correctly address the problem an accurate study of all the problem components is fundamental, as also to understand all of the mutual interactions of the problem variables and parameters. Due to these considerations this document initially presents in order all the aspects that are relevant for this work:

-the Rosetta Mission,

-the comet 67P Churyumov-Gerasimenko,

-the lander Philae.

Inside each of these dedicated chapters, at the end of each session, the repercussion on the Landing Site Selection Concept is discussed. In the following chapter these same repercussions will be recovered and expressed as constraints for the Landing Site Selection Concept. In the result section results are discussed with respect to the imposed constraints.

In order to better present the Landing Site Selection problem a preliminary conceptual scheme is presented [Figure 1]. In particular is possible to visualize the different features of the problem that will be discussed in detail in the following chapters.

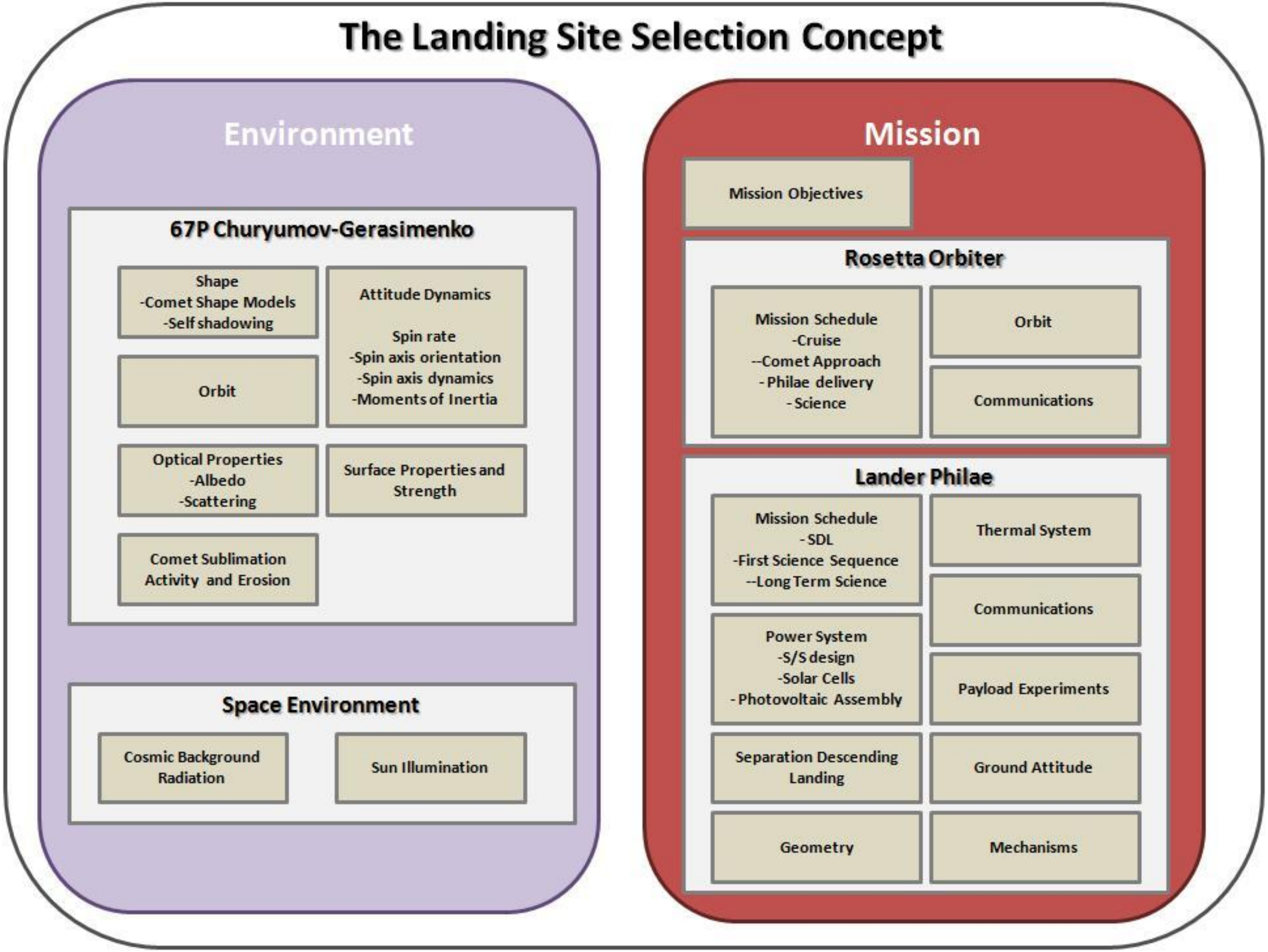

Figure 1 : LSSel Concept features

1.2 Information Updating

The information contained in this document, in particular that related to the adopted references, is constantly subjected to revision and updating: currently the Rosetta Mission is on its final orbital approach of comet 67P Churyumov-Gerasimenko, thus more accurate determination of the scenario governing parameters is fundamental to guarantee mission success in many fields. The author is aware that some of the information contained in this document may be consequently outdated, although all possible efforts were done to reduce this eventuality. It is to be underlined that particular attention was paid in order to create a tool as flexible as possible to counteract the updating of parameters governing the Rosetta mission scenario.

1.3 Document plan

In this document the most important features of Rosetta Mission are first outlined. In the following the mission environment, represented by comet 67P Churyumov-Gerasimenko, is presented; in this section particular attention is held on the characteristics and parameters affecting the Landing Site Selection Concept. As next step the lander Philae design and mission schedule is described. Philae chapter is presented after the description of 67P Churyumov-Gerasimenko as long as a preliminary discussion on the comet features is retained necessary to understand Philae design and operation plan. In the following the Landing Site Selection Concept (LSSel Concept) is discussed in detail and most of the considerations outlined in the previous sections are exposed in order to present their modelled counterparts. The following section regards the developed numerical code, the Landing Site Simulator (LSS): the numerical modelling of the problem and the different type of analysis that can be produced are reported.

Finally the LSS results are presented and discussed. As final section a critical discussion on the obtained results and on the current mission scenario is held.

2. The Rosetta Mission

The ESA Rosetta Mission was decided in 1993 and constitutes one of the most challenging European missions to date. The main objective of the mission is the rendezvous with comet 67P Churyumov-Gerasimenko that will take place after 10 years of interplanetary travel, started with the launch in May 2004. Rosetta orbital transfer permits to the mission to insert into 67P Churyumov-Gerasimenko through an energetically optimized trajectory, but also permits to have a close encounter with two asteroids: 2867-Steins and 21-Lutetia.

Rosetta mission takes its name from the Rosetta Stone which was recovered in Rashid (or Rosetta) in 1979 and permitted to interpret the ancient script of hieroglyphs. Philae is an island close to Aswan where another stele, that confirmed the interpretation, was found. Interpretation of hieroglyphs permitted decipher documents on the early history of humankind. Similarly the Rosetta Mission challenging objectives are to reveal the primordial composition and evolution of the Solar System that are secreted in the most ancient and unmodified bodies of the Solar System, the comets.

2.1 Scientific Objectives

Cometary matter has been submitted to the lowest level of processing since its condensation from the proto-solar nebula and might even have preserved presolar grains [1]. Hence comets should constitute a unique repository of information, both on the sources that contributed to the proto-solar nebula and to the condensation process that resulted in the formation of planetary bodies.

Rosetta Mission is the first to be designed for a long-term, dedicated and accurate study of a comet and represent one possible solution to obtain unaltered cometary material. From terrestrial observation indeed only the coma composition can be observed which is typically altered both by the sublimation process and the interaction with solar light and wind.

Past mission approached cometary nuclei, but few were designed for comet observations and none were designed to have a dedicated orbit in order to perform a prolonged and in-situ study of the nucleus at different Sun distances.

Primary **scientific objective** of Rosetta Mission is to study the origin of comets, the relationship between cometary and interstellar material and its implication with regard to the origin and evolution of the Solar System [1]. An additional objective is to characterize the main belt of asteroids. The measurements to be made in support of the objective of this mission are [1]:

- Global characterisation of the comet nucleus, determination of dynamics properties, surface morphology and composition.
- Determination of the chemical, mineralogical and isotopic compositions of volatiles and refractories in a cometary nucleus.
- Determination of the physical properties and interrelation of volatiles and refractories in a cometary nucleus.
- Study of the development of cometary activity and the processes in the surface layer of the nucleus and the inner coma (dust/gas interaction).
- Characterisation of main belt asteroids including dynamic properties, surface morphology and composition.

2.2 Main Mission Phases

Rosetta launch was successfully addressed in March 2004 [1]. During the **interplanetary transfer** a number of fly-bys was scheduled to optimize its trajectory, the sequence is Earth, Mars, Earth, Earth [1] (see [Figure 2]). In the meanwhile asteroids 2867-Steins and 21-Lutetia are encountered. Planets fly-bys and asteroids encounters are useful both for trajectory optimization and data collection, but also to assess correct functioning and calibration of on-board instruments and subsystems [2].

After a long period of hibernation of almost 2.5 years, in January 2014 the orbiter will be awakened and in May 2014 the **rendezvous** of comet 67P Churyumov-Gerasimenko will be carried out at about 4AU from the Sun. This is the moment where the mission main phase begins, in September 2014 the orbiter will be inserted in the comet orbit at 3.4AU. At this period a fundamental phase of global observation and mapping of the nucleus will take place at distances down to 1km. In this phase in particular the surface features, the spin axis orientation, the rotational period and the gravity filed will be observed and measured, all these information indeed is fundamental for planning the next mission phases i.e. the landing site selection and the subsequent descending manoeuvre [1]. It is to be underlined that in these phases the comet is retained to be almost inactive, although some indetermination exists.

Philae landing on the comet surface is scheduled at November 11th 2014 at a distance of about 3AU from the Sun. Philae mission on the comet is designed to last from 3AU to 2AU far from the Sun, afterwards thermal constraints will probably lead to mission end, however the goal is to reach even 1.3AU distances (so close to perihelion) through an accurate mission planning [2].

On the other hand **Rosetta orbiter** will continue to follow 67P Churyumov-Gerasimenko through perihelion and will prosecute its studies nominally until 2AU. Comet peak of activity is at perihelion, which makes this position on the orbit both the most scientifically interesting and contemporarily the most stressing for the spacecraft due to particles jettison and thermal heat.

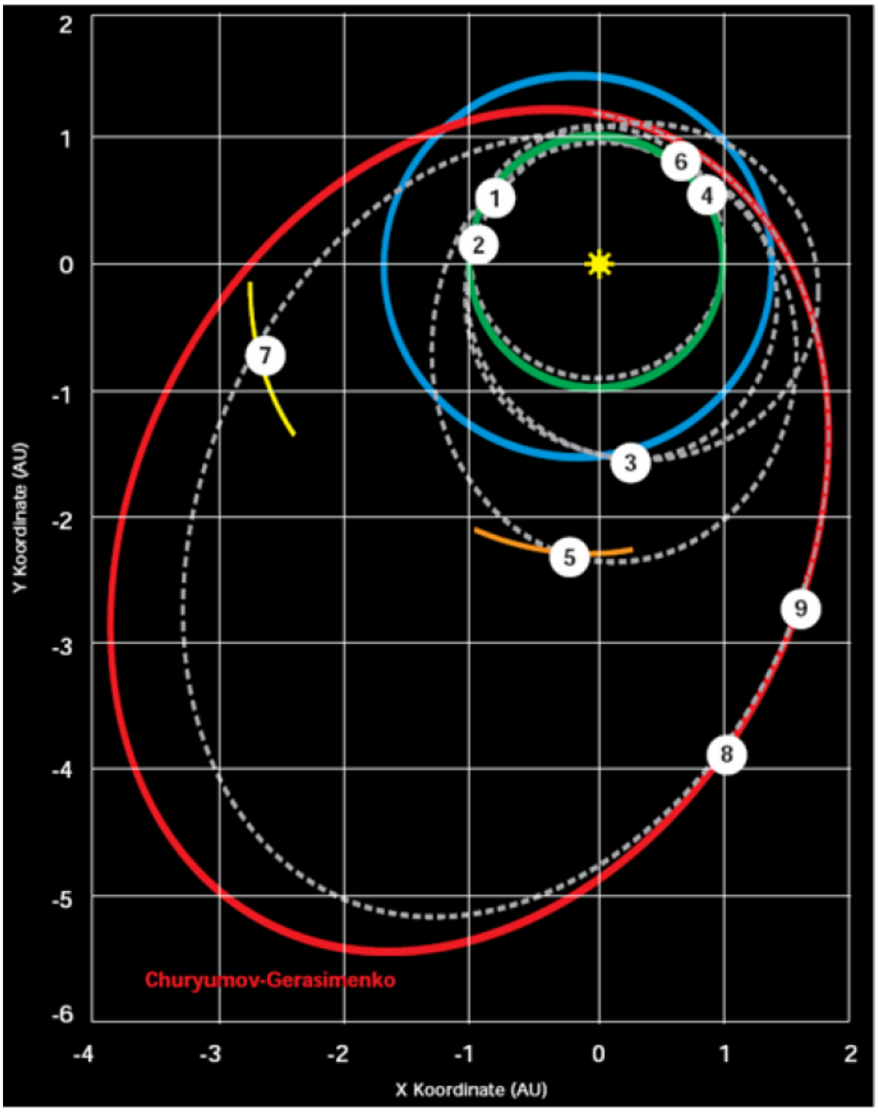

Figure 2: Trajectory of Rosetta.
1 Launch, March 2004,
2 Earth swing-by, March 2005,
3 Mars swing-by, February 2007,
4 Earth swing-by, November 2007,
5 Fly-by at 2867 Steins, September 2008,
6 Earth swing-by, November 2009,
7 Fly-by at 21 Lutetia, July 2010,
8 Rendezvous with 67P C–G., May 2014,
9 Landing, November 2014. Credits [3].

2.3 The Spacecraft

A brief description of the spacecraft is presented [1] [4] (see [Figure 3]). The total mass at launch was about 2900kg, divided between 1720kg of propellant, 165kg of scientific payload and 100kg for Philae. Rosetta spacecraft is 3-axis stabilized and its core is constituted by a 2.8x2.1x2.0m aluminium box. On the top of this box the Payload Support Module is located where all scientific instruments are mounted. On the other hand the subsystems are placed on the base, in the Bus Support Module.

For **power** production two opposed extended appendages carry the solar panels constituted by dedicate-developed Low Intensity Low Temperature solar cells. Each solar panel is 14m long and displaying 30m^2 surface. Power production capabilities are 850W at 3.4AU up to 8700W close to perihelion. Solar panel wings can rotate of ±180° on the appendage axis for Sun exposure optimization.

Earth **communication** is guaranteed through a 2.2m steerable high gain antenna attached at the back panel, while in the front panel Philae is stowed and will communicate with the orbiter through a medium gain antenna.

Rosetta orbiter **attitude** during close comet observation is designed to have the instruments pointing towards the comet, while the antenna and solar panels are pointed towards Earth and Sun respectively.

Thermal control in the hot case is ensured through thermal radiators and louvers located in the back of the spacecraft, while in the cold case through heaters. Insolation is guaranteed through MLI blankets.

For **propulsion** 10 bi-propellant thrusters of 24N are used and can be also exploited also for attitude control.

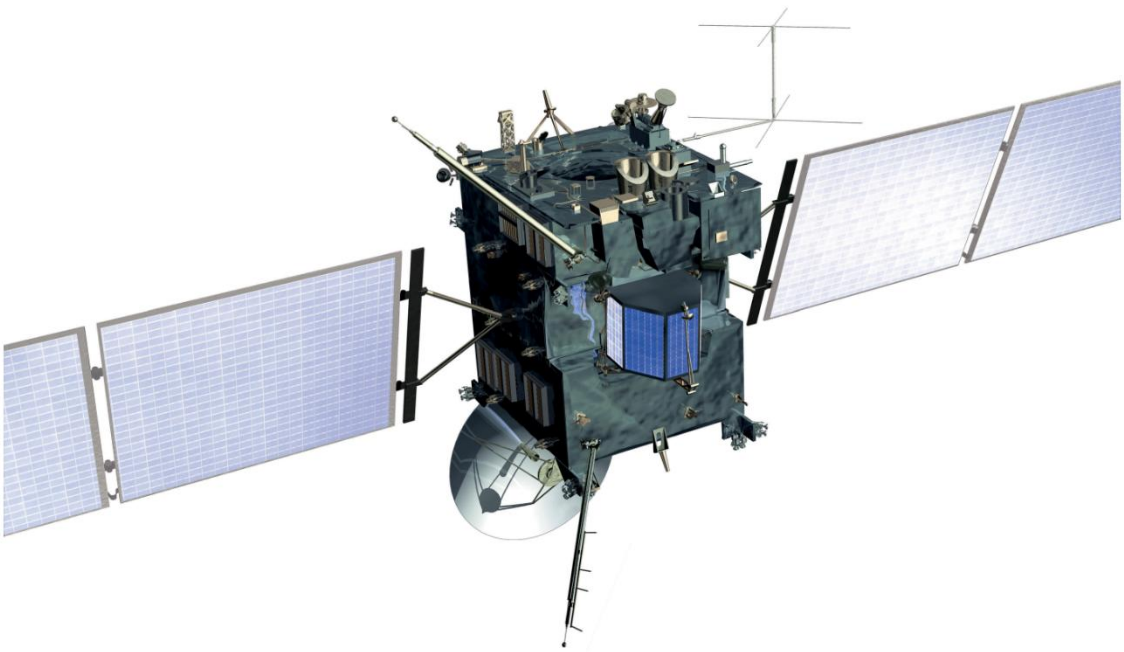

Figure 3: Rosetta orbiter layout. In particular the lander Philae can be observed, mounted in the front panel. Credits: ESA/AOES Medialab.

3. Comet 67P Churyumov-Gerasimenko

The following discussion is intended to give a picture of the current available scenario of comet 67P Churyumov-Gerasimenko (hereafter 67P C-G). A number of articles is presented, in particular the techniques used to obtain the results and their accuracy are reported. The values of the parameters used in the LSS simulations are described in the dedicated chapter [The Landing Site Selection Concept] and descend directly from the considerations that are outlined in this chapter.

Comet 67P C-G represents the primary mission objective of the Rosetta Mission [Figure 4]. Understanding 67P C-G features and characteristics is fundamental to correctly address the mission planning, as also the Landing Site Selection.

In this chapter in particular a number of data and results are presented whose accuracy strongly affects the results of the Landing Site Selection, for this reason the methods used to obtain the data are presented as well.

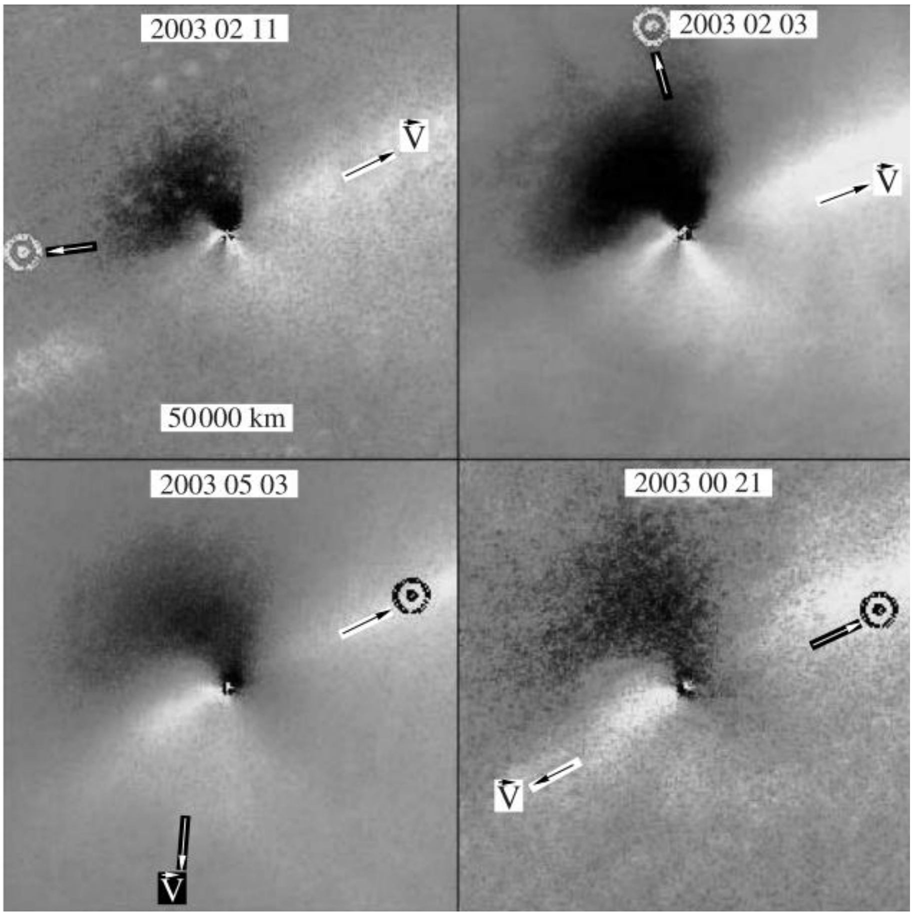

Figure 4 : Structurally enhanced broad-band R images showing the evolution of the distinct features detected in the coma of comet 67P Churyumov-Gerasimenko between February and June 2003. The projected direction of the Sun and the movement of the comet are indicated. Credits [1].

67P C-G was chosen as **primary mission objective** after that a mission departure delay caused the unfeasibility to reach the baseline primary objective comet 46P Wirtanen [5]. At the moment of the comet baseline choice change, few was know about 67P Churyumov-Gerasimenko, therefore a number of terrestrial observation was scheduled to understand the new Rosetta Mission target. The observation plan that ESA scheduled was aimed to lay out a number of few dedicated and optimized observations of the comet, in order to be able to characterize its properties with least uncertainty. This technique also favoured the development of a small number of articles, so that the reliability of the authors is known, discrepancies and ambiguities are reduced and the articles are interconnected or have strong references between each other. Clearly, repetitiveness and reliability of observations is fundamental to assess whether the present data available on the comet is relevant and accurate.

All the data reported below about comet 67P C-G regard only the characteristics that are retained to be inherent and influencing the LSSel Concept.

Repercussions in the LSSsel Concept

The results obtained from the developed model for the Landing Site Selection is primarily affected by the consistency of data available on the comet. Consequently the Landing Site Simulator was created to be easily updated in the contingency that more recent data on the comet were available. In general terms the LSS permits to study the landing site selection of Philae for any of the Solar System bodies. This generality in the problem approach permits to create a tool that is portable for the study of similar problems and that is contemporary able to quickly adapt to the evolution of the Philae mission scenario or to the data related to it.

3.1 References

One of the most recent articles that excellently resumes all the previous works, gives estimation on the reliability of the data and accurately describes the techniques used to obtain the results is “A portrait of the nucleus of 67P Churyumov-Gerasimenko” by Lamy et al. dated 2006 [5]. This work is to be considered the reference document for this thesis, regarding the 67P C-G properties. Other fundamental information on the comet are available thanks to the DLR department of Köln.

In order to give an estimation of the reliability of the data associated with 67P C-G the authors and the methods used for the observations and to retrieve the data are reported.

3.2 Astronomical Observations

The three most relevant **observations** regarding 67P CG are reported in [Table 1]:

Observation Denomination	Telescope	Comet Sun Distance	Date	Related Articles	Notes
HST	Hubble Space Telescope	2.50AU	12-13 March 2003	[5][6][7]	
MIPS	Spitzer Space Telescope	4.47AU	25 February 2004	[5][8]	
NTT	New Technology Telescope - ESO	5.60AU	10-12-14 May 2005	[5][9]	Inactive comet

Table 1: 67P C-G astronomical observations

All the three instruments appears between the most sophisticated instrument of astronomical observation currently existing and permit to have a sufficient spatial resolution in order to correctly distinguish the cometary nucleus from the surrounding coma. These dedicated observation followed after that 67P C-G was indicated as the primary Rosetta Mission objective.

Observation through astronomical telescopes are available only in determined times windows, this is related to the following aspects:

- **Sun distance**: few of the parameters (e.g. nucleus density, shape, mass) can be obtained directly, rather using indirect methods. In particular light curve analysis is a technique that permits to obtain the comet shape and spin period, but to be correctly applied a minimum distance of about 2.5-3AU of the comet from the Sun is necessary. Such distance guarantees scarce comet activity, therefore it is possible to clearly distinguish the comet nucleus from its surrounding coma. The need of such minimum distance for observations clearly affects the spatial resolution of imaging, indeed the minimum Earth-comet distance occurs in a much closer neighbourhood (67P C-G perihelion is at 1.28AU). In addition this constraints also prevents high spatial resolution observations during the perihelion passage, that is also the moment where sublimation forces acts stronger on the evolution of the comet nucleus and orbit.
- **Solar elongation**: not only the Sun distance, but also the angle seen from Earth between the comet and the Sun is fundamental as long as it permits to have a proper observation perspective and illumination: i.e. when solar elongation is zero the comet is in conjunction with respect to the Sun, so no observation is possible, when solar elongation is 180° the comet is in opposition.

Below [Figure 5] a diagram of suitable future observation windows is reported, as purposed in [5].

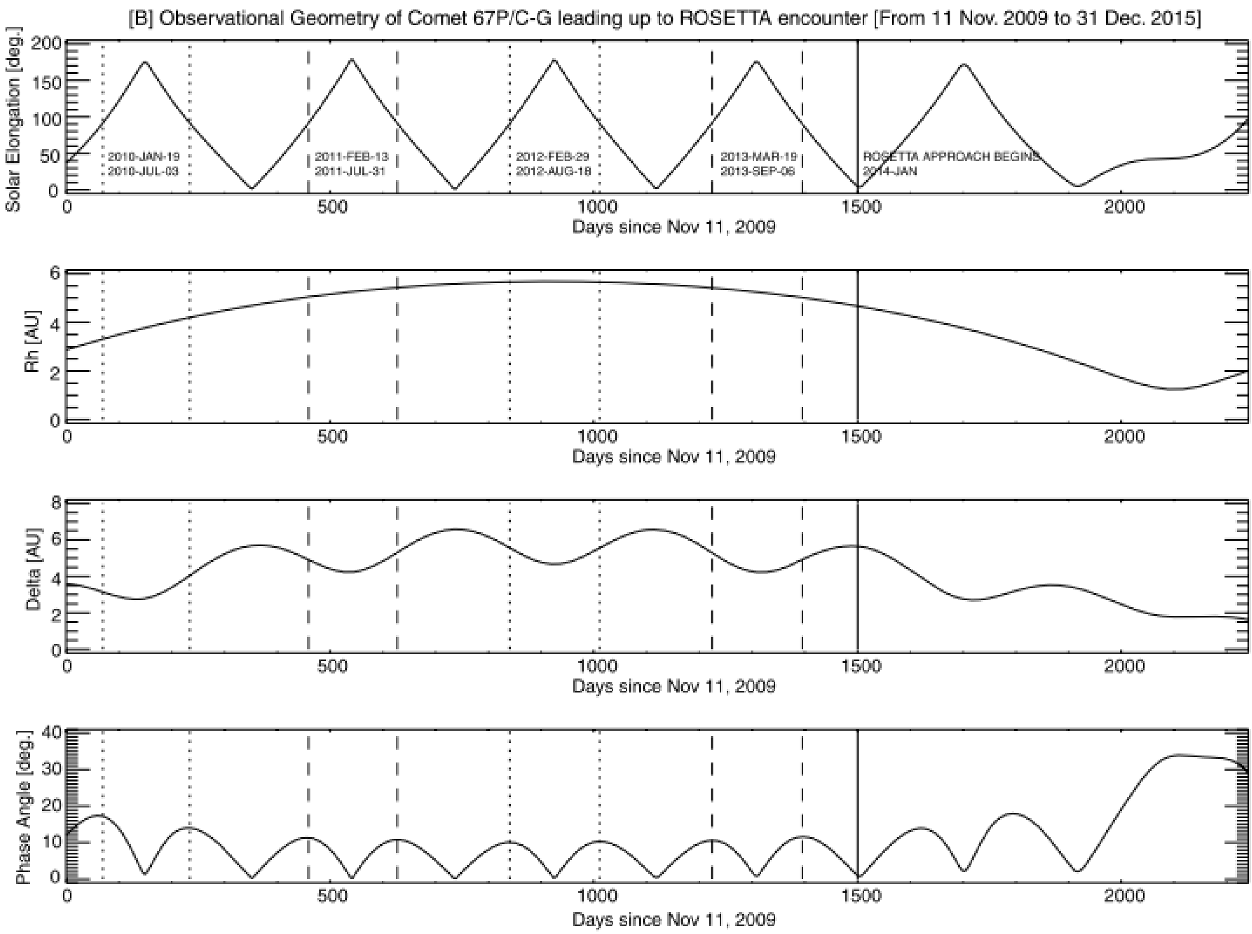

Figure 5: Purposed astronomical observations of 67P CG. Credits [5]

Repercussions in the LSSel Concept

Presently all the data available is related to the articles deriving from observations that are reported in [Table 1], with the exception of the work of Vincent et al [10] on 67P C-G spin axis orientation that is related to 2010 observations [Figure 5]. However the 67P C-G shape model provided by the DLR of Köln that is implemented in the LSS, derives directly from the work of the reported observations and articles.

3.3 Orbit and Comet Origins

3.3.1 Origins of 67P C-G

Comets are believed to be the primitive leftover of the Solar System formation process, among all celestial bodies they are believed to be the only few that were not modified during the Solar System evolution[2]. Thus, they contain information on the compositional mixture from which the planets formed about 4.6 billion years ago. They carry records of the Solar System's very early phase and are a key for the understanding of its origin and development. In addition, comets may have played an important role for the origin of life, since they may have transported organic matter to the early Earth [2].

The **origins of 67P C-G** are strictly connected with its orbital history: 67P C-G is a comet of the Jupiter family. Jupiter-family comets are a dynamically distinct group with low orbital inclinations with respect to the ecliptic and orbital periods shorter than 20 years [9]. Their origin has been shown computationally to be the Kuiper belt region, situated beyond Neptune. Typically the size of these comets is about few kilometres.

The influence of giant planets such as Jupiter, Saturn and Neptune can lead to the activation of this objects: the perihelion is moved into the inner Solar System and sublimation dynamics begin to take place.

The **orbital history of 67P C-G** is well known only since 1969, and was studied in six consecutive passages of the comet. Before 1969 calculations appear chaotic due to a wide number of perturbations. According to the work of Królikowska [11] however, in the time interval between 1000BC and 4000AD the aphelion of 67P C-G seems to be under the control of Jupiter encounters, which is the phenomena that has largely the most significant effect on the orbit of 67P C-G. Perturbations due to repeated close encounters with Jupiter influenced 67P C-G perihelion placing it in the inner Solar System and the comet was consequently activated.

One of the main objectives of Rosetta is to deepen the comprehension of the Jupiter family comets, their origin and composition.

3.3.2 Non-gravitational perturbations

If the main character responsible for gravitational perturbation of 67P C-G orbit is Jupiter, effects of mass jettison due to comet surface sublimation are strictly connected with non-gravitational perturbations of 67P C-G. Królikowska [11] exploited some thousands of observations available during six consecutive passages of the comet occurred from 1969, in order to study the orbital perturbations. This paragraph is the only one that is not related to the observations reported in [Table 1] as long as for orbital determination lower spatial resolution is needed: observations can be more frequent as long as lower scale telescopes are necessary and there is no restriction for perihelion observations: i.e. there is no need to distinguish the comet nucleus from its coma.

In the work of Królikowska [11] orbital integration was used taking into account of gravitational perturbation of all nine planets.

The fundamental equation used to retrieve the non-gravitational forces is the following [Eq. (1)]:

$$F_i = A_i g(r) \qquad (1)$$

where i=1,2,3 are relative to the radial, transverse and normal components, respectively. A_i are the non-gravitational parameters that, multiplied by the function $g(r)$, simulates the ice sublimation rate and gives the non-gravitational force in components. The shape of $g(r)$ can be represented in two ways, the first neglecting the asymmetry of ice sublimation with respect to the perihelion, the second taking into account of this effect (Model Ia and Ib in respectively in [Table 2]).

The shape of $g(r)$ is the following [Eq.(2)]:

$$g(r) = \alpha \left(\frac{r}{r_0}\right)^m \left(\left(\frac{r}{r_0}\right)^n\right)^k \quad (2)$$

where m, n, k are coefficients that represents the experimental curve of sublimated ice production, r is the heliocentric distance which is r_0 at perihelion. When the asymmetric curve is considered the function $g(r)$ is shifted through: $g'(r+\tau)$. Due to thermal inertia considerations indeed, the profile of ice production, and its peak in particular, is shifted after the perihelion of τ, which is the delay of ice sublimation peak counted in days after the perihelion passage.

	Model Ia	**Model Ib**
A_1	0.054440 ±0.002665	0.088327±0.003598
A_2	0.0098084±0.0000173	-0.0013637±0.0009429
A_3	0.030187±0.002189	0.033855±0.002152
T [days]	--	34.314±2.128
T [days]	20020818.28695(7)	20020818.28685(6)
q [AU]	1.29064789(25)	1.29064249(15)
e	0.63175088(7)	0.63175242(4)
ω [°]	11°40976(8)	11°40848(7)
Ω [°]	50°92865(7)	50°92965(7)
i [°]	7°12415(1)	7°12413(1)

Table 2 : Non-gravitational parameters and orbital elements of 67P CG as estimated by Królikowska. Credits [11]

Results obtained from Królikowska shows the non-gravitational parameters useful for orbit integration in a short time period. In particular the value of τ is in great agreement with astronomical observations light curves. Consequently results of Model Ib are to be considered more accurate.

<u>Repercussions in the LSSel Concept</u>

Orbital elements integrated in the LSS are obtained updated from JPL website. JPL orbital elements derive from the work reported above and are updated with more recent observations. Is to be noted that data reported in [Table 2] differs from JPL ephemeris as long as they are referred to different dates. The procedure to integrate orbital elements and the values used in the LSS are reported in the dedicated chapter [Orbit modelling]. The orbital parameters are between the most accurate data available for the comet, this is again related to the fact that orbital determination requires lower scale telescopes and more relaxed observation windows than those necessary to constrain the nucleus features.

3.4 Rotational Period

A number of articles try to estimate the rotational period of comet 67P C-G, only the most accredited and reliable are reported. The work of Lamy et al [5] resumes the most relevant articles and provides a picture of the current scenario. Observed rotational periods of comets range between 5-70hrs, but its vast majority lays between 5-18hrs [6].

Lamy et al [6] through HST observation of 67P C-G [Table 1] first estimated 67P C-G rotational period. The combined estimation using six different methods led to a value of P_w=12.41hrs with a standard deviation of σ=0.41hrs, assuming a double peaked light curve.

Exploiting the NTT observation of 67P C-G [Table 1] Lamy et al [5] constrained this value even further obtaining a value of P_w=12.72±0.05hrs using a Fourier fit to the R-filter light curve of the comet [Figure 6]. Also light curve inversion was used to retrieve the rotational period, this leads to even narrower ranges of values, but data appear to be noisy so that there is uncertainty on the local minima to be taken into account, consequently these results are discarded.

Repercussions in the LSSel Concept

The rotational period of 67P C-G is one of the better constrained parameters of the comet. It is to be noted however, that a variation on the rotational period would not affect the results of daily and seasonal average insolation and the results of daily and seasonal average generated power. A variation on the rotational period could on the other hand affect the thermal response of Philae, as long as the lander would be exposed to longer periods of shade and sunlight.

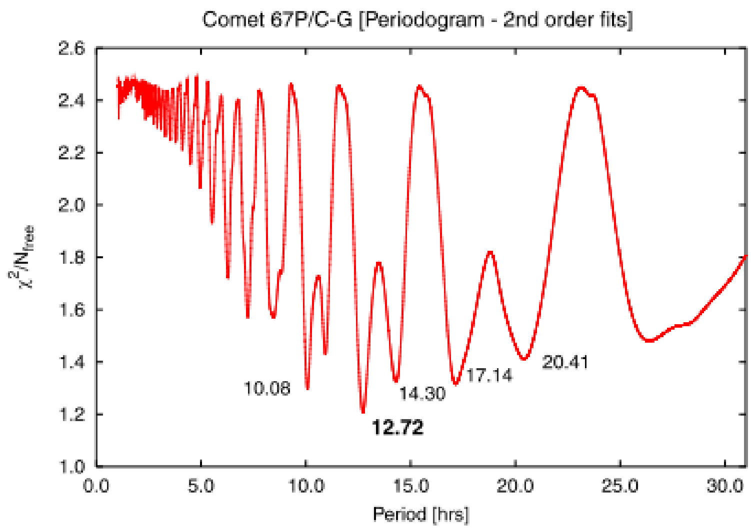

Figure 6: Resulting periodogram from Fourier fits to the R-filter light curve of comet 67P C-G extracted from time-series imaging obtained from NTT observations. Credits [5]

3.5 Moments of Inertia

The rotational state of the nucleus can be modelled as a **prolate body** rotating around its largest principal axis of inertia (the shorter in dimension, considering an homogenous body), although the comet shape is far different from a prolate spheroid as will be discussed in [Shape]. This rotational state is also to be considered as the most stable in energetic terms and is consequently taken as an assumption from some articles.

The work by Davidsson Gutierrez [7] based on the HST nucleus observations [Table 1] combined with previous orbital observations of 67P C-G is the first milestone for the estimation of the moments of inertia of the comet. By considering model comet nuclei with a wide range of sizes, prolate ellipsoidal shapes, spin axis orientations, and surface activity patterns, they placed constraints on the nucleus properties of 67P C-G. This is done by requiring that the model bodies simultaneously reproduce the empirical nucleus rotational light curve, the water production rate as function of time, and non-gravitational changes (per apparition) of the orbital period, longitude of perihelion and longitude of the ascending node.
Two different thermophysical models are used in order to calculate the water production rate and non-gravitational force vector due to nucleus outgassing of the model objects. Both thermophysical methods foresee a cometary surface described as a prolate rotating body, that is divided in active regions mainly composed by icy particles and inactive regions whose composition of the surface is mainly made of dust, which prevents sublimation effects. Both methods estimate the water production using energy balance equations, that describe the thermophysical dynamics of a rotating body periodically exposed to the Sun, displaying a given thermal inertia and a thermal profile that varies with the depth below the cometary surface. Density and composition of the comet is considered constant along the cometary depth. The second thermophysical model (EBEM – energy balance equation model) is a simplified version of the first (LEAM – layer energy absorption model), in particular heat conduction on the comet is neglected.
Requiring that the water production rate best fits the measurements, obtained through a third order polynomial interpolation of the water production calculated by several observations, they obtained that the nucleus of 67P C-G has a semi-major axis of ~2.5km, a semi-minor axis of ~1.8km and a bulk density that ranges between 100-370kg m^{-3}. This result is based on the evidence that sublimation is the main cause of orbital elements variation, once gravitational force effect is subtracted, as described by Królikowska [11]. Results obtained from Davidsson Gutierrez also permit to set more constraints on the nucleus properties that will be discussed below.

Lamy et al [6] interprets the light curve obtained with HST observation [Table 1] as a prolate body rotating around its largest moment of inertia axis [Figure 6]. This technique, as is discussed in [Orientation of the Spin Axis] also permitted to obtain the rotational period, the shape and the spin axis direction of 67P C-G.

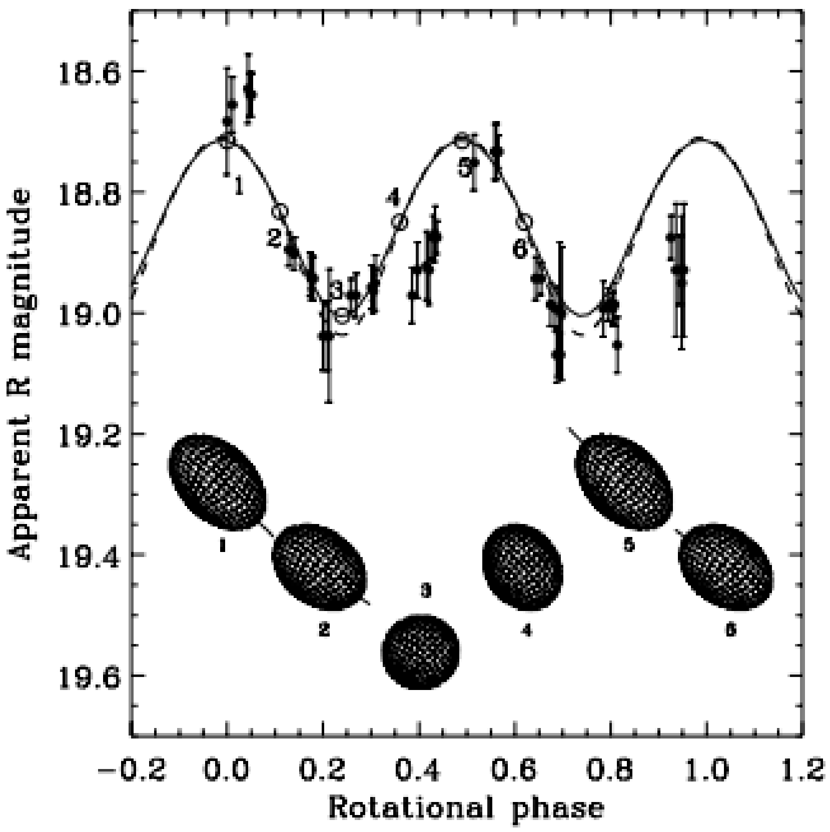

Figure 7: Light curves (apparent R magnitude) of the nucleus of comet 67P C-G. The filled circles are the observational data points from the HST observation. The solid line corresponds to the best fit prolate spheroid with the Hapke photometric parameters of asteroid 253 Mathilde. The dashed line corresponds to the projected cross-section of the illuminated fraction of the spheroid visible to the observer. The cross-section of the nucleus is displayed at different rotational phase angles labelled 1 to 6 (open circles).Credits [6].

Repercussions in the LSSel Concept

The constraining assumption in this paragraph is to schematize 67P C-G as a prolate body rotating around its largest principal inertia axis, so that no nutation or precession is considered. Clearly in the case of a body subjected to external forces, i.e the outgassing effect acing on 67P C-G and planet gravitational perturbations, dynamics on the spin axis orientation are present as long as these forces can likely produce also torques. Nutation or precession do not seem to produce noticeable effects as long as in different apparition of the comet the spin axis orientation do not change significantly. However the indetermination on the spin axis direction is so elevate (see [Orientation of the Spin Axis]), that a parametric study on the variation of the spin axis orientation considered as inertial is of primary interest. Consequently nutation and precession effects will be neglected.

3.6 Orientation of the Spin Axis

The spin axis orientation is the environmental parameter that affects the most the results of the Landing Site Selection on 67P C-G, as long as it directly determines contemporarily:

- the **amplitude of cometary seasonal variations for fixed location on the cometary surface** e.g. if the spin axis is normal to the orbital plane there is no presence of seasons, the more the comet spin axis deviate from this geometry the more seasonal effects occur. For season it is intended the effect of variation of Sun illumination angles of the comet in the cometary orbit, given by the inclination of the spin axis with respect to the orbital normal.

- the location where the **seasons occur in the comet orbit**: the elevate eccentricity of the orbit produce strong difference on the comet evolution and insolation depending on the location on the orbit where the season occurs: e.g. if the South Pole summer occurs in perihelion the insolation will be extremely elevate in this season due to Sun proximity, contrary for the North Pole that would be in shade.

The spin axis orientation is between the most undetermined parameters of the comet, this is related to the fact that at least three clearly determined and angularly separated views are necessary to establish the spin axis direction of a rotating body displaying an undetermined complex shape. Obtaining these views is challenging as long as at close distances from the Sun, shorter than 2.5-3AU, the comet nucleus can not be separated clearly from the surrounding coma, in the other hand at larger distances the viewing geometry as seen from Earth do not change significantly [5], this can be seen also in [Figure 5].

However also in this case a number of articles give estimation of the spin axis direction using different methods; the deriving results are concentrated in two distinct regions [Figure 8]. The drawback is that the angular range of the two regions has the magnitude of some tens of degrees.

To give an initial glance of the current scenario [Figure 8] from Lamy et al [5] is reported as it best resumes the work of the most reliable articles on this subject. The areas represent the position of the spin axis as reported from different authors. The reference frame is the Earth-centred EME2000.

Davidsson and Gutierrez [7] through the thermophysical model described above in [Rotational Period] and together with an analysis of the light curves, estimated the spin axis orientation, starting from a map of initial guess. Davidsson and Gutierrez report the spin axis orientation in the Argument-Inclination (Φ,I) plane. Description of such angles can be found in [12] or below in [Comet 67P C-G Shape] as long as these angles are used in the Landing Site Simulator implementation. Transformation between (Φ,I) plane and (RA,DEC) plane can be found in [Appendix 1].

As a result the spin axis argument of 67P C–G as calculated by Davidsson and Gutierrez is likely to be close to either $\Phi = 60° \pm 15°$ or $\Phi = 240° \pm 15°$. For these values of Φ, the empirical values of orbital period variation ΔP and longitude of perihelion variation $\Delta\omega$ (and for some obliquities, also the variation of the ascending node $\Delta\Omega$) are fulfilled, and the calculated water production rate reproduces the observed rates better than for other spin axis orientations (this is valid for both LEAM and EBEM). For the LEAM, the modelled water production rates are virtually as good as a third degree polynomial fit, while the EBEM fits are just slightly worse.

The spin axis obliquity I can only be constrained if it is considered likely that the right ascension variation is $0.0'' \leq \Delta\Omega \leq 2.0''$, as also indicated by Królikowska [11] estimates (however, since the RMS residual between the theoretical and observed orbits do not improve significantly when the non-gravitational parameter A3 is included as a free parameter, its value remains uncertain). If $\Delta\Omega = 1.0 \pm 1.0''$, then $100° \leq I \leq 140°$ for $\Phi \approx 60°$,i.e. the rotation is retrograde. Similarly, if $\Phi \approx 240°$ then $40° \leq I \leq 80°$, i.e. the rotation is prograde. Both the LEAM and EBEM yield very similar results in this respect.

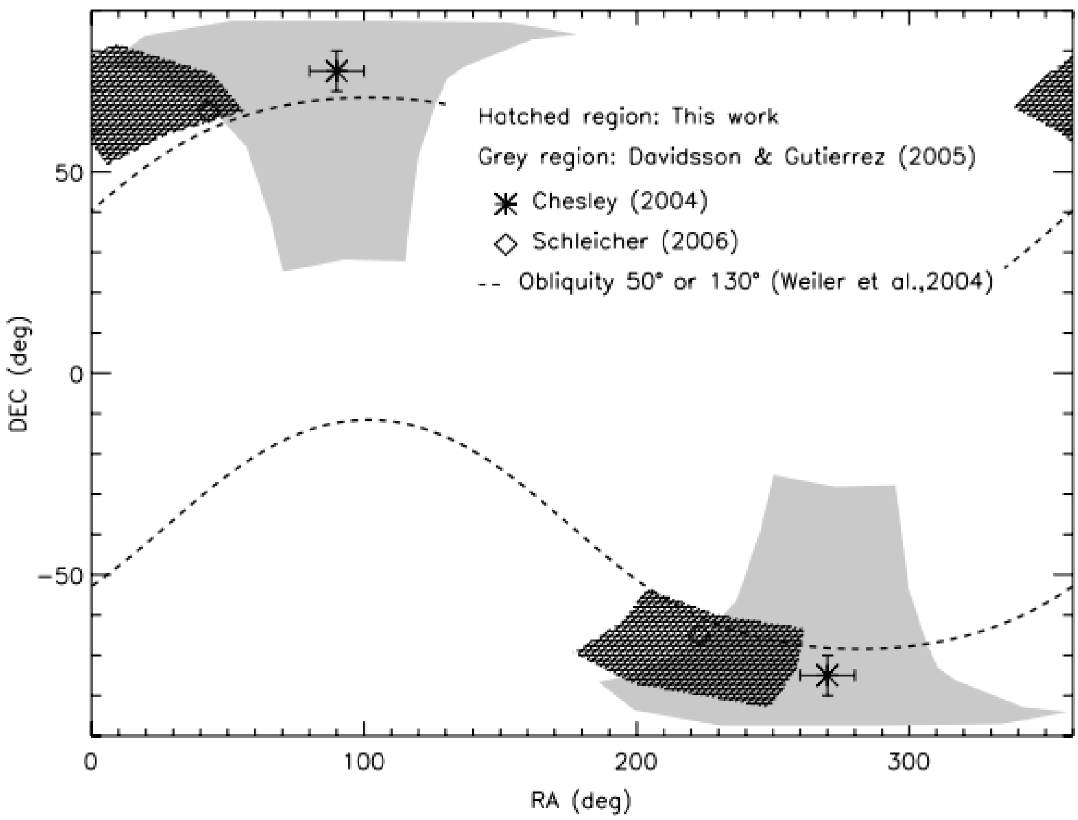

Figure 8: Constraints on the direction of the rotational axis of the nucleus of comet 67P C–G. Credits [5]

Chesley in 2004 [13] also modelled the non-gravitational accelerations seen as outgassing forces produced by body-fixed jets that thrust according to the insolation level. This study resulted in several possible pole orientations yielding a reasonable fit to the orbit. He estimated that the pole orientation of 67P C-G is within 10° of RA = 90° and DEC = 75°, with no constraint on the sense of rotation i.e. the opposite direction is equally possible.

Schleicher in 2006 [14] estimated the spin axis direction using a method that exploits hydrodynamical structures of comets (jets, fans). The assumption on the basis of this method is that these structures movement evolves only due to effects related to the rotation of the cometary nucleus. What can be typically observed is a jet that is performing a conical revolution, where the axis of the cone coincides with the spin axis of the comet. Schleicher used observations taken in January 1996 where a strong sunward radial feature in 67P C-G coma was observed, and through a Monte Carlo simulation of the possible orientation of the conical axis found that the possible solution for the rotational axis is either RA ≈ 57° and Dec ≈ + 65° or the opposite direction RA ≈ 223° and Dec ≈ − 65°, since the sense of rotation is unconstrained.

An estimation of the spin axis orientation is given by Lamy et al in 2006[5], they used the light curve inversion method applied to the HST observations of 2003 [Table 1]. Light curve inversion is a technique that uses of all data points (both relative and calibrated photometry) and finds a physical model, albeit with a large number of free parameters, that accurately reproduces the photometric data down to the noise level. The simultaneously determined parameters describe the sidereal period, the pole direction, the shape and the light-scattering properties of the body. To restrict the range of possible solutions (one light curve is not enough to constrain the inversion), Lamy et al [6] imposed the realistic condition for the spin axis to be close to the principal axis corresponding to the maximum moment of inertia in order to ensure a stable rotation. This is expected to be the case for a moderately active but relatively large nucleus, where effects of torques are not major.

Light curve inversion yields to two unconnected solutions A and B, the pole direction is given in ecliptic coordinates λ and β. The reason under the existence of two solutions is related to the fact that data are currently scarce: only two observation geometries are available. The light curve inversion in principle is a method that gives no ambiguity on the sense of rotation contrary to the methods presented above, however a $\lambda \pm 180°$ ambiguity exists for objects close to the ecliptic plane. 67P C-G orbital inclination is about 7°, so there is some degeneracy left, consequently solutions A and B are in pairs: [A1 A2] and [B1 B2] with mirror shape solutions. Ambiguity is not strictly on 180° as long as the orbit inclination is not strictly 0°.

Due to considerations related to the results obtained in the previous reported works, Lamy et al. could discard the A2 and B1 solutions, so that the results obtained is A1 with $\lambda = 51° \pm 20°$ and $\beta = 54° \pm 10°$ and corresponds to a prograde rotation. A1 presents the best fit to the data but only very marginally better than solution B2 which has $\lambda = 245° \pm 20°$ and $\beta = -50° \pm 10°$ and corresponds to a retrograde rotation.

One last estimation on the spin axis orientation is given by Vincent et al [10], they observed the evolution of coma jets during the 2010 apparition [Figure 5] to determine the jet conical axis orientation that coincides with the comet spin axis (the same technique adopted by Schleicher [14]). The result was obtained using the Coma Structures SIMulator (COSSIM) which was previously validated with comets 9P Tempel and 81P Wild2. Results show that the spin axis orientation did not change significantly between the 2003 and 2009 apparitions, as long as they can be superposed to Lamy's [5]. Spin axis orientation is estimated to be RA = 40°, DEC = 70° in the prograde case or RA = 220°, DEC = -70° for the retrograde. All values are accurate at ±10°.

Repercussions in the LSSel Concept

The influence of the spin axis orientation on the LSS results is extremely elevate and affect a wide number of parameters as will be discussed in [Critical Discussion]. Consequently a parametric study on the variation of the spin axis inclination between the indicated ranges was produced.

In addition due to information available from the DLR of Köln the currently preferred solution for the spin axis orientation is Lamy et al [5] B2 retrograde solution that coincides with Vincent et al [10] retrograde solution: RA=220° DEC=-70°. Uncertainty on the spin axis orientation is assumed as ±10° both in RA and DEC as Vincent et al [10] suggest.

3.7 Dynamics of the Spin Axis

Sublimation-driven forces are mainly responsible for the evolution of the rotational state of 67P C-G, both in short and secular effects. This process is described by Gutierrez et al. [15] exploiting the results of the work of Lamy et al [6]. The equation governing the timescale for a change of the rotation period, or of the angular momentum due to the sublimation-induced torques, can be approximated by [Eq. (3)]:

$$\tau \sim \frac{I\,\omega}{d\,Z(r_h)\,f_n\,\pi\,r_n^2\,m_g\,\eta\,v_g(r_h)} \qquad (3)$$

where I is a characteristic value for the moments of inertia, ω is the angular velocity, r_n is the mean radius of the nucleus, d is the moment arm, f_n is the surface active fraction (assumed constant), m_g is the mass of water molecules, $r_h$is the heliocentric distance, $v_g(r_h)$ is the initial gas velocity, η is the momentum transfer coefficient (the sensitivity of the body to change momentum), and $Z(r_h)$ represents the water sublimation rate (per unit area). One of the most complicated parameters to be determined is η, reference for its estimation can be found in Jorda Gutierrez [16].

Due to the values of the parameters reported, changes in the spin axis dynamics occurs within 3AU where sublimation effects are considerable.

Gutierrez et al. [15] compared three different shapes (generic triaxial ellipsoid, near prolate body, irregular shape) each of them characterized by four different surface activity patterns (randomly generated maps that divide active and inactive regions on the surface). Two initial conditions were set: the “unexcited case” correspondent to a rotation dynamics with zero initial precession and “excited case” correspondent to rotation dynamics with initial precession. They exploited the same thermophysical method used by Daviddson Gutierrez [7] described in [Moments of Inertia] to best fit the water production curve observed for 67P C-G.

When different shapes are compared, bodies with irregular shapes show slightly larger changes than others, in particular when compared to prolate spheroids that show the smallest changes. The difference factor is between 3-10 and is related to the following aspects:

- the near prolate body show the largest moment of inertia and mass, so the spin axis stability is more elevate
- the near prolate body due to geometry of its surface has necessarily a very small torque along the largest principal axis
- the near prolate body has significant cancellation of the torque due to symmetry considerations

For the particular activity patterns used in the study, the effects of the sublimation-induced torque on bodies initially rotating in the excited mode are lower than those on bodies initially rotating in the state of minimum energy (pure spin). In principle this is related to the largest rotational energy associated with the excited case.

Patterns showing activity located mostly at the extremities of the body (named a3 and a4 [Figure 9])produce large negative torques parallel to the shortest principal axis, consequently the effect of spin rate change is more noticeable. Thus the body loses energy and is more subjected to spin axis orientation change.

As results of the Gutierrez et al work the observed changes during the comet nucleus observations phases of Rosetta range from 0.05h to a few hours. A typical value for the change, considering all the simulations, is around 0.4 h. Considering all the simulations, the rate of change of the spin period ranges 0.001-0.05h/day.

In all the simulations, the orientation of the angular momentum vector changes by a few degrees [Figure 10]. The typical angular rate of change of the angular momentum vector at aphelion is less than 10e-5°/day. At the time of the lander release, this rate is less than 0.001°/day and at perihelion it is between 0.01-.1°/day. This leads to typical spin axis orientation change up to 10° during the whole Rosetta mission rendezvous.

In the simulations, the angular momentum vector makes a small loop (#4 in [Figure 10]) and almost comes back to its original position. This behaviour is due to cancellations of the torques in the orbital frame, i.e. the effects of the torques in the pre-perihelion branch of the orbit is nearly cancelled in the post-perihelion branch.

Repercussions in the LSSel Concept

As discussed in [Rotational Period] the change in rotational period does not strongly affect LSS results, except for the thermal behaviour. As presented the maximum values foreseen for spin axis orientation change during the whole Rosetta mission encounter is about 10° covering from the initial encounter at 3AU up to 2 AU post-perihelion . This mission period is overestimated for Philae as long as its mission duration will likely be shorter due to thermal effect that will lead to overheating before perihelion, therefore before the largest a variations on the spin axis occurs.

All these considerations together with the elevate spin axis orientation indetermination lead the LSSel Concept to neglect the spin axis dynamics and rather concentrate the efforts in a parametric study of the spin axis orientation considered as inertial.

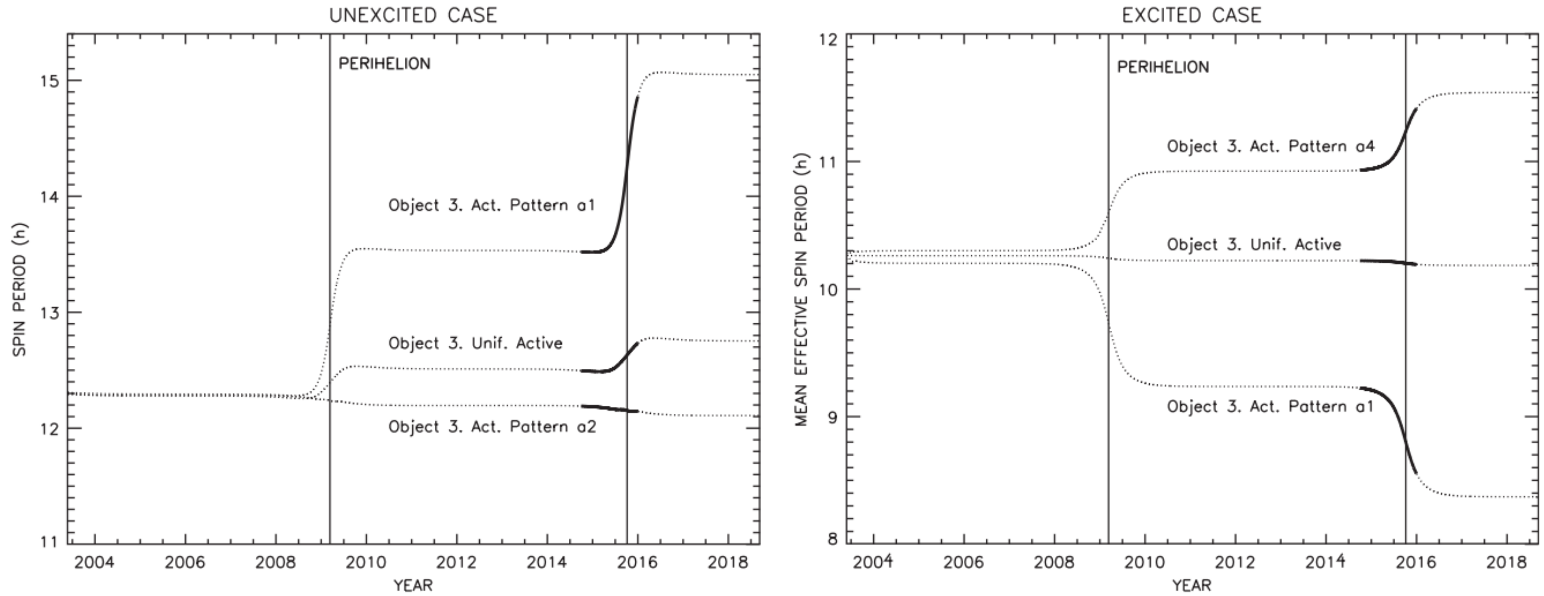

Figure 9: The evolution of the spin period for the irregular object (the most affected to change) is shown with three different activity patterns on its surface.. In the plot on the left, the body is initially rotating without precession. The excited cases are shown in the plot on the right.. The continuous part of the lines shows the respective spin evolutions during the comet nucleus observations phases of Rosetta, covering from the initial encounter up to 2 AU post-perihelion. Vertical lines mark times of perihelion passages where visibly the most significant change occurs. Credits [15]**.**

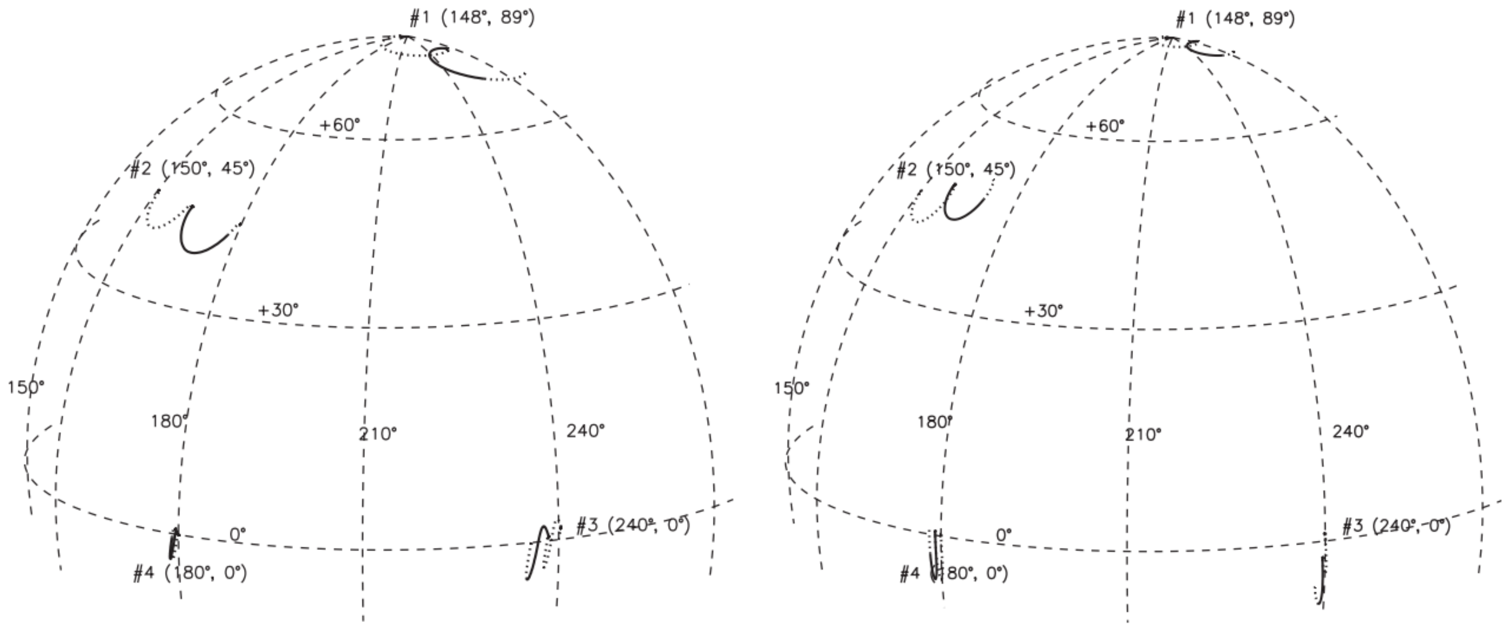

Figure 10 : The path (in orbital coordinates) of the angular momentum for the irregular body with the activity pattern a1 for the different initial angular momentum orientations. In the plot on the left, the nucleus is initially rotating in pure spin. The excited cases are shown in the plot on the right. The continuous part of the lines represent the path of the angular momentum vector during the comet nucleus observations phases of Rosetta. Credits [15]

3.8 Shape

There are three shape models that can be used to represent the shape of a comet nucleus, each of them is strictly connected with the information available and consequently presents different levels of accuracy on the representation. Such information is related to the resolution and type of observations and contemporarily to the methods used to retrieve the data.

The three models will be presented following the criterion of increasing level of complexity (so increasing sharpness in the representation of the surface characteristics) and for each of them the authors, the methods and the observations will be laid out.

3.8.1Ellipsoidal shape

The most basic technique to represent 67P C-G shape is using an ellipsoidal model. This method requires only three parameters for a pure geometrical reconstruction: the three semi-major axis of the comet. Information on the nucleus mass or density is needed to obtain also the inertia moments.

Due to the scarce capability of this method to represent irregularities and longitudinal variation of the comet shape, this topic will be only briefly treated. It is to be noted that this shape description is highly interesting for a preliminary investigation of the comet illumination, in particular when there is few information of the surface features of a body.

The shape of the body is described by the following equation [Eq.(4)]:

$$\begin{cases} x = e_x \; cos(\varphi)\, cos(\lambda\,) \\ y = e_y \; cos(\varphi)\, sin(\lambda\,) \\ \quad z = \; e_z \; sin(\varphi) \end{cases} \qquad (4)$$

where (x,y,z) are the body coordinate expressed in principal inertia axis, and z is the rotational axis of the body. Consequently latitude φ and longitude λ are defined. The semi-axis of the ellipsoid are $(e_x\,, e_y, e_z)$ respectively.

The body surface is smooth, so that the local normal vector of a point of given (λ,φ) coordinates is defined by the derivation [Eq. (5)]:

$$\begin{cases} dx_0 = \dfrac{2x}{e_x^2} \\ dy_0 = \dfrac{2y}{e_y^2} \\ dz_0 = \dfrac{2z}{e_z^2} \end{cases} \qquad (5)$$

Dimensions of 67P C-G semi-axis are obtained from works discussed above and are reported in [Table 3]. The prolate spheroids are symmetrical with respect to the rotational axis so that the semi-minor axis is $e_x = e_y$ and the semi-major axis is e_z .

Work	**Shape**	**Semi-major axis [km]**	**Semi-minor axis [km]**	**Axis Ratio**	**Equivalent Sphere Radius [km]**
Davidsson Gutierrez [7]	Prolate spheroid	2.5	1.8	1.4	N/A
Lamy et al[17]	Prolate spheroid	2.39	1.75	1.37	1.94±0.02
Lamy et al [6]	Prolate spheroid	2.41	1.55	1.55	1.98±0.02
Lowry et al [9]	Prolate spheroid	2.94	2.07	1.42	2.26±0.03

Table 3 : Summary of 67P C-G ellipsoidal dimension purposed from different works

3.8.2 Spherical Harmonics Shape

A further step in surface detail representation is the Spherical Harmonics Shape. Theoretically speaking this representation can’t be assumed to describe a 3D body shape with less accuracy with respect to the Tessellated Triangular Shape. However regarding the currently available representation of comet 67P C-G the spherical harmonics shape is rarely used.

The advantage of this method is that the shape is represented by the composition of longitudinal and latitudinal superposed series of sine, therefore the surface is always derivable with continuity.

This description permits to have an accurate representation of the gravity field and topography of a body. For brevity equations are not reported but can be found in the work of Wieczorek [18].

In literature the work of De Sanctis et al [19] purpose a Spherical Harmonic shape of 67P C-G [Figure 11] in order to reconstruct the shape obtained by Lamy et al [6].

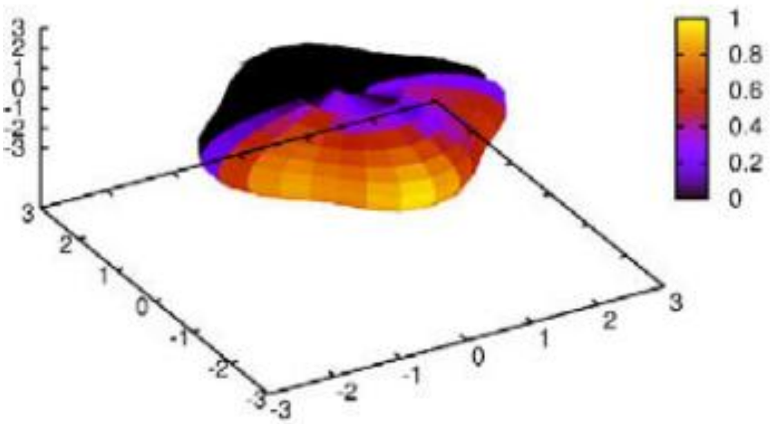

Figure 11: Shaded Spherical Harmonic shape of 67P C-G as purposed by De Sanctis et al [19]. Credits [19].

3.8.3 Tessellated Triangular Shape

The Tessellated Triangular Shape is the most accurate technique available for 67P C-G representation. It is based on a 3D triangular discrete mesh model that, given the vertices coordinates of the comet with respect to its centre of mass, permits to identify the cometary surface through triangular plates. In the 67P C-G representation the coordinate axis correspond to the principal inertia axis.

The Tessellated Triangular Shape is ideal for an irregular body shape, as 67P C-G appears, as long as it theoretically permits to achieve any desired spatial resolution (clearly accordingly to the data available) and can easily represent any type of surface irregularity. The drawback is that the surface is not smooth, although this feature has no influence on the development of this thesis work. Equations that permits to handle the Tessellated Triangular Shape are described in [Tessellated triangular plates shape].

The reference work that permitted to estimate the currently most detailed shape of 67P C-G is again the work of Lamy et al [5], from results deriving from this article descends directly the Tessellated Triangular Shape used in the LSS.

Lamy work refers to HST and NTT observations as reported in [Table 1]. Light curves deriving from such observations showed a highly asymmetric behaviour, this implies that the observed cometary nucleus corresponds to the varying cross-section of a rotating body having a complex shape, showing a pronounced deviation from the typical light curve of a simple prolate spheroid. In addition the difference in the light curve shapes between HST and NTT observations implies that the comet was seen at two different aspect angles [5]. In principle, large-scale surface unhomogeneities (i.e. surface composition) could also be advocated, but are not supported by the presently available images that the in situ space missions have returned from four different cometary nuclei [5]. Light curve inversion technique as described in [Orientation of the Spin Axis] was applied to both observations. It is possible to perform two types of inversion: convex and non-convex modelling. As Lamy et al [5] describe, there is a fundamental accuracy issue that lays between these approaches: the convex approach is performed in the parameter space describing the Gaussian image of a shape, this image is then transformed into shape information in the radius space. Thank to the Minkowski stability this inversion is stable against the inaccuracy of some other assumptions that are to be imposed in the model, i.e. the model of light scattering. Non-convex inversion is performed in the radius space directly and can not take advantage of the Minkovski stability, consequently is more liable to be affected by systematic errors and by the choice of the scattering model. As long as the available observations were limited, the non-convex approach was applied as is to be considered more efficient. To counteract the non-convex approach drawbacks, an additional inertia tensor regularization was enforced to the rotational state to remain close to principal axis rotation, so that unphysical pole solutions were discarded. Also a constraint on the shape smoothness was imposed.

As consequence of this assumption, that directly descends from the nature of the available observations, it is to be noted that only the global shape of the nucleus is really constrained by the light curves, and not the small scale variations such as local concavities which may be artifacts of the non-convex inversion.

Two uncorrelated solutions denoted as A and B are purposed in the Lamy et al. work and are only typical samples of possible models. Nevertheless, it is to be noted that the number of other solutions is already limited with the adopted data set, and that their global shape characteristics are roughly similar to those of the solutions presented. The solutions that produce the best fits to the observations are reported in rows in [Figure 12]: the upper row corresponds to the prograde solution A1, the lower row corresponds to the retrograde solution B2 as described in [Orientation of the Spin Axis].

Finally in the work of Lamy was necessary to rescale the model as long as the light curve inversion method gives dimensionless results. To scale the model the thermal flux was used as long as it is strongly controlled by the radius dimension. In [Table 4] 67P C-G shape characteristics reported, as indicated by Lamy et al [5].

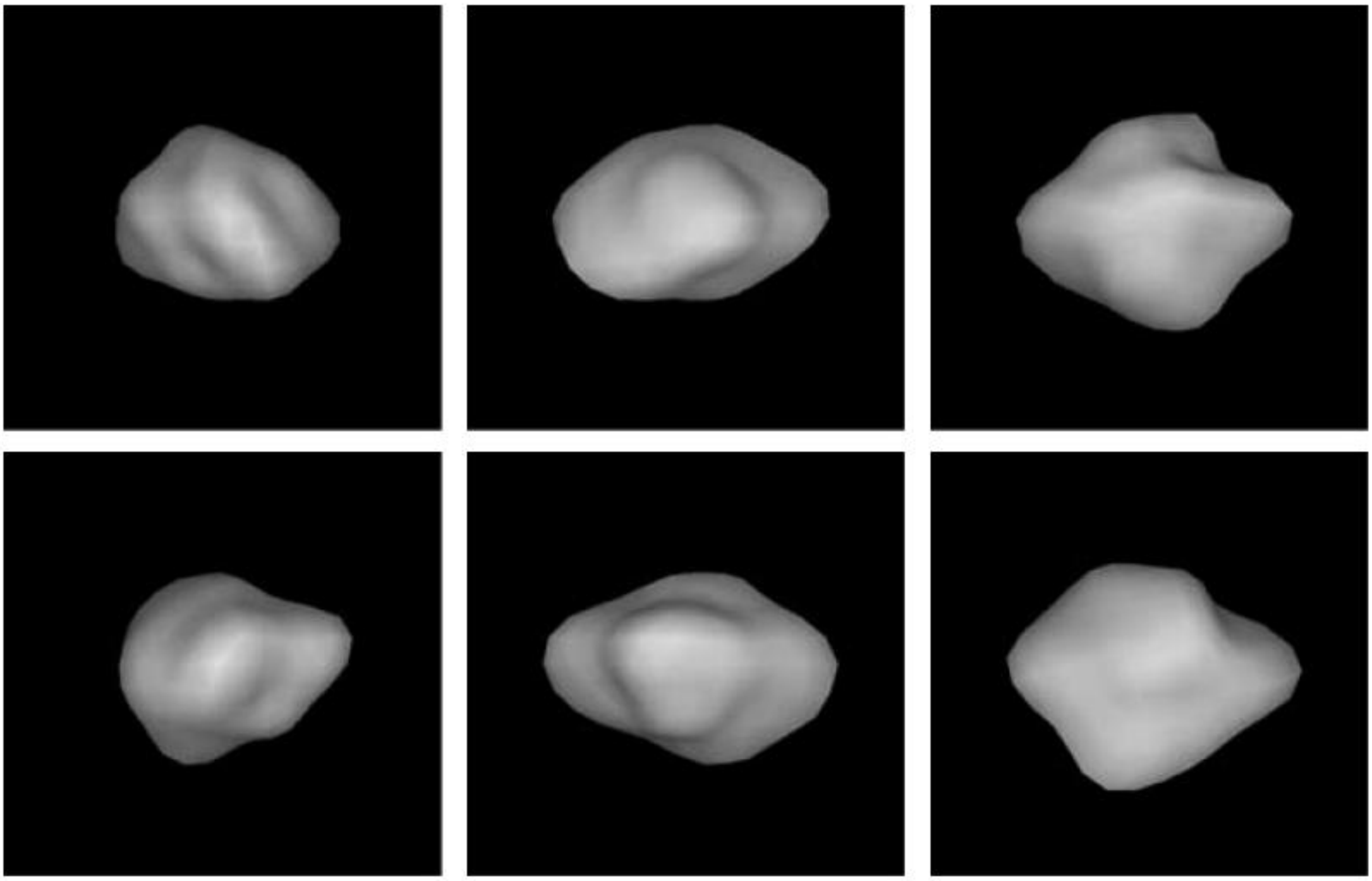

Figure 12: Prograde A1 (top row) and retrograde (bottom row) solution for 67P C-G shape solution. For each solution three views are reconstructed at three different rotational phase angles: 350° (left panel), 80°(central panel), and polar 80° view (right panel). Credits [5].

Solution	A1 (prograde)	B2 (retrograde)
X length	4.74 km	4.49 km
Y length	3.77 km	3.53 km
Z length	2.92 km	2.93 km
Volume	21.2 km^3	21.3 km^3
Area	40.2 km^2	40.1 km^2
Mass (500 kg/m^3)	1.0e13 kg	1.0e13 kg
Mass (100 kg/m^3)	2.1e12 kg	2.1e12 kg
Mass (370 kg/m^3)	7.8e12 kg	7.9e12 kg
I_x/I_z	0.70	0.67
I_y/I_z	0.86	0.86

Table 4 : Parameters of the nucleus of 67P C-G resulting from Lamy et al [5]. Credits [5]

For academic reasons is to be reported that the Tessellated Triangular Shape can also be extended in order to represent not only the cometary surface but also the internal volume of its nucleus through a 3D solid volumetric mesh. The discretization of the internal nucleus volume permits to associate a different mass and density for each element to represent an inhomogeneous body. This model is extremely useful to accurately describe the gravitational field of 67P C-G at short distances.

The work of Anderson and Udrea [20] exploits a similar methodology, they reconstruct the shape of 67P C-G using the 3D projections available from Lamy et al. [6] and create a 3D volumetric mesh. To model the gravity field they fill the volume of 67P C-G with spherical elements that can be packed using different configurations. By associating a mass to each spherical element they can model the cometary gravity field. This method is considered useful for preliminary orbital dynamics analysis and rapid trajectory propagation.

Repercussions in the LSSel Concept

The implemented shape in the LSS is the Tessellated Triangular Shape as long as:

- it best permits to describe the cometary characteristics and irregularity
- gives not only a latitudinal but also longitudinal variation effect on the shape
- is the most detailed description of 67P C-G currently available

All these features make the Tessellated Triangular Shape the preferable representation of 67P C-G. It is to be noted however that, as the works presented above suggests, this cometary shape is not definitive and may be subjected to relevant changes.

The advantage on this representation lays also in the capability of extrapolating suitable landing sites in a body showing an irregular surface: particular topographic formations located at particular latitudes may be evidenced, so that the results may be generalized for topographic features existing in a generic irregular shaped body.

As indicated also in [Orientation of the Spin Axis], due to information available from the DLR of Köln, the currently preferred solution for the spin axis orientation is Lamy et al. [5] B2 retrograde solution. Consequently the shape model adopted in the LSS corresponds to the one on the bottom row of [Figure 12]. The shape model used in the LSS is reported in details in [Tessellated triangular plates shape] .

3.9 Albedo

Albedo of the nucleus is a fundamental parameter, as long as in first approximation permits to determine the size of the nucleus when the photometric inversion method is used. As discussed in [Tessellated Triangular Shape] photometric inversion permits to obtain the shape of a body, but a scaling factor is necessary to obtain the real dimensions of the nucleus.

Albedo of cometary nuclei typically lays in a restricted range of 0.02-0.06 [5]. Albedo of 67P C-G was assumed to be 0.04 during the HST results for the determination of the nucleus size and shape [6]. In order to have the least indetermination the MIPS observation campaign [Table 1] was used from Lamy et al [5] to determine independently the scaling factor and the albedo, through a radiometric technique which combines visible and thermal measurements to independently determine the size and the albedo. For low albedo nuclei, the thermal measurements directly yield the size; then this size combined with visible measurements gives the albedo. Results yielded to an albedo of 0.044 although some uncertainty remains as long as is not easy to have a clear definition of the albedo of an irregular shape body, and observations had to be biased of 0.1mag to counteract the opposition effect [5].

Repercussions in the LSSel Concept

There is a repercussion on the LSSel Concept which is relative to the very low value of albedo. If values of albedo were much higher, as typical value of snow-ice albedo are, it would be possible to hypotheses to select a landing site which benefits of reflected sunlight coming from an extended adjacent reflective surface. This could permit to increase Philae generated power or to have a more efficient thermal control of Philae as long as the lander could be exposed only partially to direct sunlight.

Comet 67P C-G values of albedo can be associated to those of a dirty snowball, so no positive effects of reflected light can be imputed. On the contrary this permits a simplification on the modeling as long as light reflection effects can be neglected, this is further treated in [Illumination Assumptions].

3.10 *Surface*

3.10.1 Temperature and Surface Strength

The surface temperatures during the day are estimated to be in the range of -80°C to 20°C, depending strongly on the orbital position. During the night the surface temperature is estimated to be below -200°C [3].

The surface strength is estimated to be of the order of few 2-8kPa, taking into account of the comet ice to dust ratio and its porosity[21].

<u>Repercussions in the LSSel Concept</u>

Temperature on the surface of 67P C-G affect the lander thermal control. Philae indeed is designed to resist until 2AU distance from the Sun, closer distances may lead to overheating. This aspect consequently has strong consequences in the LSSel Concept and will be discussed in [Philae Thermal Subsystem].

Surface strength on the other hand is an issue for the Separation Descending Landing manoeuvre, as long as its upper limit affects the lander structural resistance, while the lower limit may lead the lander to sink into the comet surface. This aspect is extensively treated in [Separation-Descending-Landing].

3.10.2 Comet activity and erosion

Lamy et al [5] observe that a total water production of 2.2e9 kg is obtained when the production rate of water of 1e28 molecule/s is integrated over 450days before and after perihelion, which corresponds to the cometary active path on the orbit. If an active area of 4% out of the 40km^2 of cometary surface is assumed, each square meter of active area must contribute with about 1000kg of ice per apparition.

If a 0.7:0.3 ice-dust mixture is assumed as cometary composition, taking into account of the relative densities of solid materials a dust-ice ratio of 0.8 is obtained. Assuming a porosity of 70% of the surface material (this assumption is supported by the fact that solid material composing the comet is estimated to have an average density of about 1100-1200kg/m^3, while cometary density ranges between 100-500kg/m^3, probably settling at 370kg/m^3 as suggested by Daviddson Gutierrez [7]) means that there is approximately 200kg for each cubic meter of porous ice-dust material. Consequently active areas of 67P C-G erode at a rate of about 5m per apparition.

In addition Scheicher [14] observes that the coma appears highly asymmetric when observed before and after perihelion, this scenario can be explained when isolated regions activate and deactivate in different position on the orbit due to a seasonal change in solar latitude. In particular a plausible scenario of the Scheicher observation foresees [14]:

– a source region in one hemisphere dominated by large grains which is in “summer” while the comet approaches the Sun, and which is no longer illuminated shortly after perihelion;

– a much larger source region (or regions) in the other hemisphere coming under solar illumination shortly after perihelion (seasonal effect) and producing copious amounts of gas and small-sized grains but depleted in large-sized grains.

Repercussions in the LSSel Concept

The presence of strongly active areas on the comet is clearly a constraint in the LSSel Concept scenario. Harpoons designed to grab and hold Philae on the cometary surface are not capable to withstand an erosion of the order of magnitude of meters. On the contrary as seen, to explain the water production rate of the comet it is necessary to assume only a small percentage of active surface, about 4% [5], other articles purpose different values however always lower than 7%. This feature is also supported by observations of strong sunward jets [14]. Implications are that most of the surface is either inert (possibly crusted over) or releases gases at much lower rate than computed by a nominal water vaporization model.

This activity pattern is also assumed in the work of Chesley [13] and Schleicher [14] as reported in [Orientation of the Spin Axis]. As seen there is high indetermination on this aspect, consequently the constraint that can be imposed in the LSSel Concept is to try to determine the location of this highly active areas and discard them from the suitable landing sites. Clearly these area can identified between the locations most subjected to insolation that contemporarily show suitable surface composition i.e. ice rather than dust crust.

4. The Lander Philae

Philae lander is the in-situ segment of the Rosetta Mission and represents the main character of this thesis work. Thus in this chapter a detailed discussion on Rosetta lander Philae will be presented. Particular attention will be given to the features that have repercussions on the LSSel Concept.

4.1 Briefly the Mission Scenario

The lander Philae was put under commissioning in 2004 and successfully launched in March 2004, stowed in Rosetta front panel [Figure 3]. The lander is working in nominal conditions in all its subsystems and experiments, with few exceptions that do not harm mission success [22], [2]. Presently the lander is in hibernation, this travel mode will last until the Rosetta mission main operative phase, that will begin in January 2014 as already discussed in [Main Mission Phases].

After a phase of cometary approach, a period of 67P Churyumov-Gerasimenko observation will follow in order to characterize the features of the comet that are necessary for a successful mission prosecution i.e. descending manoeuvre sequence and landing site selection.

Philae was initially designed to land on comet Wirtanen; the new target comet 67P Churyumov-Gerasimenko larger dimensions implied a partial redesign of the landing gear. In addition the lander is designed to be flexible to a wide range of cometary scenarios, so there is high confidence in mission success [3].

4.2 Philae Mission Objectives

Philae represents the in-situ segment of the Rosetta Mission, thus in its objectives the direct cometary surface observation is demanded, together with the study of the structure of the nucleus. As reported in [Scientific Objectives] the prime mission purpose of Rosetta is to study and understand the early Solar System features. Scientific objectives of the lander consequently are [3] :

- determining the composition (elemental, isotopic, mineralogical and molecular) of the cometary surface material,
- measuring the physical properties (thermal, electrical, mechanical) of the cometary surface material,
- describing the large-scale structure (panoramic imaging, particles and magnetic field, and internal heterogeneity),
- monitoring the cometary activity (day/night cycle, changing distance to the Sun, outbursts).

4.3 Philae Overall Design

Philae [Figure 13] is a 97.9kg weight fully independent lander, representing the in-situ segment of Rosetta mission. Philae indeed is designed to be autonomous from all points of views from the Rosetta orbiter, provided with all necessary subsystems. Rosetta orbiter only vital function for Philae is to act as data relay for Earth communication [4], although during transfer Philae is supported from the Rosetta orbiter through Umbilical connection.

Philae **main body** shape is a trapezoidal box, constituted of carbon fibre and carbon fibre with aluminium honeycomb. It consists of a ground plate, an experiment platform and a polygonal sandwich construction, the Solar Hood, covering the Warm Compartment and carrying the solar generator. On the external faces (named WALLs) the 6 LILT solar arrays are mounted and constitute the Solar Hood[4]. The produced power is stored in the secondary batteries, although Philae is provided also with primary non rechargeable batteries useful for the First Science Sequence (this aspect is treated extensively in [Philae Power Subsystem]). Only one face of the box is open, the Balcony, and it serves as payload support and external interface. The main body core is called Warm Compartment which is thermally insulated with respect to the external environment through an MLI blanket and contains all the vital subsystems of the spacecraft (thermal subsystem is treated extensively at [Philae Thermal Subsystem]).

Philae main body is supported on a tripodal **landing gear**, each of the three foot is provided with integrated sensors and ice screws. The latter are necessary to guarantee stability and firmness on the cometary soil. Philae is also provided with an harpoon, deployable through a 2.5m tether which is designed to grab, hold and fix the lander to the comet soil during the landing manoeuvre. This aspect will be discussed in detail in [Separation-Descending-Landing].

Philae **mechanical capabilities** permit to the lander to rotate of 360° around its z axis, this solution permits to define a “working circle” for collection of samples, deployment of instruments and orientation of the solar arrays. Philae has also a small tilting capability of about ±5°.

Philae **attitude** during the Separation Descending landing manoeuvre is guaranteed through a flywheel and also through cold gas impulsive chemical thrusters.

Communication of Philae with Rosetta is performed through a series of s-band antennas placed on the external body of the lander, antennas switch on periodically using a mechanical device.

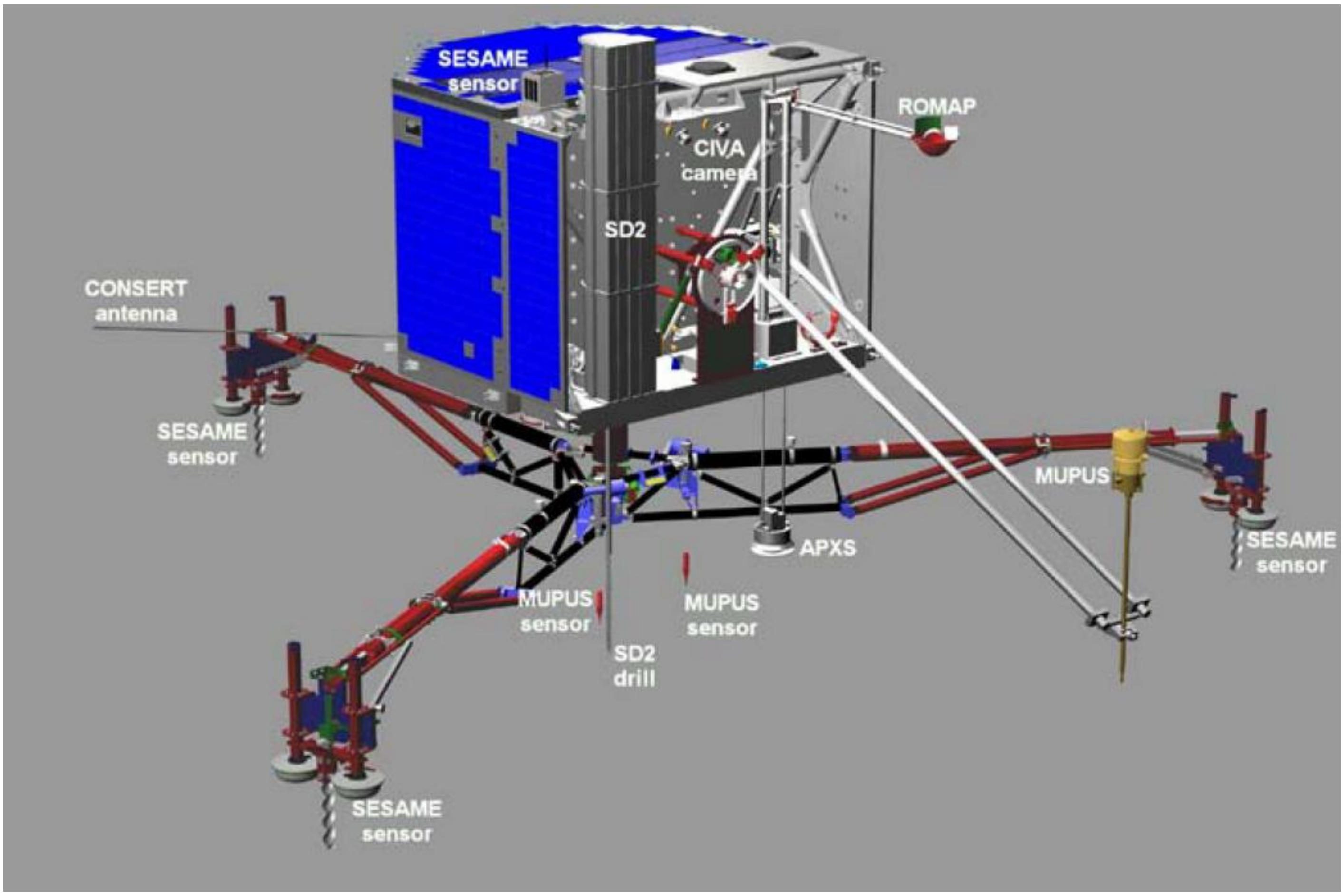

Figure 13 : Philae layout. Credits [3].

4.4 Philae Payload

Philae displays 10 scientific instruments [Table 5], each of them under the responsibility of a principal investigator. The aim of each of them is intended to comply the mission objectives outlined in [Philae Mission Objectives], in particular will characterize the composition of the cometary material down to its microscopic scale, the physical properties of the nucleus, its environment, its large-scale structure and its interior. Philae will also contribute to the monitoring of the long-term evolution (activity) of the comet[3].

Repercussions in the LSSel Concept

Repercussions on the LSSel Concept are relevant in particular in the regard of Sun exposure: most of Philae instruments probes are located in the Balcony, direct Sun exposure should be avoided, especially in the proximity of perihelion.

Instrument	Instrument Type	PI: Principal Investigator	Science Investigation	Mass [kg]
APXS	Alpha X-ray spectrometer	G. Klingelhöfer	Elemental composition of surface material	1.3
CIVA	–P: panoramic and stereo camera (b/w); –M/V: microscope, optical –M/I: microimaging IR spectrometer	J.-P. Bibring	Panoramic imaging. Microscopic imaging and analysis of the sample composition	3.4 (sharing parts with ROLIS)
CONSERT	Radio wave sounding transponder	W. Kofman	Internal structure of the nucleus by radio-wave sounding	1.8
COSAC	GCMS	H. Rosenbauer F. Goesmann	Molecular composition and chirality of samples	4.9
MUPUS	PEN: hammering device with thermal and mechanical sensors; TM: IR thermal mapper; ANC: acceleration and thermal sensors and in anchors	T. Spohn	Physical properties of the subsurface (density, porosity, thermal properties)	2.2
PTOLEMY	GCMS	C. Pillinger/I. Wright	Isotopic composition of light stable elements in samples	4.5
ROLIS	Descent and close up down-looking camera, 3 colours active illumination	S. Mottola	Descent and down looking imaging	1.4
ROMAP	Magnetometer and electron/ion sensor; Pressure sensors (1 Pirani, 1 Penning)	U. Auster	Magnetic and plasma monitoring	0.7
SESAME	CASSE: acoustic transmitters and receivers; PP: permittivity probe; DIM: 3D dust impact monitor	D. Möhlmann/K. Seidensticker	Electric and acoustic sounding, dust impact monitoring	1.8
SD2	Sample drill, sample volume check and transfer device; soil strength inference	A. Finzi	Sample acquisition (drill) and transfer	4.7
Total				26.7

Table 5 : Philae payload. Credits [3]

4.5 Philae Operative Phase

In this section the phases of Philae operative life will be discussed, together with the repercussions in the LSSel Concept.

Philae operative life begun shortly after launch, when four launch blocks were released[2]. The lander was switched on during interplanetary trajectory for checkout and calibrations i.e. the first Earth fly-by and the Mars fly-by [3]

4.5.1 Approach to 67P Churyumov-Gerasimenko

Although not regarding direct involvement of Philae (during this phase the lander will be switched off), the approach to comet 67P C-G is a fundamental phase for Philae mission scenario schedule. After a long period of hibernation of almost 2.5 years, in January 2014 the orbiter will be awakened and in May 2014 the rendezvous of comet 67P Churyumov-Gerasimenko will be carried out at about 4AU from the Sun. In September 2014 the orbiter will be inserted in the comet orbit at 3.4AU. At this period a fundamental phase of global observation and mapping of the nucleus will take place at distances down to 1km. As already reported in [Main Mission Phases] few of the cometary features are known with sufficient accuracy, consequently a phase of preliminary comet observation is necessary In this phase in particular the surface features and shape, the spin axis orientation, the rotational period, the outgassing dynamics and the gravity filed will be observed, all these information indeed is fundamental for planning Philae descending manoeuvre and landing site selection [1]. It is to be underlined that in these phases the comet is retained to be scarcely active, as will be reported in [Separation-Descending-Landing].

4.5.2 Separation-Descending-Landing

SDL (Separation Descending landing) is one of the yet most undetermined phases regarding Philae operative scenario[3]. Philae has been designed to cope with a wide range of possible comet properties as long as it is foreseen that comet features would be partially undetermined until the final approach phase [23].

However a number of articles, that will be reported below, address the SDL phase, producing interesting and relevant consequences for the LSSel Concept. A schematization is reported in [Figure 14].

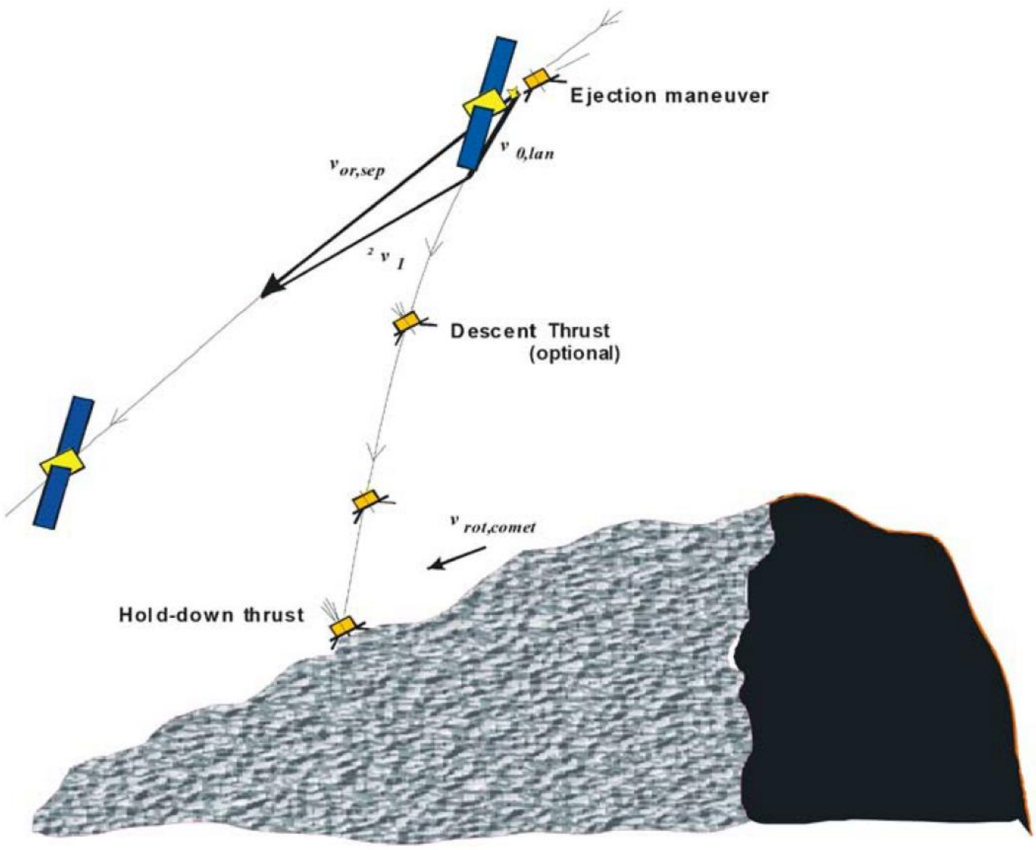

Figure 14: Schematization of Philae SDL manoeuvre. Credits [3].

Separation [21] of Philae will be carried out once Rosetta orbiter is in a dedicated delivery orbit. Separation will take place with an adjustable relative velocity between Rosetta and Philae of 5-52cm/s and will place Philae in a near-ballistic descent. The ejection manoeuvre takes place at an altitude of the order of 1 km only.

Descending [21] of the Lander is the following phase. Lander ejection velocity partly cancels Rosetta's orbital velocity, such that Philae moves on an comet-surface crossing ellipse. Descent is stabilised by a flywheel and the optional use of a cold-gas thrusters (in z direction, thus normal to the lander baseplate).

Landing [21] is one of the most critical phases. Touchdown will take place with the velocity vector parallel to the lander z-axis and the cometary surface normal to it (i.e. the baseplate parallel to the cometary surface). Typical impact velocity at the surface will be between 0.5-1m/s, impact will be withstood by the tripodal landing gear that is provided with a dedicated damping device in its central part to minimize re-bounce. Ice screws are located in the tripod feet to provide anchoring force and avoid gliding in slopes. Immediately after touchdown an harpoon is fired, which is connected to a 2.5m tether that once retracted (by rewinding the tether) will secure the lander to the comet surface exploiting a pre-adjustable pre-tension ranging 5-30N[21].

There is an issue regarding the surface strength of comet 67P C-G during touchdown, which is accurately treated by Biele et al [21]. For sake of brevity only the fundamental results will be reported. Considering realistic estimate of 67P C-G surface strength (see [Temperature and Surface Strength]), the typical touchdown velocity and the frontal area of Philae as function of the depth (i.e.: feet plus the ice screws and their brackets penetrate of approximately 20–25cm, after the legs penetrate of additional 30cm, after the baseplate touches the ground [Figure 15]) a plot of the penetration depth is obtained as function of 67P C-G surface strength, [Figure 16]. Most likely, the soft landing will lead to a typical penetration of the lander's feet of up to 20 cm. Results do not change appreciably if the bulk density of the comet is twice or half the assumed value of 300kg/m^3 (penetration depth changes by at most 8%); they depend on square touchdown velocity for high surface strength, but depend on less than proportional touchdown velocity for smaller strengths, up to 4-8kPa.

Landing gear failure is avoided by the fact that maximum design surface strength is assumed of MPa magnitude, rather depth penetration is to be considered cause if the baseplate sunk the 360° z axis rotation of Philae would be compromised, this eventuality is to be considered for tensile surface strength lower than 2kPa.

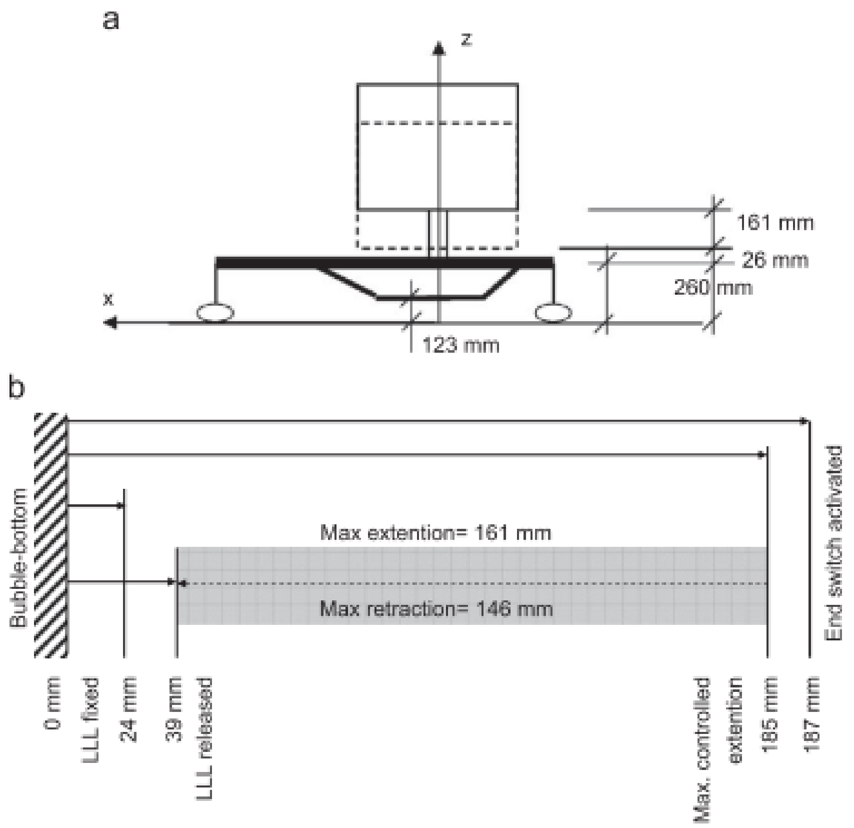

Figure 15: (a) Rosetta lander schematic side view and (b) Rosetta lander landing gear vertical range flexibility. Credits [21]

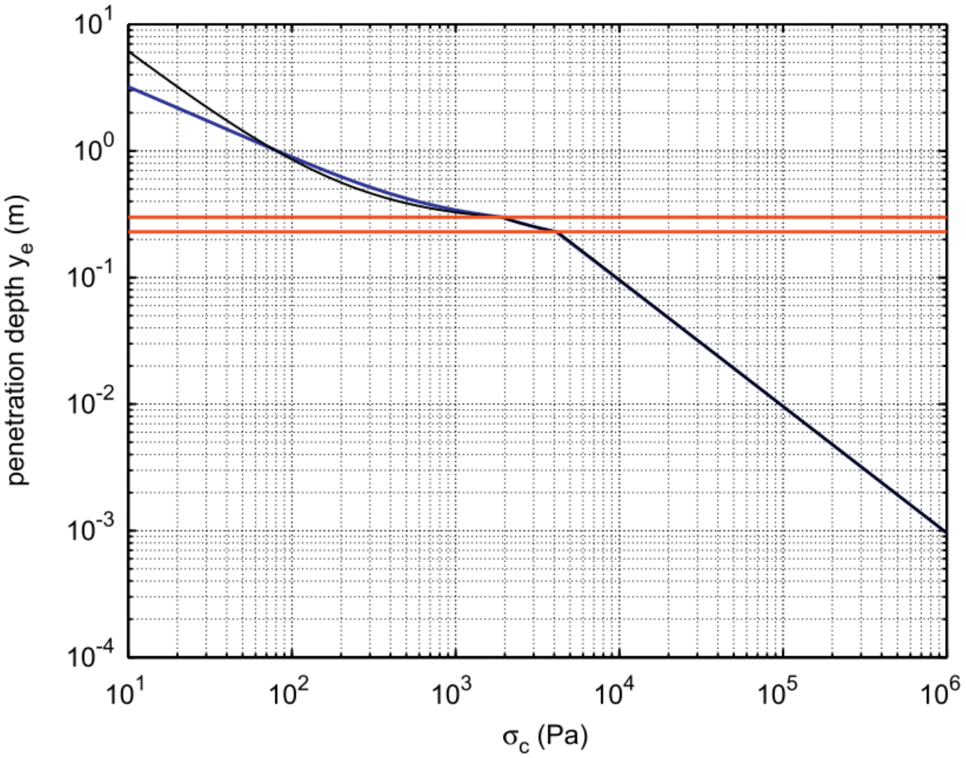

Figure 16: Modelled penetration depths of Philae as a function of compressive strength. Touchdown velocity 1m/s and bulk density of comet surface material 300kg/m^3 are assumed. The thin lack curve is the simple analytical result for zero density; only for small compressive strength the difference is evident. Note the kinks in the curves where the lander cross section changes abruptly (at 1906 and 4100Pa, respectively). Credits [21].

Contingencies on the SDL manoeuvre regard also the possible **comet activity** during this phase. In particular the ratio between gravitational and outgassing forces is to be taken into account: outgassing forces deviate the lander form a ballistic descent trajectory, but in the other hand can possibly permit a softer (slower in impact velocity) landing as long as outgassing forces act almost normally to the cometary surface. Bertrand et al [24] address this problem using HST observations [Table 1] and the A1 shape model retrieved by Lamy et al [6]. They follow analysis that can be based on two criterions: *impact velocity minimization* or *descending time minimization*. The slowest is the impact velocity the safest the landing (critical impacts are for velocities >1.2m/s), on the other hand the longer the descending trajectory the more the perturbing forces (i.e. gravitational unmodelled, outgassing) disturb the optimal trajectory. Contemporary the descending trajectory must be longer than 30mins for operational reasons: i.e. landing gear deployment and measurements. Separation manoeuvre for mechanical reasons will produce a thrust on Philae normally to its z-axis, this same axis must be orthogonal to the cometary surface at landing. Maximum release thrust is 0.529m/s, while maximum ADC thrust during descent is 1m/s. Release altitude must be greater than 1km.

Considering these constraints altogether Bertrand et al. observed that the maximum ratio between outgassing and gravitational acceleration is 8%, thus gravitational forces remain predominant in the problem [Figure 17].

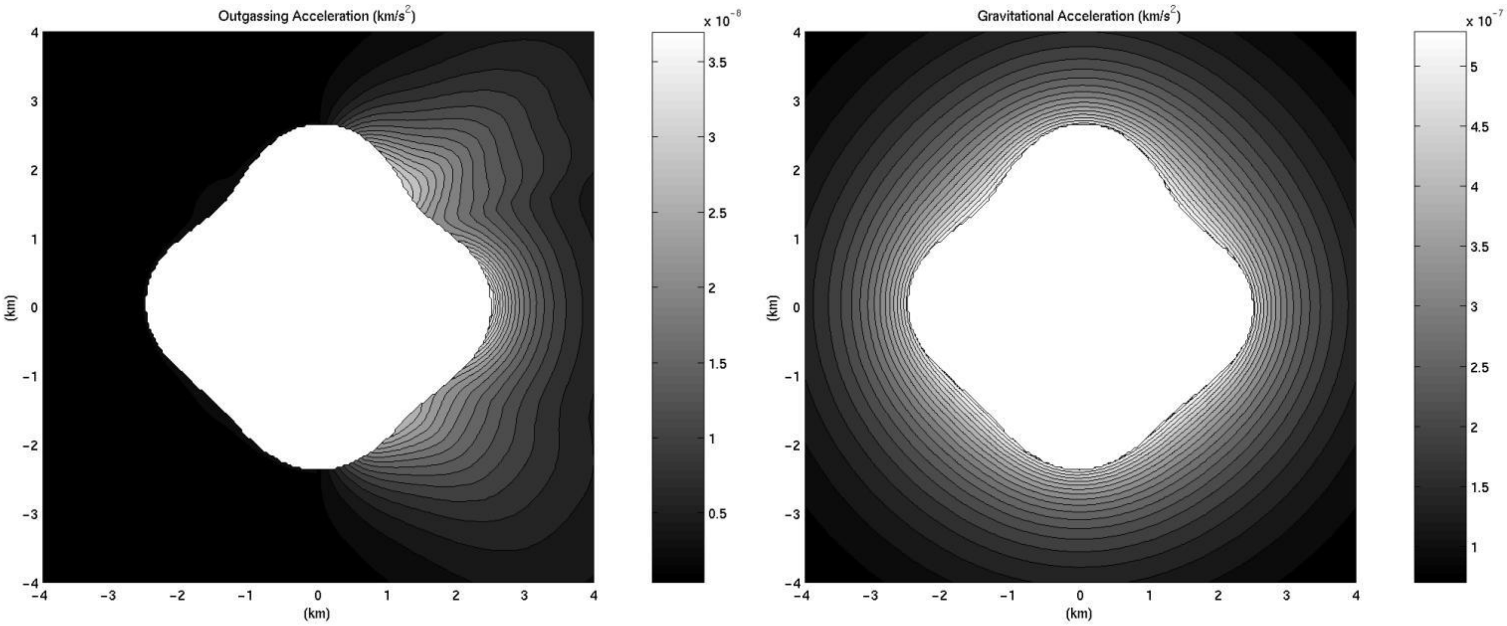

Figure 17: Outgassing and gravitational accelerations in 67P C-G equatorial plane. Outgassing accelerations have magnitude of 10^{-8}km/s^{s} while gravitational of 10^{-7}km/s^{2} Credits [24].

Results of Configuration 1 (landing site located at 0° latitude 0° longitude, Sun direction points at 0° latitude 0° longitude) are reported in [Table 6], they correspond to the minimal impact velocity that can be obtained and are an example of a suitable SDL manoeuvre.

Creterion	Impact velocity	Duration
Impact velocity	0.718 m/s	1.159 m/s
Descent duration	55 min	30 min
Separation ΔV	0.529 m/s	0.489 m/s
Descent ΔV	0.164 m/s	0.675 m/s
Release altitude	1 km	1.5 km

Table 6: SDL manoeuvre parameters, Configuration 1. Credits [24].

A very wide number of other manoeuvres can be obtained, it is to be observed however that with the technique presented not all cometary sites can be reached: depending on the Sun direction and season (given by comet spin axis orientation) the part of the nucleus reachable by the lander varies from 46% to 62%. In particular concerning effect of nucleus shape Bertrand et al. observe that reachable parts of the nucleus are located near humps and close to the equator to exploit high rotational velocity. Configuration 1 that shows the best impact velocity results displays a landing site located at the subsolar point. This proves that the outgassing forces, acting opposite to the gravitational forces and showing highest values for the subsolar point, influence notably the lander descending phase.

Results robustness and errors on the nominal landing site are evaluated taking into account dispersions on orbital parameters, separation manoeuvre and descent ADS manoeuvre (dispersions on lander attitude, outgassing forces and comet density are neglected however) and lead to highly accurate values [Table 7]:

	Max	**Min**	**Mean**	**Std**
Impact velocity	0.754 m/s	0.716 m/s	0.734 m/s	5e-03 m/s
Distance from target site	71 m	0.15 m	22 m	12 m
Latitude	1.38°	1.44°	9e-03°	0.34°
Longitude	1.61°	-1.22°	0.24°	0.41°
Landing delay	289 s	-188 s	39 s	62 s

Table 7: Landing site accuracy, Configuration 1, Impact velocity criterion. Credits [24].

Repercussions in the LSSel Concept

Contingencies on the lander penetration depth at landing will be neglected in the LSSel Concept. As seen the worst condition deriving from this issue is the baseplate sinking that would compromise Philae 360° rotation around z-axis. Clearly this eventuality would reduce noticeably the solar generated power during the mission, as long as Sun orientation of the lander is fundamental, as it will be discussed in [Philae Orientation on the Plate].

Relevant repercussions can be evicted from Bertrand et al. work, although is to be underlined that this article is dated 2004 (it was not possible to find more recent works), in particular:

- it is noticeable that not all sites in the cometary surface can be reached, as reported the best estimate foresees that 62% of the surface can be reached, particularly suitable are hills and humps located at subsolar point and/or near the equator. This is relevant also when considering repercussions deriving from Telecommunication [Communications]. In addition means that different landing sites may be available depending on the season, thus on the spin axis orientation.
- robustness of results show that is possible to land within the designed impact velocity range. Of particular relevance is the "Distance from target site" parameter, which gives a good estimation of the landing site error ellipse.

4.5.3 First Science Sequence

Philae First Science Sequence is scheduled to last 120hrs and will be operated through primary batteries (for details see [Power Subsystem Design]). Operations and experiments are guaranteed for all 10 instruments onboard, an additional margin was considered to permit nominally one repetition of experiments for each instrument to prevent possible malfunctioning or inaccuracy in the measures. A margin of 30% on the available power was applied to these estimates [3]. Some operations can be executed simultaneously in this phase.

Primary batteries will permit to have a stable and reliable source of energy, in addition the lander orientation will be fully dedicated to experiments and not to solar array optimal exposure.

It is to be noted that Philae First Science Sequence will begin immediately after separation from the Rosetta orbiter, images will be taken and other analysis will be performed during the descent phase[21]. Measurements and experiments will prosecute for the immediate120hrs following the landing.

4.5.4Long Term Science

The Long Term Science phase will be operated through the use of secondary batteries that will be recharged exploiting the 6 Low Intensity Low Temperature solar arrays mounted on the body of Philae (for details see [Power Subsystem Design]). Power production will also ensure the lander vital operations in Safe Mode i.e. thermal control, communication.

The Long Term Science phase is designed to permit to study the evolution of the comet surface scenario while 67P C-G is approaching the Sun. Experiments will be operated depending on the available power resources.

Nominally the Long Term Science phase will begin immediately after the First Science Sequence and will last until 2AU Sun distance, Philae thermal design threshold. However an extension of this phase is foreseen possibly until perihelion, to study at best the comet nucleus evolution [3].

Repercussions in the LSSel Concept

The aim of this thesis work is to optimize Philae generated power during this phase, paying particular attention to thermal constraints in order to guarantee the longest mission extension in the best conditions. The landing site free parameter is indeed a fundamental tool to achieve Philae mission extension.

4.6Philae Power Subsystem

Philae Power Subsystem is a fundamental aspect in the LSSel Concept definition, as long as its design features govern the Solar Generated Power that is the prime optimization parameter of this thesis work.

Most of the references used in this section derive from the Politecnico of Milano as it is responsible in Rosetta and Philae photovoltaic assemblies design, as also in the Philae solar generator in order to support the foreseen works during the journey to the comet and the in-situ operations.

4.6.1 Power Subsystem Design

Philae Power Subsystem manages all electrical power needed by the lander during its entire mission.

The main power source is the primary battery unit of estimated capacity 1000Wh at comet arrival and 1200Wh at launch [25]. Primary batteries are four strings with eight $Li/SOCl_2$ non rechargeable cells. As already mentioned in First Science Sequence] these batteries will support the First Science Sequence for at least 120hrs of operations.

The secondary power source is the secondary batteries unit of estimated capacity of 130Wh at comet arrival and 150Wh at launch[25]. Secondary batteries are constituted of two strings of 14 cells of lithium-ion rechargeable cells. These batteries will be refilled by the power generated with the solar arrays.

During the cruise phase Philae Power Subsystem will be supplied via the Electrical Support System through the Rosetta orbiter, this allows lander check-ups and calibrations [4].

Power distribution is ensured thank to the Philae Primary Bus. The main subsystems, the Command Data Management System (CDMS) and the Thermal Control Units (TCUs), are directly connected to the primary bus via the dedicated DC-DC converters. The other subsystems and all the experiments are connected through switches to the Primary Bus to the Secondary Bus, that is stabilized.[4].

The Wake-Up System provided for the exact and safe start of Philae operations. It monitors it the temperature and the available power are in the foreseen ranges before switching power to the start system[4].

4.6.2 Solar Cells

Rosetta mission solar cells are new deep-space cells developed to work in Low Intensity Low Temperature conditions (LILT). In facts in the 70s was found that in these conditions normal solar cells would show uncontrollable adverse effects, named as LILT degradation. The losses occurred with large statistical variation and could not be assessed from measurement at room temperatures[4].

For decades the solution for this issues has been the use of radioisotope thermoelectric generators (RTGs), but Rosetta mission was conceived to be the first to set a milestone for the solution of LILT degradation and also to counteract a number of drawbacks coming from the use of radioisotope power sources: costs, safety and impossibility to launch it in a full European mission.

LILT solar cells (see [Figure 18]) selected for Rosetta and Philae Photovoltaic Assembly (PVA) are the silicon-based 10LiTHI-ETA® 3-ID/200. Solar cells used for Philae PVA are the same mounted on Rosetta orbiter, but with different dimensions: 61.95mmx3.75mmx200μm thick for Rosetta, 32.4x33.7x200μm thick for Philae. In addition Philae cells have coverglass applied. These cells can withstand LILT degradation effects as also Flat Spot, Tunnel or Shunt on I-V characteristic of solar cell in LILT conditions.

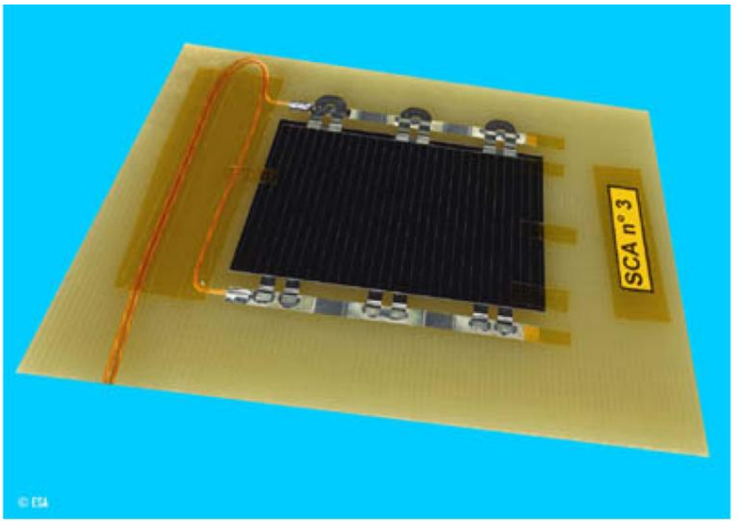

Figure 18: Philae LILT cell. Credits ESA

A team of students, researchers and professors from the Politecnico of Milano, including S. Brambillasca, F. Topputo, A. Finzi, F. Bernelli-Zazzera conducted a series of laboratory experiments for the characterization of Philae cells in order to estimated at best the in-flight behaviour of the LILT cells[25][26]. In particular a I-V curve investigation was conducted as long as it permits to retrieve characteristic parameters of the solar cells as: short cut current Isc, open-circuit voltage Voc, the maximum power point (Imp and Vmp), the fill factor FF and the cell efficiency η.

Experiments were conducted in a series of foreseen operative conditions as reported in [Table 8]:

Rosetta cells (23.39 cm^2)		
SC	**Temp(°C)**	**Fluence (1e14e/cm^2)**
1	From +25 to +150	From 0 to 9
0.03	From -155 to +25	From 0 to 9
0.11	+25	0
0.11	From -130 to +25	3.2 and 6.4
Philae cells (10.92cm^2)		
SC	**Temp(°C)**	**Fluence (1e14e/cm^2)**
0.11	+25	0
0.11	From +25 to -120	0

Table 8 : Summary of test performed on Rosetta and Philae solar cells. Credits [25]

To obtain values of the characteristic cell parameters in EOL conditions the following expression [Eq. (6)]was applied[25]:

$$X_{EOL}(T)|_L = X_{BOL}(T_{ref})\big|_L RF_X|_O - \beta_{EOL}|_O(T_{ref} - T) \qquad (6)$$

where X is the generic parameter (i.e. X = {Isc,Voc,Imp,Vmp}), EOL and BOL refer to the parameter in end of life or begin of life conditions, T and Tref are generic temperature and reference temperature respectively, RFx is the Remaining Factor of the X parameter, β is the temperature coefficient of X, L and O refers whether the measure was made on lander ,or to orbiter respectively.

In particular the characterization of Philae cells in LILT conditions will be reported, as it can be seen in [Table 4Table 8] experiments were conducted in BOL conditions, consequently the relation that can be applied to obtain the cell characteristic parameters is [Eq.(7)]:

$$X_{BOL}(T) = X_{BOL}\left(T_{ref}\right) - \beta_{BOL}(T_{ref} - T) \qquad (7)$$

where all parameters are referred to the lander in this case.

As a result the electrical parameters at 25°C and SC=0.11 were obtained, as much as the temperature coefficients.

Isc [mA]	**Voc [mV]**	**Pmax [mW]**	**Imp [mA]**	**Vmp [mV]**	**F.F. [%]**	**η [%]**
57.74	578.1	26.33	54.15	486.3	78.88	16.05

Table 9 : Electrical parameters of Philae cells at 25°C and 0.11SC. Credits [25]

dIsc/dT [mA/°C]	**dVoc/dT [mV/°C]**	**dImp/dT [mA/°C]**	**dVmp/dT [mV/°C]**
0.1048	-1.9182	0.0883	-2.1569

Table 10 : Temperature coefficients of Philae cells at 0.11SC BOL. Credits [25]

Voc temperature coefficients tendencies show good accordance for all the 10 LILT cells of Philae used for the BOL experiments performed at variable temperature and at 0.11SC (see [Figure 20]). On the other hand temperature coefficient tendencies for Isc show different groups of performances: Group1 have good performances with decreasing temperature; Group2 have worse performances as their Isc decrease faster with decreasing T (see [Figure 19]). This behaviour is clearly reflected in the Pmax performances (see [Figure 21]).

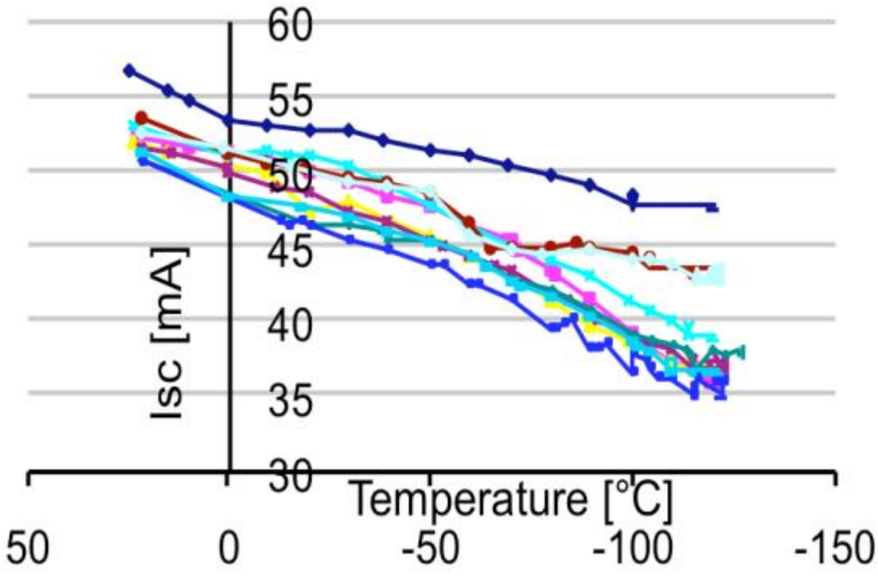

Figure 19: Isc vs Temperature at 0.1SC BOL. Credits [25].

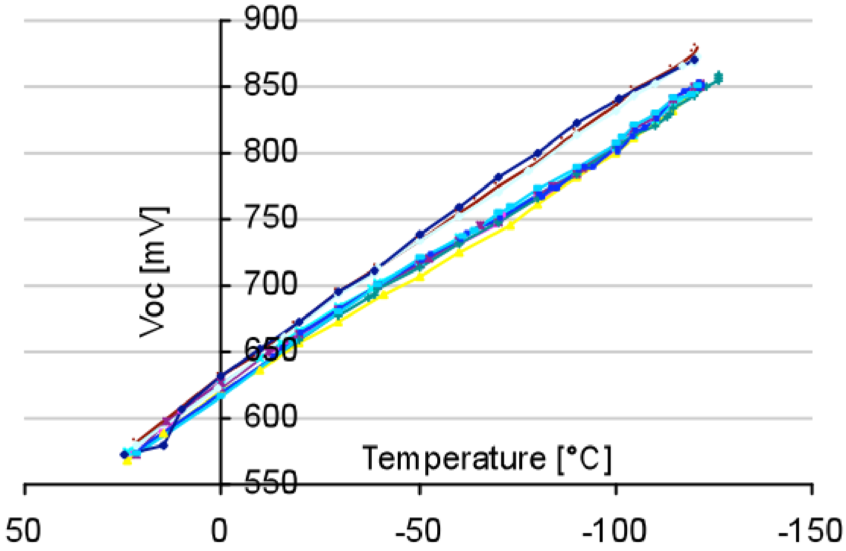

Figure 20 : Voc vs Temperature at 0.1SC BOL. Credits [25].

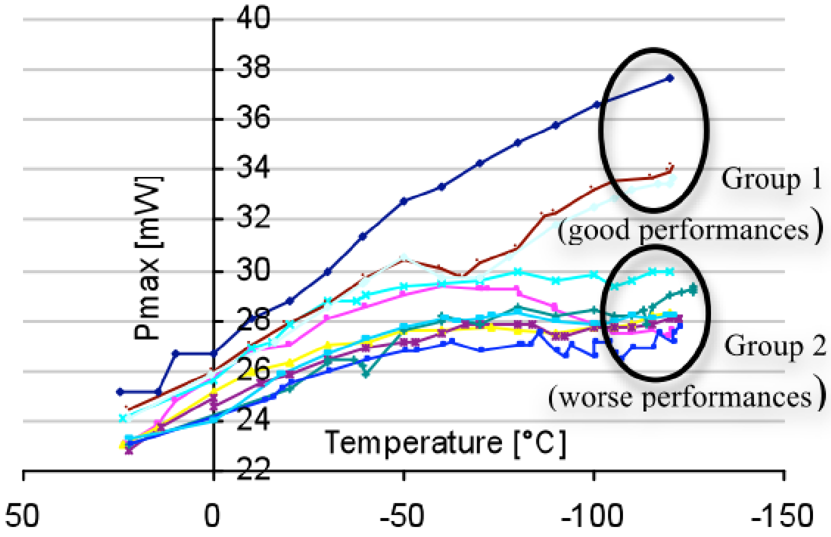

Figure 21 : Pmax vs Temperature at 0.1SC BOL. Credits [25].

Repercussions in the LSSel Concept

The model of cell described above is the one that is implemented in the Solar Array Simulator. This routine, developed at Politecnico di Milano, permits estimate the power production of Philae during the cometary phase as it is integrated in the Landing Site Simulator. Solar Array Simulator capabilities are described in [Philae Power Model].

4.6.3 Photovoltaic Assembly

Philae Photovoltaic Assembly (PVA) has a surface of $2m^2$ and was conceived to permit to the lander to produce a sufficient amount of power to support the Long Term Science phase. The Philae PVA was integrated by Galileo Avionica, under the responsibility of the Politecnico di Milano, on the lander Solar Hood built by DLR.

Philae PVA is constituted of 1224 10LiTHI-ETA® 3-ID/200 silicon solar cells organized in 6 solar arrays disposed in all but one side of Philae body, as visible in [Figure 22]. Solar arrays are directly mounted to the Solar Hood, which consists of a unique structure that collects the following panels: Wall 1, Wall 2, Wall 3, Wall 4, Wall 5 and the LID and by two detachable panels identified as Balcony 1 and Balcony 2, which are attached by means of a connector to Wall 1 and Wall 5. Electrical sections are six because the panels Wall 1 and Balcony 1 and the panels Wall 5 and Balcony 2 are wired together and constitute unique sections [Table 11]. This complex solution is due accordingly to the design requirement that the maximum power point (Vmp> 30.6V) must be respected under the following mission conditions:

- -80 ◦C @ 0.11 SC for all the Philae electrical sections
- +20 ◦C @ 0.25 SC only for Wall 1 and Balcony 1, Wall 5 and Balcony 2, LID

Solar array	Electrical Section	Solar cells per string	No. of strings
SA1	Wall1 + Balcony1	127	2
SA2	Wall 2	81	2
SA3	Wall 3	81	2
SA4	Wall 4	81	2
SA5	Wall 5+ Balcony 2	127	2
SA6	Lid	115	2

Table 11 : Philae PVA solar array sections layout. Credits [25]

The six solar panels are connected to five individual Maximum Point Power Trackers (MPPT), with SA1 and SA5 connected to the same MPPT as they are opposed and can’t be exposed to the Sun simultaneously.

Philae Solar Hood shape was conceived to optimize the Sun received by Philae and reducing at minimum the necessity of lander orientation to guarantee best Sun exposure.

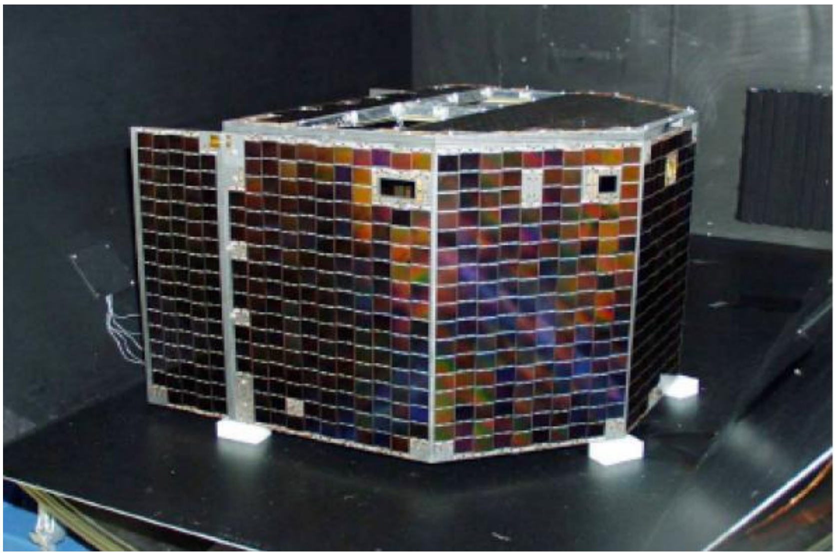

Figure 22: Philae PVA. Credits Galileo Avionica

4.6.4Power Levels and Modes

Different power levels are necessary for Philae operations. In particular the Standby Mode power levels are reported in [Table 12]: these values are constraining as the minimum power threshold that must be guaranteed to ensure a daily equilibrium between generated power and operative necessary power.

Philae Standby Mode Power Levels	
Standby 1: PSS CDMS TCU2 ON	5.11 W
Standby2: Standby 1 plus 1 secondary battery heater on	7.61 W
Standby3: Standby 1 plus secondary battery heater on, thus also TCU1 on.	10.28 W

Table 12 : Philae Standby Mode Power Levels

<u>Repercussion on the LSSel Concept</u>

The least constraining power level Standby1 is considered to produce an analysis that can estimate which cometary sites permit the daily production of at least this minimum power threshold for the entire mission duration.

4.7 Philae Thermal Subsystem

Philae have to sustain a range of thermal conditions, from the hibernation cold case, to the hot case when the comet is approaching perihelion. In order to comply with this wide range of variations the Thermal Control Subsytem of Philae was conceived separating the lander components in two thermally and physically separated locations [27]:

- **Warm compartment**: represents the lander core, it is designed to store those devices that are sensitive to extreme temperature values and do not need to directly interact with the external environment: electronics and sensitive experiments.
- **Cold Balcony**: is the lander external shell, it is designed to permit experiments interaction with the environment, to provide free filed of views for the solar generators and for the antennas.

Insulation is a prime strategy to comply thermal requirements, two MLI tents are used to thermally separate the Warm Compartment from the Cold Balcony and the external environment. The cold case is counteracted through the use of a number of heaters, while two absorbers are mounted on the solar hood lid to collect solar energy and dissipate it in the Warm Compartment. See [Figure 23].

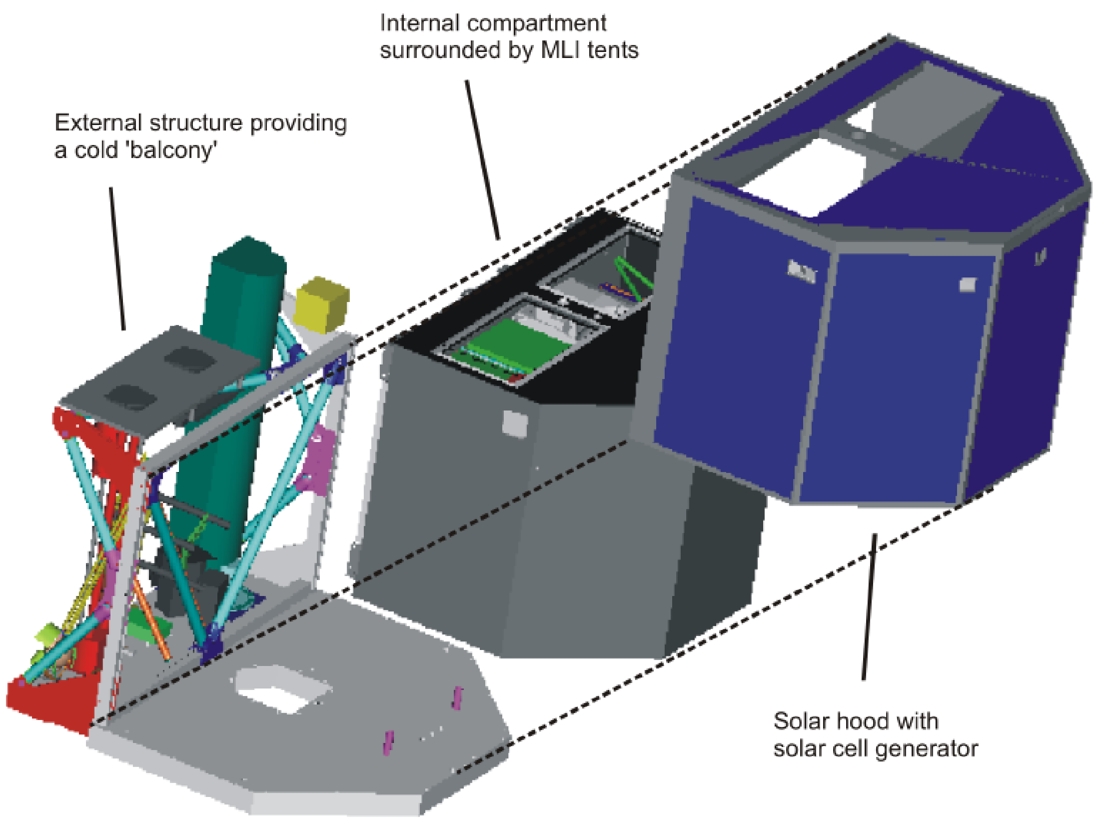

Figure 23: Philae Thermal Control System. Credits [27].

Absorber foils [27]**:** two solar absorber foils are mounted in the solar hood lid and permit to collect solar heat and to transmit it into the Warm compartment. Foils are made of copper and have surface finishing: absorbing TINOX surface on the external side and black painted surface on the internal side. Characteristics for each foil are reported in [Table 13]:

Characteristics of Philae absorbers		
Overall dimensions	65772mm²	--
External absorbing area	61123mm²	alpha/eps = 0.94/0.04
Internal emitting area	64669mm²	alpha/eps = 0.96/0.88

Table 13 : Philae absorbers characteristics. Credits [27].

MLI tents [27]: two separated MLI tents are installed, MLI tent 1 and MLI tent 2, composed respectively of 22 and 25 layers. The MLI tent 2 is wrapped around the components stored in the Warm Compartment, following their shape and dimensions. MLI tent 2 also insulates cavities that protrude the internal compartment and houses the landing gear mechanics and the electronics of CIVA camera. MLI tent 1 on the other hand is accommodated into the Solar Hood box, following the shape of the Walls and Lid of the Solar Hood., the inner surface of the Baseplate and an area facing the Balcony. MLI tent 1 separately surrounds MLI tent 2 and provides a second step of insulation. This strategy permits to achieve temperature difference of 100°C between the Solar Hood surface and the Warm Compartment. In [Figure 24] the two MLI tents wrapping and the absorbers apertures are visible.

Two **Hibernation Heaters** [27]: are necessary during the hibernation phase and all the non-operational phases. This permits to the lander, together with the MLI insulation to avoid the warm compartment to reach the lower non operational temperature of **-**55°C. Additional Heaters are installed to prevent failure of heaters when the lander is awakened from hibernation.

The **operational electronics** of the Thermal Control System are composed of two identically built, but individually operated Thermal Control Units (TCU-1 and TCU-2). Each TCU monitors 31 temperature sensors distributed over all Philae body, where 6 sensors are used simultaneously to provide heater control loops.

Temperature ranges for the Warm Compartment are the most constraining for the mission and can range as reported in [Table 14]:

Philae Warm Compartment thermal ranges	
Operative	-40°C +50°C
Non-operative	-55°C +60°C

Table 14: Thermal ranges allowed for Philae Warm Compartment

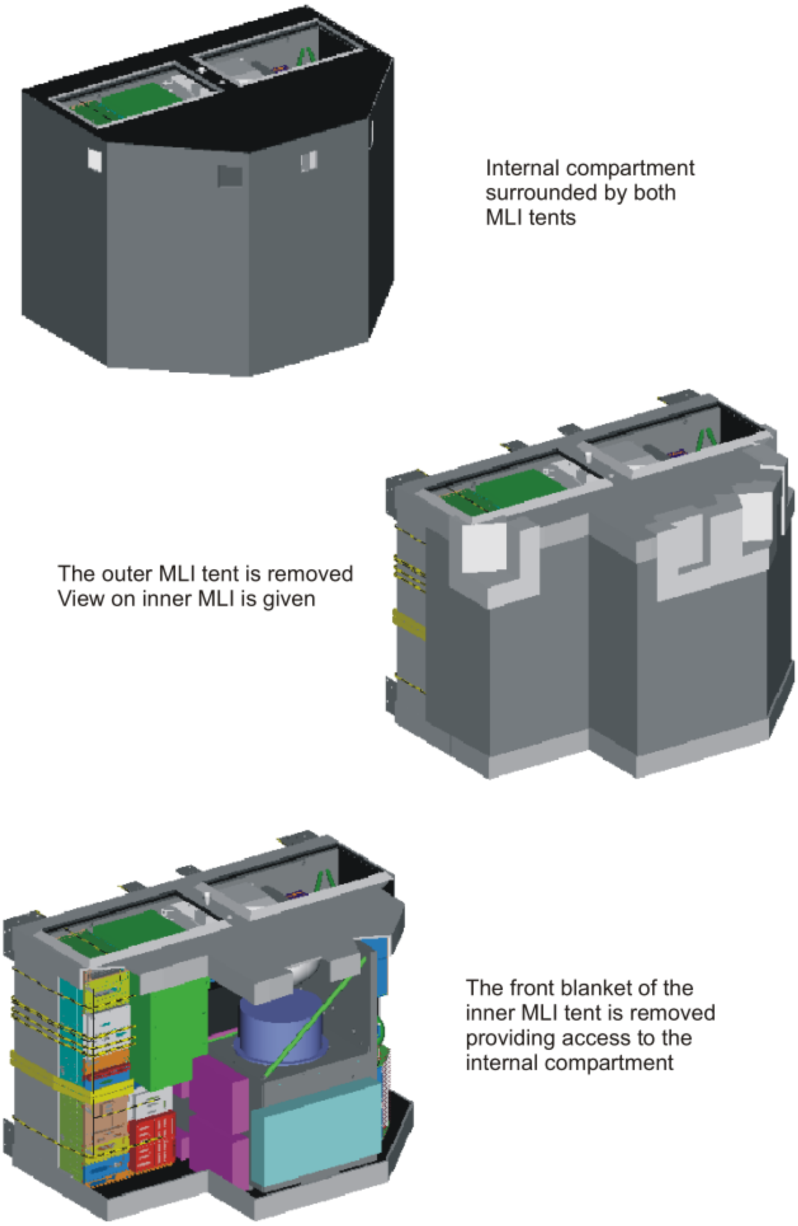

Figure 24 : Philae MLI layout. Credits

Repercussions on the LSSel Concept

The most constraining thermal condition for the mission is the hot case, when Philae on the comet surface will be approaching perihelion. The cold case in facts is fully counteracted by MLI insulation and heaters. The LSSel Concept thus foresees a thermal model that can estimates the temperature of Philae Warm Compartment in order to evaluate the dependency of the mission duration on the landing site. Different landing sites indeed have different insolation conditions, depending on the position on the surface and on the season.

4.8 Communications

Communications of Philae is guaranteed through s-band antennas located in the external face of the Solar Hood. The Rosetta orbiter acts as data relay to Earth.

Repercussions on the LSSel Concept

Cometary hills and humps are preferable for communications as long as visibility windows are optimized.

5. The Landing Site Selection Concept

This chapter describes the design and modelling choices of the LSSel Concept for addressing Philae landing site selection on comet 67P Churyumov-Gerasimenko . The considerations that follow descend directly from the LSSel Concept Repercussions, that have been discussed in the previous chapters.

The developed method is a support to define the most suitable landing site for Philae on the surface of comet 67P Churyumov-Gerasimenko. The prime variable of optimization is the power produced by Philae six LILT solar arrays, although rationales on the effects of the landing site on the thermal subsystem and other constraints are also discussed. The preliminary goals of the project is to obtain the movement of the Sun in the lander reference frame, the local insolation, the lander instantaneous available power and the lander temperature distribution, for all latitudes and longitudes in each mission time instant.

5.1 Introduction to the problem

Before introducing the LSSel Concept a number of preliminary considerations are outlined. Churyumov-Gerasimenko's features make the comet an exotic body whose illumination characteristics are quite unusual if compared to those at Earth, in particular due to the following aspects:

- Solar constant: during the approximate 6 months of Philae Long Term Science the Sun distance varies from almost 3AU down to 1.6 AU. The solar constant, that depends on the inverse of the square value of this distance, has consequently larger variations, it ranges from $SC = 0.11$ to $SC = 0.39$.
- Comet rotation: the inclination of the comet equator with respect to the ecliptic plane (i.e. the obliquity) is estimated to be about 137.8° if the B2 Lamy et al. solution is considered[5]. This means that, contrary to the large majority of the Solar System bodies, the comet has a retrograde rotation.
- Comet inclination: if again the 137.8° comet equator-ecliptic plane is considered, taking the complementary angle to 180° (therefore neglecting the retrograde rotation effect, that has no influence for considerations on the season), means that there is a relative angle of 42.2° between the comet equator and the ecliptic plane (see [Figure 28]). This means that seasons have more noticeable effect in terms of illumination if compared to Earth: cometary Polar Circles are at 47.8° North and South of the equator (polar circles are so defined assuming a spherical comet, for an irregular body as 67P C-G polar circles and tropics are defined with respect to the local site normal direction, as discussed in [Geographical Definition]), when Earth polar circles are located at about 66.5° . This means that a large part of the comet surface is not illuminated for at

least one day in the cometary year and the same areas have at least one cometary day where the Sun is almost always present in the sky.

- Comet irregular shape: the comet shape is far different from the almost spherical terrestrial geoid. The surface normal (and together the surface horizon) can differ of some tens of degrees with respect to the radial direction from the centre of the body, this creates unique illumination conditions.
- Comet rotational asymmetry: there is a strong longitudinal variation effect due to the comet shape irregularity: Earth illumination properties could be studied independently from the longitude as long as, in first approximation, is symmetrical around its spin axis. On the other hand 67P C-G is far different from a revolution solid shape.
- Illumination: at mission beginning the comet is considerable almost inactive: sublimation does not occur and a direct illumination model can be used, as discussed in [Comet activity and erosion]. While 67P C-G is approaching the Sun sublimation process activates, thus to describe this phenomena a diffused light model should be used.
- Seasons : the landing site choice is to be addressed in a period of time that is not multiple of a cometary year: Philae Long Term Science is scheduled to last a fraction of the 6.45 terrestrial years of orbital period. Consequently, in general terms, the lander will experience only a restricted range of cometary seasons. From the illumination point of view the landing occurs when it is summer for the Northern Hemisphere and winter in the Southern Hemisphere (North and South are defined with respect to the comet spin axis direction: North pole is the positive pole, South pole the negative, thus considering a retrograde rotation North pole lays in the negative orbit semi-space, South pole in the positive semi-space). Consequently, most latitudes of the Northern Hemisphere see the Sun for the entire cometary day, contrary to the Southern Hemisphere. On the other hand at the end of the 6 months the illumination conditions are similar to terrestrial spring: all latitudes see the Sun for almost half cometary day.
- Self-shadowing: the comet irregular shape creates unique illumination conditions due to its peculiar topography and orography, some sites are clearly affected by this issue.

All the features presented above increase the problem complexity and the number of parameters and variables, but contemporary permits to handle a much wider range of possibility in terms of landing sites choice.

The remainder of this report is organized as follows. First, the modelling assumptions are given, the variables and the modelling framework are discussed, and the implementation of the LSS is then discussed.

5.2 Objectives and constraints

The scope of the LSSel Concept is to support the selection of the optimal landing site such that the power produced by the solar arrays is maximized. In this perspective, the function to be maximized is the **Mission Total Power Generated**.

As discussed in the previous chapters the Mission Total Power Generated can't be considered alone, as long as a number of other requirements descend from the mission and the environment. Consequently the maximization has to be done respecting the following of constraints:

1. **Thermal Ranges**: Philae subsystems functionalities and operative ranges must be respected. In particular thermal ranges of Philae Warm Compartment are constraining and will likely lead to mission end when the comet is approaching perihelion due to overheating. Warm Compartment temperatures must be included in the operative range of -55°C to +60°C (see also [Table 14]).
2. **Daily Power Threshold**: the Daily Mean Generated Power must be major than a minimum daily power threshold, necessary to ensure at least Philae Safe Mode during each day of the mission. The minimum threshold for Philae Safe Mode is 5.11W as reported also in [Table 12].
3. **Landing Site Area Robustness**: the landing site chosen shall not be a small isolated position in the cometary surface showing suitable illumination properties, rather an extended area in order to be robust to small errors in the SDL phase. As seen in [Separation-Descending-Landing] the foreseen landing accuracy is estimated to be 22m with a standard deviation of 12m. In these estimations some perturbations were neglected however. Taking into account that, in the Tessellated Triangular Shape, plates have sides dimensions of about 300-400m, the magnitude of one plate is considered enough to comply with the landing accuracy. In addition subsolar point and/or equatorial point are preferable.
4. **Landing Site Orography**: the landing site topography/geometry/orography should be smooth enough to cope with landing accuracy, as described in [Separation-Descending-Landing] and [Communications] hills and humps are to be preferred for landing site coverage and communication visibility.
5. **Landing Site Activity**: landing sites showing strong sublimation activity should be avoided, as discussed in [Comet activity and erosion] as long as may lead to erosion of the magnitude of meters. The fraction of cometary surface liable to this effect is smaller than 7% (probably assessing at 4%), identifiable by maximum insolation values and changing with the season. The LSS will try to evidence this areas and discard them among the suitable landing sites.
6. **Instruments exposure**: as discussed in [Philae Payload] most of Philae probes are located in the Balcony, direct exposure to the Sun is to be avoided, in particular in proximity of perihelion.
7. **Comet data consistency**: as discussed in [References],[Orientation of the Spin Axis] and [Dynamics of the Spin Axis] contingency related to the data regarding the comet is to be

counteracted in the analysis. Consequently a parametrical analysis will be performed, in particular for the spin axis orientation, which is the parameter most affecting the results.

5.3 General Assumptions and Main Variables

The LSSel Concept foresees a comet model with no dynamics as discussed in [Dynamics of the Spin Axis], **kinematics** alone is necessary to describe the motion, therefore each parameter can be determined in every time instant independently from the previous and following time instants. This simplification comes from the assumption to neglect environmental torques acting to the comet and internal cometary torques as discussed in [Dynamics of the Spin Axis]. Dynamic actions on the comet can be modelled, but the uncertainty in the governing parameters of such phenomena is elevate, thus a simplified model is preferred.

Before introducing the problem main variables, it is useful to introduce the concept of season. For **season** it is intended a span of 60 cometary days. Mission duration is 360 cometary days, therefore 6 seasons of 60 cometary days are defined. For details see [Time Discretization].

5.3.1 Power Variables

The LSSel Concept permit to calculates the solar power on the cometary surface and Philae generated power. Two main variables are therefore defined:

- **Solar Power** [W/m^2] is the instantaneous solar energy square meter received per by a surface whose normal coincides with the local normal to the cometary surface. Solar Power is function of time and of position on the surface.
- **Generated Power** [W] is the instantaneous electrical power produced by Philae LILT SA and available once processed by the MPPT of Philae power subsystem.

Daily and seasonal integrations and averages of Solar Power and Generated Power are performed as long as they are fundamental to understand if a position on the comet is more preferable than others. Solar Power is distinguished from Generated Power as long as the first is a feature related to the landing site, while the former depends also on lander geometry and orientation on the comet surface. Consequently these two functions do not coincide, e.g. if the Sun was always orthogonal in a location this would not correspond to maximum Generated Power. Insolation integrations are performed in order to understand the movement of the Sun in the sky in different position in the comet and for different periods of the mission.

Thus the following results are available:

- **Daily Mean Insolation** [W/m^2]: is the Solar Power integrated over a cometary day divided by the duration of a cometary day. It is function of cometary date and landing site..
- **Daily Mean Generated Power** [W]: is Philae Generated Power integrated over a cometary day divided by the duration of a cometary day. It is function of cometary date and landing site.
- **Seasonal Mean Insolation** [W/m^2] : is the Solar Power integrated from the beginning to the end of the season and divided by the season duration. It is function of season and landing site.
- **Seasonal Mean Generated Power** [W]: is Philae Generated Power integrated from the beginning to the end of the season and divided by the season duration. It is function of season and landing site.
- **Cumulated Seasonal Mean Insolation** [W/m^2]: is the Solar Power integrated from the beginning of the mission (Philae landing date) to the end of a given season and normalized by the integration time. It is function of season and landing site.
- **Cumulated Mean Generated Power** [W]: is Philae Generated Power integrated from the beginning of the mission (Philae landing date) to the end of a given season and normalized by the integration time. It is function of season and landing site.
- **Total Mission Insolation** [J/m^2] : is the Solar Power integrated from the beginning to the end of the mission. It is function of landing site alone.
- **Total Mission Generated Power** [Wh]: is Philae Generated Power integrated from the beginning to the end of the mission. It is function of landing site alone.
- **Total Mission Mean Insolation** [W/m^2]: is the Solar Power integrated from the beginning to the end of the mission and normalized by the mission duration. It is function of landing site alone.
- **Total Mission Mean Generated Power** [W]: is Philae Generated Power integrated from the beginning to the end of the mission and normalized by the mission duration. It is function of landing site alone.

5.3.2 Thermal Variables

The thermal model of Philae, as discussed in [Philae Thermal Model, is a simplified lumped parameter model, which is constituted of two nodes, having the following variables:

- **Warm Compartment Temperature** [K]: is the temperature of the node associated with Philae Warm Compartment.
- **Solar Absorbers Temperature** [K]: is the temperature of the node associated with Philae solar absorbers.

5.3.3 Orientation Manoeuvre Variables

Philae has the capability to rotate of 360° around its z-axis, as discussed in [Philae Overall Design]. This feature is a fundamental degree of freedom of the problem, as long as it permits to the lander exposure to optimize the produced power. **Philae Orientation on the Plate** is the variable related to it.

5.4 Modeling

Selecting the landing site is a multidisciplinary problem. In this problem, the following blocks have been modelled. [Figure 25].

- Time vector design and discretization
- 67P Churyumov-Gerasimenko geometry and kinematics
- Orbit model
- Illumination model
- Shadowing
- Philae geometry
- Philae power system model
- Philae thermal system model
- Angles and reference frames
- Philae orientation on the plate

The following sections are thus intended to present how every aspect of the LSSel Concept problem is modelled and the assumptions related to it. These modelling choices (i.e. all the equations and methods that are presented), are directly reflected in the Landing Site Simulator implementation. The chapter that follows [The Landing Site Simulator] is dedicated to the Landing Site Simulator and for sake of brevity only the aspects of the problem that require a dedicated description of the implementation are reported.

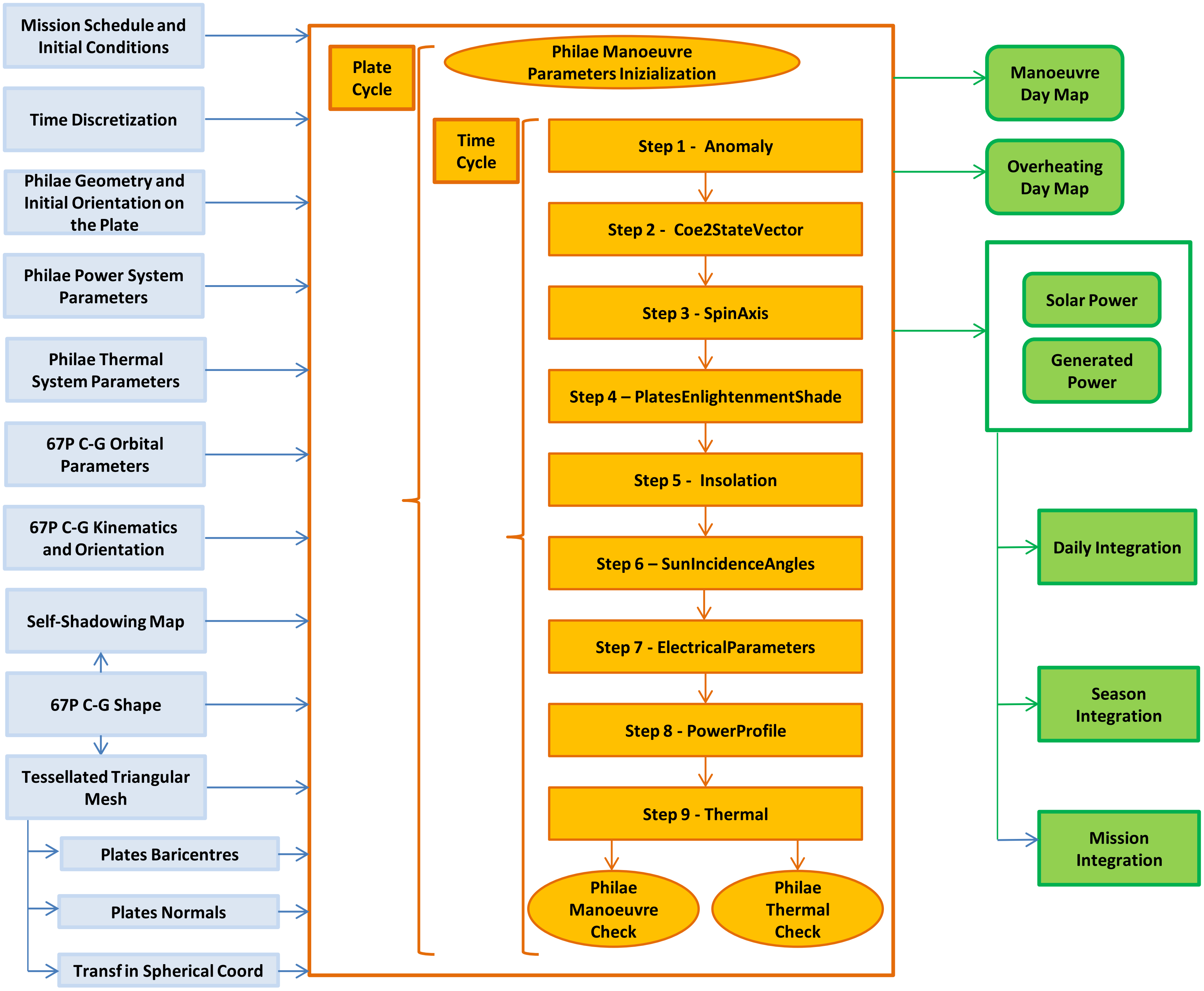

Figure 25: Philae LSSel Conceptual scheme

5.5 Time Discretization

Time is the independent variable of the problem and is discretized through the use of a **time vector** whose design derives from the assumption that the model developed of the comet simulates kinematic motion, consequently there is no need to rely on a time step small enough to ensure solution convergence: the solution calculated is (numerically) exact in mathematical terms in chosen time labels. However the time step is connected to the accuracy of:

- the integration of Solar Power and Generated Power to perform daily and seasonal spans
- the integration of the nodes temperature of the Thermal model

Thus the time step is conveniently chosen as a fraction of cometary day and the time vector length is an integer number of cometary days.

The time vector is expressed in seconds and is designed as it follows:

- <u>Begins</u> at time $t_{land} = 0[s]$ that corresponds to 00.00UT of November 11th 2014 baseline date of Philae landing. The *date2jed.m* function is used to convert Gregorian dates into JED2000. For sake of simplicity no analysis on the variation of the date of landing is considered.
- <u>Ends</u> at time $t_{end} = 1563840\,[s]$ which corresponds to 360 cometary days of rotational period $Pw = 12.72\ [hr]$. This number of days was chosen as it is an integer number of days close to the 6 months operative time-life foreseen for Philae LTS. Furthermore, it permits to have an integer number of 60 cometary days spans that are useful for results presentation.
- <u>Time discretization</u> is performed dividing the cometary day in dT=100 instants. A fraction of the spin rate has been chosen in order to manage more easily the daily and seasonal integration of Solar Power and Generated Power. It also permits to control in how many different positions the lander illumination is evaluated in each discretized day.

5.6 Comet 67P C-G Shape

Comet 67P Churyumov-Gerasimenko is described with a 512 Tessellated Triangular Plates shape [Figure 26]. The surface is constituted by using a mesh of triangular plates identified by 258 vertices. The correspondent reference document can be found in[28] and is provided by Laboratoire d'Astrophysique de Marseille updated at February 2012. This model corresponds to the B2 retrograde shape model retrieved by Lamy et al[5] and discussed in [Tessellated Triangular Shape]. The final model, provided by the DLR of Köln, was than postprocessed, in particular was:

- rescaled to obtain the correct volume calculated from observations
- rotated to bring the principal inertia axis aligned with (x,y,z) axis, in particular to align the rotational z-axis with the largest moment of inertia axis
- translated so that the origin of axis corresponds to the comet centre of mass

As a remainder, the low scale smoothness of the surface is not represented in the Tessellated Triangular Shape, only the large scale features are.

5.6.1 Tessellated triangular plates shape

In the model plate vertices are given in Cartesian coordinates (x,y,z) where:

- z axis is aligned with the comet spin axis that corresponds to the comet major inertia axis.
- x and y axis lay on the plane normal to z (the cometary equator) and the direction of x defines the prime meridian of the comet.

The origin of coordinates coincides with the cometary centre of mass. The rotation of the comet is positive with the z axis as defined by the right hand rule.

In the model two matrices permit to describe the comet **tessellated shape**.

- the matrix of the 258 vertices of the comet in Cartesian coordinates: defined as *V = [Vx; Vy; Vz]* where Vx, Vy and Vz are the arrays of vertex coordinates in x, y and z, respectively. Therefore the matrix V has dimensions (3x258) .
- the matrix that links every vertex index to the corresponding triangle: defined in the routine as *T = [T1; T2; T3]* where T1 T2 and T3 are the arrays of vertex order. The matrix T has dimensions (3x512) .

In order to have a more practical notation for the plates coordinates a tensor *CG* is defined, whose dimensions are (512x258x3):

- first tensor dimension is referred to the plate index
- second tensor dimension is referred to the vertex index
- third tensor dimension is correspondent to the x y z vertex coordinates

[28] NASA DSK Kernel SPICE toolkit. Last retrieved on 10 September 2012. Available at: http://naif.jpl.nasa.gov/pub/naif/generic_kernels/dsk/churyumov-gerasimenko/

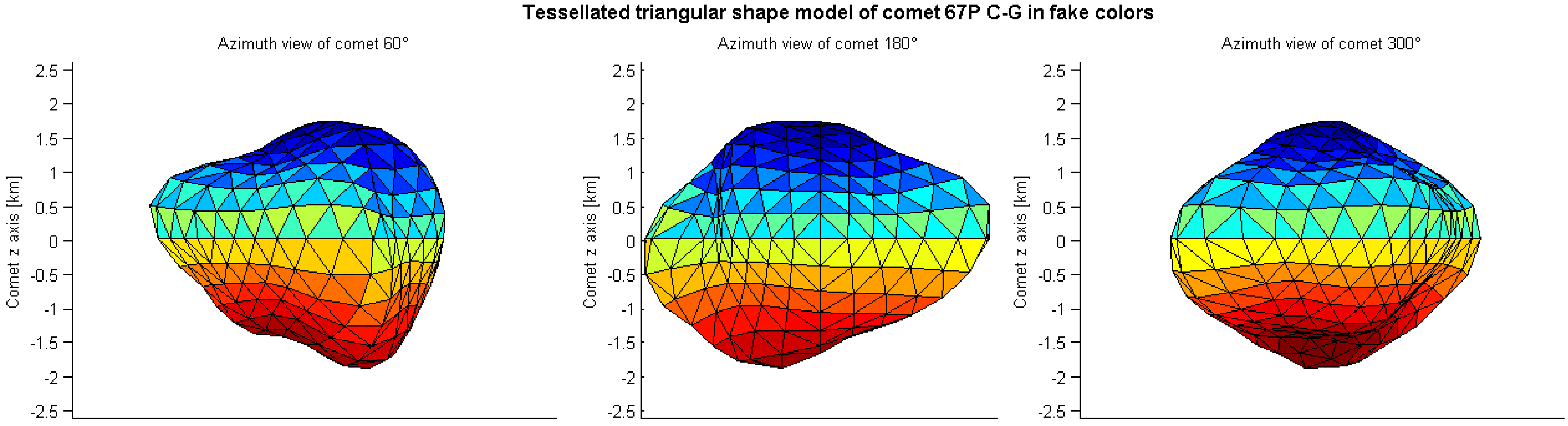

Figure 26 : 67P Churyumov-Gerasimenko shape model in fake colours

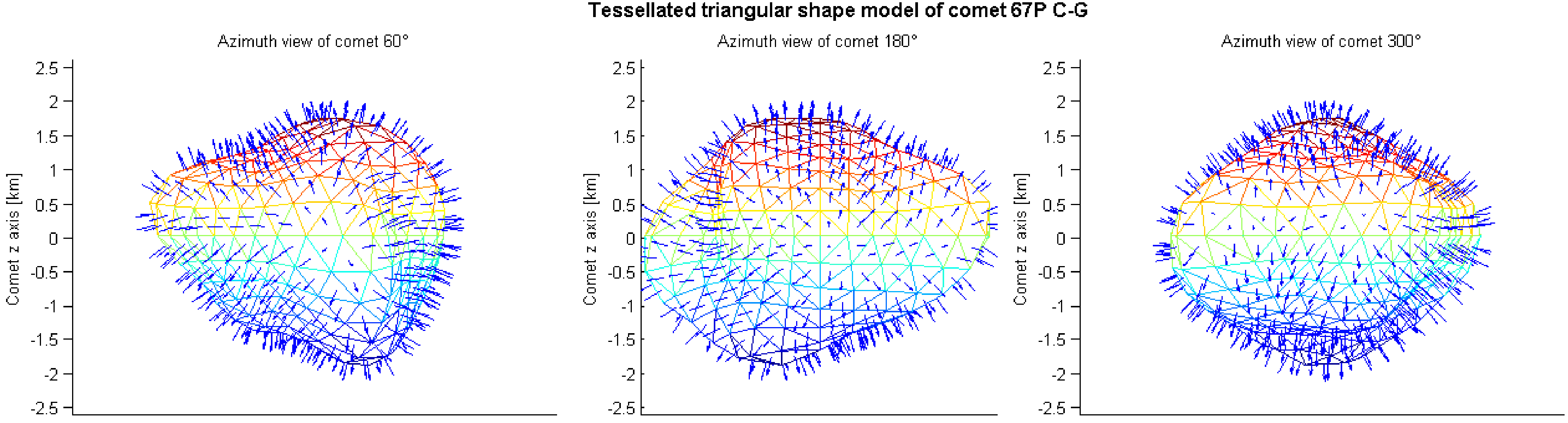

Figure 27 : 67P Churyumov-Gerasimenko normal versors

5.6.2 Plates normal versors and centres

The order in which each triangle vertices triplet is given permits to define a rotation direction that consequently imposes an outgoing **normal versor** for each plate with respect to the comet surface [Figure 27]. Thus each plate normal is obtained from the normalization of the cross product between two of the triangle sides: the first triangle side is defined subtracting the first vertex coordinates to the second vertex [Eq.(8)]; the second triangle side is defined subtracting the third vertex coordinates to the first vertex[Eq.(9)]. The normal versor is obtained normalizing the cross product between the first and the second side [Eq. (10)]. Plate normal versor directions are contained in the *CGn* matrix whose dimension is (512x3). Normal versors are applied at the plate centre.

$$v_1 = CG(i,2,:) - CG(i,1,:) \tag{8}$$

$$v_2 = CG(i,3,:) - CG(i,1,:) \tag{9}$$

$$CGn(i,:) = \frac{v_1 \times v_2}{|v_1 \times v_2|} \tag{10}$$

Triangular plates are not equilateral, thus the plate centre is calculated as the **barycentre**: the intersection between two (of the three) segments that connect each vertex with the middle point of the opposite side of the triangle. Plate centre coordinates are contained in the *CGb* matrix whose dimension is (512x3).

5.6.3 Plates locality assumption

A fundamental assumption of this model is that properties evaluated for each plate are calculated at the plate centre and then associated to the whole plate surface, in particular:

- the normal versor of each plate is applied at the plate centre
- the insolation of each plate is evaluated at the plate centre coordinates
- the power produced by Philae is evaluated at the plate centre coordinates; i.e., Philae is modelled as it is placed at the centre of the plate.

5.7 Comet 67P C-G Kinematics

67P Churyumov-Gerasimenko is modelled as a rigid body rotating around its major inertia axis that correspond to the z axis as discussed in [Moments of Inertia]. The period of rotation is $Pw = 12.72hr$, as reported in [Rotational Period]. No precession or nutation is modelled, the spin axis direction is inertial and the spin rate is constant, as discussed in [Dynamics of the Spin Axis]. However in order to counteract the indetermination on the spin axis orientation a parametric study on the variation of the spin axis direction and spin rate is performed. The orientation of the spin axis is RA = 220° , DEC=70° expressed in EME2000 reference frame, which is equivalent to I=137.8° ψ =92.4° expressed in Inclination-Argument angles. Definition of the angles is given below at [Equatorial Reference Frame - ERF], while (RA,DEC) to (I, ψ) transformation can be found in [Appendix 1].

5.7.1 Geographical Definitions

A clarification of terms is necessary. Often the **Northern/Southern Hemisphere** or **North/South Pole** terms are used, the North/South definition is to be intended as follows: comet 67P C-G has a retrograde rotation, thus its positive pole, the North Pole, points in the negative semi-space of the orbit, while its negative pole, the South pole, points in the positive semi-space of the orbit. The comet z axis expressed in CFF (see [Comet Fixed Frame - CFF] for definition) is the axis of positive rotation of the comet, as defined by the right hand rule. North and South definitions are relative to the spin direction of the comet rather than to the orbit semi-space: the North Pole is the positive pole, located for positive z values as expressed in CFF (thus located in the negative orbital semi-space), while the South Pole is the negative pole, located for negative z values as expressed in CFF (thus located in the positive orbital semi-space).

Comet Tropics and Polar Circles, for an irregular body as come 67P Churyumov-Gerasimenko, are defined with respect to the inclination of the plate normal direction with respect to the comet equator, rather than the latitude i.e. Tropics are defined by all plates that show normal inclination ranging between ±42.2°, while North Pole for plates that normal inclination major than 47.8° (which is the complementary to 90° of 42.2°). This angular value is obtained when considering the 137.8° comet equator-ecliptic plane angle: taking the complementary angle to 180° (therefore neglecting the retrograde rotation effect, that has no influence for considerations on the season), means that there is a relative angle of 42.2° between the comet equator and the ecliptic plane.

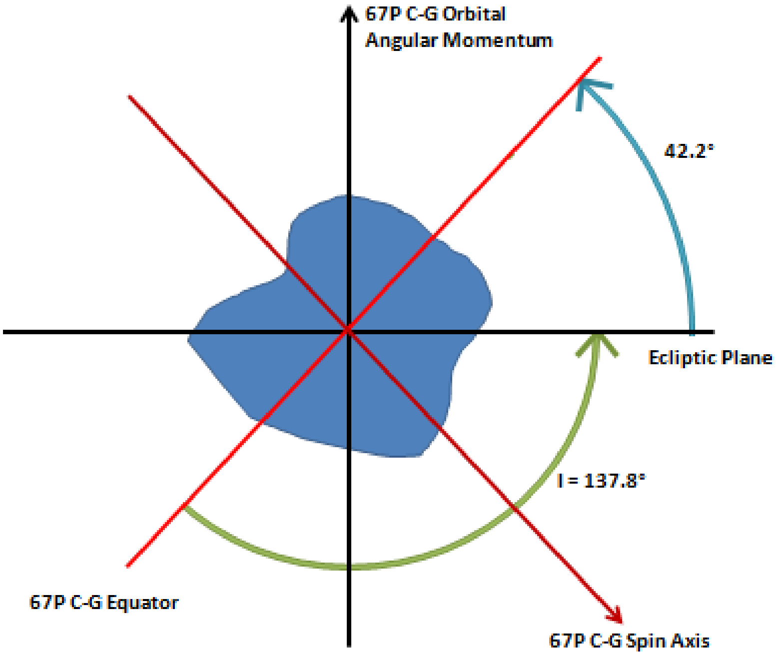

Figure 28 : 67P C-G Spin Axis Orientation

5.8 Orbit modelling

67P Churyumov-Gerasimenko orbit is modelled as inertial and is described through Kepler's parameters. The following orbital parameters have been obtained from NASA JPL website [29] [Table 15].

Orbital Parameter	Symbol	Value
Semimajor Axis [AU]	a	3.464312068995289
Eccentricity	e	0 .6410992808753628
Inclination [°]	i	7.045643228574521
Right Ascension of the Ascending Node [°]	RAAN	50.17707791542941
Argument of Pericentre [°]	ω	12.711342250349
Pericentre passage [JED]	t_{per}	2454891.857291965753
Orbital Period [days]	P	2355.179091268956

Table 15 : 67P Churyumov-Gerasimenko orbital parameters

Other useful physical constant for the orbital problem are reported in [Table 16]:

Constant	Symbol	Value
Sun Gravitational Constant [km^3/s^2]	μ_{Sun}	132712440018
Astronomic Unit [km]	AU	149597870.691

Table 16 : Orbital physical constants

In order to evaluate the comet position in the orbit for each time instant the indirect problem is solved: given an instant of time t the implicit Kepler's equation is solved for the eccentric anomaly. The mean anomaly M is given by [Eq.(11)]:

$$M = \sqrt{\frac{\mu_{Sun}}{a^3}}\, t \qquad (11)$$

from which the eccentric anomaly can be obtained through the implicit Kepler's equation [Eq (12)],

$$M = E - e\, sinE \qquad (12)$$

Kepler's equation is implicit, thus Newton-Raphson iteration method is used to solve it for the eccentric anomaly E. Once obtained the eccentric anomaly, the true anomaly ν can be obtained using [Eq.(13)]

[27] JPL NASA Small -Body Database Browser. last retrieved on 10 September 2012. Available at: http://ssd.jpl.nasa.gov/sbdb.cgi?sstr=67P;orb=0;cov=0;log=0;cad=0#orb

$$\tan\frac{E}{2} = \sqrt{\frac{1-e}{1+e}}\,\tan\frac{\nu}{2} \tag{13}$$

that can be written explicitly to solve the true anomaly ν [Eq. (14)]:

$$\nu = 2\arctan\left(\sqrt{\frac{1+\mathrm{e}}{1-\mathrm{e}}}\,\tan\frac{\mathrm{E}}{2}\right) \tag{14}$$

Besides true anomaly ν, also the orbital radius R is a fundamental quantity to be evaluated in each time label as long as it permits to evaluate the Sun irradiance at orbital radius distance; it can be obtained through [Eq (15)]:

$$R = \frac{p}{1 + e\cos\nu} \tag{15}$$

where $p = a(1 - e^2)$.

5.9 Illumination Assumptions

As many of the aspects of 67P Churyumov-Gerasimenko also the illumination conditions show exotic characteristics. At mission beginning at about 3AU the comet is foreseen to have a distance from Sun sufficient to be considered almost inactive, light scattering and attenuation due to sublimated particles is negligible. On the other hand at the end of mission the comet will approach perihelion and the distance from the Sun will be short enough to likely fully activate the comet sublimation, in this condition a diffused light model should be used. There is indetermination on the moment at which the sublimation process will activate.

From the illumination point of view the inactive condition can be treated simply using a **direct illumination model**: the light reaching the surface of the comet is equal to the irradiance evaluated at that orbital radius distance and the light source is considerable a point at infinitum distance that emits a uniform wavefront. Thus no air mass effect is modelled: the light scattering is considered negligible at all elevation angles taken from the surface, because of the cometary extremely rarefied coma. Solar irradiance, expressed in [W/m^2], at a given Sun distance is calculated as [Eq.(16)]:

$$I_{rr\,AU} = \left(\frac{I_{sun1AU}}{R_{AU}}\right)^2 \qquad (16)$$

where $I_{sun1AU} = 1366.1 W/m^2$ is the Sun constant evaluated at 1AU according to the standards reported in [30] and R_{AU} is the orbital radius expressed in AU.

The active condition instead should be treated with a **diffused light model**: scattering deriving from suspended particles is so elevate that the light may be considerable diffused, when seen in the semisphere of the landing site sky. The implementation of such phenomena requires a gasdynamic accurate model of the sublimated particles that are subjected to gravity forces, solar wind, comet spin effect and more.

Due to the fact that both a gasdynamic model is considered to be too complex to be implemented and that currently there is no accurate information on the parameters governing this phenomena, also for the active condition of the comet a direct illumination model is used.

As discussed in [Albedo], cometary **albedo** is estimated to be 0.044. This low value, together with the low values of irradiance, permit to neglect the contribute of reflected light in the solar generated power computation.

Thus **insolation** [W/m^2] over a generic cometary site where the Sun elevation over the horizon is h_{Sun} can be calculated as [Eq. (17)]:

$$P_{Sun} = Irr_{AU} \cos\left(\frac{\pi}{2} - h_{Sun}\right) = \left(\frac{I_{sun1AU}}{R_{AU}}\right)^2 \cos\left(\frac{\pi}{2} - h_{Sun}\right) \tag{17}$$

The equation [Eq.(17)] is valid only if $h_{Sun} > 0$, differently $P_{Sun} = 0$.

5.10 Comet Self-Shadowing

In order to produce a model as realistic as possible, cometary self-shadowing was implemented, for an irregular body as 67P C-G this aspect can’t be neglected. The model of shadowing comes in two steps:

- the first is preliminary and designed to identify which plates are liable to shade each plate, this permits to reduce the number of operations to be solved and is carried out in the LSS by the function *FindShade*
- the second step is designed to evaluate in each simulation time label whether a given plate is shaded or not. This is realized in the LSS by the function *TriangleRayIntersection* which is contained into the *PlatesEnlightenmentShade* function (these functions are described in [The Landing Site Simulator])

5.10.1 Shadowing Liability

This preliminary step permits to evaluate whether the i-th plate is liable to shade the j-th plate. The principle that was followed to identify the shade-liability is: the j-th plate can be shaded by the i-th if at least one of the vertices of the i-th plate is contained in the positive semi-space of the j-th plate. The positive semi-space of the j-th plate is identified as follows: the plane where the j-th plate lays defines two semi-spaces, the positive one is identified by the normal outgoing from the body: i.e. positive semi-spaces are in the outer volume of the comet. The following equation [Eq. (18)] defines the plane of the j-th plate:

$$a_j\left(x - x_{1j}\right) + b_j\left(y - y_{1j}\right) + c_j\left(z - z_{1j}\right) = 0 \qquad (18)$$

where a_j, b_j, c_j are coefficients that can be determined using the three vertices that define the j-th plate $(x_1 y_1 z_1)_j$, $(x_2 y_2 z_2)_j$, $(x_3 y_3 z_3)_j$ solving the following determinants (the j subscript is omitted):

$$a_j = \begin{vmatrix} y_2 - y_1 & z_2 - z_1 \\ y_3 - y_1 & z_3 - x_1 \end{vmatrix} \qquad (19)$$

$$b_j = -\begin{vmatrix} x_2 - x_1 & z_2 - z_1 \\ x_3 - x_1 & z_3 - x_1 \end{vmatrix} \qquad (20)$$

$$c_j = \begin{vmatrix} x_2 - x_1 & y_2 - y_1 \\ x_3 - x_1 & y_3 - y_1 \end{vmatrix} \qquad (21)$$

The equation of the positive semi-space of the j-th plate can be easily found using the inequality[Eq. (22)]

$$a_j\left(x - x_{1j}\right) + b_j\left(y - y_{1j}\right) + c_j\left(z - z_{1j}\right) > 0 \qquad (22)$$

Thus when calculating, for instance, if the first vertex of the i-th plate is contained in the positive semi-space of the j-th plate the equations can be written as follows [Eq. (23)], where $(x_{1i}\ ,\ y_{1i}\ ,\ z_{1i})$ are the coordinates of the first vertex of the i-th plate.

$$a_j(x_{1i} - x_{1j}) + b_j(y_{1i} - y_{1j}) + c_j(z_{1i} - z_{1j}) > 0 \qquad (23)$$

In equation [Eq. (23)] is visible that the inequality must be greater than 1e-6: it is necessary to set this small threshold to avoid numerical errors, otherwise the j-th plate tends to recognize its surrounding plates as always shading: this is due to the fact that the j-th plate would see its vertices shadowing itself when considered as belonging to the surrounding plates.

This preliminary calculation permits to obtain a map of interrelation between plate shadowing, the **Shadowing Liability Map,** which is useful to reduce the number of calculations needed to evaluate the shadowing. The impact of shadowing in the calculation time is extremely elevate, in facts for every given time instant it is necessary to evaluate whether each plate is shaded by all the others, therefore the process must be repeated $n_{calculations} = n_{time\ instants}\ n_{plates}^2$. This technique permits to reduce $n_{calculations}$ of a factor 17, acting drastically on the n_{plates}^2 factor.

For exemplification two figures are reported. [Figure 29] represents the Shadowing Liability Map, it shows the number of plates liable to shadow each plate, it is visible that plates located in the comet concave surface have no shadowing liability, whereas convex regions show possible shadowing up to almost a hundred plates. The second figure [Figure 30] is an example of the shadowing liability for plate #30 (in red): the surrounding orange-coloured plates have at least one vertex contained in the positive semi-space of plate #30

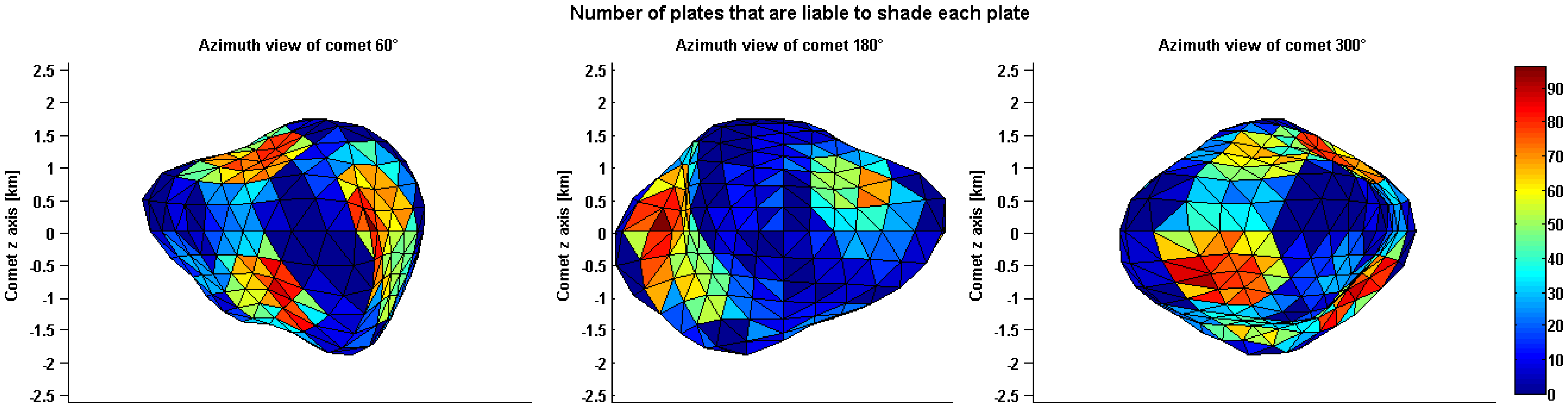

Figure 29 : Comet 67P C-G Shadowing Liability Map

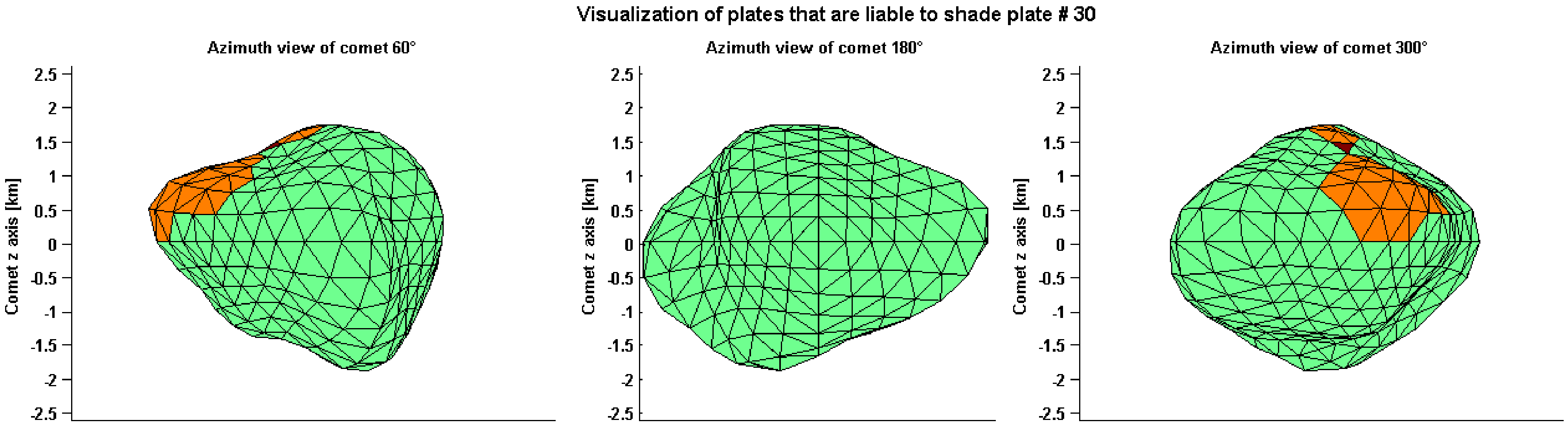

Figure 30 : Example of shadowing liability on plate 30 (in red)

5.10.2 Shadowing

This second step necessary to solve the shadowing issue is evaluated in each mission time label and permits to calculate if the j-th plate is actually shaded by the i-th at a given time instant of the simulation. The function is applied only if the following conditions are , in order, verified:

- the j-th plate is liable to be shaded by other plates
- in the j-th plate the Sun is above the plate horizon
- the j-th plate is liable to be shaded by the i-th, as identified in the Shadowing Liability Map

Each time one of the above conditions are not verified, shadowing can not occur. In the LSS the conditions are evaluated in order and if not respected the shadowing label is turned into 0 (no shadowing occurs at the j-th plate in that given time instant). This preliminary check is executed once again to reduce the computation time.

If all the three conditions presented above are respected it is then necessary to evaluate if the j-th plate is shadowed, in a given time label, by any of the i-ths plates that are identified in the Shadowing Liability Map. This problem is modelled by finding the intersection between a line (the Sun incidence on the j-th plate centre) and a triangle (the i-th plate), where:

- the line is identified by the j-th plate centre and the instantaneous direction of the Sun. Consequence of this assumption is that if the centre of the plate is shaded then all the plate is, this is in agreement with the hypothesis reported in [Plates normal versors and centres]).
- the triangle is identified by the vertices coordinates of the i-th plate, as indicated in the Shadowing Liability Map.

Intersection between line and triangle can be found as purposed by Möller and Tumbore [31], this method can be easily implemented and guarantees short computation time. Below the Möller and Tumbore [31] prove is reported.

A ray, $R(t)$, with origin O and normalized direction D is defined as function of the distance from the origin, t as [Eq. (24)]:

$$R(t) = O + tD \tag{24}$$

A point, $T(u, v)$, on a triangle of vertices (V_0, V_1, V_2) is given by [Eq. (25)]:

$$T(u, v) = (1 - u - v)V_0 + uV_1 + vV_2 \tag{25}$$

where (u, v) are the barycentric coordinates, which must fulfil $u \geq 0$, $v \geq 0$ and $u + v \leq 1$. Computing the intersection between the ray, $R(t)$, and the triangle $T(u, v)$, is equivalent to $R(t) = T(u, v)$ which yields to [Eq. (26)]:

$$O + tD = (1 - u - v)V_0 + uV_1 + vV_2 \qquad (26)$$

Rearranging the terms gives the following linear system [Eq. (27)] that permits to calculate both the intersection in barycentric coordinates and the distance from the ray, t:

$$[-D, \quad V_1 - V_0, \quad V_2 - V_0] \begin{bmatrix} t \\ u \\ v \end{bmatrix} = O - V_0 \qquad (27)$$

If $u \geq 0$, $v \geq 0$ and $u + v \leq 1$ are simultaneously respected there is intersection between ray and triangle (the intersection belongs to the triangle), thus shadowing occurs. Differently if any of the conditions are not respected, there is no intersection and shadowing does not occur.

This prove can be interpreted geometrically as translating the triangle to the origin and transforming it to a unit triangle in y-z plane with the ray intersection aligned with x. This is illustrated in [Figure 31], where $M = [-D, \quad V_1 - V_0, \quad V_2 - V_0]$.

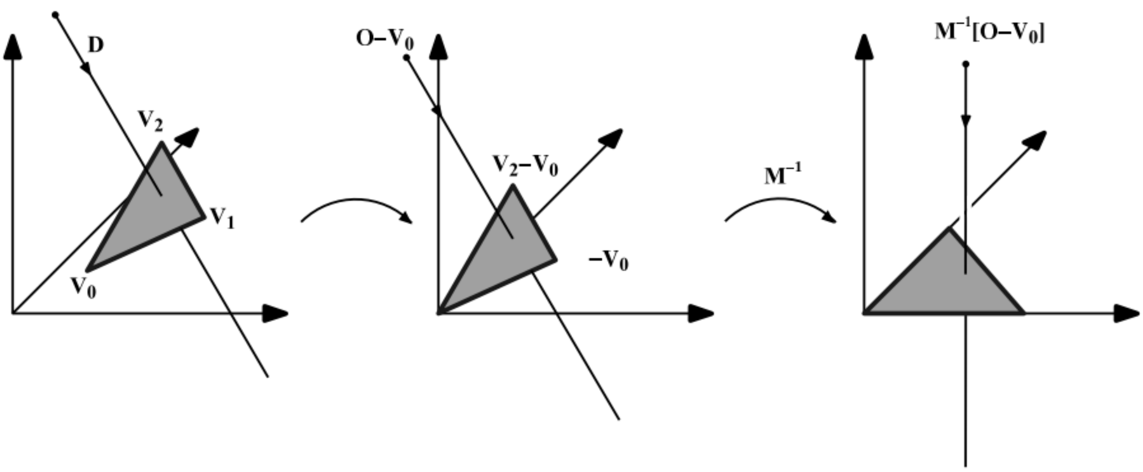

Figure 31 : Ray-triangle intersection, geometric interpretation. Credits [31].

5.11 Philae Geometry

This section aims to introduce to the notation used to describe Philae geometry, in particular to the nomenclature used for the solar arrays. The [Figure 32] shows the orientation of the Lander Reference Frame (that will be defined in [Lander Reference Frame – LDR]) with respect to the Solar Arrays. Each Philae SA has a different nomenclature so that each panel is uniquely identified.

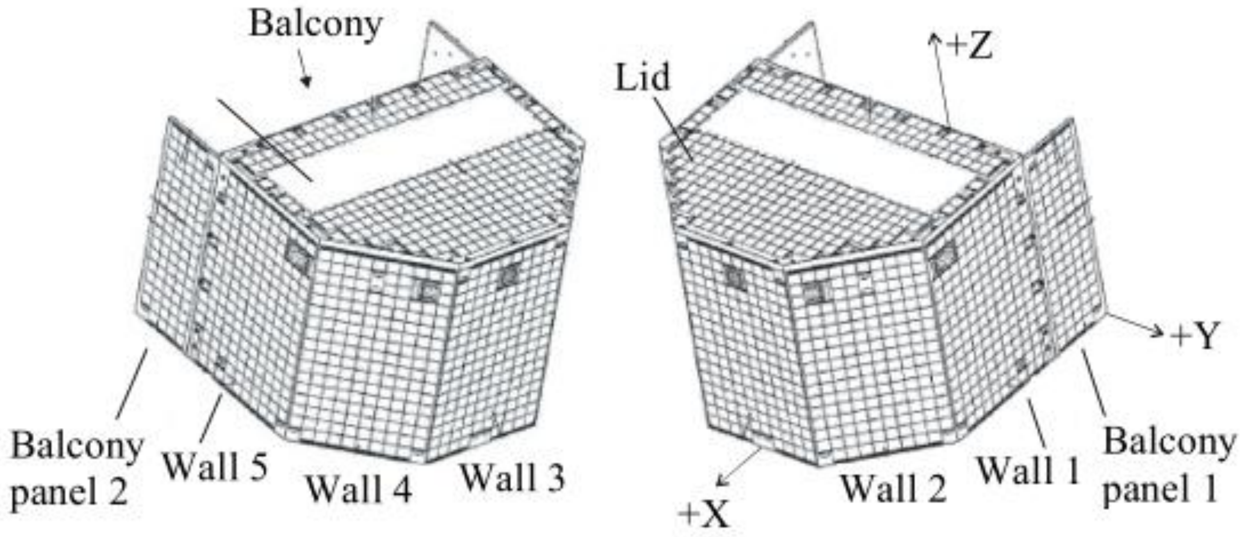

Figure 32: Philae SA nomenclature

5.12 Philae Power Model

This section is dedicated to the description of the modelling of Philae Power System, in particular to the Solar Array Assembly in order to produce a realistic estimation of the Power Generated by Philae. The modelling description that is presented below is used for the implementation of the Solar Array Simulator (SAS). The SAS is a tool developed from the Politecnico di Milano and is constituted of both software and hardware components. In this thesis work some functions contained in the SAS software are used to simulate the instantaneous power generated by Philae. All references can be found in the Philae Solar Array Simulator user manual [32].

The aim is to model the power generated by each Philae SAs, for this purpose the following equations can be used to evaluate the I/V curve [Eq. (28)]:

$$\mathrm{I(V)} = \mathrm{I_{SC}} - \mathrm{B}(\mathrm{e}^{\frac{\mathrm{V}}{\mathrm{C}}} - 1) \tag{28}$$

with

$$B = (I_{SC} - I_m)e^{-\frac{V_m}{C}} \tag{29}$$

$$C = \frac{V_m - V_{OC}}{\ln\left(1 - \frac{I_m}{I_{SC}}\right)} \tag{30}$$

where $\mathrm{I_{SC}}$ is the short cut current, $V_{OC}$is the open circuit voltage, V_m and I_m the voltage and current at Maximum Power Point. Thus the SA panel power can be calculated as [Eq. (31)]:

$$P = V * I(V) \tag{31}$$

In order to provide an accurate I/V curve a multi-flash test campaign was performed to obtain the necessary parameters. The following [Table 17] reports the baseline parameters of the SA, as measured at the Solar Hood I/F connector to the MPPT, with a Multi Flash lamp, irradiance of 1SC=1360W/m^2 at laboratory condition temperatures of 25°C. The SA assembly design is referred to the description reported in [Photovoltaic Assembly]

Panel	V_{OC} **[V]**	I_{SC}**[A]**	V_m **[V]**	I_m**[A]**	P_m **[W]**	**Eff [%]**
Wall1/Balcony1	81.01	1.041	63.66	0.971	61.80	16.38
Wall2	51.40	1.010	41.05	0.940	38.58	16.04
Wall3	51.70	1.044	40.45	0.980	39.65	16.48
Wall4	51.70	1.042	40.75	0.971	39.57	16.45
Wall5/Balcony2	81.16	1.040	63.56	0.977	62.09	16.46
Lid	73.51	1.046	57.91	0.974	56.39	16.51

Table 17: Solar Array Multi Flash test results

Data of [Table 17] is referred to laboratory conditions. For a correct estimation of the generated power an adaptation to the lander operative environment is necessary, thus is to be modelled :

- Irradiation angle θ, defined as the angle between the panel normal and the Sun direction
- Operative environment parameters as: Cumulated Radiation Dose, Array Temperature, Distance to Sun and Damaged Strings.

Once this parameters have been set is possible to obtain the adapted values $\mathrm{I}_{\mathrm{SC-adapt}}$ $V_{OC-adapt}$ $V_{mp-adapt}$, $I_{mp-adapt}$ useful for power calculations in maximum power tracking conditions, also labelled as “Normal Mode”, thus using [Eq. (32)]:

$$P_{mp-adapt} = V_{mp-adapt} * I_{mp-adapt} \qquad (32)$$

Irradiation angle for each panel is given once the Sun direction is expressed in SAA, as defined in [Solar Aspect Angles – SAA] . Sun direction in SAA can be calculated using interconnected rotation matrices as reported in [Handling the Transformation Matrices]. This permits to evaluate the irradiation angle of the Sun with respect to Philae, than each SA orientation is to be identified in order to evaluate the irradiation angle for each panel. To evaluate the irradiation angle θ with respect to each solar panel the [Eq. (33)] expression can be used, only if the Sun irradiation angle is included in the α and β domain of that panel [Table 18], differently the panel is not exposed to the Sun. The following expression permits to calculate the irradiation angle for each panel:

$$cos\theta = \cos(\alpha_{Sun} - \alpha_{Normal}) \cos\,(\beta_{Sun} - \beta_{Normal}) \qquad (33)$$

where $\alpha_{Sun}\beta_{Sun}$ are the Sun angles in SAA and $\alpha_{Normal}\beta_{Normal}$ are the panel normal angles in SAA.

Panel	$\boldsymbol{\alpha_{Domain}}$	$\boldsymbol{\beta_{Domain}}$	$\boldsymbol{\alpha_{Normal}}$	$\boldsymbol{\beta_{Normal}}$
Wall1/Balcony1	$-90° < \alpha < 90°$	$\beta > 0$	0°	0°
Wall2	$-45° < \alpha < 135°$	$\beta > 0$	45°	0°
Wall3	$0 < \alpha < 180°$	$\beta > 0$	90°	0°
Wall4	$45° < \alpha < 180°$OR $-180° < \alpha < -135°$	$\beta > 0$	135°	0°
Wall5/Balcony2	$90° < \alpha < 180°$ OR $-180° < \alpha < -90°$	$\beta > 0$	-225°	0°
Lid	$-180° < \alpha < 180°$	$0° < \beta < 90°$	0°	90°

Table 18 : Philae Solar Arrays SAA exposure domains

The table below [Table 19] presents the value of characteristic parameters used to evaluate the adapted parameters:

Parameter	**Value**
MPPT Efficiency	0.75
Accumulated Equivalent Radiation Dose at 1MeV [1e14e/cm²]	6.4
Solar Array Temperature [°C]	-100

Table 19: Philae characteristic power parameters

In particular is to be noted that the MPPT efficiency is assumed constant as also the Solar Array Temperatures. The Accumulated Equivalent Radiation Dose is assumed in EOL conditions. Consequently the value of power used to estimate the lander Generated Power is

$$P_{Gen} = \eta \, P_{mp-adapt} \qquad (34)$$

where η is the MPPT efficiency.

5.13 Philae Thermal Model

Philae Thermal Model is a schematization of the Philae Thermal System that permits to study the lander heat fluxes and temperatures. The schematization used is a **non-stationary lumped parameter** model that permits in particular to estimate temperature of Philae Warm Compartment and Solar Absorbers. The model that is presented is a rough simplification of the real thermal behaviour of Philae, as long as currently no more detailed data are available on Philae Thermal System. Consequently results related to this aspect are treated separately in the [Thermal Results] section and can only be considered as preliminary.

In particular, due to the contingency related to Philae mission end caused by overheating, as discussed in [Philae Thermal Subsystem] the modelling assumptions that are presented aim to describe at best Philae hot case.

Although the simplification of the model a number of preliminary considerations can be obtained, in particular regarding the relative thermal behaviour between different locations on the comet surface.

As discussed in [Philae Thermal Subsystem], Philae Thermal Subsystem is designed to permit to the lander to survive until about 2AU, this value is strongly dependent on the insolation characteristics of the landing site. The purpose of this section is to model the dependence of Philae mission duration on the landing site choice.

5.13.1 Lumped Parameters Analytical Approach

Philae Thermal model can be schematized through a lumped parameters model, constituted of two nodes:

- **node 1**: corresponds to Philae Warm Compartment
- **node 2**: corresponds to the two Philae Solar Absorbers

The heat transfer between these two components is considered major in the problem, thus in first approximation the **Warm Compartment** can be retained adiabatic, except for the heat transfer with the Solar Absorbers. This assumption neglects the heat transfer between the Warm Compartment and the external environment, in particular the MLI insulating effect is considered as ideal. Clearly, conduction and radiation occur through the MLI, as it will be seen this assumption is too constraining for the problem, thus the heat transfer is also simulated between these components. A further assumption is that also **Solar Absorbers** can be considered adiabatic in their lateral thickness surface, and can transfer heat only through the external face with the environment and the internal face with the Warm Compartment. In addition also **internal power dissipation** due to Joule effect is to be taken into account: for energy balance all the electrical power used instantaneously by Philae is converted in thermal heat, except for the fraction that is transmitted through the antennas. The power condition that is chosen as baseline to simulate Philae hot case is the Standby Mode Level1as reported in [Table 12].

A figure of the thermal model schematization is reported [Figure 33]

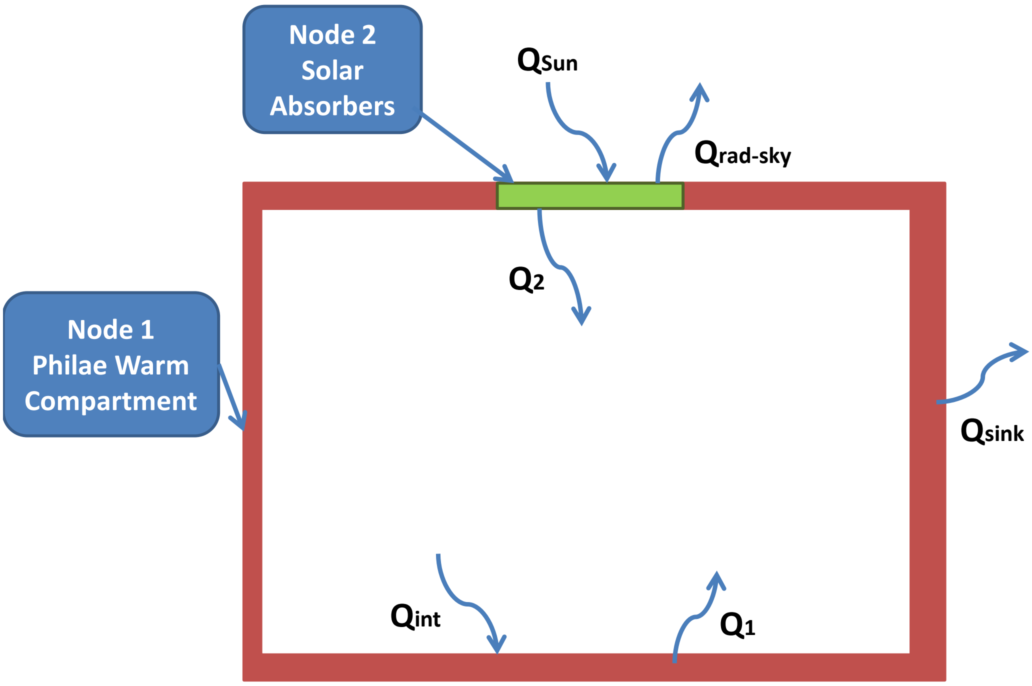

Figure 33 : Schematization of Philae Thermal Model

Equation describing a non-stationary lumped parameter model are presented. The energy balance for a body of volume V, surface S, density ρ, specific heat capacity c, can be written through the integral of the Fourier equation [Eq. (35)]:

$$\int_V \rho c \frac{\partial T}{\partial t} dV = - \int_S \bar{q} \cdot \bar{n} \, dS \qquad (35)$$

in the case of a lumped parameter model, the quantities of the problem do not depend on the space variable, thus it can be written [Eq. (36)]:

$$\rho c \frac{dT}{dt} \int_V dV = -\frac{Q}{S} \int_S dS \qquad (36)$$

which is [Eq. (37)],

$$\rho c \frac{dT}{dt} V = -Q \qquad (37)$$

the heat capacity of a body can be defined as [Eq. (38)]:

$$C = \rho c V \qquad (38)$$

thus the lumped parameter equation governing the heat balance of a body can be written as [Eq. (39)]:

$$C\frac{\partial T}{\partial t} = -Q \qquad (39)$$

where Q is the total heat fluxes that is considered positive when outgoing the boundary of the body. Now if the total heat flux is separated into components and is considered positive when ingoing the boundary of the body the equation becomes [Eq. (40)]:

$$C\frac{\partial T}{\partial t} = \sum_i Q_i \qquad (40)$$

Equation [Eq. (40)] holds for each node of the lumped parameters model.

5.13.2 Lumped Parameters for Philae Thermal Model

It is now possible to express the lumped parameter energy balance for each node of the model through [Eq. (40)], in particular the summation of the heat fluxes of each node must be written explicitly. Before writing the problem heat fluxes is necessary to introduce all the problem physical constants and parameters that are reported in [Table 20] [Table 21] respectively.

Physical Constant	Symbol	Value
Stephan-Boltzmann Constant [J/s m^2K^4]	σ	5.6704e-8
Cosmic Background Radiation Temp [K]	T_{sky}	2.7
Solar Irradiance @ 1AU [W/m^2]	I_{Sun}	1366.1

Table 20 : Philae Thermal Model physical constants

Parameter	Symbol	Value
Absorptivity of Absorbers external surface	α_{2e}	0.94
Emissivity of Absorbers external surface	ε_{2e}	0.04
Emissivity of Absorbers internal surface	ε_{2i}	0.88
Absorbers external Area [m^2]	A_{2e}	2*64669e-6
Absorbers internal Area [m^2]	A_{2i}	2*61123e-6
Copper Density [kg/m^3]	ρ_{copper}	8954
Copper Specific Heat Capacity [J/kgK]	c_p	384
Warm Compartment Heat Capacity [J/K]	C_{WC}	34889.8

Table 21 : Philae Thermal Model parameters of the problem

Taking as a reference the schematization on [Figure 33], it is possible to write the heat balance for the nodes. Heat fluxes can be explicited for node 1 – Philae Warm Compartment – as [Eq.(41)]:

$$C_1 \frac{\partial \mathrm{T_1}}{\partial \mathrm{t}} = -\mathrm{Q_1} + \mathrm{Q_{int}} - Q_{sink} \tag{41}$$

whereas for node 2 – Solar Absorbers – can be written as [Eq. (42)]:

$$C_2 \frac{\partial \mathrm{T_2}}{\partial \mathrm{t}} = -\mathrm{Q_2} + \mathrm{Q_{Sun}} - Q_{rad} \tag{42}$$

Values of heat fluxes are reported in the following. From these equations temperature variation in time can be explicited and written for a generic time instant i. Integration is than performed using Euler's forward formula to obtain temperatures at the nodes [Eq.(43)], [Eq. (44)]:

$$T_{1\,i+1} = T_{1\,i} + \frac{\partial \mathrm{T_{1\,i}}}{\partial \mathrm{t}} \mathrm{dt} \tag{43}$$

$$T_{2\,i+1} = T_{2\,i} + \frac{\partial \mathrm{T_{2\,i}}}{\partial \mathrm{t}} \mathrm{dt} \tag{44}$$

Below all the heat fluxes are specified for the problem. Beginning from the heat transfer with the external environment, the contribution given by the **Sun irradiance** is [Eq. (45)]:

$$\mathrm{Q_{Sun}} = \alpha_{2e} \mathrm{A_{2e}}\, \mathrm{I_{rrAU}} \sin\beta \tag{45}$$

where the solar irradiance $\mathrm{I_{rrAU}}$ at a given orbital radius distance is evaluated with [Eq (16)] while β is the angle of elevation of Sun above the lander horizon. If β is positive the contribution of $\mathrm{Q_{Sun}}$ is calculated, otherwise is set to zero.

The contribution of heat **radiation of the two Solar Absorbers** with the deep space sky is [Eq. (46)]:

$$\mathrm{Q_{rad}} = \varepsilon_{2e} \mathrm{A_{2e}}\, \sigma\, (\mathrm{T_2^4} - \mathrm{T_{sky}^4}) \tag{46}$$

Heat transfer between the **two Solar Absorbers and the Warm Compartment** is given by radiation, the equivalent resistance schematization is reported in [Figure 34]. In first approximation the Warm Compartment radiation is assumed as black body radiation, thus emissivity and absorptivity are unitary: $\varepsilon_{WC} = \alpha_{WC} = 1$. This means that for heat transfer schematization the physical node 1 of the Wall Compartment corresponds to the black body thermal node of the Warm Compartment E_{b1}. In the other hand the Solar Absorbers internal faces are not black, thus an equivalent non-black thermal node J_2 must be considered as intermediate node between the Solar Absorbers black body node E_{b2} and the Warm Compartment black body thermal node E_{b1} .

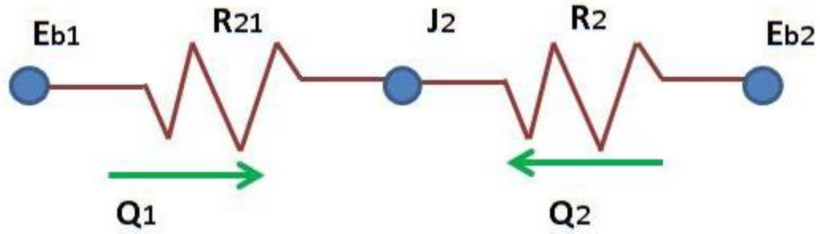

Figure 34 : Solar Absorbers/Warm Compartment resistive model

The heat balance for J_2 node is $Q_2 + Q_1 = 0$ that can be explicited as [Eq. (47)]:

$$\frac{E_{b2} - J_2}{R_2} + \frac{E_{b1} - J_2}{R_{21}} = 0 \tag{47}$$

where the thermal resistance R_2 represents the link between the black and non-black thermal nodes of the Solar Absorbers [Eq. (48)]:

$$R_2 = \frac{1 - \varepsilon_{2i}}{\varepsilon_{2i} A_{2i}} \tag{48}$$

while R_{21} represents the link between the Solar Absorbers and Warm Compartment reciprocal radiation geometry. The first equivalence of [Eq (49)] can not be explicited as long as the equivalent area of the Warm Compartment A_1 is unknown, as also the Warm Compartment to Solar Absorbers view factor F_{12}. Exploiting the reprocity theorem of view factors the second equivalence can be explicited: A_{2i} is known, whereas $F_{21} = 1$.

$$R_{21} = \frac{1}{A_1 F_{12}} = \frac{1}{A_{2i} F_{21}} \tag{49}$$

As previously discussed $Q_{\text{int}} = 5.11\text{W}$ is assumed constant, while Q_{sink} requires a dedicated discussion as long as it is the parameter that affects the most thermal results.

A first thermal model was developed without the Q_{sink} contribute, the resulting Warm Compartment temperatures are too elevate for any location on the comet surface, assessing at about 450-550K. From preliminary results without Q_{sink} it was observed that the instantaneous and daily average temperatures are well beyond the thermal ranges even at mission beginning, thus this modelling is considered inadequate to describe the mission scenario.

Consequently a second thermal model was developed adding the contribute Q_{sink} , whose aim is to simulate the heat dispersion through the two MLI blankets surrounding Philae Warm Compartment. It was observed that a suitable value for Q_{sink} ranges between 10-15W of heat loss, assumed constant: this value permits for most of locations on the comet surface to have a mission duration for Philae of 180 or more cometary days, which is a good estimation of the possible duration of the mission on the comet. As discussed in [Philae Thermal Subsystem] indeed, Philae Thermal Subsystem is designed to permit to the lander to survive until about 2AU. However if a constant $Q_{sink} = 10 - 15W$ is assumed for the whole mission in any location, some plates, in particular those that show very low insolation, display a strong decrease of the temperature leading in some cases to unphysical negative temperatures. This can be interpreted as: the heat loss must depend on the Warm Compartment temperature, the higher the Warm Compartment temperature, the more elevate the heat loss is. In addition in the earliest phases of the mission heaters are switched on, to counteract heat dispersion, this aspects must be consequently be included in the shape of Q_{sink}.

A third thermal model was than developed, taking into account of this last considerations, where the shape of the heat sink Q_{sink} is thus assumed as a linear piece-wise law, defined with respect to the average temperature admissible for Philae Warm Compartment $T_{meanWC} = \frac{T_{maxWC}+T_{minWC}}{2} \sim 273.15K$

- $Q_{sink} = 0W$ for $T_{1meanday} < T_{meanWC}$
- $Q_{sink} = 15W$ for $T_{1meanday} > T_{maxWC}$
- Q_{sink} is connected linearly in the interval $T_{meanWC} < T_1 < T_{maxWC}$ so that Q_{sink} is continuous in the entire temperature domain.

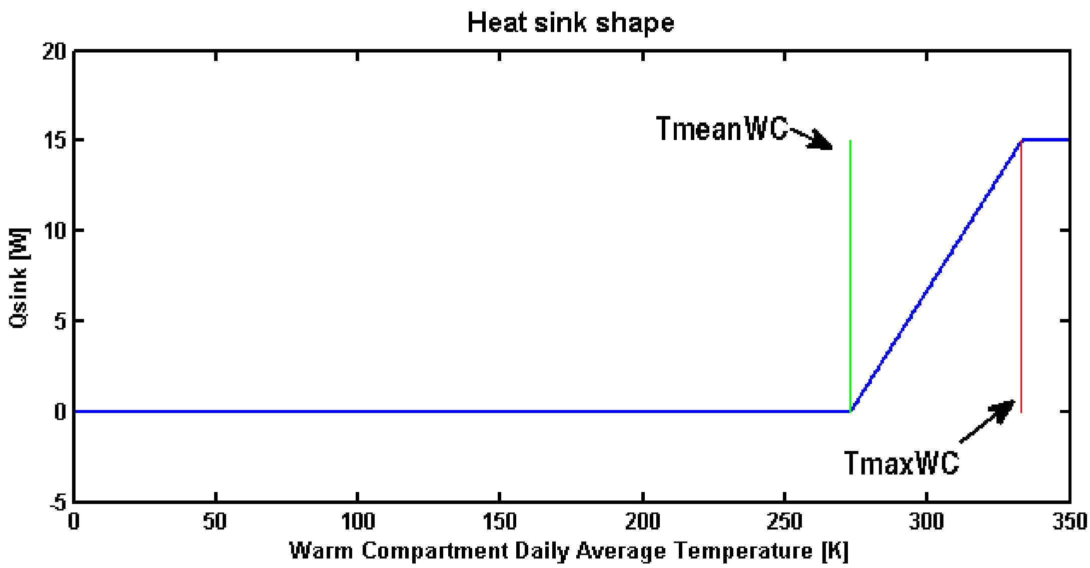

Figure 35 : Assumed heat sink profile

The designed trend of Q_{sink} can be conceived as: for $T_{1meanday} < T_{meanWC}$ heaters are switched on and heat dissipation can be counteracted thus $Q_{sink} = 0W$, for $T_{1meanday} > T_{maxWC}$ heaters are switched off and Q_{sink} increases with increasing Warm Compartment temperatures.

In [Figure 36] the thermal behaviour of a sample of plates is reported. The green line is the maximum admissible Warm Compartment temperature, while in red is the daily mean Warm Compartment temperature and in blue the instantaneous Warm Compartment temperature. It can be observed that the instantaneous temperature oscillates of few degrees around the mean temperature. The abscissa axis is represented by the "Time Instant" which is discretized as reported in [Time Discretization], cometary day number is 1/100 of the "Time Instant" reported value. A short initial temperature transitory is present due to the initial guess temperature values.

In addition in order to have least temperature oscillation due to the presence of the heat sink , at each time label Q_{sink} is evaluated considering the average temperature of the previous cometary day: $T_{1meanday}$. Q_{sink} profile is reported in [Figure 36].

This Q_{sink} shape permits to have a suitable value for Philae mission duration on all plates and contemporary guarantees that the model has physical behaviour in the cold temperature range

The heat sink profile is the strongest assumption related to Philae Thermal Model and results are directly influenced by it. In particular Philae Thermal Model is conceived to simulate the mission hot case for all the cometary plates in order to estimate the mission duration. The value that affect most the results is the maximum value of $Q_{sinkmax} = 15$W: if $Q_{sinkmax}$ is augmented the mission duration is extended for all plates as long as a major heat dispersion is achievable, vice versa if $Q_{sinkmax}$ is diminished. The advantage of this schematization is that the same profile is applied for all the Philae simulated landing sites on the comet.

Thus results related to the absolute mission duration are considered unreliable as long as there is contingency on the correct value to associate to $Q_{sinkmax}$, whereas the relative behaviour between different plates, i.e. the relative difference between mission duration in different cometary sites, can be discussed.

Finally is to be remarked that this study on Philae thermal behaviour on comet 67P C-G can only be considered as preliminary, a more detailed thermal model is necessary to obtain reliable results. Clearly also the profile of thermal dispersion through MLI depends on the landing site, this aspect is neglected in this thermal model, thus in this model is assumed that the dependence of heat dispersion through MLI on the comet location is on second order with respect to the dependence on the comet location of the other heat fluxes.

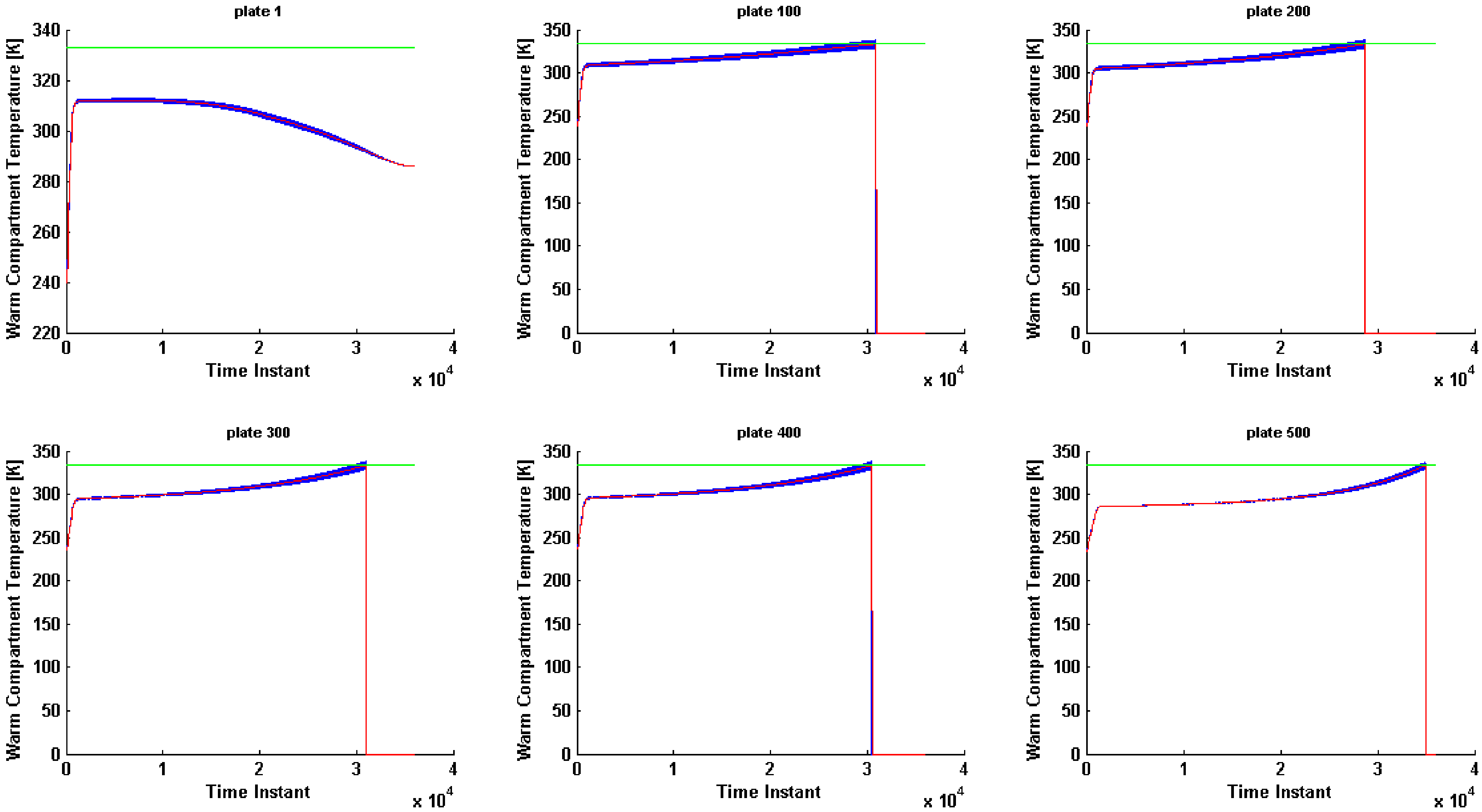

Figure 36 : Examples of Warm Compartment behaviour in different plates

5.14 Angles and Reference Frames

In order to understand the LSSel Concept model an introduction to the variables and reference frames is fundamental. Six reference frames are considered in the problem:

- Orbital Reference Frame, that projected at infinitum corresponds to the ecliptic frame
- Equatorial Reference Frame, defined by the comet spin axis and equator
- Comet Fixed Frame
- Local Site Frame, defined for each plate
- Lander Reference Frame
- Solar Aspect Angles

All the transformation matrices that will be presented are orthogonal rotation matrices, so that the inverse transformation can be obtained taking the transpose of the transformation matrix.

5.14.1 Orbital Reference Frame - ORF

The Orbital Reference Frame, projected at infinitum corresponds to the ecliptic frame. Is centred in the comet and is defined by the tern (R,T,N) so that axis R is directed as the orbital radial direction, N is the direction of the orbital angular momentum thus normal to the orbital plane, T complete the dextrorotatory tern.

5.14.2 Equatorial Reference Frame - ERF

In order to define the Equatorial Reference Frame an introduction on the cometary spin axis orientation is necessary. The spin axis orientation in space defines the mutual orientation of the ORF with respect to the ERF. The spin axis orientation is given in angles (Φ,I) as described by Sekanina [12]. This representation was chosen as long as it permits to have a physical interpretation of the variables. Angles (Φ,I) are defined as it follows,- see also [Figure 37]below:

- **Argument Φ** $\in [0, 2\pi[$ is measured from the vernal equinox of the comet, counter-clockwise, to its subsolar meridian at perihelion, or equivalently, is the angular distance measured clock-wise from the negative velocity vector of the comet at perihelion, to the projection of the spin vector onto the orbital plane.
- **Obliquity I** $\in [0, \pi]$ is the angle between the orbital and equatorial planes of the comet, or equivalently, the angle between the angular momentum vector of the orbit and the spin vector of the comet.

Therefore N is the comet ascending node, R the comet north pole and P points the direction of the angular momentum of the orbit.

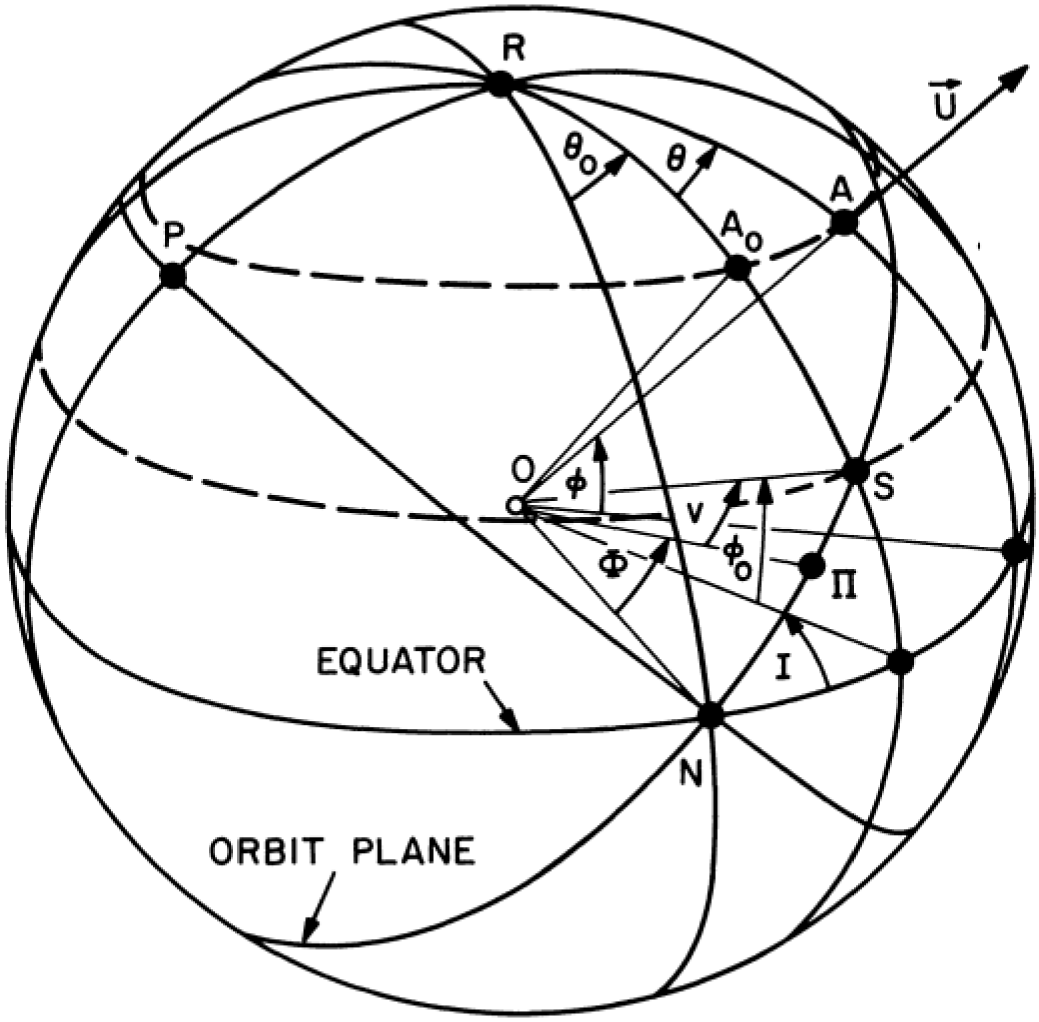

Figure 37: Representation of comet orientation in space. Credits [12].

The equatorial coordinates of a point on the comet surface are defined in the Equatorial Reference Frame as:

- **Latitude φ** defined in the interval [π /2;- π /2] . Counted from the comet equator and positive for the northern hemisphere.
- **Right Ascension (θ_0 + θ)** defined in the interval [0; 2π [. The angle θ_0 is the rotation of the subsolar point S with respect to the ascending node N. It is worth pointing out that the subsolar point S moves on the ecliptic plane and creates an angle υ, counted from the subsolar point at perihelion Π, that is equivalent to the orbital true anomaly. θ is the angle counted on the equator from the projection of the subsolar point S, counter-clockwise to the projection of the chosen point on the comet A. The projection of A moves on the equator at the comet spin rate.

The last angle defined in Sekanina's model is φ_0, which is the declination of the subsolar point S counted counter-clockwise from the equator.

<u>TRANSFORMATION ERF → ORF</u>

Transformation of coordinates from ERF to ORF is performed through two rotations [Eq. 107(50)]. Given a vector of coordinates $[s_1 , s_2 , s_3]$ in ERF will be transformed in the vector $[s_r , s_t , s_n]$ in ORF, exploiting first a rotation of I around the comet nodal axis, than a rotation of $(\Phi + \upsilon)$ in the orbital plane.

$$\begin{bmatrix} s_r \\ s_t \\ s_n \end{bmatrix} = \begin{bmatrix} \cos(\Phi+\upsilon) & sin(\Phi+\upsilon) & 0 \\ -sin(\Phi+\upsilon) & cos(\Phi+\upsilon) & 0 \\ 0 & 0 & 1 \end{bmatrix} \begin{bmatrix} 1 & 0 & 0 \\ 0 & \cos(I) & \sin(I) \\ 0 & -\sin(I) & \cos(I) \end{bmatrix} \begin{bmatrix} s_1 \\ s_2 \\ s_3 \end{bmatrix} \quad (50)$$

5.14.3 Comet Fixed Frame - CFF

The difference between the Equatorial Reference Frame and the Comet Fixed Frame is a rotation in longitude on the comet equatorial plane, that corresponds to define an initial rotation condition of the comet at the moment when mission begins. This angle called η is counted counter-clockwise from the ascending node to the cometary x axis, that corresponds to the **prime meridian**. In this schematization η is considerable as a variable parameter, due to the fact that the synchrony between comet rotation and revolution is currently unknown. However the influence of the choice of the parameter η in the overall mission duration is considered negligible at this stage of the work, so it will be assumed fixed and equal to zero: at landing date the prime meridian is considered aligned with the cometary ascending node.

The chosen A point [Figure 37]on cometary surface is defined by the coordinates in the CFF:

- **Latitude φ** [π /2;- π /2] positive in the Northern Hemisphere
- **Longitude λ** [-π; π] counted counter-clockwise from the x axis direction.

<u>TRANSFORMATION CFF → ERF</u>

Transformation of coordinates from CFF to ERF is performed through a rotation on the comet equatorial axis of the an angle $(\theta_0 + \theta - \eta)$ as reported in [Eq. (51)]. As seen $(\theta_0 + \theta)$ is the right ascension in ERF while η is the position of the comet prime meridian at the moment of the comet landing. Therefore a vector of coordinates $[s_x , s_y , s_z]$ in the CFF can be obtained from the ERF coordinates through:

$$\begin{bmatrix} s_x \\ s_y \\ s_z \end{bmatrix} = \begin{bmatrix} \cos(\theta_0+\theta-\eta) & \sin(\theta_0+\theta-\eta) & 0 \\ -sin(\theta_0+\theta-\eta) & cos(\theta_0+\theta-\eta) & 0 \\ 0 & 0 & 1 \end{bmatrix} \begin{bmatrix} s_1 \\ s_2 \\ s_3 \end{bmatrix} \quad (51)$$

5.14.4 Local Site Frame - LSF

The aim of the Local Site Frame is to define a reference frame centred in the centre of each cometary plate in order to permit to study locally the movement of the Sun, coordinates of the plate centre are given in latitude φ and longitude λ.

Sekanina [12] describes the method to obtain the orbital coordinates of the normal vector to a point that is located over a spherical cometary surface. In the actual case the comet is schematized as a tessellated irregular shape and its major inertia axis is coincident with the axis of spin, indeed the model needs to be generalized.

Due to the fact that the comet shape is not spherical, in general the normal to the plate is not aligned with the radial. The radial is defined as the direction taken from the comet centre of coordinates to each plate centre of coordinates. Thus a local reference frame, the Local Site Frame, whose normal is aligned with the plate normal and not to the radial, is to be defined. This issue leads to consequences that will be discussed in [Philae Orientation on the Plate].

LSF is defined for each plate centre of coordinates as suggested in [33] as it follows:

- local vertical of the landing site V is perpendicular to the horizontal plane tangent to the landing site (as given by 67P Churyumov-Gerasimenko shape model)
- the axis E is the cross product of the comet pole axis with the local vertical to the landing site
- the axis N lays in the plate plane and is defined such that the tern (E,N,V) is dextrorotatory

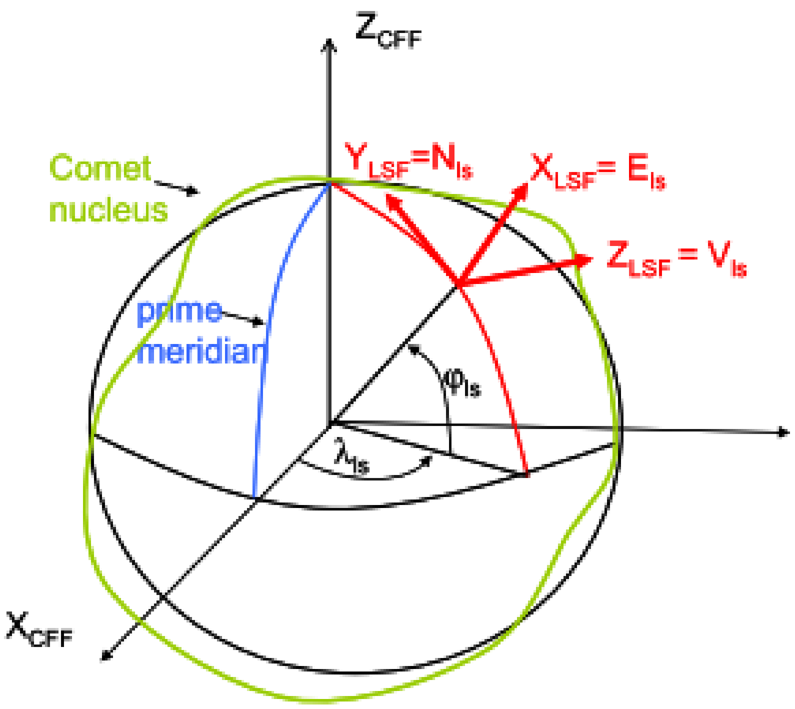

Figure 38 : Local Site Frame definition. Credits [33]

Due to the fact that LSF is a local frame it is useful to define elevation and azimuth:

- **Azimuth α_1** [-π; π] counted counter-clockwise from the axis E.
- **Elevation β_1** [π /2;- π /2] counted from the plate horizon, positive in the Zenith-containing hemisphere

<u>TRANSFORMATION LSF</u> → <u>CFF</u>

Transformation of coordinates from LSF to CFF is performed as suggested again in [33] through the following rotation matrix [Eq. (52)], where the vector $[s_E\ , s_N\ , s_V]$ is expressed in LSF coordinates. Where $[n_1\ , n_2\ , n_3]$ are the component of the LSF local vertical Z_{LSF} expressed in CFF coordinates.

$$\begin{bmatrix} s_x \\ s_y \\ s_z \end{bmatrix} = \begin{bmatrix} -n_2 & -n_1 n_3 & n_1 \\ n_1 & -n_2 n_3 & n_2 \\ 0 & n_1^2 + n_2^2 & n_3 \end{bmatrix} \begin{bmatrix} s_E \\ s_N \\ s_V \end{bmatrix} \tag{52}$$

5.14.5 Lander Reference Frame – LDR

The Lander Reference Frame is fixed to the lander, the x axis in oriented towards WALL3, y oriented towards WALL1 and z is the normal to the lander plane.

Again due to the fact that LDR is a local frame is useful to define elevation and azimuth:

- **Azimuth α_2** [-π; π] counted counter-clockwise from the lander x axis.
- **Elevation β_2** [π /2;- π /2] counted from the lander plane, positive in the hemisphere containing the positive z axis of the lander.

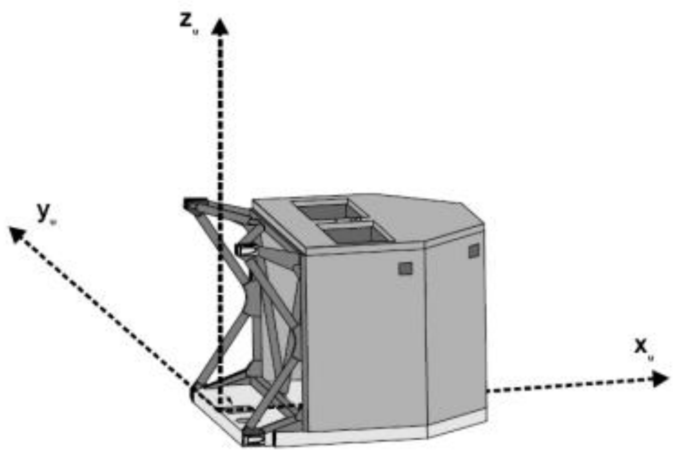

Figure 39 : Lander Reference Frame definition. Credits [33]

For simplicity the LRF is conceived coincident with the LSF at the moment of landing. Any rotation of the LRF around the z axis is defined by the angle θ.

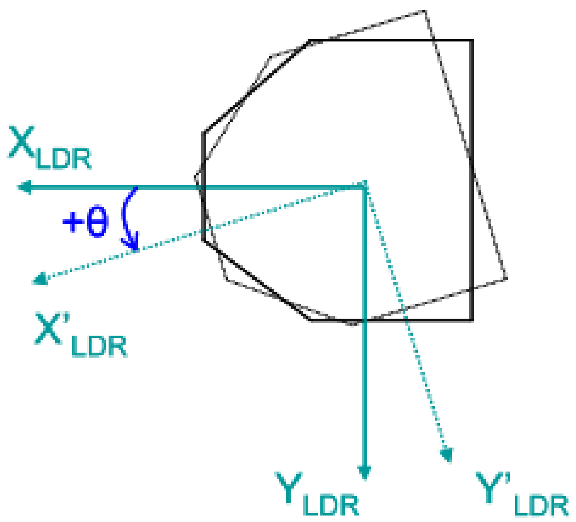

Figure 40 : Lander Reference Frame rotation. Credits [33]

<u>TRANSFORMATION LSF</u> → <u>LRF</u>

Transformation of coordinates from LSF to LRF is performed through the following rotation matrix [Eq. (53)], where the vector [s_I , s_{II} , s_{III}] is expressed in LSF.

$$\begin{bmatrix} s_I \\ s_{II} \\ s_{III} \end{bmatrix} = \begin{bmatrix} \cos\theta & \sin\theta & 0 \\ -\sin\theta & \cos\theta & 0 \\ 0 & 0 & 1 \end{bmatrix} \begin{bmatrix} s_E \\ s_N \\ s_V \end{bmatrix} \qquad (53)$$

As it will be discussed in below in [Philae Orientation on the Plate] the angle of rotation of the lander with respect to its initial position is given by [Eq. (54)]

$$\theta = \alpha_{\mathrm{rot}} + \pi\,\delta \qquad (54)$$

where:

- $\boldsymbol{\alpha_{rot}}$ is the lander initial orientation at mission beginning
- $\boldsymbol{\pi\,\delta}$ represents to a 180° rotation manoeuvre of the lander that will be performed during the mission. δ is a switch whose value is zero at mission beginning and one when the manoeuvre is performed.

5.14.6 Solar Aspect Angles – SAA

Solar Aspect Angles are used as input for Philae Solar Array Simulator, they are strictly connected with the LRF, indeed the domain α ranges [-180°,180°], while β ranges [-90 , 90] as defined in the [32].

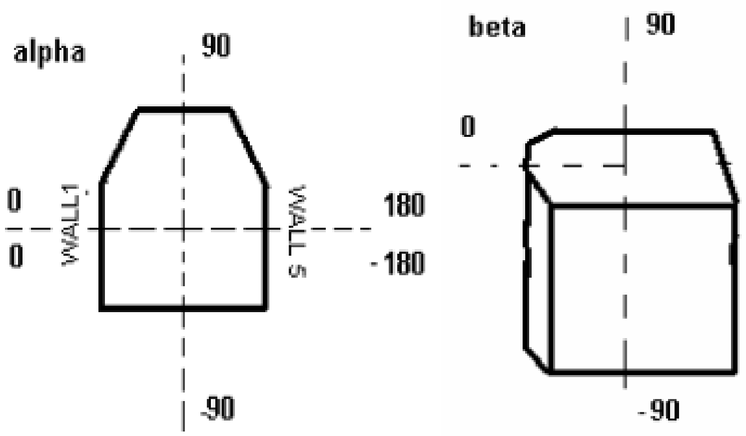

Figure 41 : Solar Aspect Angles definition. Credits [32]

5.14.7 Handling the Transformation Matrices

Transformation matrices are designed to be permit rapid transformations between reference frames. For instance in the LSS is necessary to study the Sun movement in the plate reference frame, the LSF. To produce this analysis is necessary to evaluate the Sun direction in LSF coordinates in each chosen time label. The Sun direction corresponds to the opposite direction of the R axis of the ORF, thus a transformation of coordinates between ORF and LSF is necessary. To perform this is simply necessary to interconnect the transformation matrices presented in the previous sections. For a clearer presentation also intermediate passages are presented.

The Sun in ORF can be expressed as the opposite direction of the R axis [Eq. (55)]:

$$\begin{bmatrix} s_r \\ s_t \\ s_n \end{bmatrix} = \begin{bmatrix} -1 \\ 0 \\ 0 \end{bmatrix} \qquad (55)$$

and can be expressed in ERF using the following transformation [Eq. (56)], which is the inverse transformation of [Eq. (51)]

$$\begin{bmatrix} s_1 \\ s_2 \\ s_3 \end{bmatrix} = \begin{bmatrix} 1 & 0 & 0 \\ 0 & \cos(I) & \sin(I) \\ 0 & -\sin(I) & \cos(I) \end{bmatrix}^T \begin{bmatrix} \cos(\Phi + \upsilon) & sin(\Phi + \upsilon) & 0 \\ -sin(\Phi + \upsilon) & cos(\Phi + \upsilon) & 0 \\ 0 & 0 & 1 \end{bmatrix}^T \begin{bmatrix} s_r \\ s_t \\ s_n \end{bmatrix} \qquad (56)$$

or can be transformed to the CFF reference frame using [Eq. (57)]:

$$\begin{bmatrix} s_x \\ s_y \\ s_z \end{bmatrix} = \begin{bmatrix} \cos(\theta_0+\theta-\eta) & \sin(\theta_0+\theta-\eta) & 0 \\ -sin(\theta_0+\theta-\eta) & cos(\theta_0+\theta-\eta) & 0 \\ 0 & 0 & 1 \end{bmatrix}^T \begin{bmatrix} 1 & 0 & 0 \\ 0 & \cos(I) & \sin(I) \\ 0 & -\sin(I) & \cos(I) \end{bmatrix}^T \begin{bmatrix} \cos(\Phi+\upsilon) & sin(\Phi+\upsilon) & 0 \\ -sin(\Phi+\upsilon) & cos(\Phi+\upsilon) & 0 \\ 0 & 0 & 1 \end{bmatrix}^T \begin{bmatrix} s_r \\ s_t \\ s_n \end{bmatrix} \quad (57)$$

The process of interconnection can continue to bring the Sun direction into the LSF, now for sake of brevity it is assumed to know already the Sun in CFF coordinates, thus to know $\begin{bmatrix} s_x \\ s_y \\ s_z \end{bmatrix}$ as calculated in [Eq. (57)]. To move in the LSF the transformation is [Eq. (58)]:

$$\begin{bmatrix} s_E \\ s_N \\ s_V \end{bmatrix} = \begin{bmatrix} -n_2 & -n_1 n_3 & n_1 \\ n_1 & -n_2 n_3 & n_2 \\ 0 & n_1^2+n_2^2 & n_3 \end{bmatrix}^T \begin{bmatrix} s_x \\ s_y \\ s_z \end{bmatrix} \quad (58)$$

in the LRF can be expressed as [Eq. (59)]:

$$\begin{bmatrix} s_I \\ s_{II} \\ s_{III} \end{bmatrix} = \begin{bmatrix} \cos\theta & \sin\theta & 0 \\ -\sin\theta & \cos\theta & 0 \\ 0 & 0 & 1 \end{bmatrix} \begin{bmatrix} -n_2 & -n_1 n_3 & n_1 \\ n_1 & -n_2 n_3 & n_2 \\ 0 & n_1^2+n_2^2 & n_3 \end{bmatrix}^T \begin{bmatrix} s_x \\ s_y \\ s_z \end{bmatrix} \quad (59)$$

Rotation matrices are orthogonal, this guarantees that the initial versor $\begin{bmatrix} s_r \\ s_t \\ s_n \end{bmatrix}$ when transformed in LRF $\begin{bmatrix} s_I \\ s_{II} \\ s_{III} \end{bmatrix}$ is still a unitary vector.

6. The Landing Site Simulator

Once introduced to the LSSel Concept Model, in particular to all the assumptions and schematizations useful to address the problem, it is now possible to present the implemented tool, the Landing Site Simulator. The LSS represents the simulation counterpart of the LSSel Concept and is useful to obtain fundamental results to understand the features of the landing site selection problem. The platform used to develop the code tool is Matlab.

Most of aspects schematized in the LSS are straightforward implementation of the equations presented in the [The Landing Site Selection Concept] and for sake of brevity are not discussed. This chapter aims to describe the structure, the functionalities and the results that can be obtained with the LSS.

6.1 Simulations

Below is reported [Figure 42] representing the available simulation of the LSS.

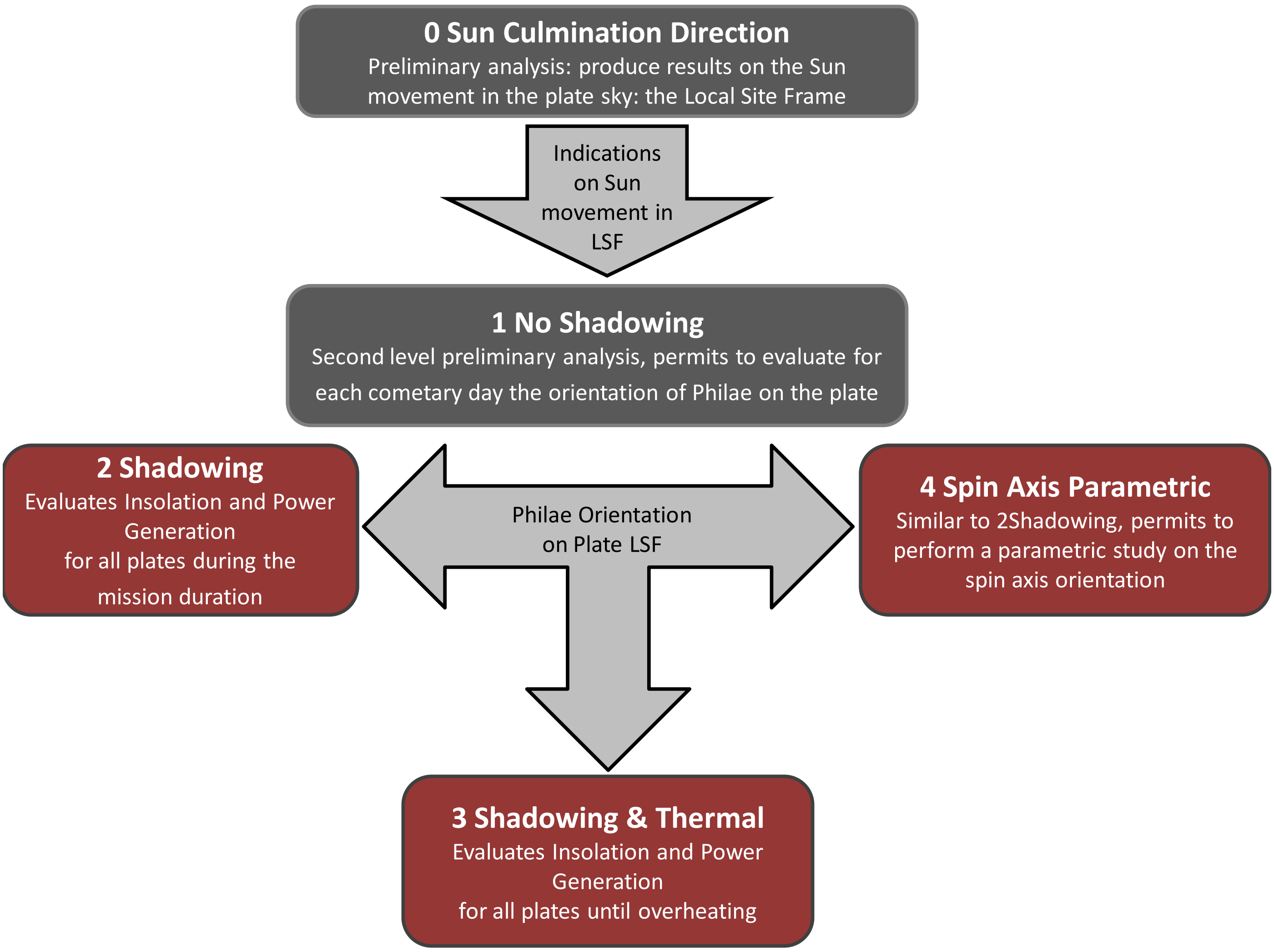

Figure 42 : LSS available simulations and mutual interconnections

There are 5 different types on analysis that can be performed with the LSS [Figure 42]:

- **0 Sun Culmination Direction**, permits to study the Sun movement in the Local Site Frame for all cometary sites, in particular to study the effects of the irregular shape of comet 67P C-G on the illumination conditions.
- **1 No Shadowing**, permits to perform a preliminary analysis on the Insolation and Power Generation neglecting the comet self-shadowing. In particular it is useful to evaluate the optimal orientation of Philae in the LSF for all plates and for all the mission duration.
- **2 Shadowing**: loads the orientation of Philae in the LSF for all plates and for the entire mission duration and evaluates Insolation and Power Generation for the entire mission, taking into account of comet shadowing.
- **3 Shadowing & Thermal**: loads the orientation of Philae in the LSF for all plates and for the entire mission duration and evaluates Insolation and Power Generation from mission beginning until overheating, taking into account of comet shadowing.
- **4 Spin Axis Parametric**, similar to the simulation *2 Shadowing* permits to study the effects of a parametric variation on the spin axis orientation.

6.2 Simulation-0 Sun Culmination Direction

In the Sun Culmination Direction tool the LSS model the following aspects as reported in [Table 22]

Aspect	Modelling	Reference
67P C-G Shape	Tessellated Triangular Shape	[Comet 67P C-G Shape]
67P C-G kinematics	Inertial spin axis, constant rotation rate	[Comet 67P C-G Kinematics]
Orbital Parameters	Kepler’s parameters	[Orbit modelling]
Mission Schedule	Philae mission nominal	[Time Discretization]
Time discretization	Fraction of rotational period	[Time Discretization]
Illumination	Direct illumination	[Illumination Assumptions]
Reference Frames	Interconnected orthogonal rotation matrices	[Angles and Reference Frames]
Philae Orientation	--	
Shadowing	--	
Power	--	
Thermal	--	

Table 22 : Sun Culmination Direction simulation modelling

Once the preliminary modelling of [Table 22] is loaded in the *0 Sun Culmination* tool, the next phase is the routine core. The core is a double-nested for cycle, the external cycle is on the N = 360*dT time instants and the internal over the L = 512 cometary plates. The core of the routine permits to evaluate the position of the Sun for each time chosen time label in each plate, expressed in the LSF. To perform this calculation [Eq. (59)] and previous are implemented, as described in [Handling the Transformation Matrices]. Results obtained from this simulation are available in the results chapter in [Philae Orientation on the Plate].

6.3 Simulation- 1 No Shadowing

This second preliminary routine permits to evaluate the orientation of Philae in the plate expressed in LSF for each plate in each cometary day. Thus the output of this simulation is the angle of rotation of LSF with respect to the LRF as described in [Eq. (53)] and [Eq.(54)].

Aspect	Modelling	Reference
67P C-G Shape	Tessellated Triangular Shape	[Comet 67P C-G Shape]
67P C-G kinematics	Inertial spin axis, constant rotation rate	[Comet 67P C-G Kinematics]
Orbital Parameters	Kepler's parameters	[Orbit modelling]
Mission Schedule	Philae mission nominal	[Time Discretization]
Time discretization	Fraction of rotational period	[Time Discretization]
Illumination	Direct illumination	[Illumination Assumptions]
Reference Frames	Interconnected orthogonal rotation matrices	[Angles and Reference Frames]
Philae Orientation	Optimum evaluation	[Philae Orientation on the Plate]
Shadowing	--	
Power	--	
Thermal	--	

Table 23: No Shadowing simulation modelling

The structure of the routine is reported in [Figure 43]. Once the problem aspects are loaded as presented in [Table 23], the core is a double-nested for cycle, the external cycle is over the L = 512 cometary plates and the internal on the N = 360*dT time instants.

For each plate and at every time instant a sequence of eight steps is applied, each step is correspondent to a specific dedicated function.

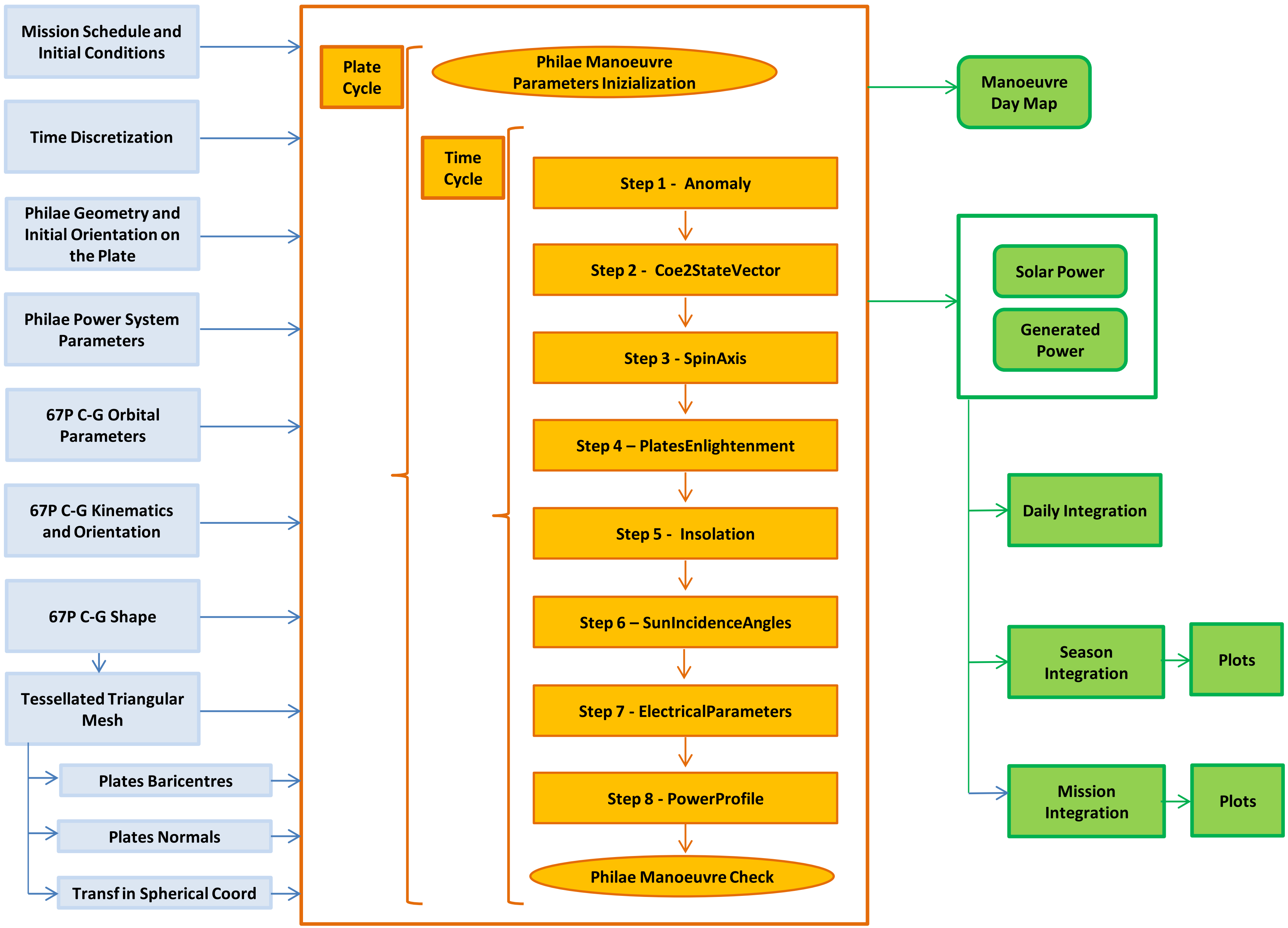

Figure 43 : Simulation 1No Shadowing block scheme

Step 1. Anomaly

Given the time instant, the semi-major axis and eccentricity of the orbit, returns the eccentric and true anomaly as described in [Orbit modelling]. Anomalies are evaluated from the time of the pericentre passage t_{per}. Integration time starts at 0 sec so it is necessary to add the time of landing counted from the perihelion passage to the date of landing to obtain the correct value. Eccentric anomaly is obtained numerically solving Kepler's equation exploiting Newton-Raphson method.

Step 2. Coe2StateVector

Given the classical Keplerian orbital elements returns the Cartesian state vector. The aim of this function is to plot 67P Churyumov-Gerasimenko orbital position.

Step 3. SpinAxis

The function SpinAxis, given the angles Φ and I, that defines the orientation of the cometary spin axis with respect to the orbital plane, returns the value of the instantaneous position of the subsolar point counted counter-clockwise from the ascending node. References can be found in [Comet 67P C-G Kinematics]

Step 4. PlatesEnlightenment

This function permits to evaluate the Sun direction in the Comet Fixed Frame, in the Landing Site Frame, in the Lander Reference Frame and in Solar Aspect Angles exploiting the transformation matrices presented in [Angles and Reference Frames]. This function is fundamental in the routine as long as it both permits to study the Sun movement in different reference frames and to evaluate the Solar Aspect Angles input for the Solar Array Simulator.

Step 5. Insolation

Given the orbital radius, the Sun elevation over the plate and the solar constant returns the Solar Power and the Solar Irradiance at such distance, exploiting the insolation equation [Eq. (17)] and the assumptions discussed in [Illumination Assumptions].

Step 6. SunIncidenceAngles

This function is part of the SAS and computes the Sun-incidence angles useful to compute the solar array power, as described in [Philae Power Model].

Step 7. ElectricalParameters

This function is also part of the SAS and computes the four main electrical parameters (Voc, Isc, Vmp, Imp) over the simulation time. This function was modified from the SAS original version: three fake walls were created WALL7 WALL8 WALL9, they have same physical properties, degradation, temperature and dimensions of WALL2 WALL3 WALL4 respectively, but have opposite exposition direction. Fake walls are useful to evaluate whether Philae daily best orientation is with the lander x axis pointing towards $\alpha_1 = -90°$ or $\alpha_1 = 90°$ expressed in LSF (see [Local Site Frame - LSF] for definition of the angle). This aspect is further treated in the results section [Philae Orientation on the Plate].

Step 8. PowerProfile

This function is also part of the SAS and computes the power profile at the simulation time. The power is calculated both at section level (Pmp) and overall (Ptot). Permits also to calculate the summation of the instantaneous of power produced by WALL7+WALL8+WALL9 and WALL2+WALL3+WALL4.

Philae Manoeuvre Check at the end of each cometary day the summation of the instantaneous of power produced by WALL7+WALL8+WALL9 and WALL2+WALL3+WALL4 are integrated over the past day. If the daily power produced by WALL7+WALL8+WALL9 is major than the power produced by WALL2+WALL3+WALL4, the lander is rotated of 180° to guarantee optimal exposure for power generation. Days of manoeuvres are saved.

6.4Simulation–2 Shadowing

This simulation aims to calculate the Insolation and Generated Power over the entire mission duration and, differently from the previous, simulates comet self-shadowing. Input for this simulation is Philae manoeuvre day map: as is discussed in Philae Orientation on the Plate], the orientation of Philae can be determined univocally only if the plate horizon is flat. Many plates of 67P C-G shape do not display a flat horizon, this is also the condition that creates comet self-shadowing. This issue is solved calculating the best orientation of Philae assuming a flat horizon for all the plates, thus exploiting *1NoShadowin*g simulation, the same manoeuvres are than performed in this *2Shadowing* simulation. This is the reason why this *2Shadowing* simulation must load the Manoeuvre Day Map. Clearly this a simplification of the problem, consequence related to it are discussed in [Philae Orientation Operations on the plate]. Modeling assumptions are reported in [Table 24].

Aspect	Modelling	Reference
67P C-G Shape	Tessellated Triangular Shape	[Comet 67P C-G Shape]
67P C-G kinematics	Inertial spin axis, constant rotation rate	[Comet 67P C-G Kinematics]
Orbital Parameters	Kepler's parameters	[Orbit modelling]
Mission flag-dates	Philae mission nominal	[Time Discretization]
Time discretization	Fraction of rotational period	[Time Discretization]
Illumination	Direct illumination	[Illumination Assumptions]
Reference Frames	Interconnected orthogonal rotation matrices	[Angles and Reference Frames]
Philae Orientation	Optimal	[Philae Orientation Operations on the plate]
Shadowing	Shadowing liability map + Shadowing	[Shadowing Liability] [Shadowing]
Power	Solar Array Simulator	[Philae Power Model]
Thermal	--	

Table 24: 2Shadowingsimulation modelling assumptions

This simulation is identical to *1NoShadowing* simulation, there are only two differences:

- the Step4 – PlatesEnlightenment is called Step4 – PlatesEnlightenmentShade ad long as shadowing is implemented. The simulation creates the Shadowing liability map and exploits it inside the PlatesEnlightenmentShade step to evaluate whether for that time label and plate shadowing occurs. The reference equations for the problem modelling are reported in [Comet Self-Shadowing].
- the Manoeuvre Check is now performed simply following the Manoeuvre Day Map.

Results obtained from this simulation can be found in [Insolation] [Generated Power]and permit to evaluate Insolation, Generated Power and their daily and seasonal integrations, as indicated in [Power Variables]. This simulation permits also to integrate Generated Power daily to check whether the constraint [Constr. 2] is respected.

6.5 Simulation – 3Shadowing & Thermal

This simulation permits to model contemporarily all the aspects presented in the LSSel Concept. However, due to scarce reliability on the Thermal Model, the results related to it are treated separately and can only be considered as preliminary. The structure of this simulation is visible at [Figure 44].
Once again the modelling assumptions of this simulation are reported in the dedicated [Table 25].

Aspect	Modelling	Reference
67P C-G Shape	Tessellated Triangular Shape	[Comet 67P C-G Shape]
67P C-G kinematics	Inertial spin axis, constant rotation rate	[Comet 67P C-G Kinematics]
Orbital Parameters	Kepler's parameters	[Orbit modelling]
Mission flag-dates	Philae mission nominal	[Time Discretization]
Time discretization	Fraction of rotational period	[Time Discretization]
Illumination	Direct illumination	[Illumination Assumptions]
Reference Frames	Interconnected orthogonal rotation matrices	[Angles and Reference Frames]
Philae Orientation	Optimal	[Philae Orientation Operations on the plate]
Shadowing	Shadowing liability map + Shadowing	[Shadowing Liability] [Shadowing]
Power	Solar Array Simulator	[Philae Power Model]
Thermal	Lumped parameters non-stationary	[Philae Thermal Model]

Table 25 : 3Shadowing&Thermal modelling assumptions

Simulation steps are identical to the *2Shadowing* simulation, there are only two differences:

- a Step 9 – Thermal is added and permits to simulate the thermal behaviour of Philae for all plates in every chosen time label, as described in [Philae Thermal Model].
- Seasonal integration are performed for each plate from mission beginning until overheating.

Available results in [Thermal Results] are seasonal and mission integration of Insolation and Generated Power until overheating, also a map of overheating day is produced.

6.6 Simulation – 4Spin Axis Parametric

This simulation is identical to the two simulations *1NoShadowing* and the following simulations, only the spin axis orientation is changed to produce a parametric analysis on the variation of this parameter. Four analysis of this kind are performed [Table 26], corresponding to the maximum and minimum boundaries of spin axis orientation variation: $I = 220° \pm 10°$, $\psi = -70° \pm 10°$

Simulation	Inclination I	Argument ψ
SpinAxis1	230	-70
SpinAxis2	210	-70
SpinAxis3	220	-60
SpinAxis4	220	-80

Table 26 : Spin Axis Parametric Analysis

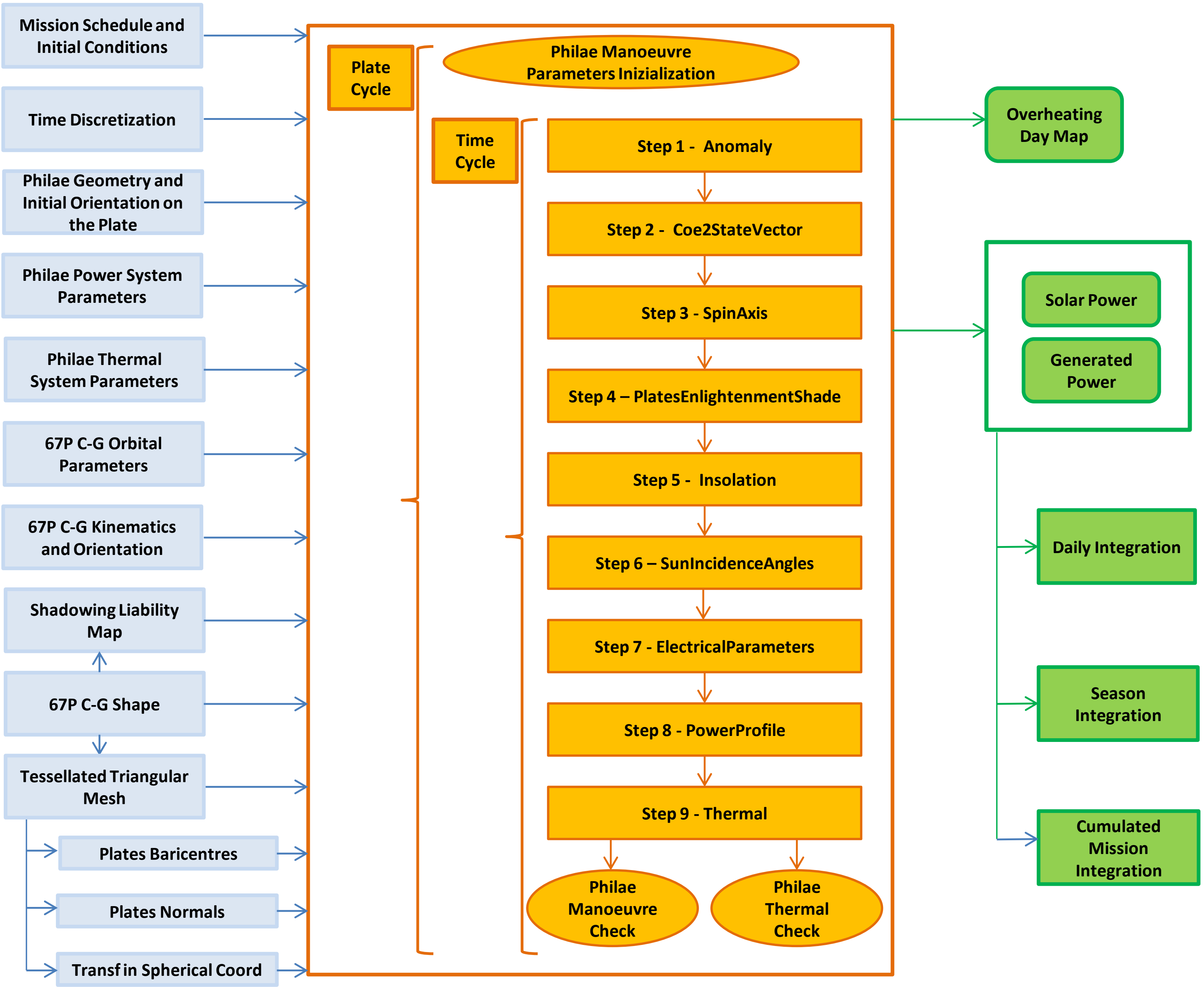

Figure 44: Simulation 3Shadowing&Thermal block scheme

7.Results

Results presented in this chapter are related to the LSS simulations as presented in [The Landing Site Simulator]. First the Orientation of Philae on the plate is discussed, than the most suitable landing sites are evidenced for each performed analysis.

7.1 Results Layout

Due to the elevate irregularity of 67P Churyumov-Gerasimenko, results are shown in three **cometary 3D views**. Projections are parallel to the comet z axis and have an azimuth angle with respect to the comet x axis of 60° 180° and 300° respectively. This sequence of angles was chosen as long as it is the only one found that permits to visualize all the comet location using only three projection, in addition projection are separated uniformly in azimuth of 120°.Projection are designed to maintain the aspect ratio of the comet.

Results are also presented projecting 67P Churyumov-Gerasimenko in a **2D latitude-longitude** plot.

7.2 Philae Orientation on the Plate

This section is dedicated to the results related to the optimal orientation of Philae on comet 67P C-G. As discussed in [Philae Overall Design] thanks to Philae mechanical capabilities a **rotation manoeuvre around LRF z axis** is possible. Such rotation requires electrical power to be performed and as long as the aim of this study is to maximize the power produced by Philae, the manoeuvre can’t be counterproductive. Thus is fundamental to control and reduce at minimum the need of Philae yaw manoeuvres. Due to these considerations the hypothesis of Sun tracking is discarded from the beginning.

To understand which is the most efficient positioning of Philae in each plate some considerations need to be done about the Landing Site Frame.

7.2.1 Cardinal Points

The Landing Site Frame is defined as a local frame is typically defined also for Earth surface. It is to be noticed however that in the case of Earth the local frame is defined in each location with respect to the plumb line direction (also known as the Zenith), that is almost coincident with the local radial. In 67P Churyumov-Gerasimenko shape model the radial direction and the plate normal do not coincide and their angular separation can be up to of some tens of degrees. As a consequence, it can't be assumed a priori that in the LSF the E axis corresponds to East and the N axis corresponds to North in the terrestrial sense: indeed if the LSF was defined in a spherical flat body N would correspond to the opposition direction of the Sun daily culmination and E would correspond to the direction of sunrise at equinoxes (this would be the terrestrial interpretation of North and East in the Northern Hemisphere for a spherical flat surface Earth model). In particular in a spherical flat surface local frame the direction of South coincides with the direction of Sun culmination every day of the year. These properties would be still valid when defining an equivalent flat sphere local frame for the comet, but such reference frame is useful only to describe a spherical flat surface comet, thus has no interest for this study.

These cardinal points properties can't be assessed a priori for the LSF and in particular the invariance over the year of the direction of Sun culmination in the LSF.

7.2.2 Philae Optimal Orientation

All these considerations are useful when the orientation of the lander in each plate is to be optimized. In order to guarantee to the lander the most efficient illumination condition, in terms of daily generated power in a given landing site, it was proven by Topputo et al. [34] that the normal to WALL3 must be pointing towards the direction of Sun culmination This result is supported by Philae symmetry with respect to the WALL3 normal.

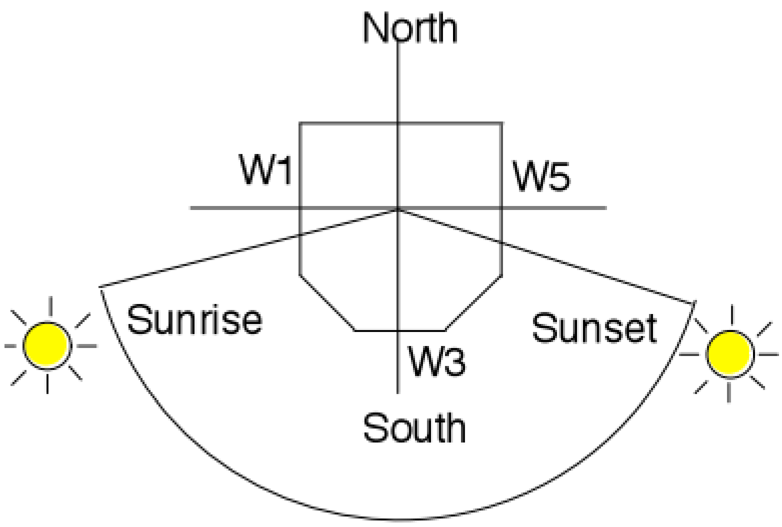

Figure 45 : Movement of the Sun in the lander plane seen from below

This result is valid when:

- North and South are defined in a local site frame that is referred to a spherical flat body, thus when the radial to the body coincides with the local normal.

- the lander reference frame plane is parallel to the horizon
- the day has a typical day-night cycle

Indeed in such hypothesis the Sun culminates at South in every location on the Northern Hemisphere and North in every location in the Southern Hemisphere. In addition in this hypothesis the Sun performs a symmetrical curve in the sky with respect to the culmination direction. The conditions of validity of this result are not always respected in 67P C-G surface over the entire mission duration, thus these results need to be extended.

7.2.3 Cardinal Points in LSF and Sun Movement in the Sky

To establish if these results could be extended also to an irregular cometary shape the movement of the Sun in the LSF was studied for different positions in the comet and for different days over the mission duration.

The Sun movement in the LSF is reported in the series of figures below. Sun movement is plotted in each plate for the entire mission span (360 days) with a 10 days mutual separation. The chosen plates represent a significant sample of the different possible behaviors, as function of the latitude and longitude.

For each plate also the value of inclination of the normal with respect to the comet equator, thus expressed in CFF φ angle, is reported, as long as it is fundamental for results interpretation.

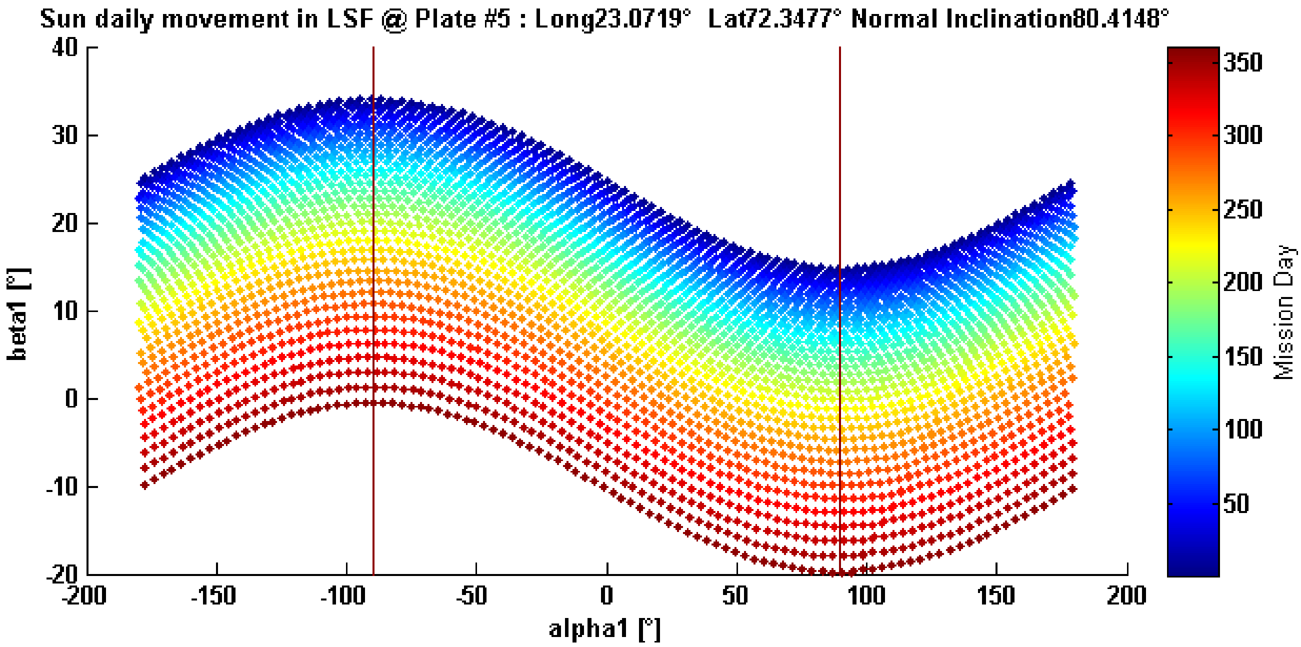

Figure 46 : Plate 5 Sun movement in LSF

Plate 5 [Figure 46**]**, normal inclination 80.41°: is a typical North Pole plate, at mission beginning the Sun is always above the horizon at middle elevation angles, while at mission end the Sun never rises above the horizon. Culmination is always for $\alpha_1 = -90°$.

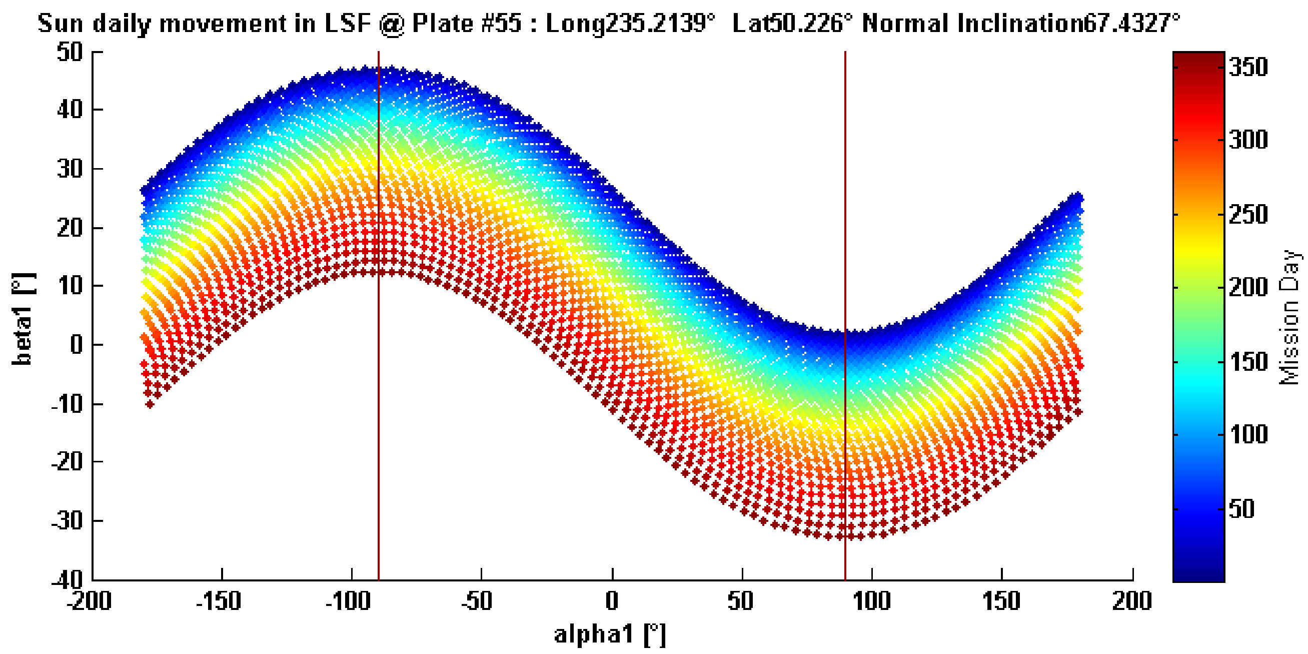

Figure 47 : Plate 55 Sun movement in LSF

Plate 55 [Figure 47**]**, normal inclination 67.43°: located at middle latitudes, due to the elevate inclination of 67P C-G spin axis at mission beginning can see the Sun over the horizon for the entire day, while at mission end experience only a short day. Culmination direction is always for $\alpha_1 = -90°$.

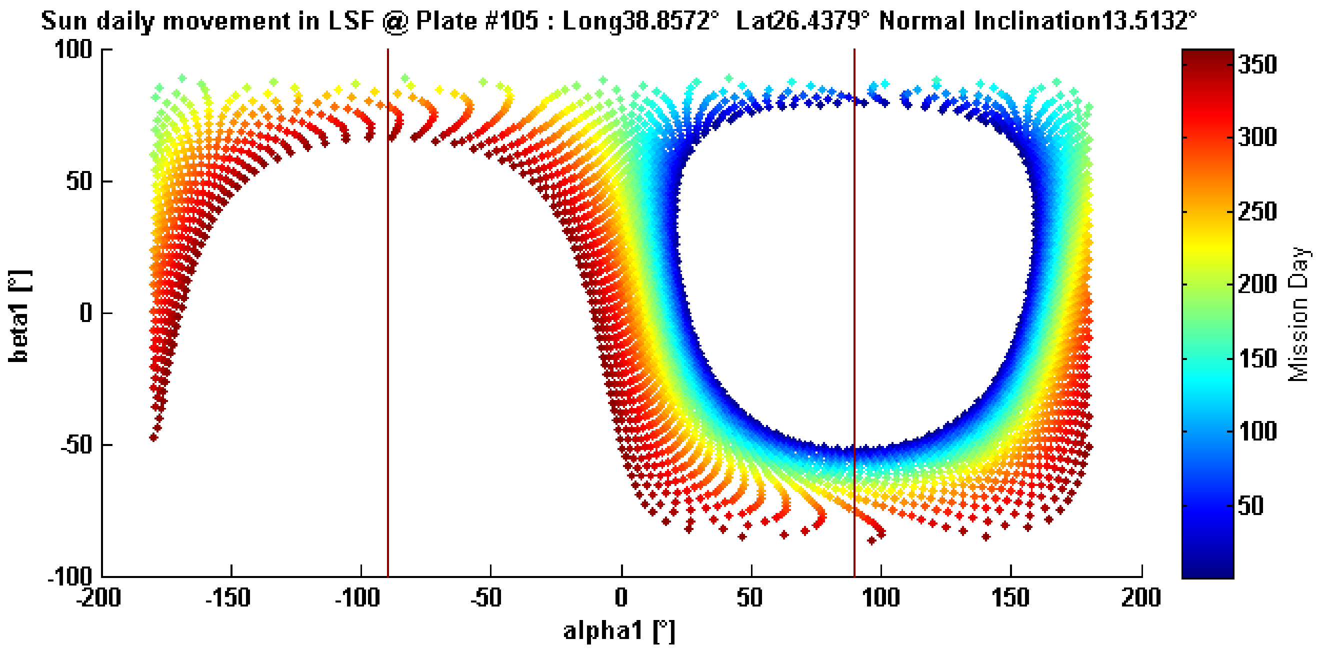

Figure 48 : Plate 105 Sun movement in LSF

Plate 105 [Figure 48**]** normal inclination 13.51°: located at low latitude, show very exotic illumination conditions: at mission beginning sees the Sun moving only in restricted range of horizontal angles. while at mission end presents a normal day/night cycle. Between days 150 and 220 show a typical Sun Culmination Change in Opposition: culmination direction moves from $\alpha_1 = +90°$ to $\alpha_1 = -90°$ due to the fact that the Sun elevation angle trespass the 90° threshold.

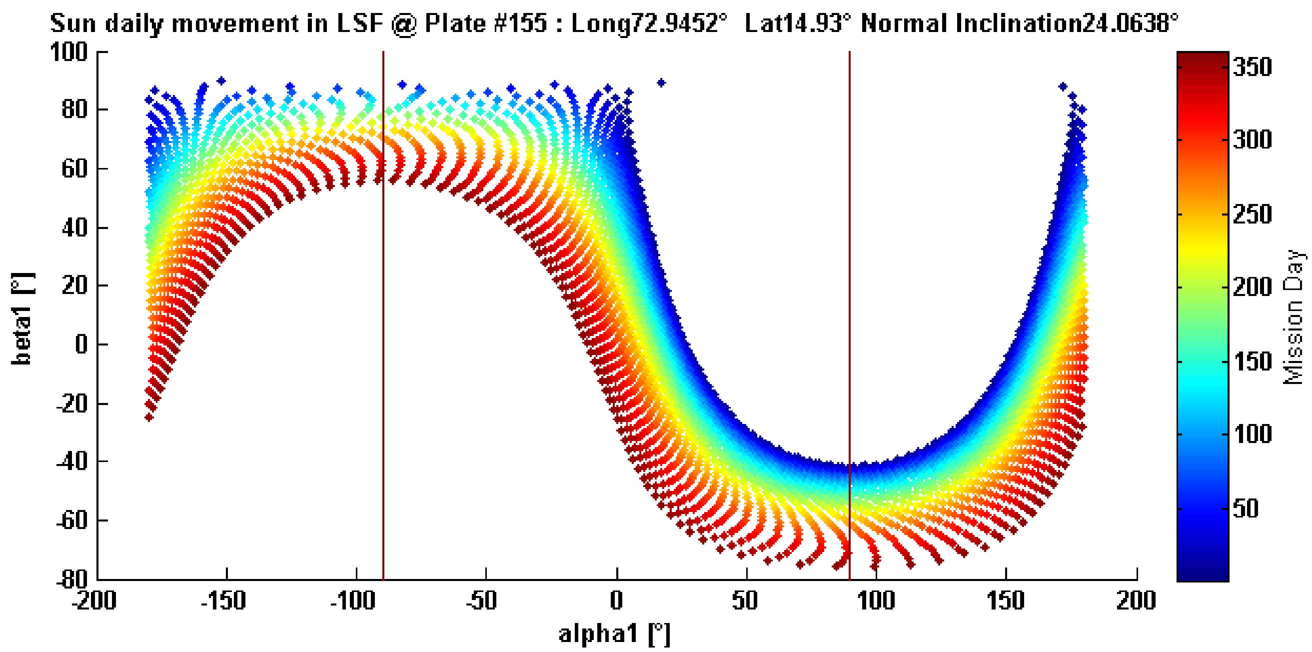

Figure 49 : Plate 155 Sun movement in LSF

Plate 155 [Figure 49**]** normal inclination 24.08°: is also at low latitude, it can be noticed that has a behavior very similar to Plate 105, except for the fact that Sun Culmination direction change occurs at the first day. This plate show a lower latitude if confronted with Plate 105, but has a more inclined normal. This is due to 67P C-G irregular shape.

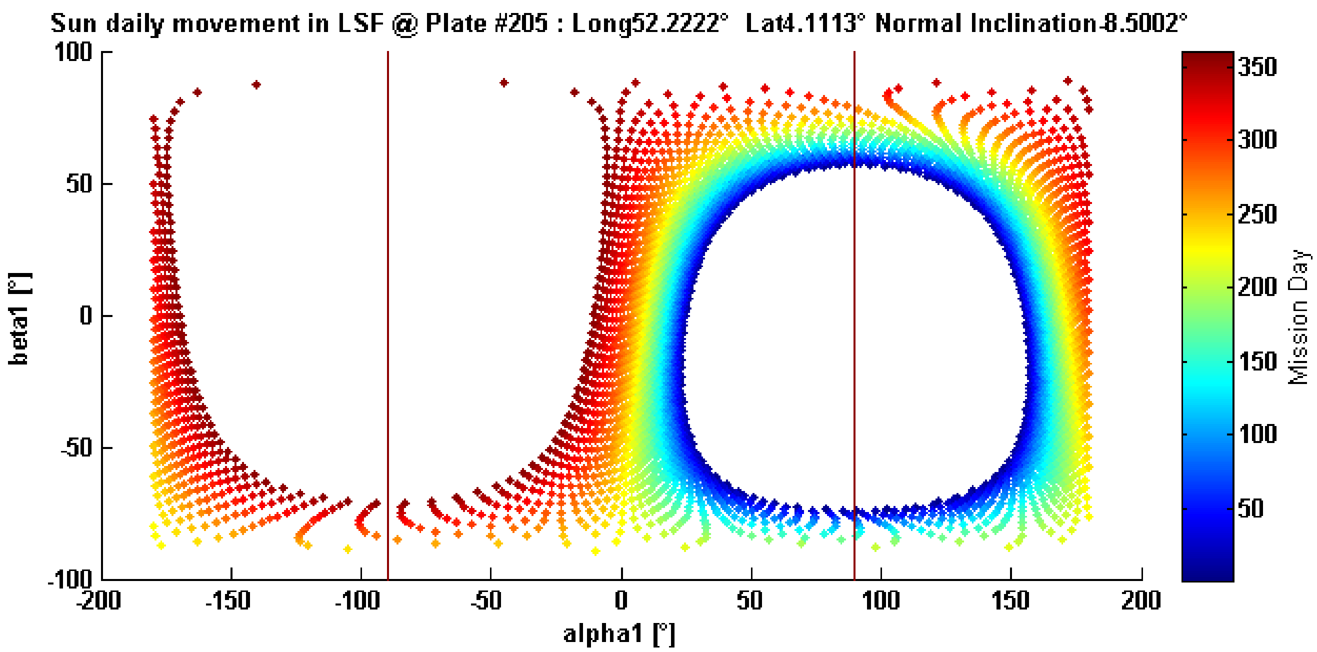

Figure 50 : Plate 205 Sun movement in LSF

Plate 205 [Figure 50**]** normal inclination -8.05°: show a condition opposed to Plate 155, here the Sun Culmination change into opposition occurs at the last cometary day. It is to be noted that, although showing positive latitude value, this plate has a negative normal, thus presents illumination conditions typical of the Southern Hemisphere.

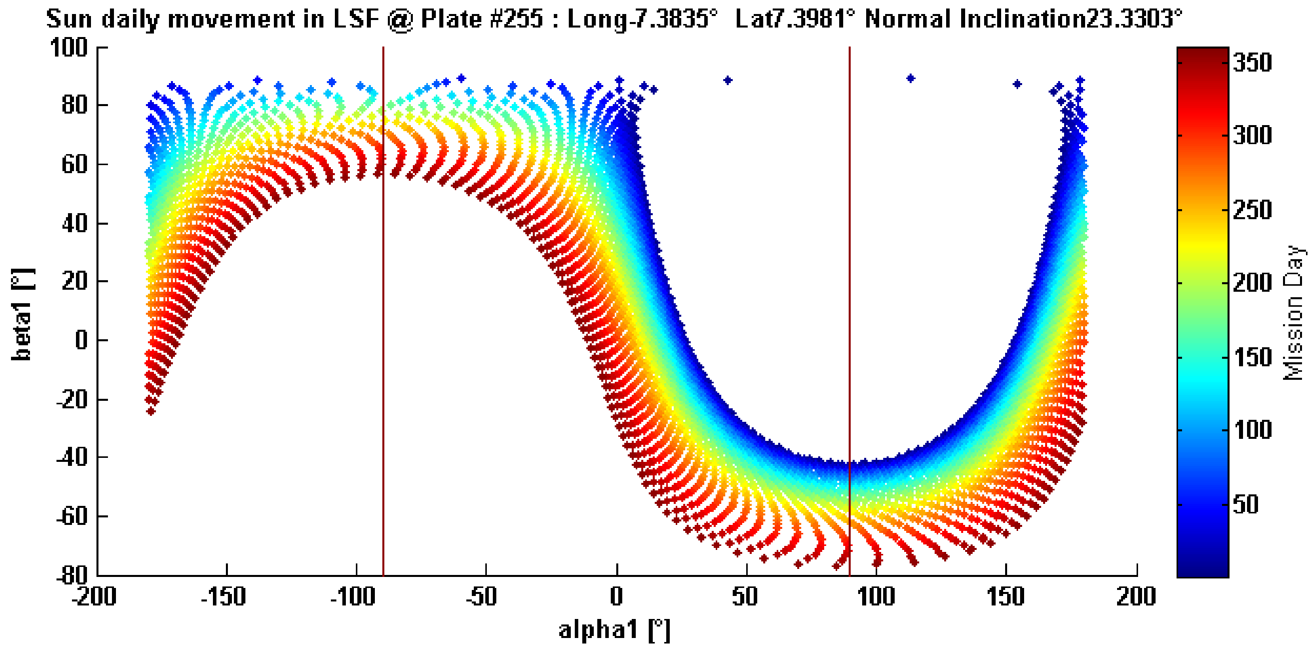

Figure 51 : Plate 255 Sun movement in LSF

Plate 255 [Figure 51**]** normal inclination 23.33°: although showing lower latitude if confronted with Plate 155, it has almost the dame inclination of the normal, thus the Sun Culmination change into opposition occurs the same day. This confirms that the behavior of the Sun in the LSF is governed by the inclination of the normal of the plate with respect to the comet equatorial plane, rather than the latitude of the plate.

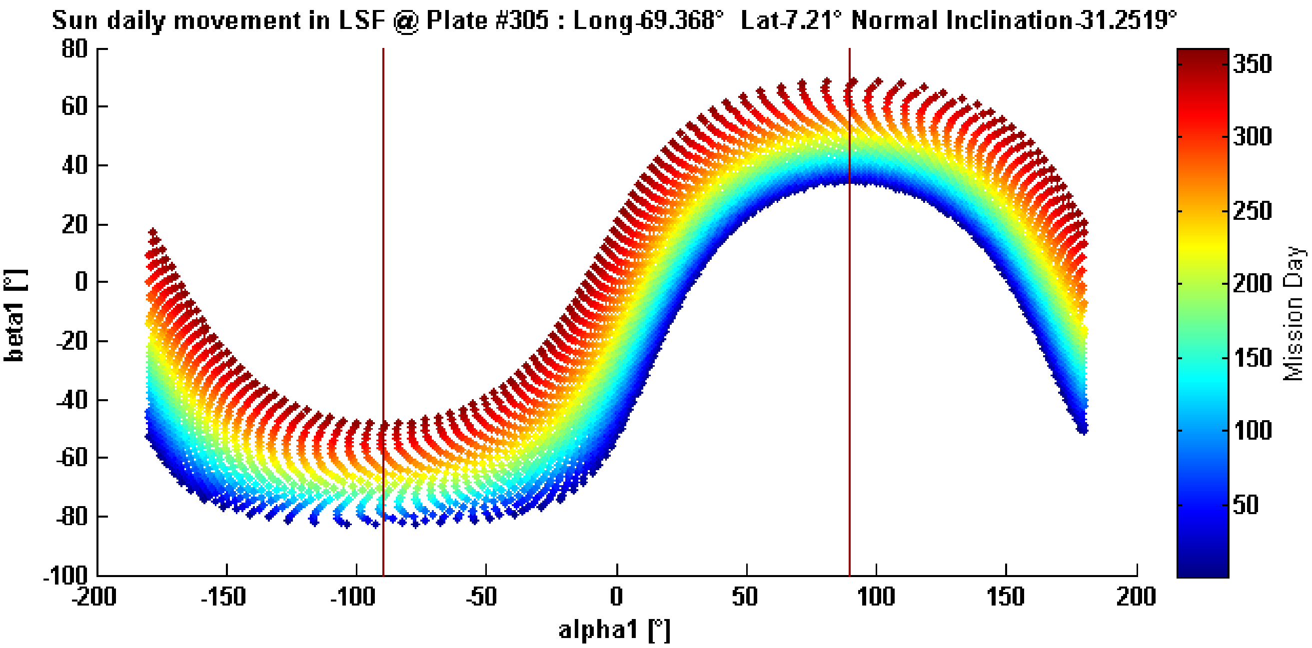

Figure 52 : Plate 305 Sun movement in LSF

Plate 305 [Figure 52] normal inclination -31.25°: this plate is out of the Transition Belt, the locus of cometary sites that are subjected to Sun Culmination direction change. Now culmination is always for $\alpha_1 = 90°$.

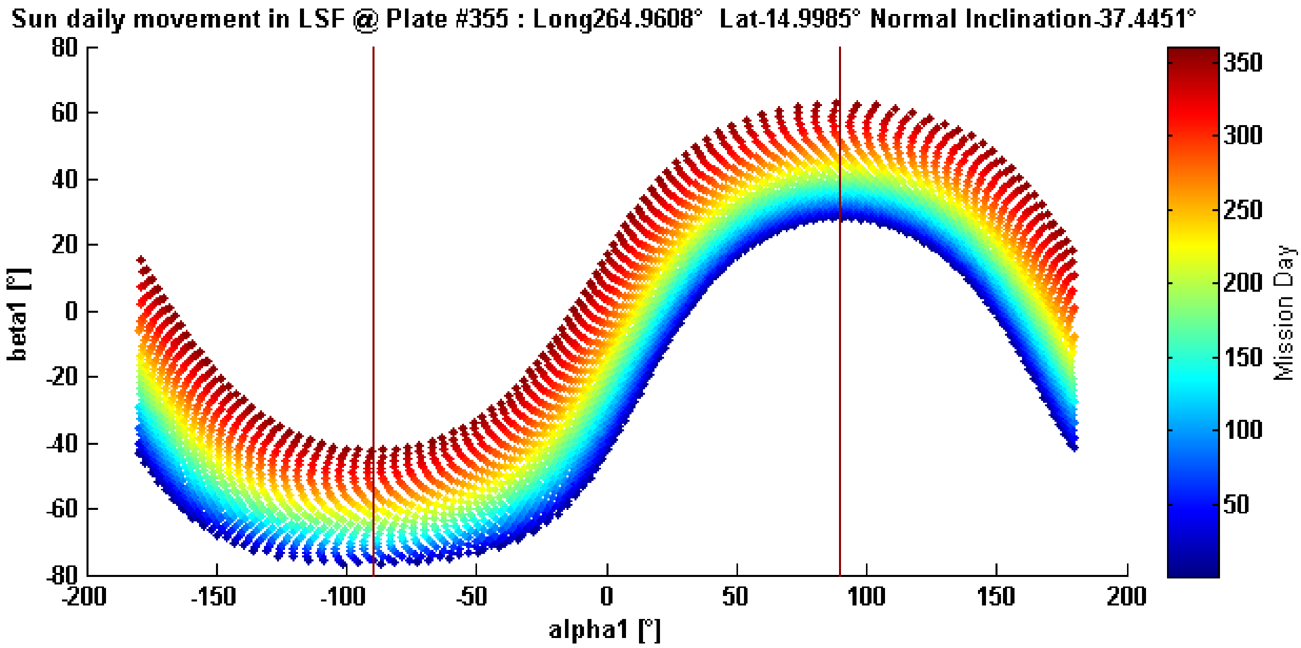

Figure 53 : Plate 355 Sun movement in LSF

Plate 355 [Figure 53] normal inclination -37.44°: the Sun movement in the sky is very similar to the condition of Plate 305.

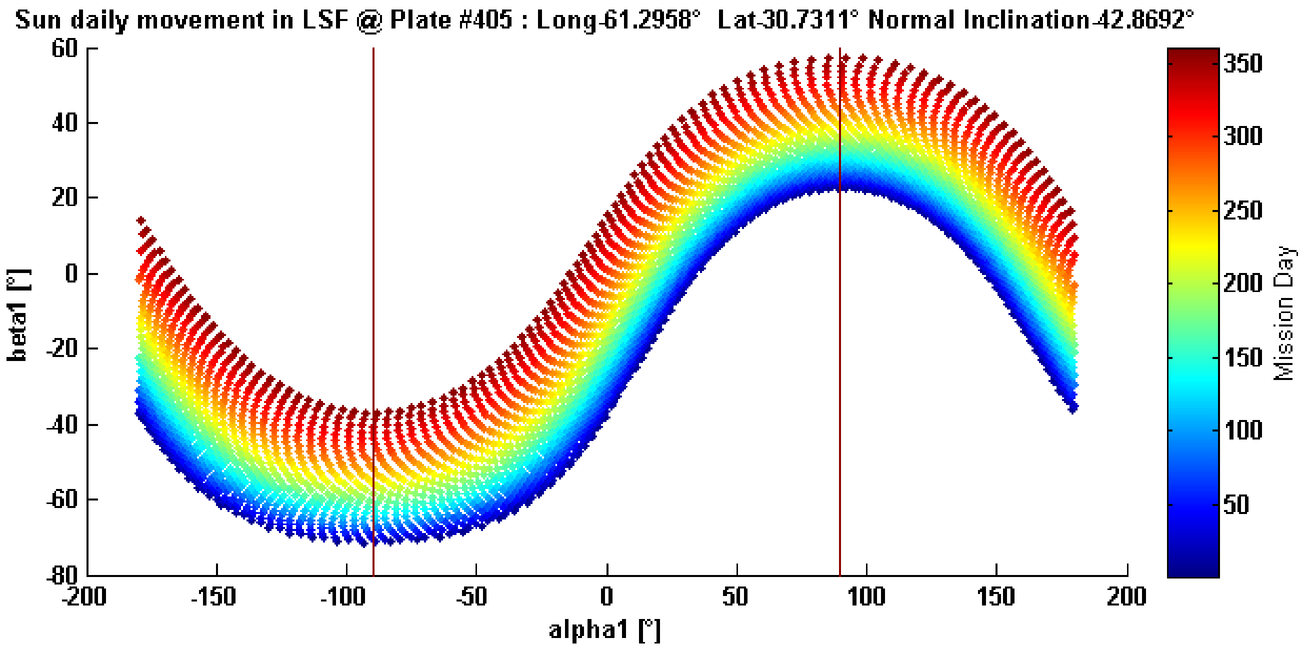

Figure 54 : Plate 405 Sun movement in LSF

Plate 405 [Figure 54] normal inclination -42.87°, the illumination condition is very similar to Plate 305 and Plate 355. In the Southern Hemisphere the illumination conditions are less exotic if confronted with the Southern Hemisphere, this is due to the fact that during the mission the season is changing from Northern Hemisphere summer to autumn: the Transition Belt is located in the Northern Hemisphere.

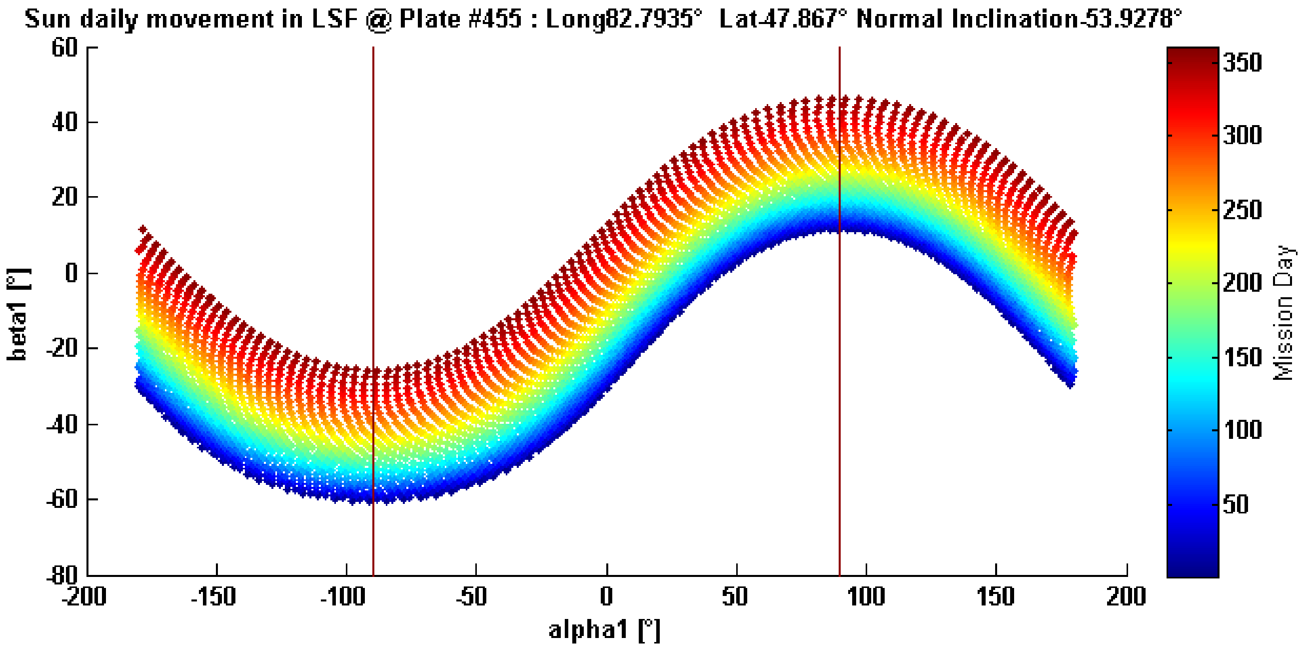

Figure 55 : Plate 455 Sun movement in LSF

Plate 455 [Figure 55] normal inclination -53.93°: the normal is more inclined than the previous plates, this is a plate close to the South Pole, at mission beginning indeed the day is very short.

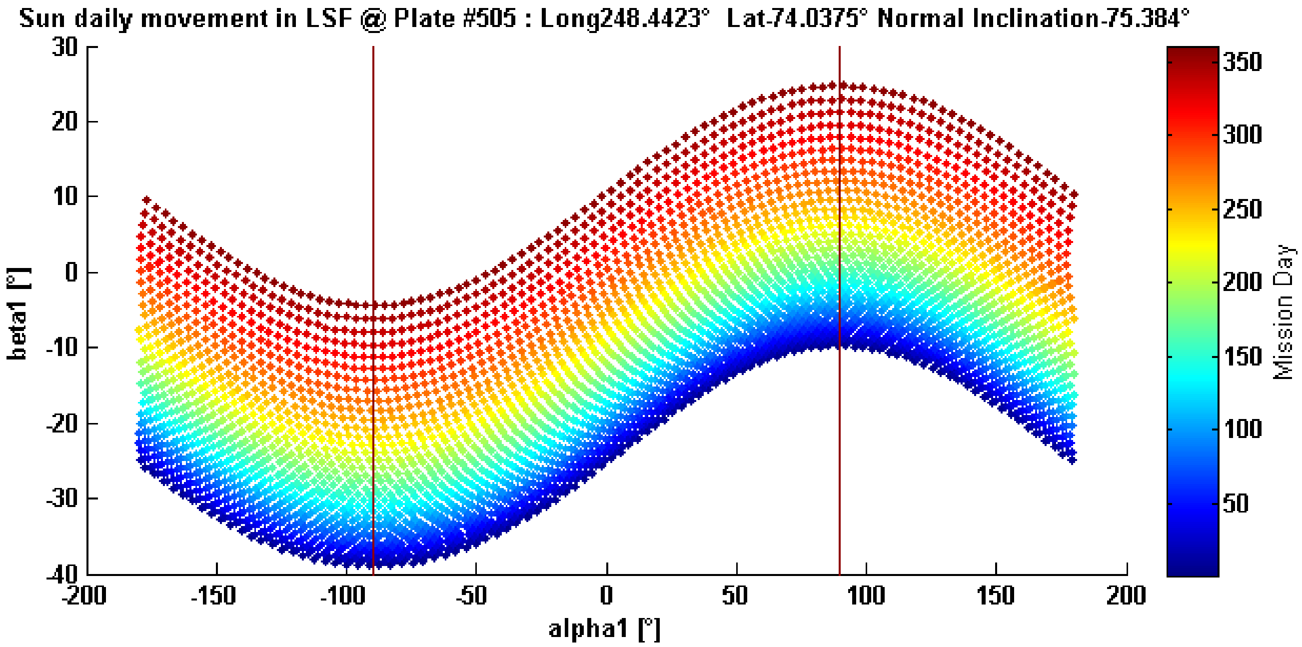

Figure 56 : Plate 505 Sun movement in LSF

Plate 505[Figure 57] normal inclination -75.38°: this is a typical South Pole plate illumination condition, at mission beginning the Sun never rises above the horizon, the contrary at mission end.

From the results deriving from this analysis, the following aspects have been demonstrated:

- The projection in the horizon of the Sun Culmination direction has the same orientation every day of the cometary year and this direction corresponds to the direction of N axis of the LSF or to its opposite (this issue will be further discussed in detail in [Change into opposition of culmination direction]).
- A Transition Belt is present in the comet: a number of plates show during the mission duration a Sun Culmination change into opposition.
- The Sun performs a symmetrical curve with respect to the Sun Culmination direction.
- The plate illumination conditions are related to the inclination of the normal with respect to the comet equator, rather than the latitude.

If results obtained from Topputo et al [34] (as reported in [Philae Optimal Orientation]) are considered together with the results just exposed the following can be assessed: once the lander plane is assumed to be parallel to the cometary plate surface and WALL3 is rotated such that faces the Sun Culmination direction in the horizon, the optimization in terms of Generated Power is guaranteed. However there is an illumination condition that was not considered in Topputo et al work: the condition when the Sun is above the horizon during the entire cometary day. In this condition Philae best orientation is facing WALL3 towards the direction of Sun minimum height over the horizon, which is opposed to the Sun Culmination direction. This is related to the fact that 5 out of 6 solar panels of Philae are disposed orthogonally to the lander plane: if the Sun is low above the plate horizon these plates have best exposure. This aspect is further treated in [Generated Power].

7.2.4Change into opposition of culmination direction

While studying the invariance of the Sun culmination direction in the LSF [Cardinal Points in LSF and Sun Movement in the Sky] for each plate a fundamental aspect emerged: the **change into opposition of the Sun culmination direction** for a number of plates during the mission duration.
As long as the inclination of 67P Churyumov-Gerasimenko equator with respect to its orbital plane is 42.575° (is the complementary angle to 180° of the spin axis inclination angle I=137.425°, the complementary angle is taken so that the retrograde rotation is neglected, as long as it does not influence considerations on the seasons), the illumination conditions experience a wide variation in terms of elevation of Sun culmination in the LSF. In addition the mission scenario is set in a period of time in which the comet has a rapid angular motion in its orbit due to proximity to perihelion, this means that season variations are fast. The combined effect of these two issues lead the Sun culmination elevation to be daily increasing for some latitudes up to trespassing the threshold of 90°. This means, for those plates, that if at mission beginning the Sun culmination direction is N, during the mission changes to the opposition of N. Vice versa if the culmination direction is the opposition of N during the mission changes to N. This effect is also present at Earth but in a narrower range of latitudes due to the minor inclination

of Earth equator with respect to its orbital plane: it is possible to experience the variation of Sun culmination direction only in the latitudes included in the Tropics.
This is valid also for 67P Churyumov-Gerasimenko if Tropics are identified as all the plates that show normal inclination with respect to the equatorial plane included in $-42.5° < \varphi_{\mathrm{Normal}} < 42.5°$ [Figure 57] [Figure 58] . If confronted with Earth in one cometary year a wider range of position on the comet experience the change of Sun culmination direction. Clearly in one cometary year the change occurs twice.

In the case of study the mission 6 months duration is only a fraction of the cometary year, in this period the comet passes from a Northern Hemisphere summer(or Southern Hemisphere winter) condition at the beginning of the mission to a Northern Hemisphere autumn (or Southern Hemisphere spring) condition at the end of the mission, consequently the change in culmination direction occurs only once.

7.2.5Philae Orientation Operations on the plate

A maximum of two orientation manoeuvres is necessary during the entire mission duration in order to guarantee to Philae the best exposure in terms of generated power [Figure 59] [Figure 60] [Figure 61].

First Orientation Manoeuvre is reported in **[**Figure 59**]** for blue plates the initial orientation is with $\theta = \alpha_{rot} = \frac{\pi}{2}$ for red plates $\theta = \alpha_{rot} = -\frac{\pi}{2}$ (for definition of this angles see [Lander Reference Frame – LDR]): once Philae reaches the cometary surface an initial orientation manoeuvre is necessary to orient it towards the Sun culmination direction, or to its opposite direction if the Sun is above the plate horizon for the entire cometary day. There is some indetermination on the geometric condition necessary to establish if Philae is to be oriented towards the Sun culmination direction or its opposite i.e. in a day showing only a small fraction of period with the Sun below the horizon it may be still more convenient to orient Philae towards the opposite direction of the Sun culmination. Due to the complex Philae geometry and wide variety of illumination conditions finding an analytic solution is extremely challenging. This issue is solved creating 3 fake walls, named WALL7 WALL8 WALL9, designed to have exactly the same physical properties, degradation, surface dimensions and temperature of WALL2, WALL3, WALL4, but exposed in the opposite sense of these three walls respectively. The Solar Array Simulator evaluates daily the mean power produced by the summation of WALL 2+WALL3+WALL5 and confronts it with the daily mean power produce by the fake WALL7+WALL8+WALL9: when the power of the least is major than the power of the former Philae is rotated of 180°.

This fundamentally permits to evaluate in each time label of the mission to evaluate whether the best exposition of Philae is towards the Sun culmination direction or its opposite. In addition this techniques permits to evaluate automatically the day of Sun culmination direction change, thus when the Second Orientation Manoeuvre occurs.

Second Orientation Manoeuvre: is reported in [Figure 60][Figure 61], the day of mission reported in each plate is the day at which this second manoeuvre must be performed, thus when δ=1 and the angle θ between LRF and LSF becomes $\theta = \alpha_{rot} + \pi\,\delta$ (for angles definition see [Lander Reference Frame – LDR]). If the day of the second manoeuvre is set to zero, no Second Orientation Manoeuvre is necessary.

The Second Rotation Manoeuvre must be performed by Philae when the Sun culmination direction changes into opposition, the lander must be rotated in its plane of 180°. The Sun culmination change of direction creates a very inefficient illumination condition as long as Philae would show the BALCONY to the Sun culmination direction, and the Sun would perform a symmetrical curve with respect to it. In addition this condition is not favourable also in terms of operations: Philae scientific payload is mounted in the BALCONY and designed in order to operate in the shade. Therefore when this condition occurs Philae will have to perform a 180° rotation around its z axis to maintain an optimal exposition.

A second orientation manoeuvre is also necessary for those plates that at mission beginning show WALL3 oriented towards the opposite to the Sun culmination direction as long as they see the Sun for the entire cometary day: when the season changes during the mission the Sun begins to set below the horizon in the opposite direction of Sun culmination, thus Philae need to be rotated of 180° towards the culmination direction.

Philae Orientation Change Transition: during the analysis a transition of few cometary days was observed when Philae has to perform the 180° rotation. This means that the summation of daily power of WALL2+WALL3+WALL4 is very similar to the one produced by WALL7+WALL8+WALL9 for some days of transition. Transition can last up to 5-7 days, than the orientation of Philae stabilizes. In this respect the day of manoeuvre reported in [Figure 60][Figure 61] are related to the last day of transition, thus to the first day of Philae orientation stabilization. This period of transition occurs only for few tens of plates, the large majority of plates show a sharp transition that occurs in a single day.

In general terms the results of the previous sections permit to divide the plates into four categories, depending on the number of manoeuvres and the comet location, they are now presented for decreasing latitudes. It is to be remarked that Philae orientation manoeuvre is optimized automatically and orientations are reported in **[**Figure 59**]** [Figure 60][Figure 61] , these general considerations are useful for results interpretation only.

North Pole two Orientation Manoeuvres plates: a number of plates on the comet North Pole at mission beginning see the Sun above the horizon for the entire cometary day, for those plates the best orientation is when WALL3 is oriented towards the opposite direction of Sun culmination. During the mission the season for the North Pole changes from summer to autumn, thus the Sun begins to set below the North Pole plates horizon, the sunset occurs in the opposite direction of Sun culmination, this means that Philae most efficient orientation for power generation is with WALL3 pointing towards the Sun culmination direction, thus Philae is rotated of 180°. Philae will then keep this orientation until mission end.

High Latitudes one Orientation Manoeuvre plates: immediately below North Pole there is a belt of plates that do not see the Sun for the entire cometary day at mission beginning, thus the initial orientation for Philae is with WALL3 facing the Sun culmination direction. For these plates no further manoeuvres are necessary during the mission, besides the initial orientation after landing.

Transition Belt two Orientation Manoeuvres plates: immediately below the previous category there is the Transition Belt: the belt of plates that are liable to Sun culmination direction change into opposition. These plates are located in the Tropics as defined in [Change into opposition of culmination direction], thus they can not see the Sun for the entire cometary day: at mission beginning Philae is oriented towards the Sun Culmination direction. A Second Orientation manoeuvre is necessary if the Sun culmination direction changes. The Sun culmination direction changes in the plates that are liable to it depending on the duration of the mission: the first to change culmination direction are those that have the most inclined normal with respect to the comet equatorial plane, as observed in [Cardinal Points in LSF and Sun Movement in the Sky].

Transition Belt one Orientation Manoeuvre plates: is identified by those plates liable to Sun culmination direction change, thus located into the Tropics, that do not need a second orientation manoeuvre as long as the mission duration is too short to provoke the Sun culmination direction change.

Below this last category the same categories can be found but reflected in the Southern Hemisphere, thus with inverted seasons. Southern Hemisphere plates landing sites are not interesting for the mission as long as too scarce power generation is guaranteed at mission beginning to permit a daily sustainable power balance, as is discussed also in [Generated Power]. For these reasons behaviour of these plates is not analyzed.

As a consequence to these results two more observations are to be remarked:

- results just reported depend strongly on the spin axis orientation: Philae initial orientation, the day of the second manoeuvre and the necessity to perform it are dependent on the spin axis orientation.
- in this analysis shadowing effects are neglected, as reported also in [Simulation- 1 No Shadowing] : if the plate is shaded the lander orientation is only close to optimum and the best orientation should be studied day by day simulating which is Philae best orientation through a 360° degree of freedom rotation.

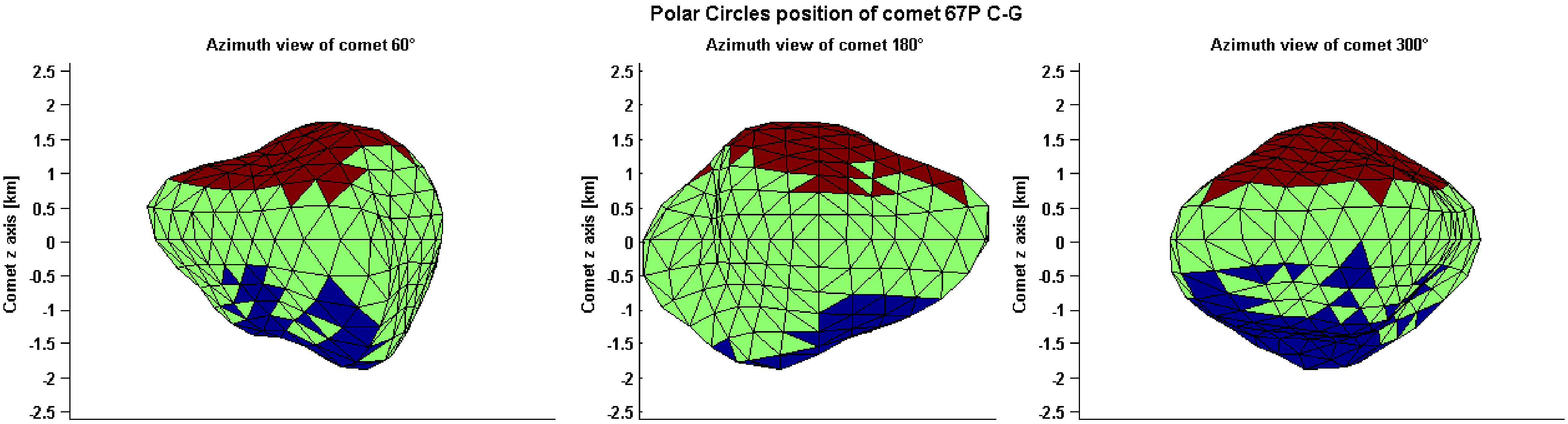

Figure 57 : Comet 67P C-G Polar Circles

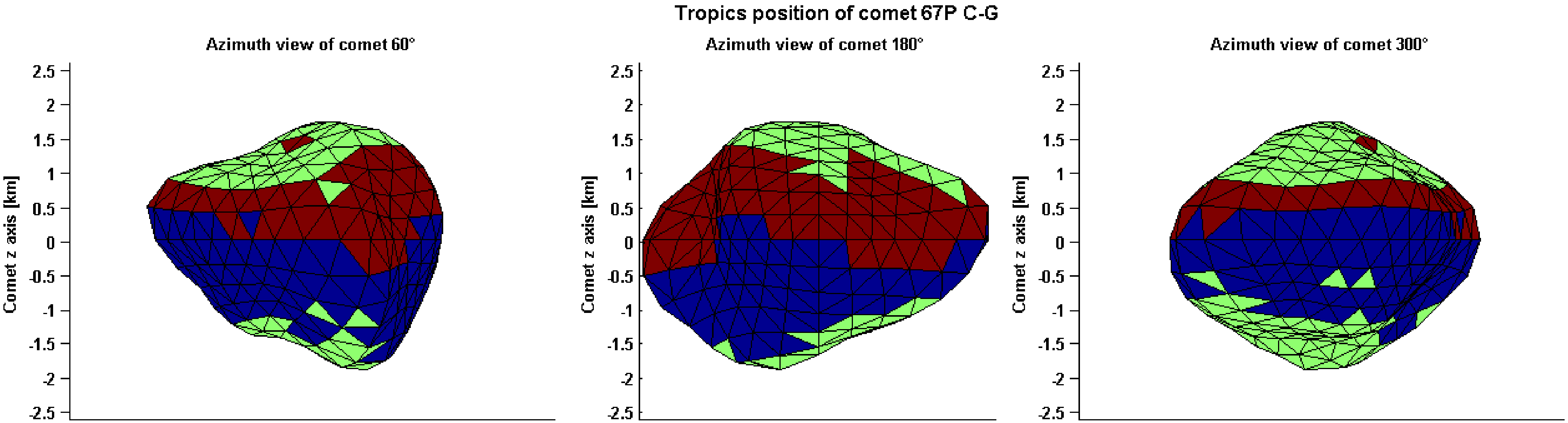

Figure 58 : Comet 67P C-G Tropics

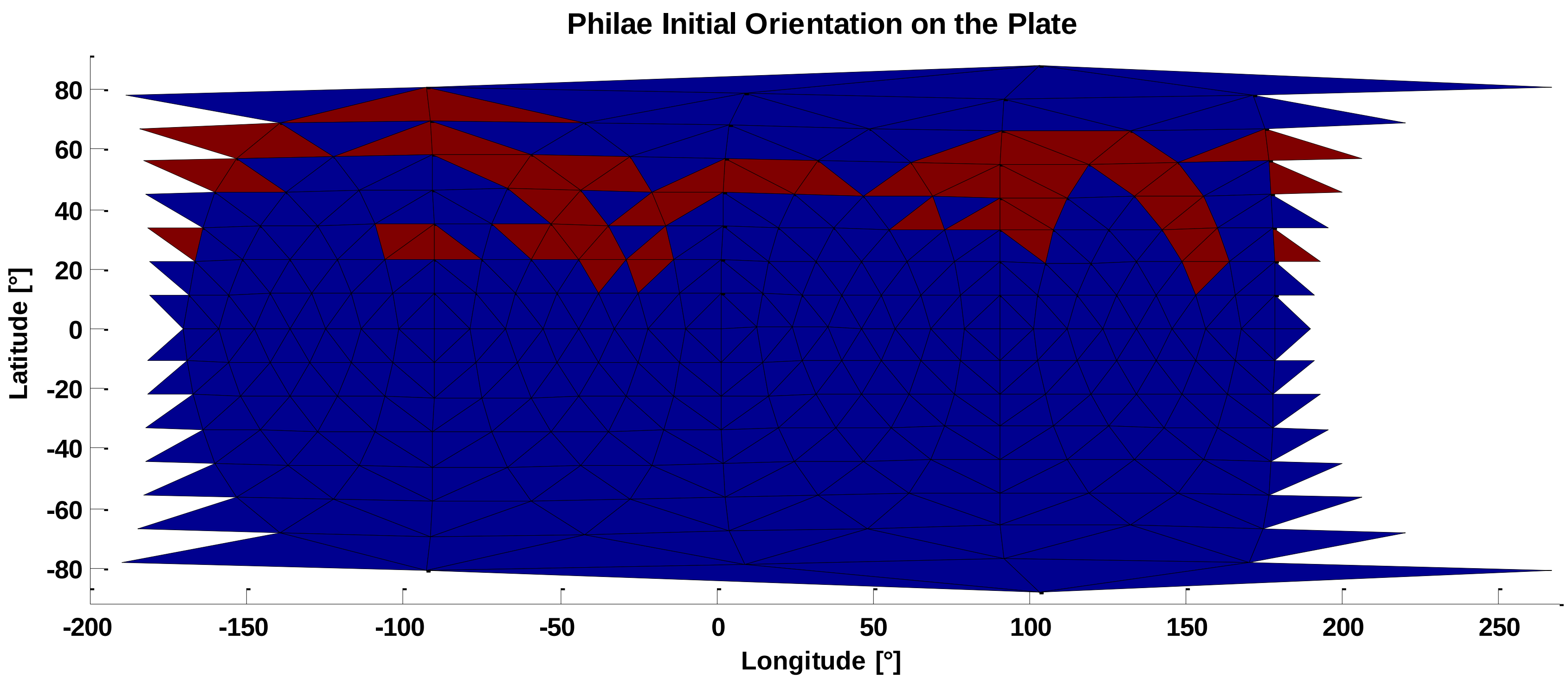

Figure 59 : Philae Initial Orientation on the plate

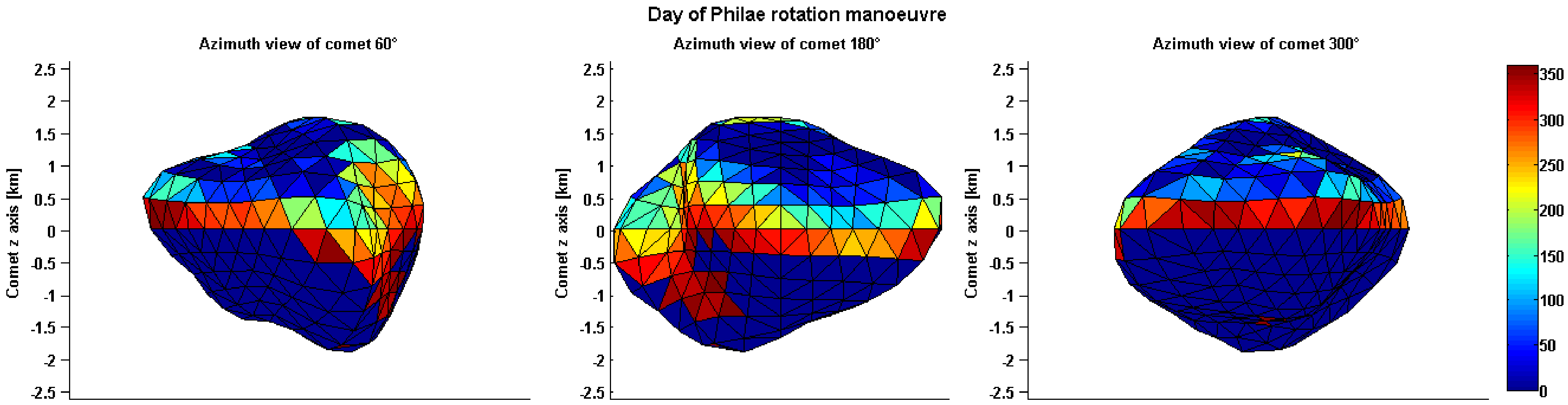

Figure 60 : Philae Day of rotation manoeuvre

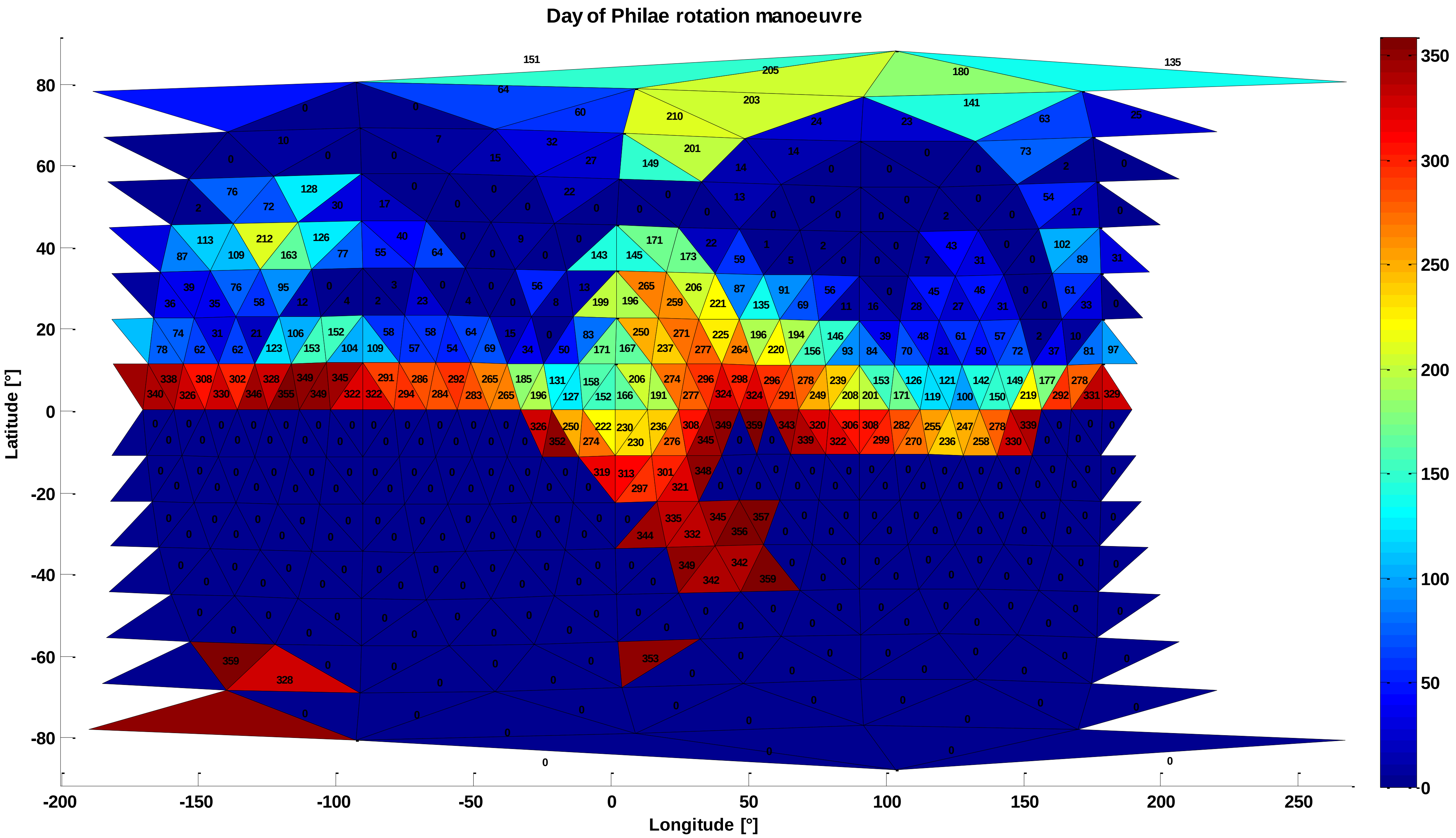

Figure 61 : Philae Day of rotation manoeuvre

7.3 Insolation

Total Mission Insolation [W/m^2], [Figure 62][Figure 63] it can be observed the highest values of insolation are located in low-middle latitudes of the Northern Hemisphere and for some latitudes of the Southern Hemisphere. The strong longitudinal diversity of the comet is also noticeable: given a latitude position, the plate normal inclination varies depending on the longitude, so different illumination condition can be found for the same latitude in the comet. Once again this is related to the plate normal inclination with respect to the comet equator, but effects related to shadowing are also noticeable.

The locations most subjected to Insolation shows values of 90W/m^2 and are located in the Northern Hemisphere Tropics and partially in the Southern Hemisphere Tropics. As discussed in [Comet activity and erosion] areas most subjected to Insolation are those where major erosion occurs as long as they are the locations where jets and fans may be present. Comet activity that lead to erosion of magnitude of meters is estimated to be 4-7% of the cometary surface. This fraction of extremely active surface may be located in a portion of the area that show higher insolation that contemporarily show suitable surface composition: erosion is likely to be major where surface composition is mainly constituted by ice and minimal in sites that show dust crust.

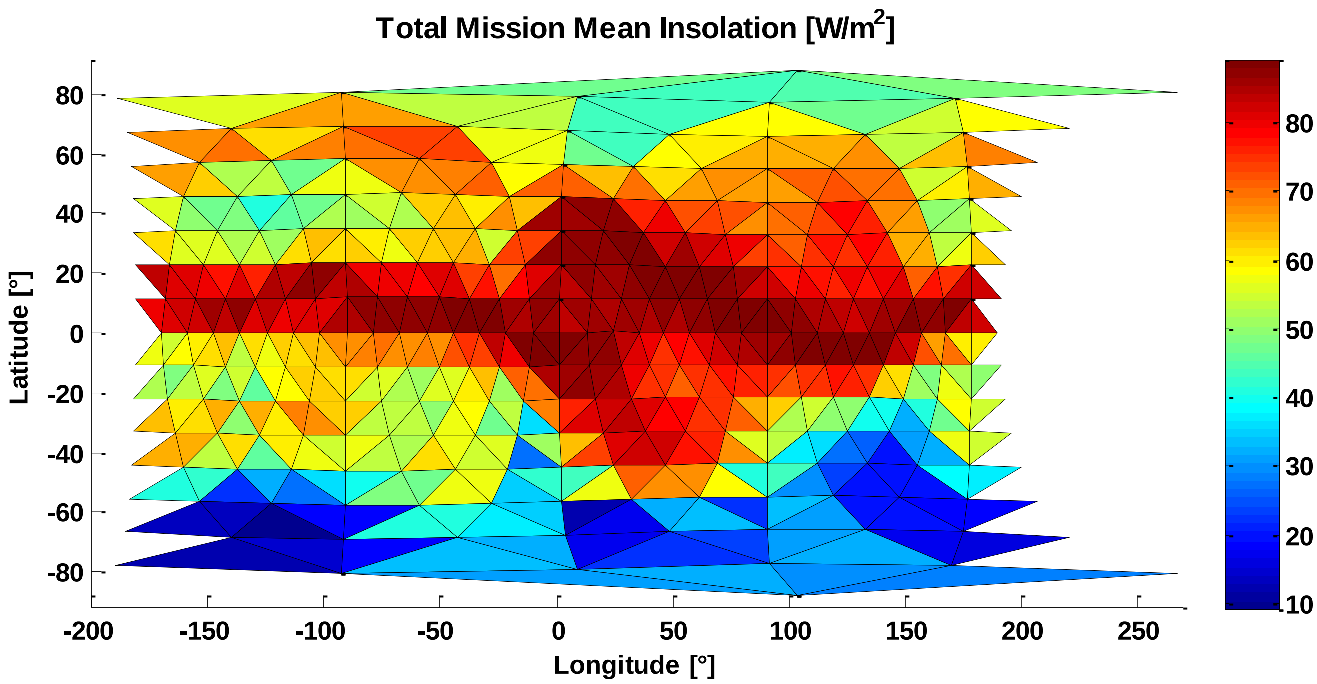

Figure 62 : Total Mission Insolation 2D Map

Seasonal Mean Insolation [W/m^2]: from [Figure 64] to [Figure 69]: show that illumination conditions change during the mission from a Northern Hemisphere summer to a Northern Hemisphere autumn, the subsolar point moves towards South. At Season6 is noticeable that the most suitable insolation conditions move from the Northern Hemisphere to the Southern Hemisphere. Maximum values of Seasonal Mean

Insolation increases noticeably during the mission duration, this is clearly due to the fact that the comet is approaching perihelion and the value of Solar Constant increases. At mission beginning [Figure 64] the solar constant is very low SC=0.11 but in this period North Pole plates can see the Sun for the whole cometary day at medium altitudes on the horizon, consequently the Mean Insolation maximum value is about 60W/m^2, about half the Sun irradiance at that distance.
In the other hand at mission end [Figure 69] the solar constant increases noticeably up to SC=0.39 but in this period at the Equator the Sun performs typically a 180° arch in the sky (culmination is close to the zenith) during half cometary day. Thus the Sun is present for half cometary day at average middle elevation angles, as a consequence the Mean Insolation at mission end is only about one third of the irradiance at that distance.
South Pole sites in the other hand are in a winter condition, the Sun never rises above the horizon, for some locations the insolation is null at mission beginning. These sites can be discarded from the suitable landing sites as long as no power can be generated.

If Seasonal Insolation is seen from the **comet activity/erosion** point of view, is evident that different cometary sites are likely to activate in different orbital position, thus in different period of the mission. At mission beginning the Northern Hemisphere shows highest insolation thus is the area where comet activity is mainly localized. However in this period the comet is retained to be scarcely active due to the fact that insolation values are still low. Consequently it can’t be assessed whether this area can constitute a risk for the mission. When Seasonal Mean Insolation values increase the locations of maximum values change, moving towards South. At mission end the strongest cometary activity will be likely localized in the Southern Hemisphere, in this period strong sublimation probably takes place as long as maximum insolation values are about 2.5 times the initial maximum values. These conclusions are in agreement to Scheicher [14] conclusions as reported in [Comet activity and erosion], who noticed from observation that across perihelion the active locations of the comet change hemisphere.
It is to be noted that the movement during the mission of the location of comet activity is in agreement with the landing sites that are purposed in the following section [Generated Power], localized at high latitudes in the Northern Hemisphere. If the condition of activity at mission beginning can be sustained, in particular in the SDL phase, these sites provide the safest locations for the further mission duration.

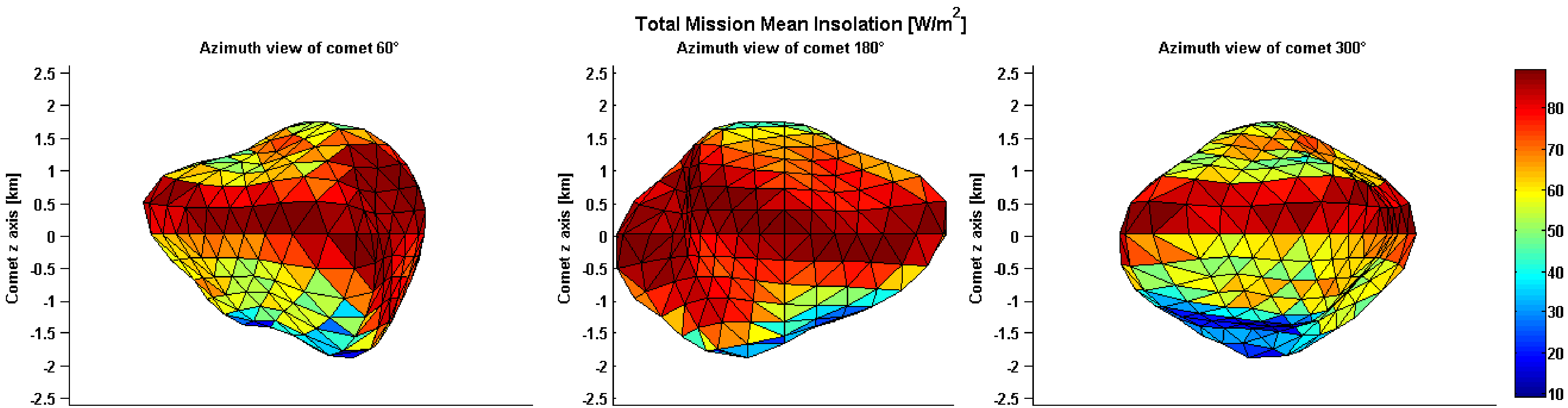

Figure 63 : Total Mission Mean Insolation

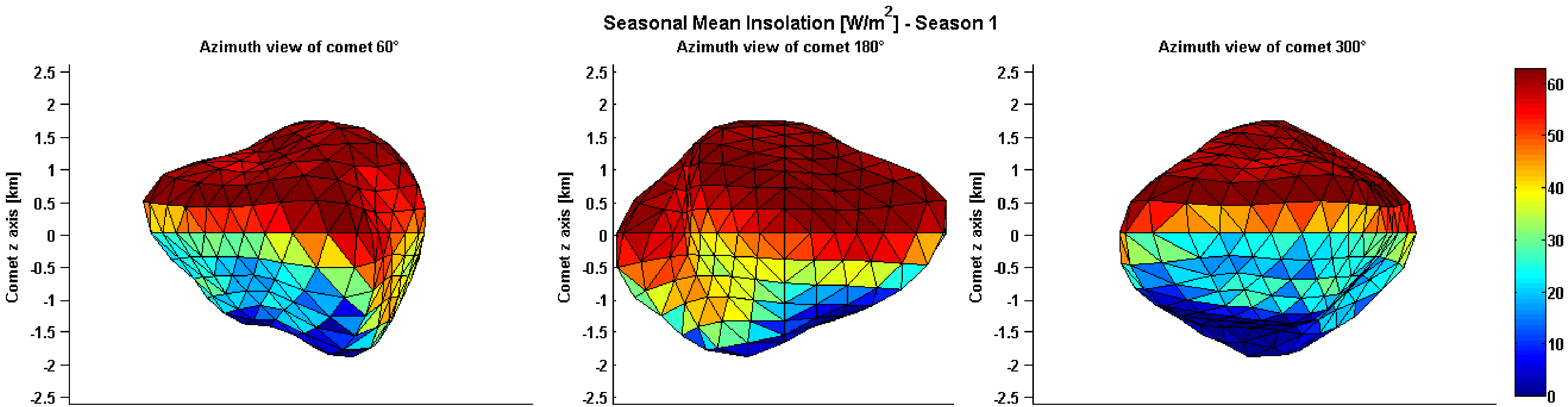

Figure 64 : Seasonal Mean Insolation - Season 1

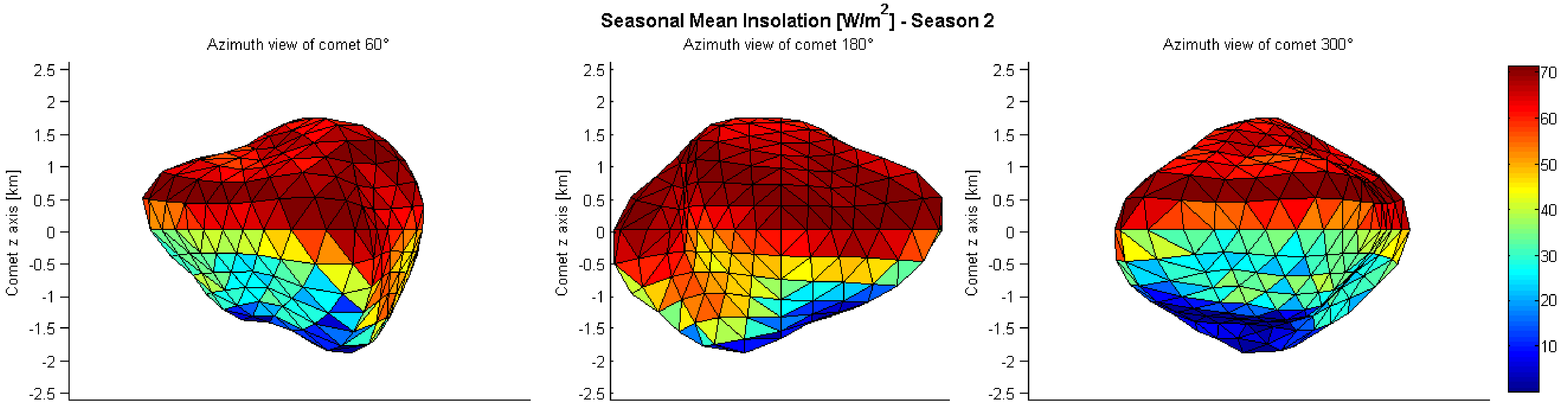

Figure 65 : Seasonal Mean Insolation - Season 2

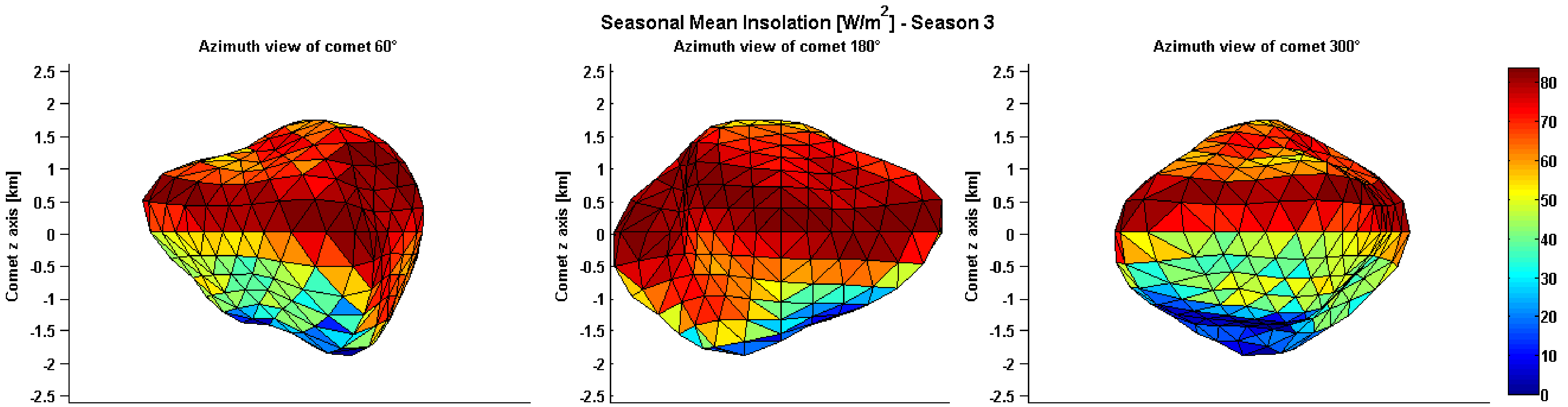

Figure 66 : Seasonal Mean Insolation - Season 3

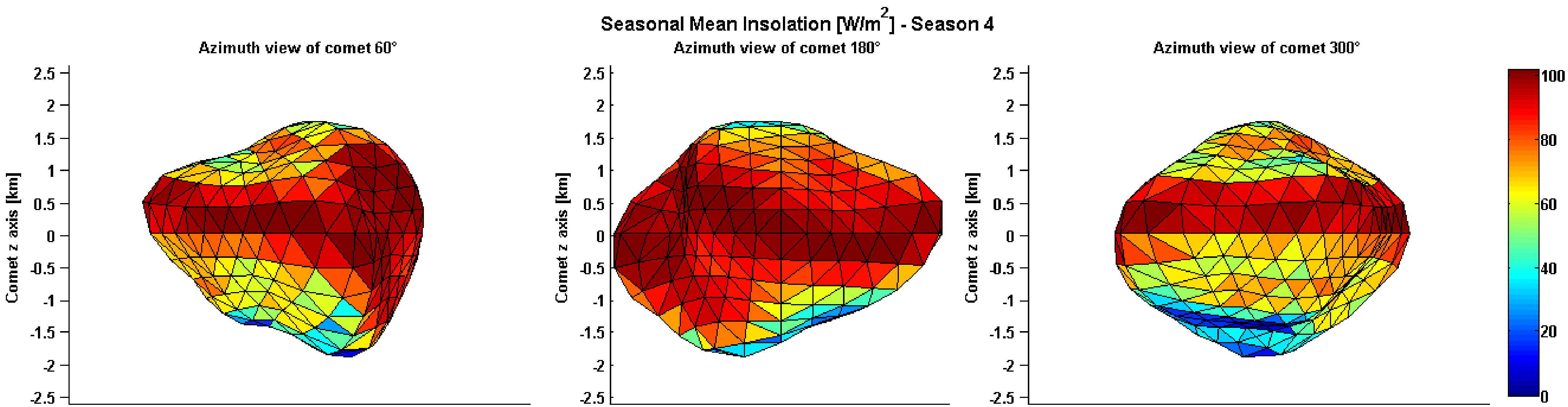

Figure 67 : Seasonal Mean Insolation - Season 4

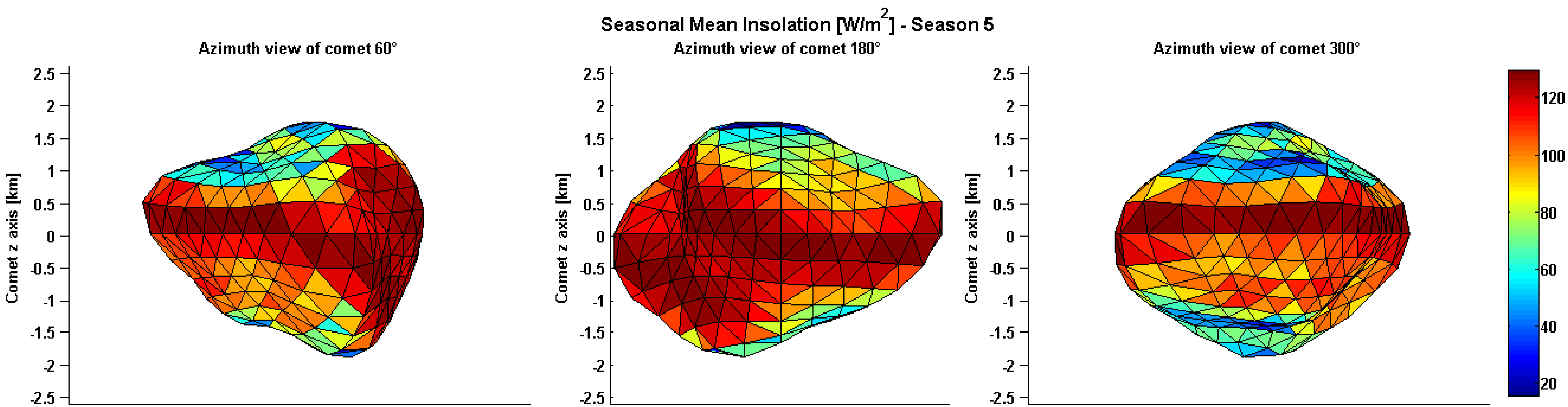

Figure 68 : Seasonal Mean Insolation - Season 5

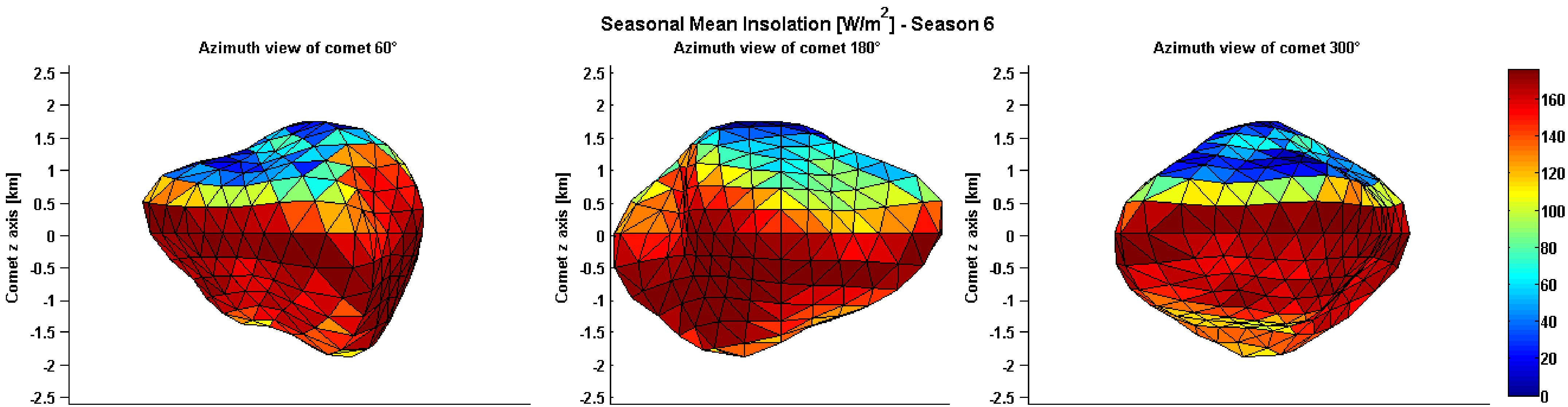

Figure 69 : Seasonal Mean Insolation - Season 6

7.4 Generated Power

Before introducing to the results related to the Generated Power, it is to be recalled that the power generated was calculated assuming the orientation of Philae as described in [Philae Orientation Operations on the plate], thus for plates liable to shadowing the Generated Power is only close to optimum. To optimize the generated power when a plate is shaded it would be necessary to evaluate the daily generated power for all 360° possible orientations of Philae in the plate. This procedure is computationally too demanding to be simulated, in addition the generated power obtained with the presented method is estimated to be not far from optimum. Results of this section are related to [Simulation–2 Shadowing].

Total Mission Mean Generated Power [W] [Figure 70] [Figure 74] shows best performances in the Northern Hemisphere, in particular for plates located in hills/humps at latitudes ranging 15°÷80°. The 10 plates showing highest values of Mission Generated Power are reported in [Table 27]. As visible these plates show a very small range of normal inclination with respect to the comet equator and are located, as visible also in [Figure 70] similarly to the disposition of plates that have initial orientation for $\theta = \alpha_{rot} = -\frac{\pi}{2}$ as visible in [Figure 59] and discussed in [Philae Orientation Operations on the plate]. This means that the category of plates named **High Latitudes one Orientation Manoeuvre plates** (see [Philae Orientation Operations on the plate]) are those that show best Power Generation condition for the overall mission. This category of plates have a narrow range of inclination with respect to the comet equator, from 46.4° to 59.2°.

Mission Mean Generated Power [W]	Plate #	Normal Inclination [°]	Latitude	Longitude [°]
9.8145	133	59,19	26.93	263,76
9.7742	132	57,31	30.77	257,56
9.7666	38	56,79	53.16	20,61
9.7551	26	56,86	60.25	165,40
9.7508	99	56,90	42.21	-11,85
9.7393	23	56,07	63.38	115,03
9.7352	140	55,75	26.84	-35,78
9.7240	21	55,84	59.45	79,91
9.7229	22	55,96	59.35	101,21
9.7212	120	55,42	26.01	157,78

Table 27 : Mission Mean Generated Power best performance plate

In [Figure 72] are reported the 56 most suitable plates in terms of Total Mission Generated Power, if confronted to the 56 High Latitudes one Orientation Manoeuvre plates of [Figure 59], 53 out of 56 coincide.

This proves that High Latitudes one Orientation Manoeuvre plates have particular illumination conditions that render them the most suitable in term of generated power for the overall mission. The 56 plates showing best Total Mission Generated Power have power values that range from 8.96W and 9.81W. High Latitudes one Orientation Manoeuvre plates have power values that range from 8.84 W to 9.81W.

The location of the most suitable areas is restricted to a smaller area in the Northern Hemisphere if compared with the Total Mission Insolation. This is due to a fundamental aspect: for an optimal power production a generic suitable location is a plate that is exposed at Sun for most of the cometary day with a relatively low Sun elevation angle: Insolation indeed is evaluated with the cosine of the angle between the plate normal and the Sun direction, therefore is elevate when the Sun is high in the plate horizon, while Generated Power is produced through solar arrays that are disposed vertically with respect to the plate horizon (with the exception of WALL6), consequently their efficiency is at best when the Sun is low in the horizon. This is possible also as long as in the comet there is no air mass effect: the light scattering is considered negligible at all elevation angles, because of the cometary extremely rarefied atmosphere, as assumed in [Illumination Assumptions].

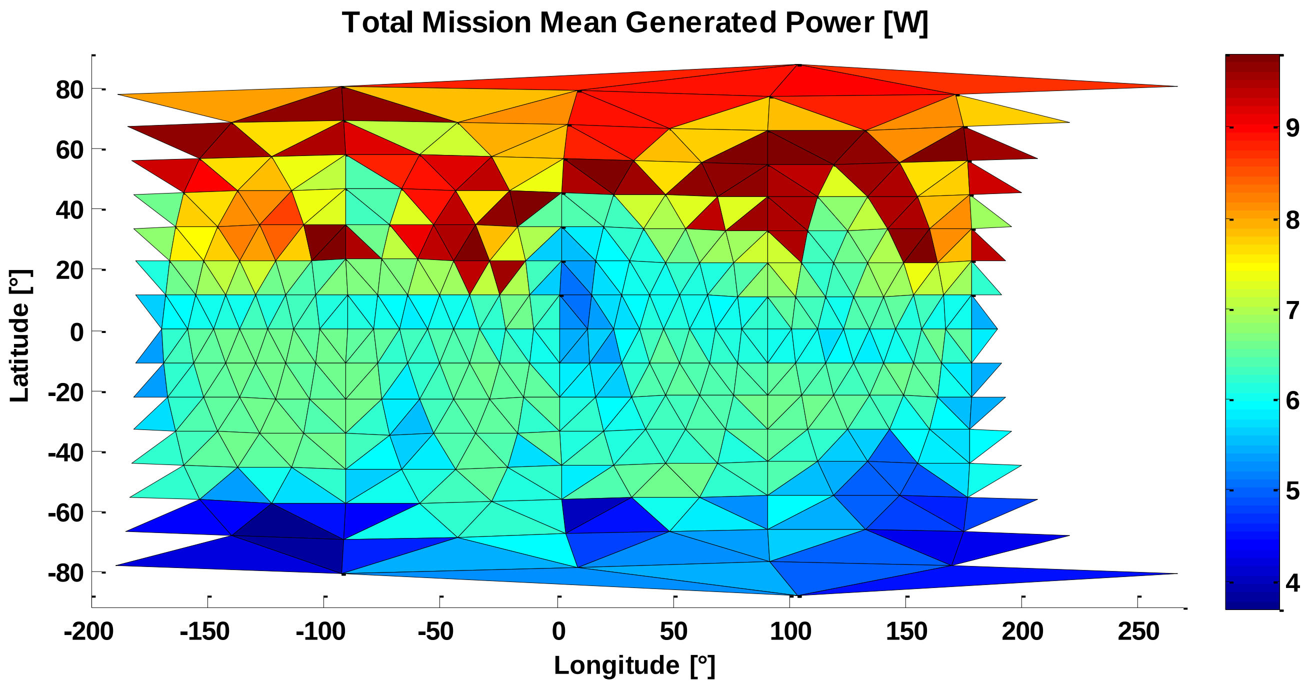

Figure 70 : Total Mission Mean Generated Power

Total Mission Mean Generated Power show also a strong longitudinal variation, this is due to the effects of shadowing, thus to the comet irregular shape. For a clearer understanding of this aspect also results of Total Mission Mean Generated Power without shadowing are reported in [Figure 71] and [Figure 75]. When compared the two series of figures permit to outline the overall loss of generated power due to shadowing effects in most of cometary surface. The comparison of shaded and non-shaded analysis permits to outline the advantage of a landing site located in hills/ humps, where no attenuation related to shadowing is observable. The confrontation of the two figures permit also to assess that effects of shadowing can not be neglected as long as best generated power performances are reduced in value and the most suitable sites are located in a more restricted area .

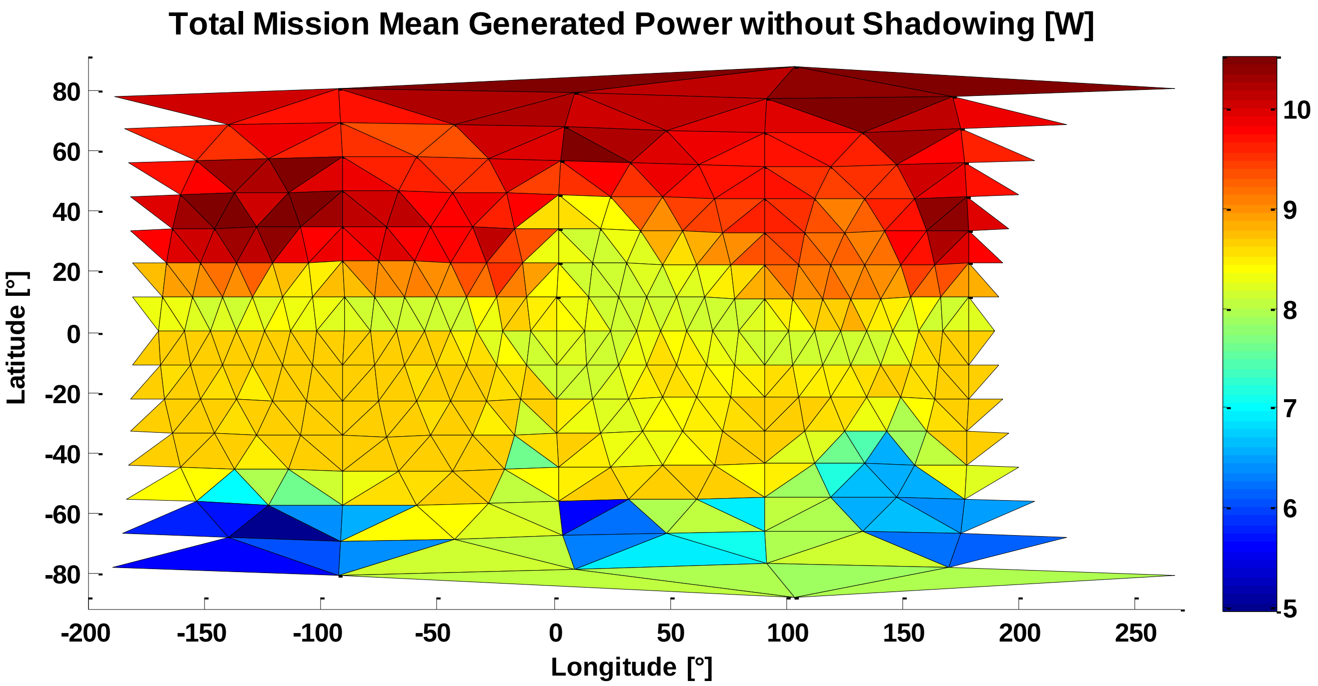

Figure 71 : Total Mission Mean Generated Power without Shadowing

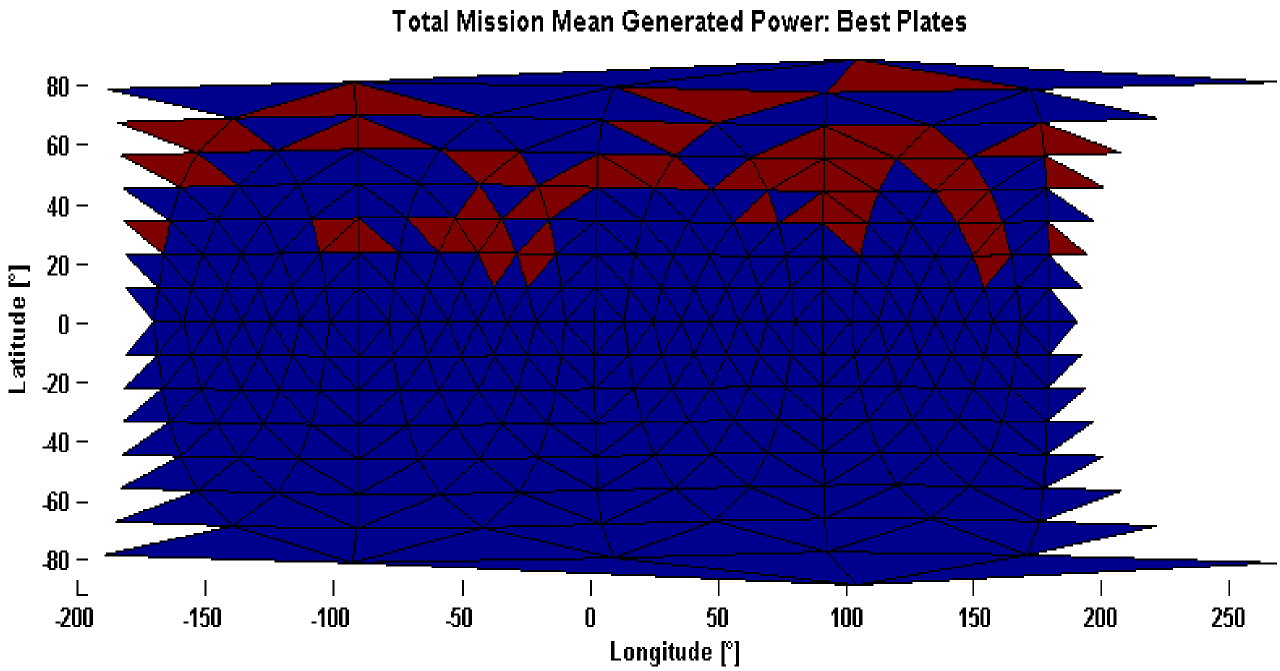

Figure 72 : Plates showing best Total Mission Mean Generated Power

It is to be remarked that the results presented above are relative to simulations that display the same mission duration of 360 days. This means that to obtain the values of **Total Mission Generated Power** for each plate expressed in [Wh] is necessary to multiply the results by the mission duration in seconds and convert from Joule to Wh.

The result in [Figure 73] is dedicated the **plates that respect over each cometary day the Minimum Daily Power Thresholds**. Plotted thresholds are the following:

- light blue, plates that for all cometary days can produce at least daily mean 4.11W
- yellow plates that for all cometary days can produce at least daily mean 5.11W
- red plates that for all cometary days can produce at least daily mean 6.11W. None of these plates trespass the 7.11W threshold.

It can be noticed that plates presented above that show best power generation conditions, named as High Latitudes one Orientation Manoeuvre plates, are only included in the lower 4.11W threshold. This is due to the fact that for the first days of the mission these plates show power levels that are lower than 5.11W (this can be noted also in plots reported in [Appendix 2]). If the first cometary days are neglected these plates can be included in the minimum 5.11W threshold. In terms of Power thresholds the plates that respect the 6.11W Daily Minimum Power Threshold can be separated in two categories, defined as follow.

North Pole 6.11W Threshold plates: are the plates that show 6.11W Daily Minimum Power Threshold and are located in latitudes greater than 50°. This category show best performances in terms of Daily Minimum Power Threshold and contemporarily permit elevate Total Mission Mean Generated Power, assessing at about 8.5W. These plates have the advantage of presenting the best power generation condition in the comet in the first cometary days, when the Solar Constant is the lowest, as visible also in Season1 and Season 2 results of [Seasonal Mean Generated Power].

Middle latitude Northern Hemisphere 6.11W Threshold plates: are the plates that show 6.11W Daily Minimum Power Threshold and are located in latitudes ranging between 25° and 50°. This category show best performances in terms of Daily Minimum Power Threshold and assess Total Mission Mean Generated Power at about 8W.

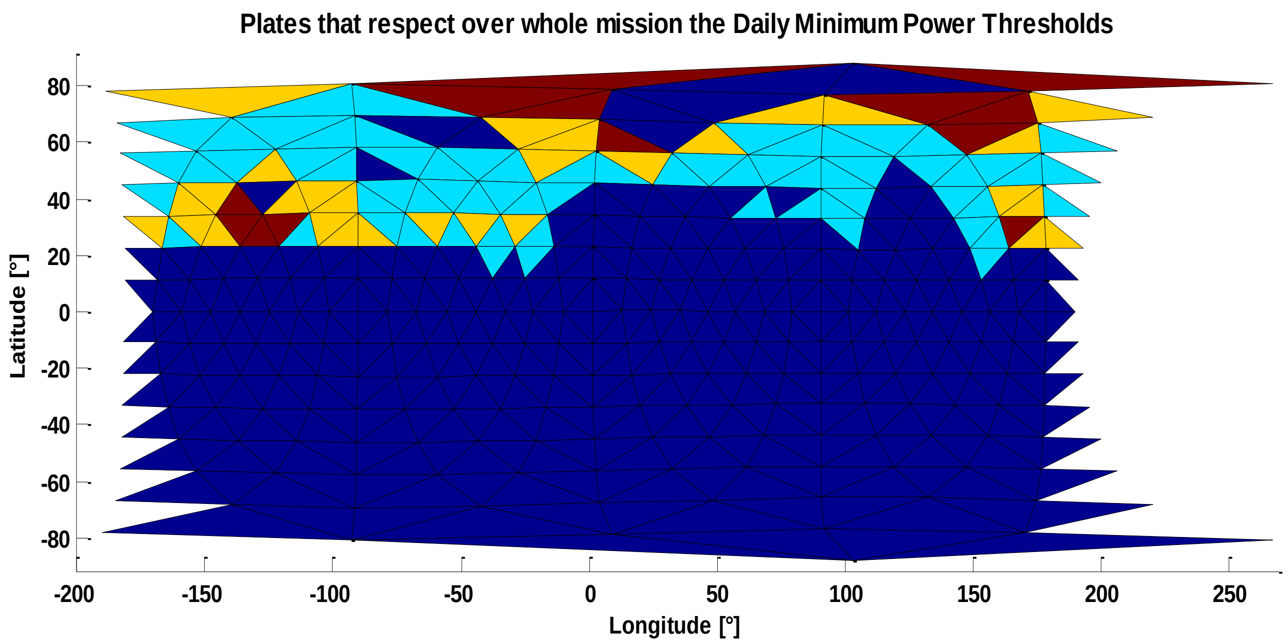

Figure 73: Daily Minimum Power Thresholds

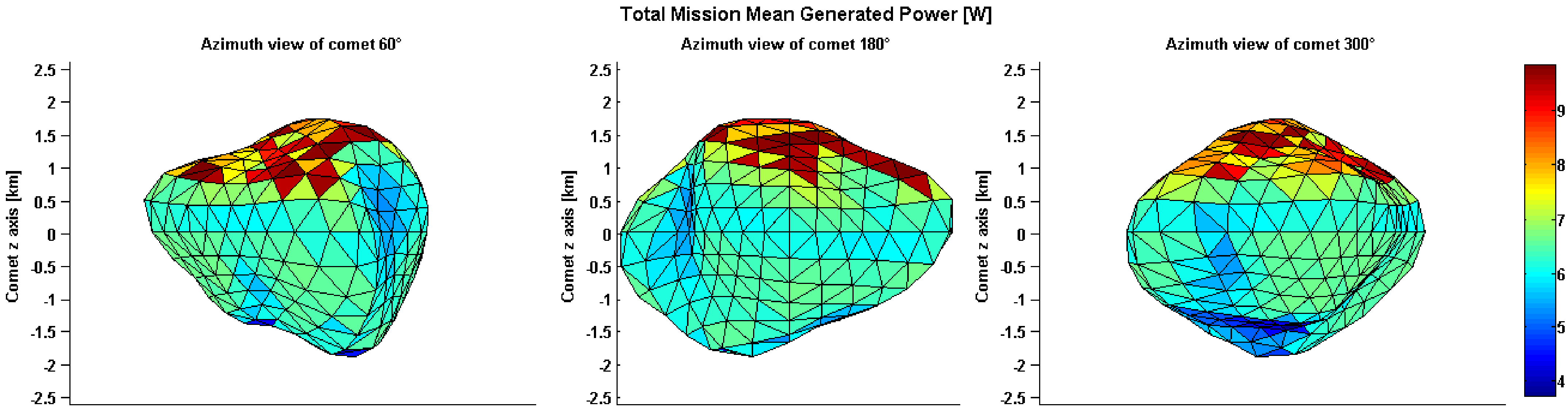

Figure 74 : Total Mission Mean Generated Power

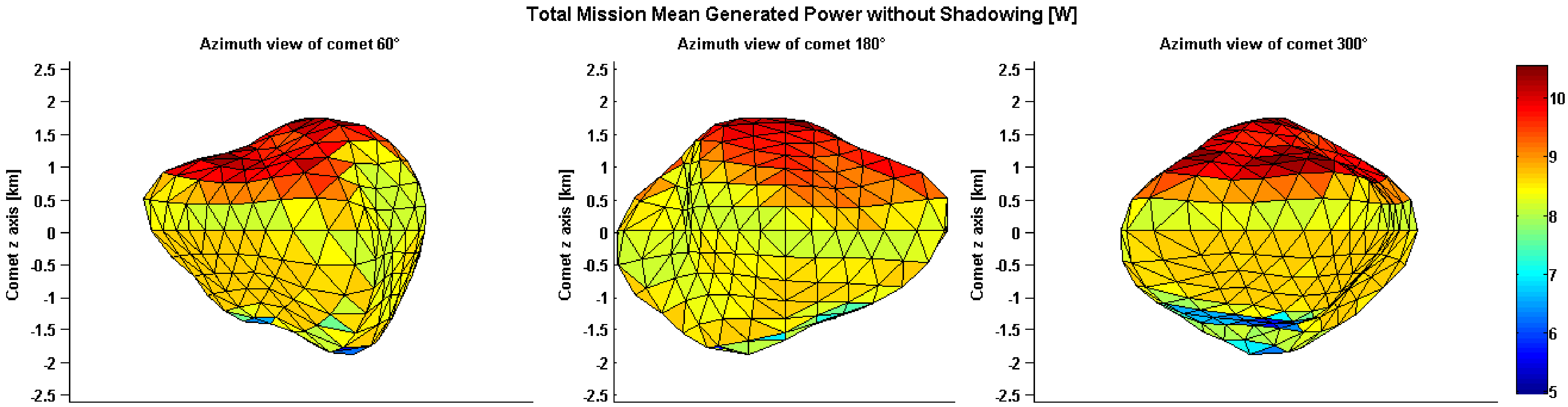

Figure 75: Total Mission Mean Generated Power without Shadowing

7.4.1 Seasonal Mean Generated Power

In the figures below the Seasonal Mean Generated Power [W] is reported and discussed season by season.

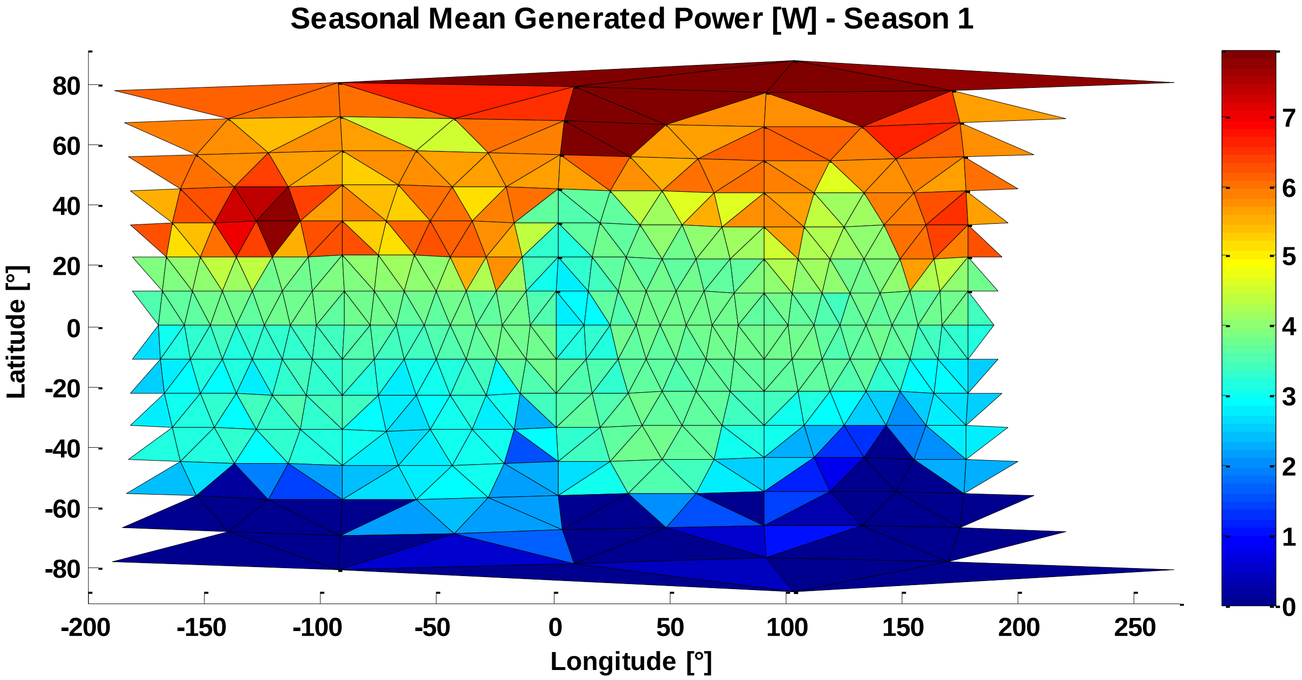

Figure 76 : Seasonal Mean Generated Power - Season 1

Season 1 [Figure 76**][**Figure 82**]:** best power generation is guaranteed for North Poles plates that reach values close to 8W, while the Northern Hemisphere show overall good performances. Southern Hemisphere plates show values close to zero for latitude lower than -50°, this result permits to discard plates at these latitudes.

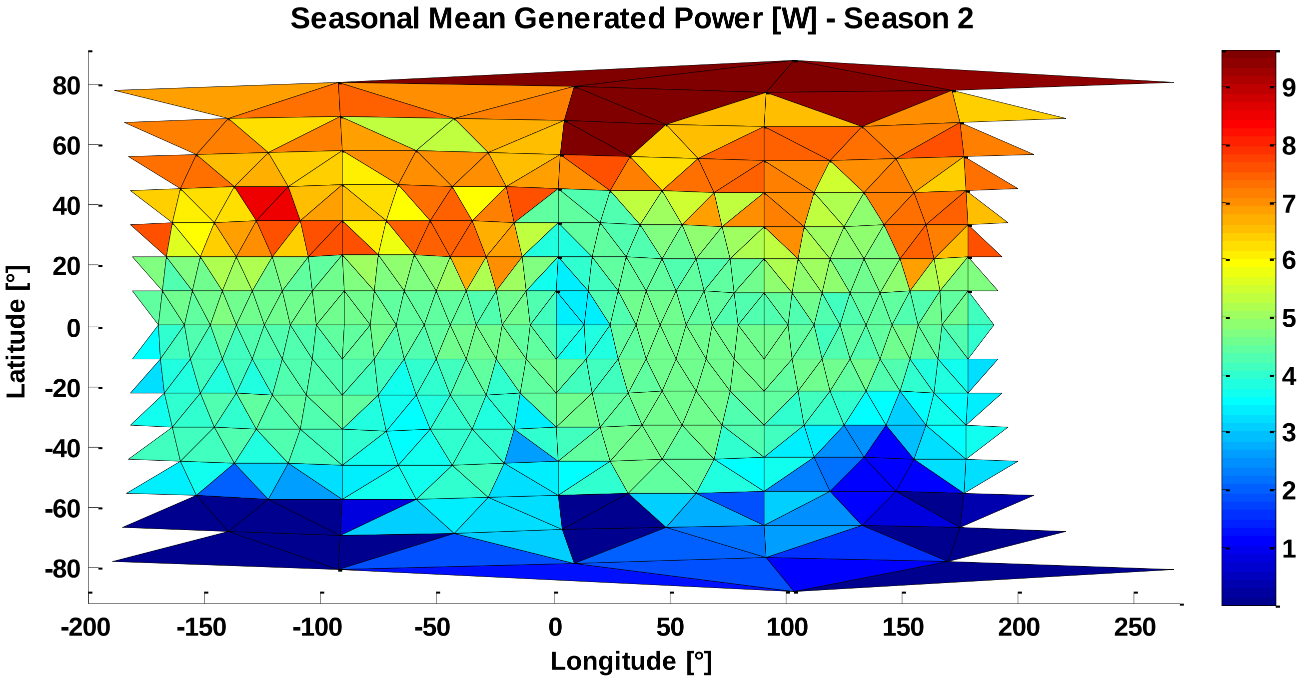

Figure 77 : Seasonal Mean Generated Power - Season 2

Season 2 [Figure 77**][**Figure 83**]:** the spatial distribution of performance is very similar to season one, although higher values of generated power can be noticed: already from Season 2 the approach to perihelion and the insolation increase in noticeable.

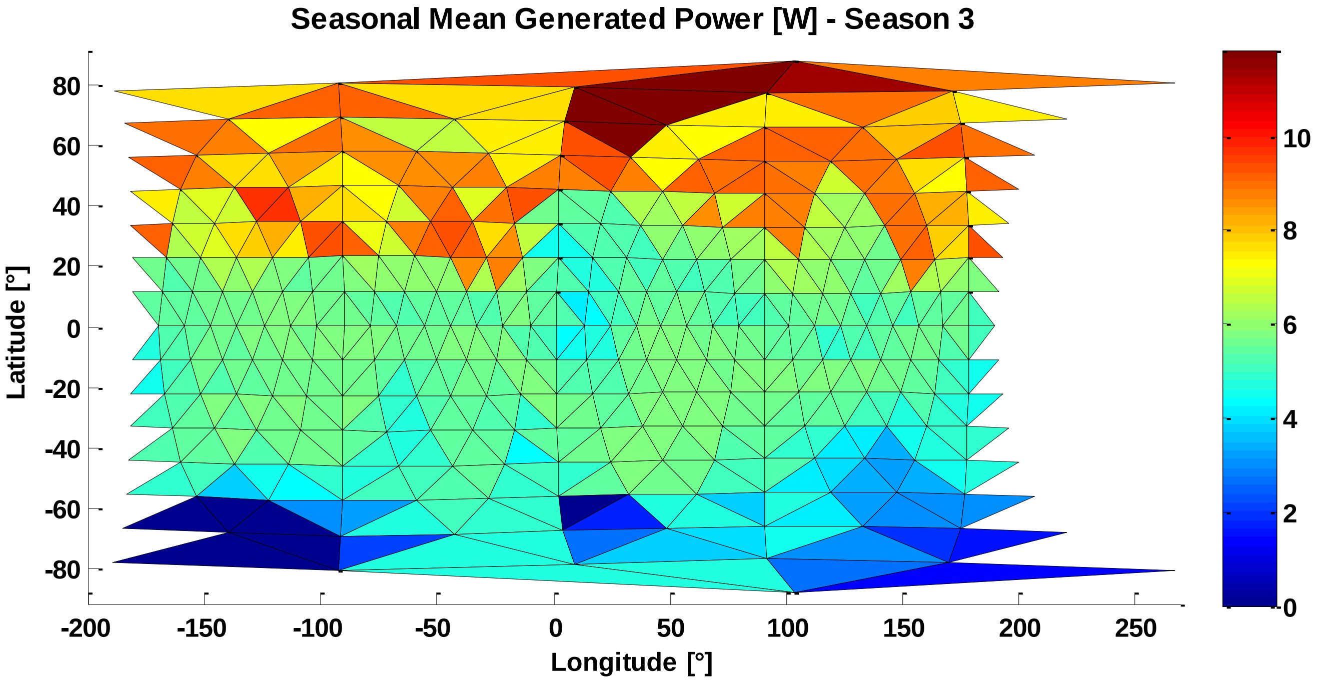

Figure 78 : Seasonal Mean Generated Power - Season 3

Season 3[Figure 78**][**Figure 84**]:** displays spatial features similar to Season1 and Season 2. Again the increase of mean power generation is noticeable, best plates can produce almost up to 11W.

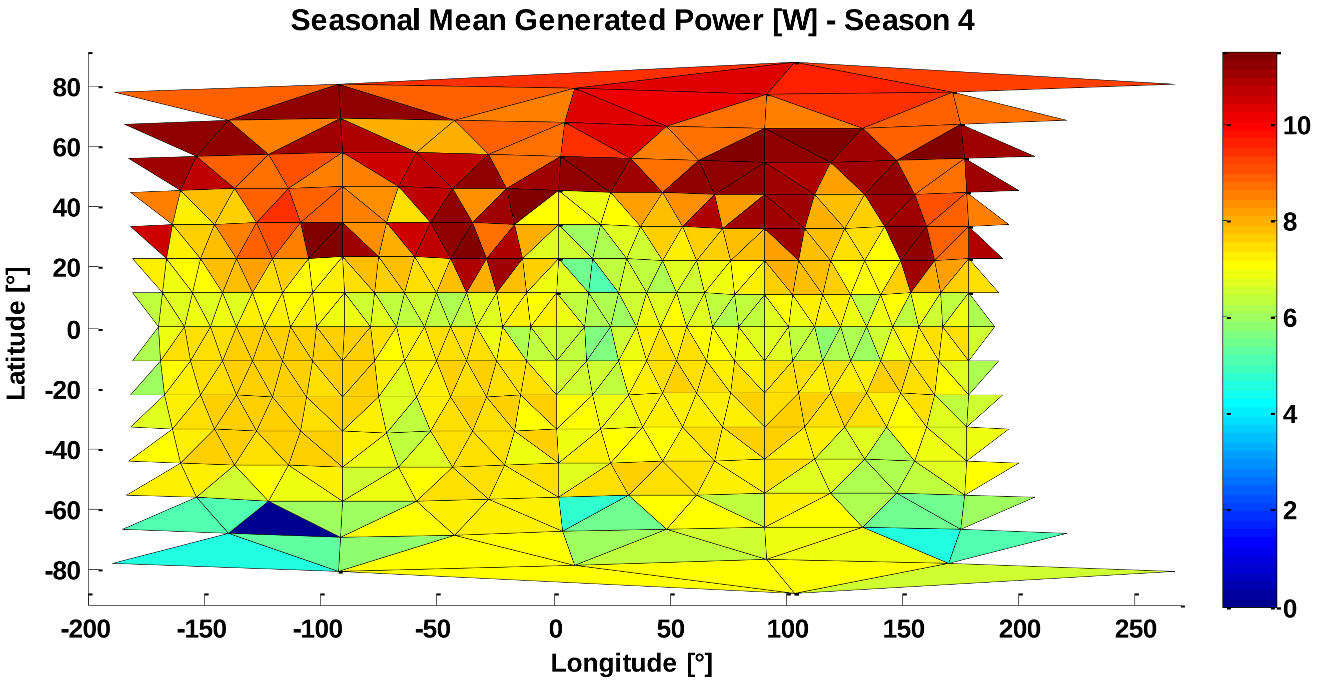

Figure 79 : Seasonal Mean Generated Power - Season 4

Season 4 [Figure 79][Figure 85]: this season show best performances for the same map of plates that have best mission performances (see [Figure 70] [Figure 74]). Season 4 thus provides a fundamental contribution to asses suitable power generation conditions for these plates. The reason under this is related to the fact that these plates have suitable normal inclination to take advantage of prolonged low elevation insolation and contemporary are located in hills/humps where shadowing effects are minimal.

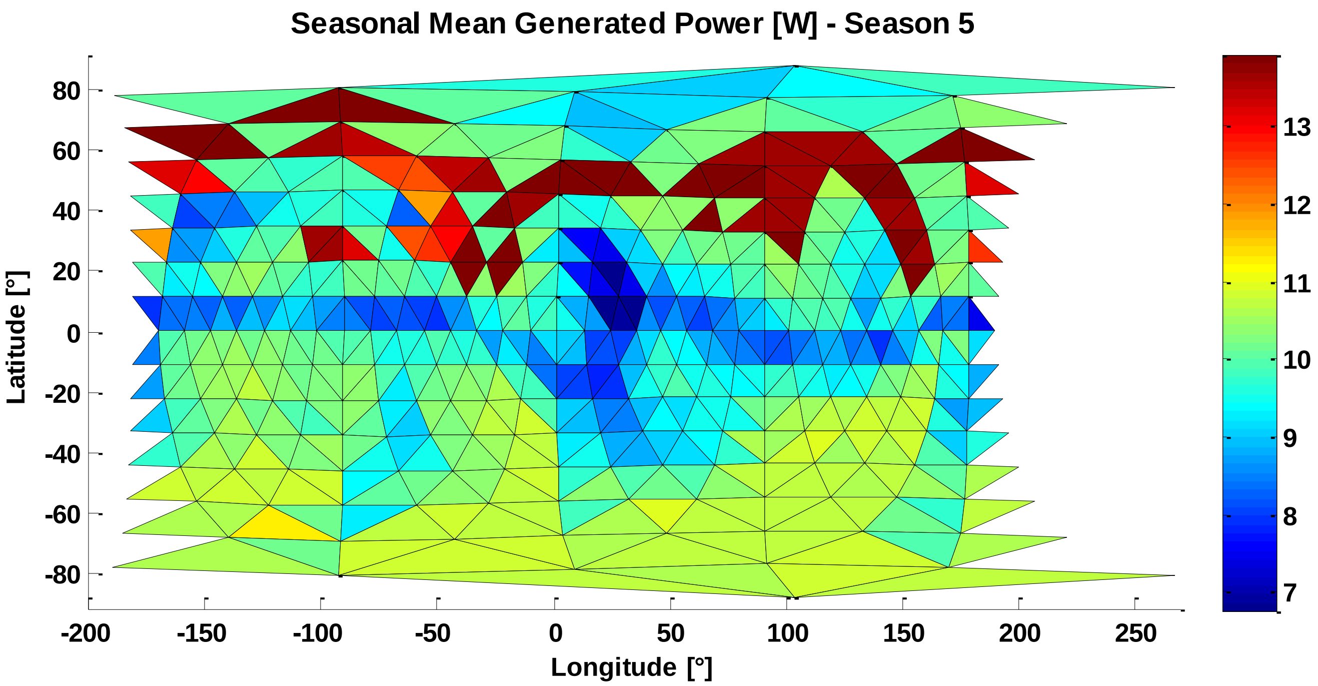

Figure 80 : Seasonal Mean Generated Power - Season 5

Season 5 [Figure 80**][**Figure 86**]**shows best performances for the same plate map of Season 5, the power generation gap with respect to the surrounding plates has the magnitude of some [W] in some cases.

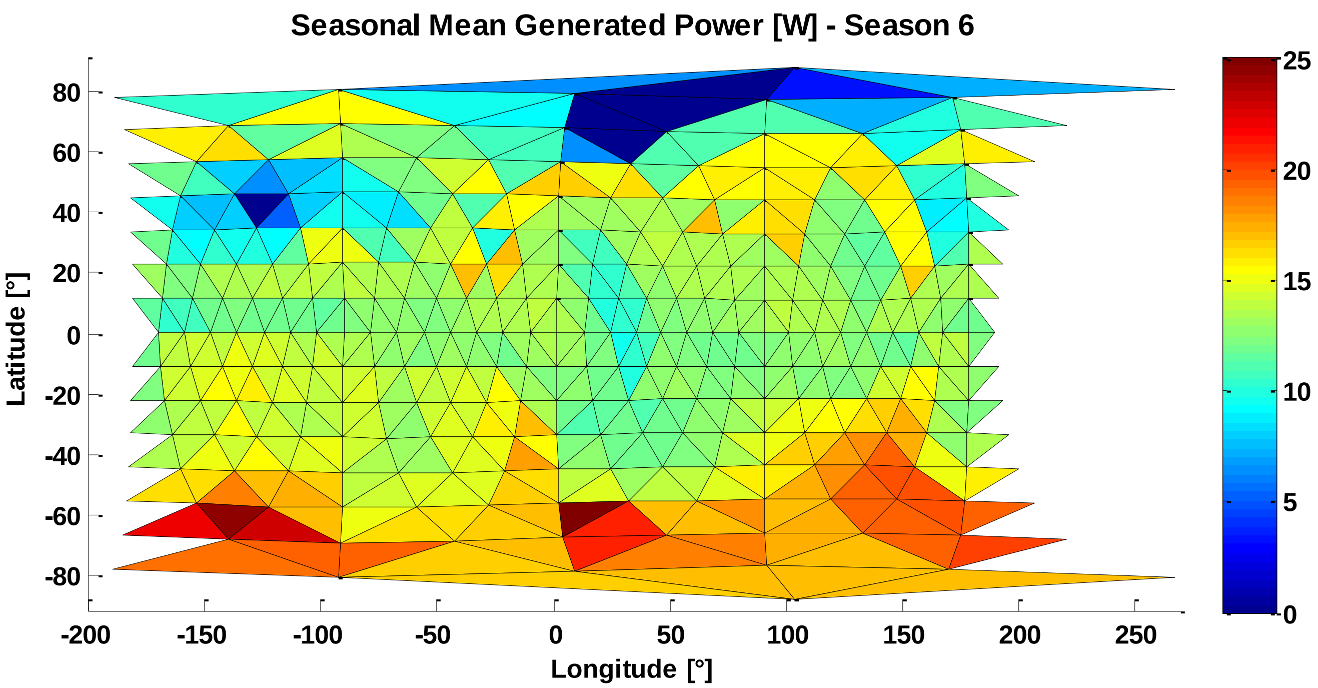

Figure 81 : Seasonal Mean Generated Power - Season 6

Season 6 [Figure 81**][**Figure 87**]**is the Season where there best conditions move from the Northern to the Southern hemisphere, maximum values reach 25W, but are related to plates that displayed very low power generation in the previous seasons, thus these results are not relevant. Is important to notice, on the other hand, the values close to zero for some of the plates that showed best generation for the first seasons.

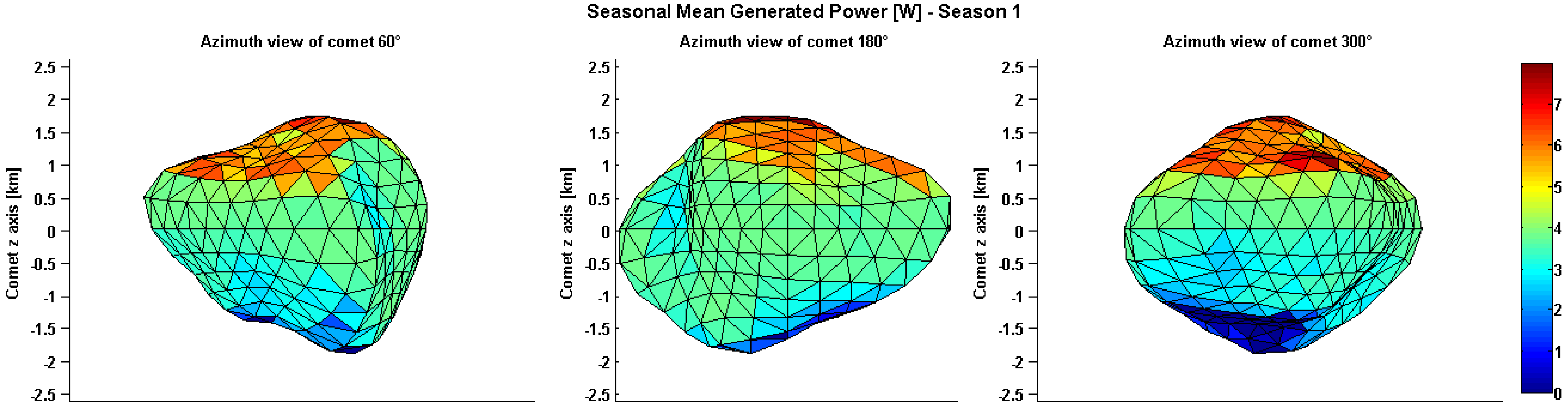

Figure 82 : Seasonal Mean Generated Power – Season 1

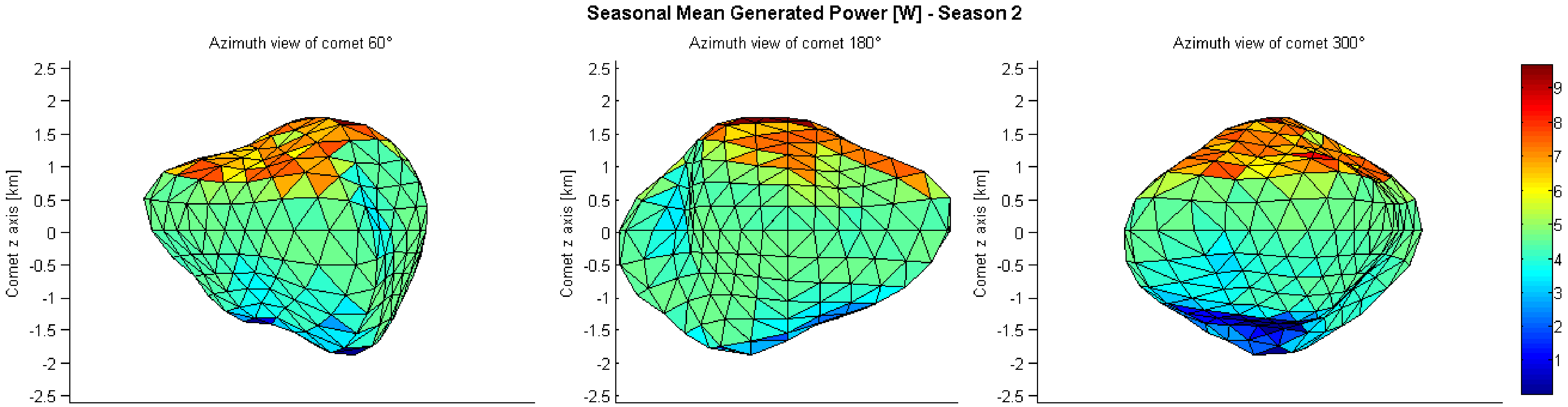

Figure 83 : Seasonal Mean Generated Power - Season 2

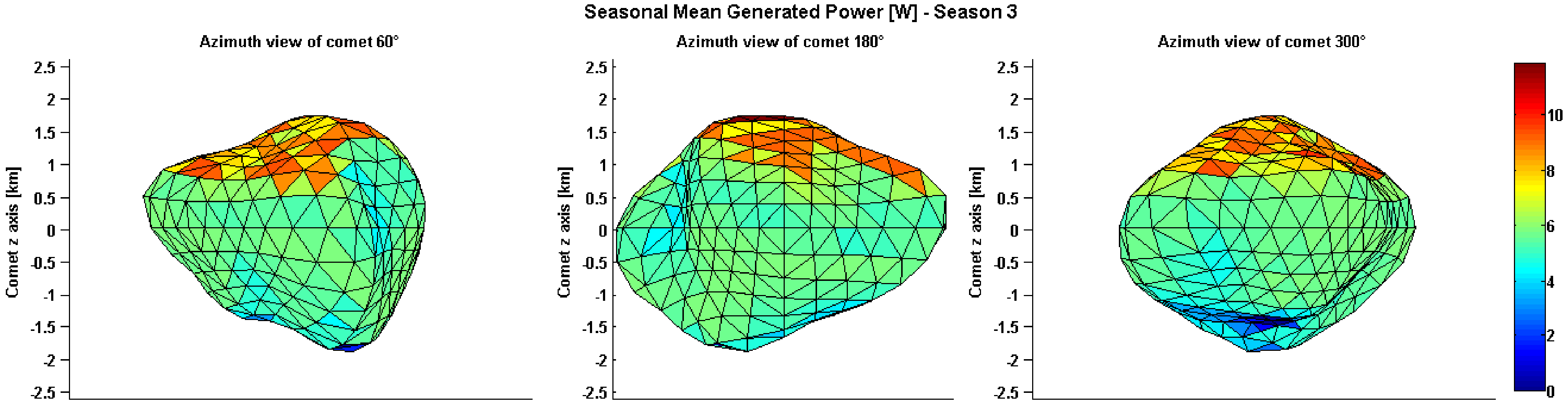

Figure 84: Seasonal Mean Generated Power - Season 3

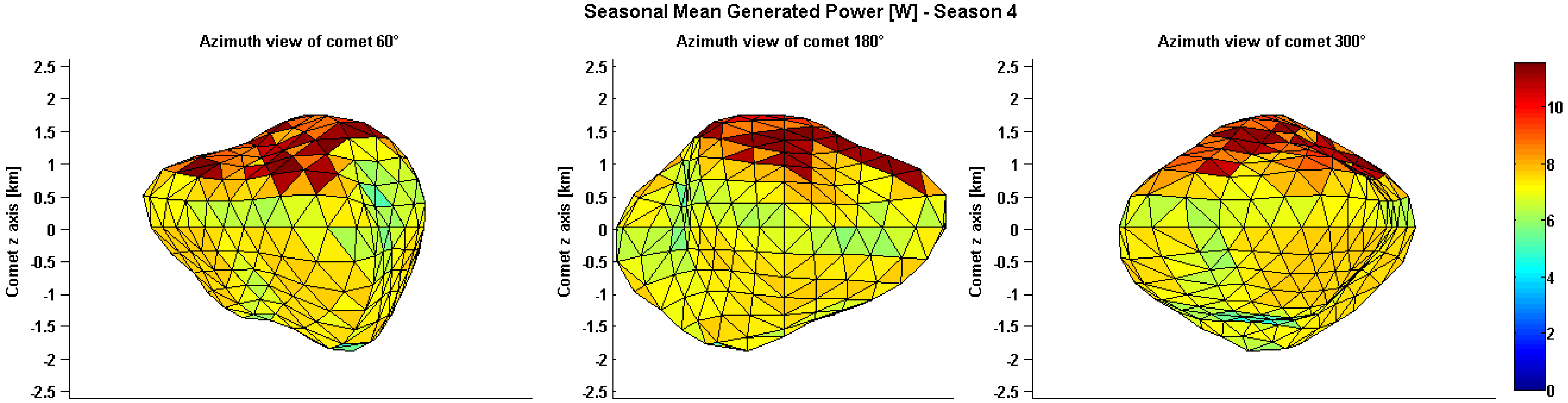

Figure 85 : Seasonal Mean Generated Power - Season 4

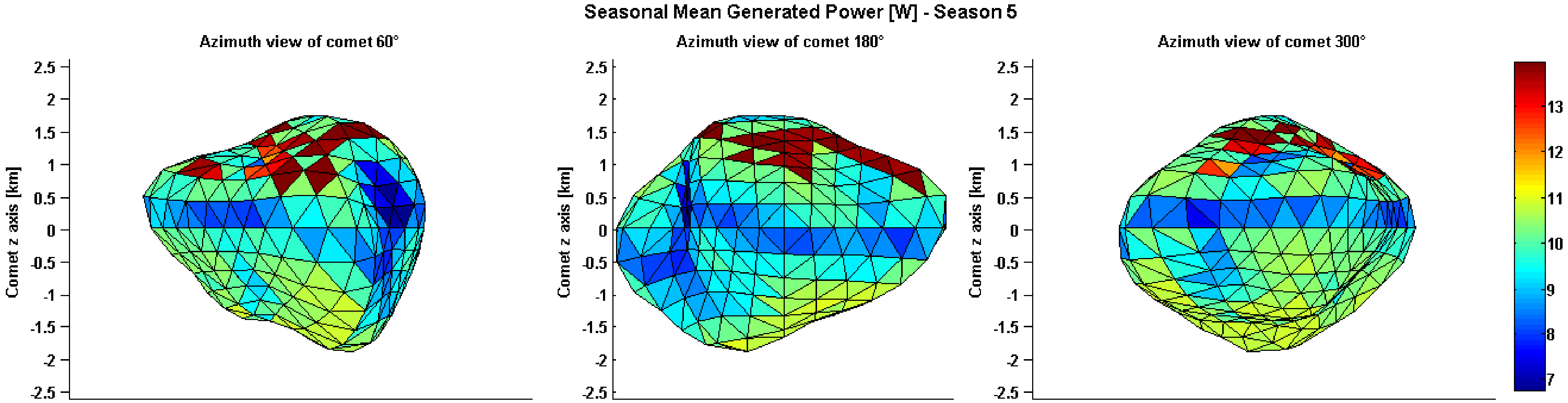

Figure 86 : Seasonal Mean Generated Power - Season 5

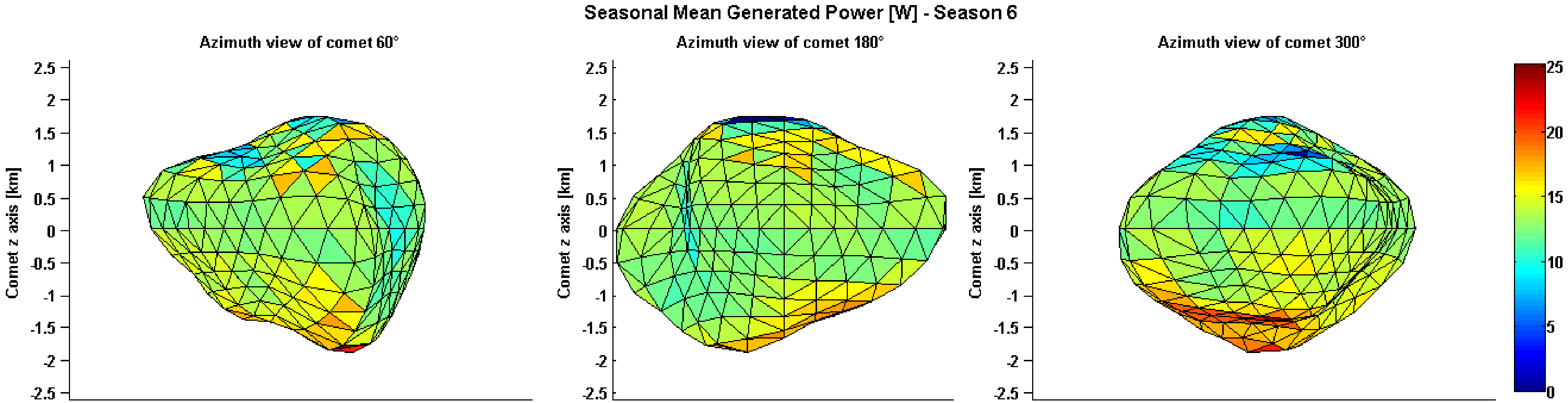

Figure 87 : Seasonal Mean Generated Power - Season 6

7.5 Thermal Results

Results of this section are related to[Simulation – 3Shadowing & Thermal]. This analysis can be only considered as preliminary due to the thermal model assumptions, as described in [Philae Thermal Model]. In particular the obtained results are not useful to determine the exact day of overheating, rather to obtain the relative trend of overheating between plates. This is closely related to the maximum value of Q_{Sink} as described in [Lumped Parameters for Philae Thermal Model], increasing or decreasing this value the mission duration can be uniformly extended or shortened respectively, thus only the relative behaviour between plates can be analyzed.

Day of Philae Overheating [Figure 90**][**Figure 91**]** only a restricted number of plates are liable to overheating and are located in particular in the Southern Hemisphere. Plates of **[**Figure 91**]** that display mission end the day 360 are to be interpreted as plates that can complete the 360 days of mission without thermal constraints.

If these results are interpreted with the typical temperature behaviour of plates located in different cometary sites (as reported in [Figure 36], it is to be remarked for interpretation of this figure that increasing plate number is related to decreasing latitude) it can be concluded that overheating is strongly linked with season and insolation. In facts plates located in the Northern Hemisphere suffer the highest values of insolation at mission beginning, but the Solar Constant low value do not lead to harmful temperatures for the Warm Compartment; during the mission the Solar Constant increases, while the season contemporarily changes: temperatures in the Warm Compartment decrease and no overheating occurs. On the other hand plates that suffer of overheating show a trend of mission end day that in general terms increases for decreasing latitudes: the season changes and insolation show higher values for lower latitudes season by season. This same trend is noticeable for the peak Warm Compartment temperature: the lower the latitude the later occurs. The Northern Hemisphere plates have the earliest Warm Compartment peak temperature, but are advantaged as long as the Solar Constant is not elevate enough to lead to mission end. On the other hand, whenever SC values are elevate enough to lead to mission end, the mission end day follows in general terms its North to South trend. Exceptions to this trend are related to plates that show elevate shadowing. As a conclusion not only the Solar Constant, but also the Subsolar Point play a fundamental role to determine overheating.

Cumulated Mean Generated Power before Overheating:[W] [Figure 88**][**Figure 92**].** This result permits to estimate the mean power produced by each plate until overheating. All plates that have been selected in the section [Generated Power] do not suffer of overheating, thus they still show the better performances in terms of generated power.

Mission Cumulated Generated Power before Overheating [Wh] [Figure 89**]** is the Cumulated Mean Generated Power before Overheating multiplied by the mission duration before overheating. This result is an indicator of the amount of generated power that can be produced by each cometary site before overheating. The most performing sites are the same presented in [Figure 88][Figure 92], but the ratio between maximum and minimum values increases with respect to the previous results. This is related to the fact that all the most suitable landing sites in terms of produced power do not suffer of overheating, other plates that have lower mean generated power values suffer of overheating: their mission duration is shorter and this is reflected in the Mission Cumulated Generated Power.

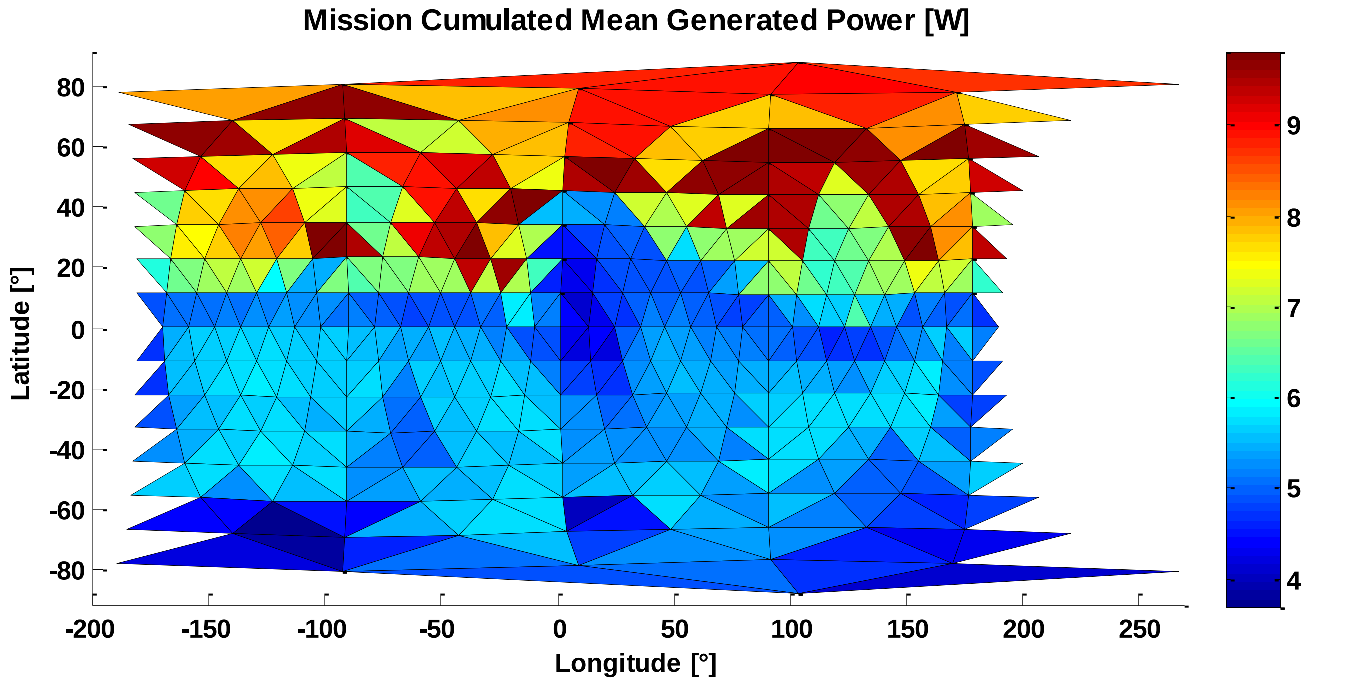

Figure 88 : Cumulated Mean Generated Power before Overheating

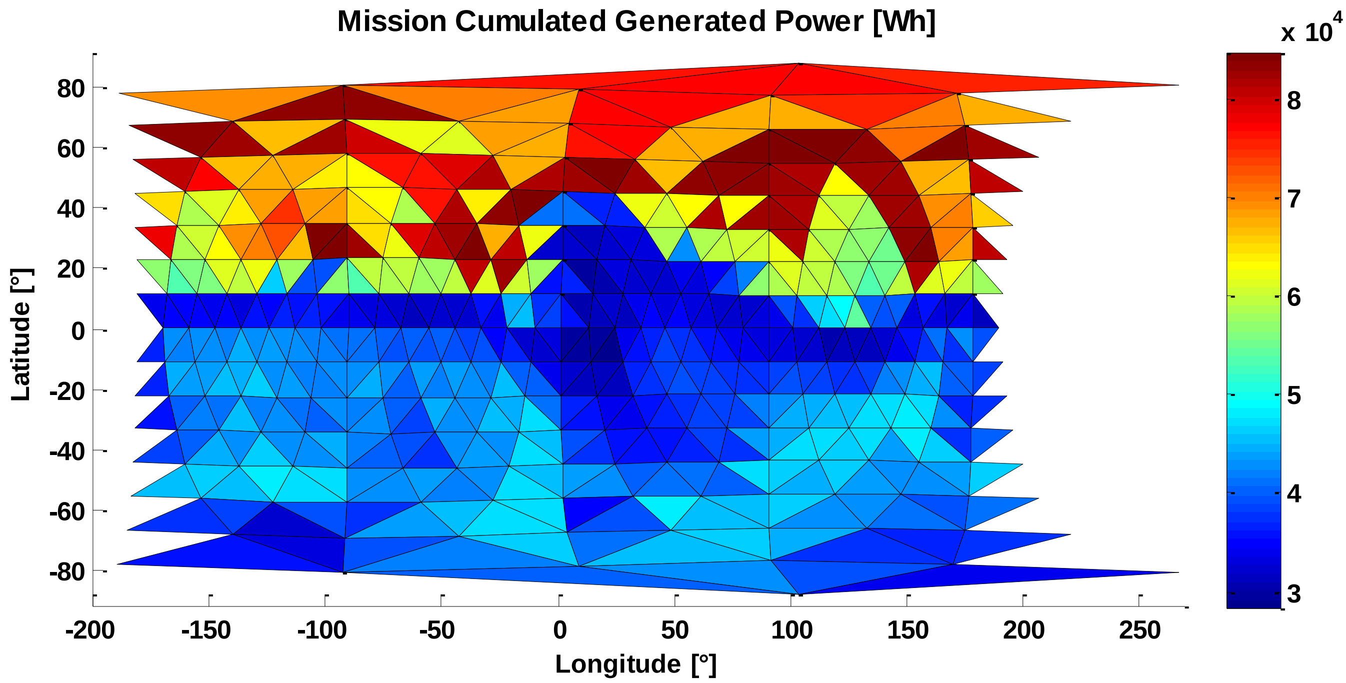

Figure 89 : Mission Cumulated Generated Power

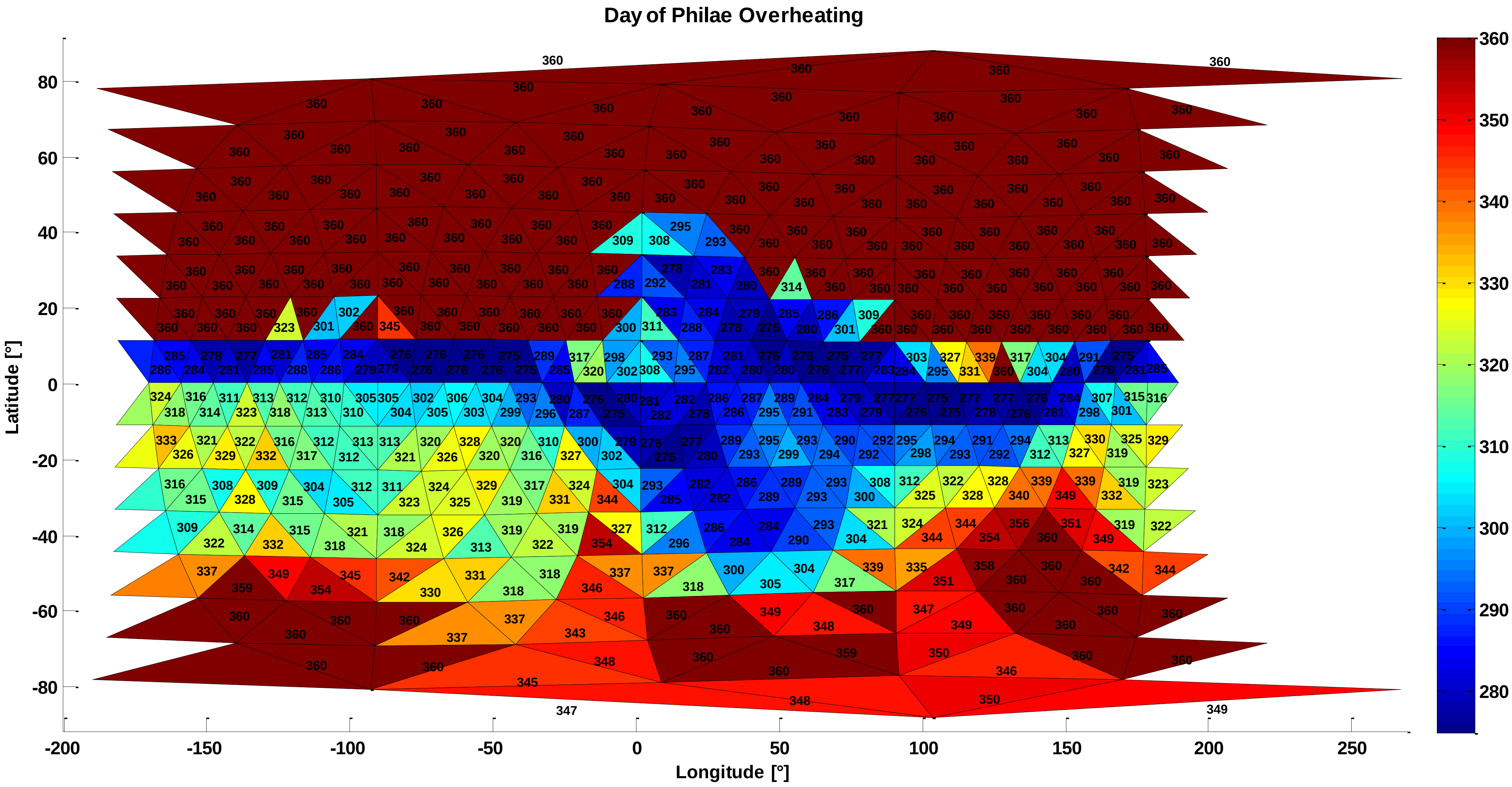

Figure 90 : Day of Philae Overheating

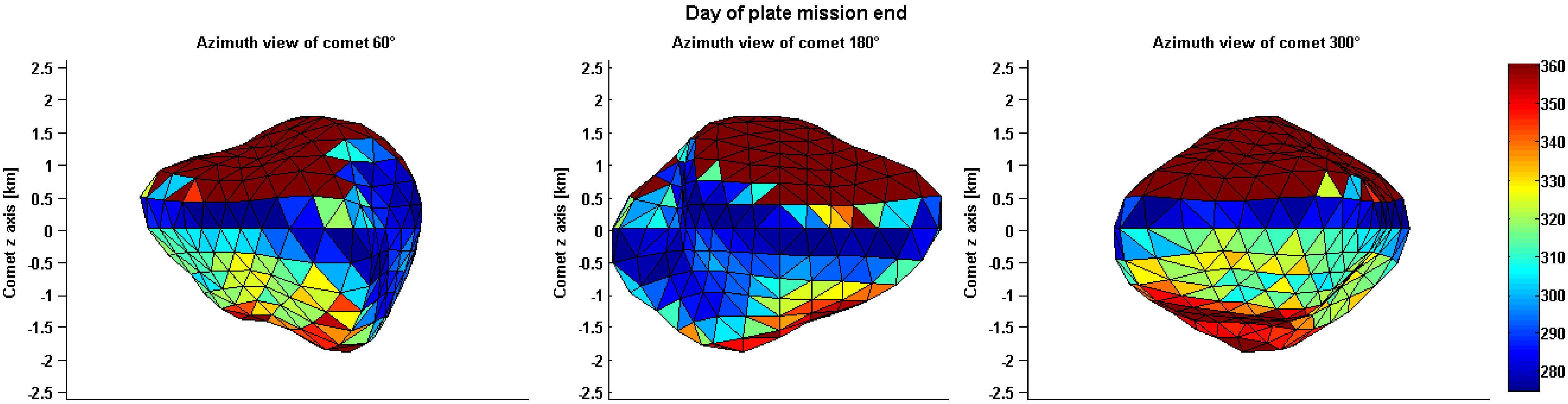

Figure 91 : Day Of Philae Overheating

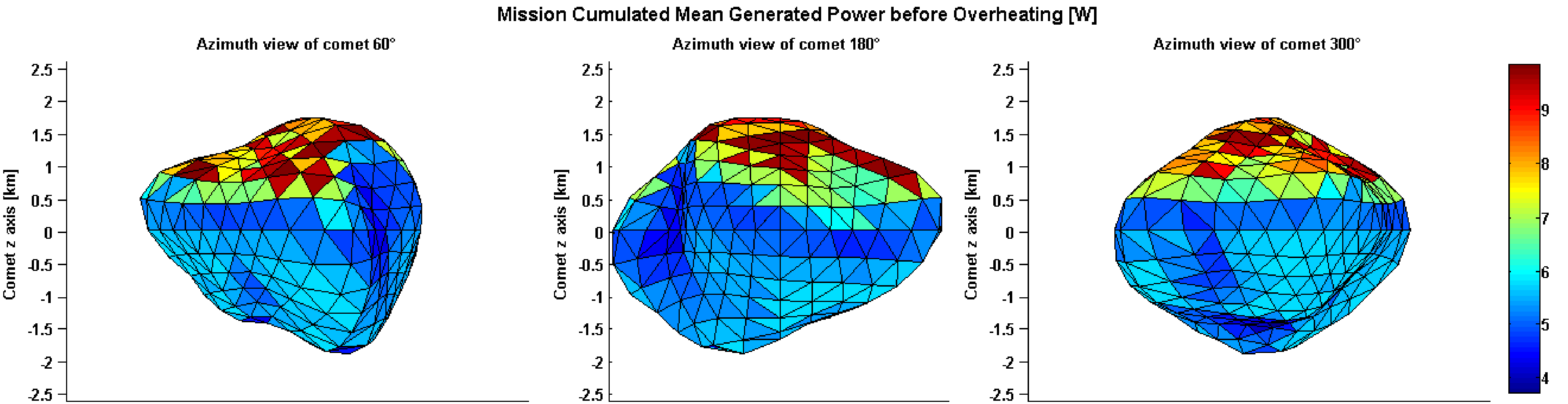

Figure 92 : Cumulated Mean Generated Power before Overheating

7.6 Spin Axis Parametric Orientation

For sake of brevity only the total mission results are reported for this section, which are related to the 4 simulations as presented in [Simulation – 4Spin Axis Parametric]: each simulation is dedicated to one of the four range boundaries of the Spin Axis Orientation possible variation.

Inclination variation [Figure 93][Figure 94] for Inclination I+10°, [Figure 95][Figure 96] for I-10°. As is visible the variation of inclination do not create wide variations in terms of Mission Insolation, while the Total Mean Generated Power changes, both in the most suitable location and in the maximum values. In particular in the case of I+10° most suitable sites in terms of Total Mean Generated Power are a vast area in the Northern Hemisphere, while in the case of I-10° suitable sites are located in small areas of Northern Hemisphere showing elevate values of normal inclinations.

Argument variation [Figure 97**][**Figure 98**]**for Argument Ψ+10°, [Figure 99][Figure 100**]** for Argument Ψ-10°. The variation of Argument do not create wide variations in terms of Mission Insolation over the entire mission, while the Total Mean Generated Power changes, both in the most suitable location and in the maximum values. In the case of Ψ+10° most suitable sites in terms of Total Mean Generated Power are a vast area in the Northern Hemisphere, while for Ψ-10° conditions are very uniform overall the comet and almost symmetrical with respect to the equator.

These results permit to state two conclusions:

- the choice of the landing site is strongly dependent on the Spin Axis Orientation, due to the indetermination related to it, the conclusions that are outlined for the nominal Spin Axis Orientation can be retained only as indicative.
- the Spin Axis Orientation variation with respect to the nominal value may lead to more favourable or adverse conditions with respect to the nominal solution, even for small variations of the orientation.

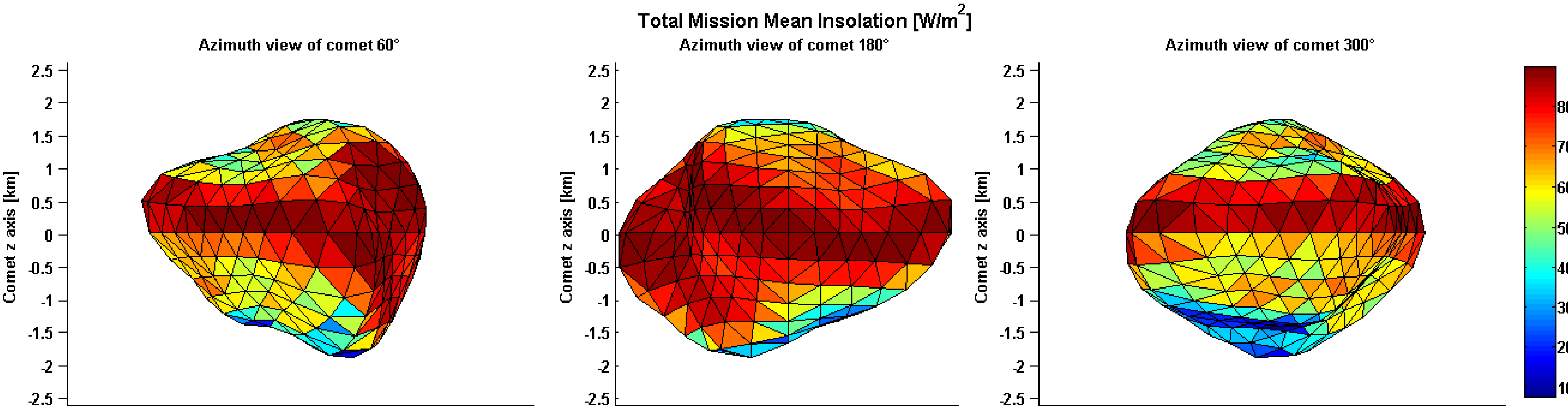

Figure 93 : Total Mission Mean Insolation - Inclination I +10°

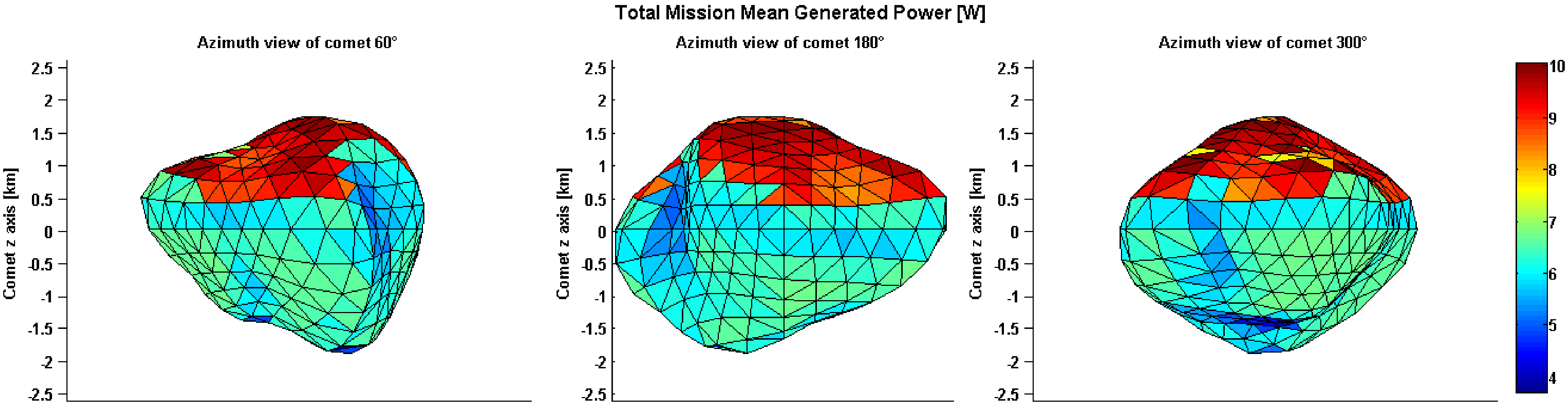

Figure 94 : Total Mission Mean Generated Power - Inclination I +10°

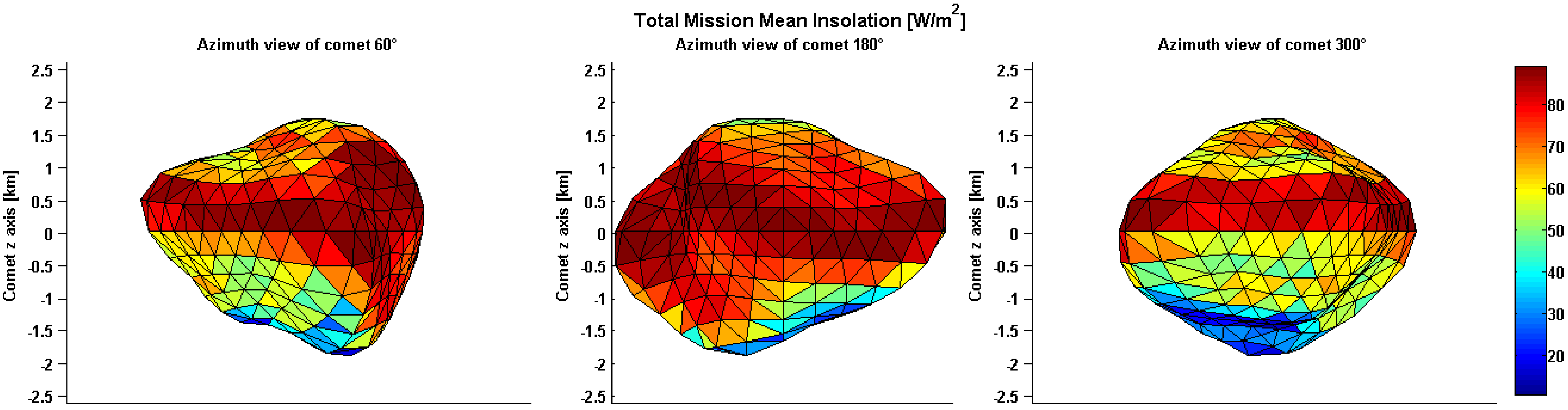

Figure 95 : Total Mission Mean Insolation - Inclination I -10°

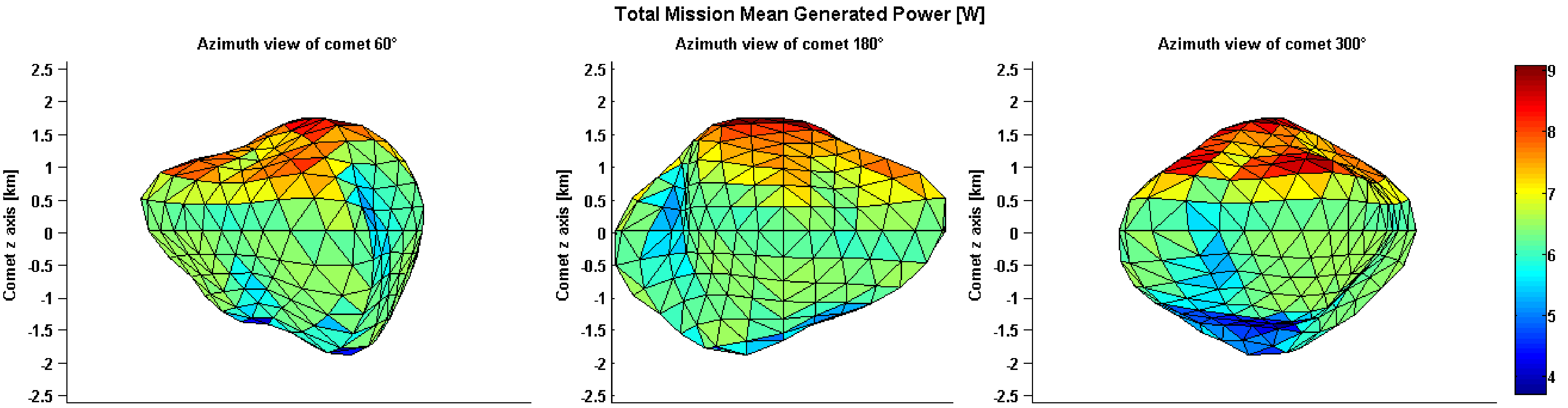

Figure 96 : Total Mission Mean Generated Power - Inclination I -10

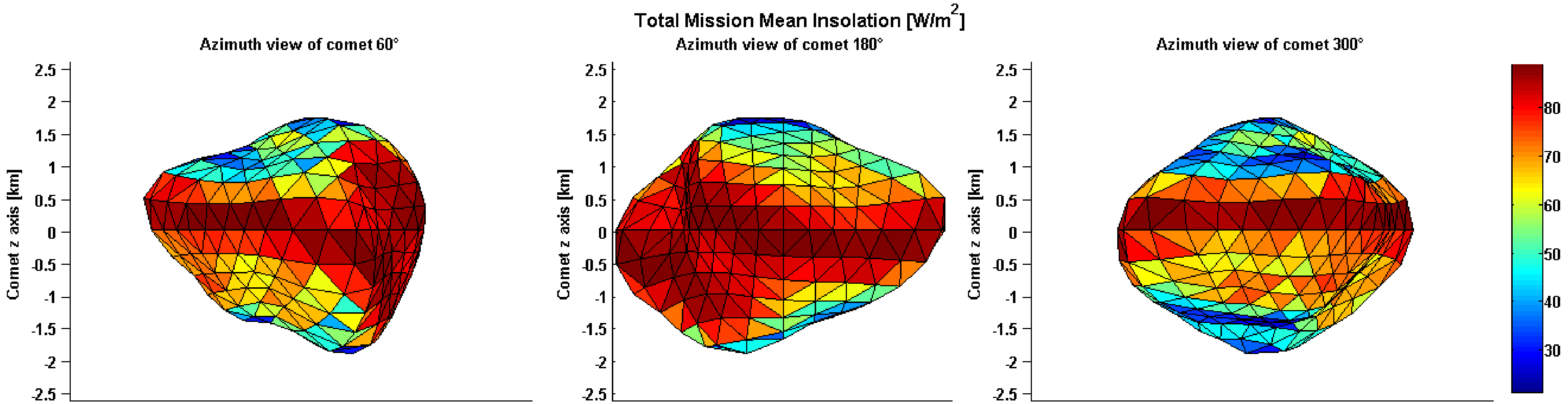

Figure 97 : Total Mission Mean Insolation –Argument Ψ +10°

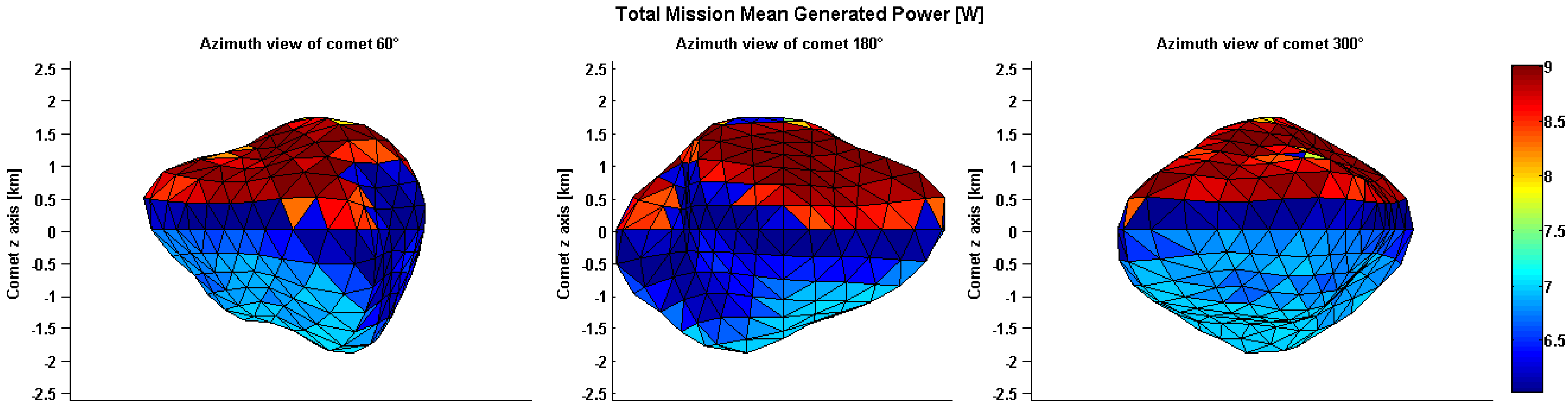

Figure 98 : Total Mission Mean Generated Power –Argument Ψ +10

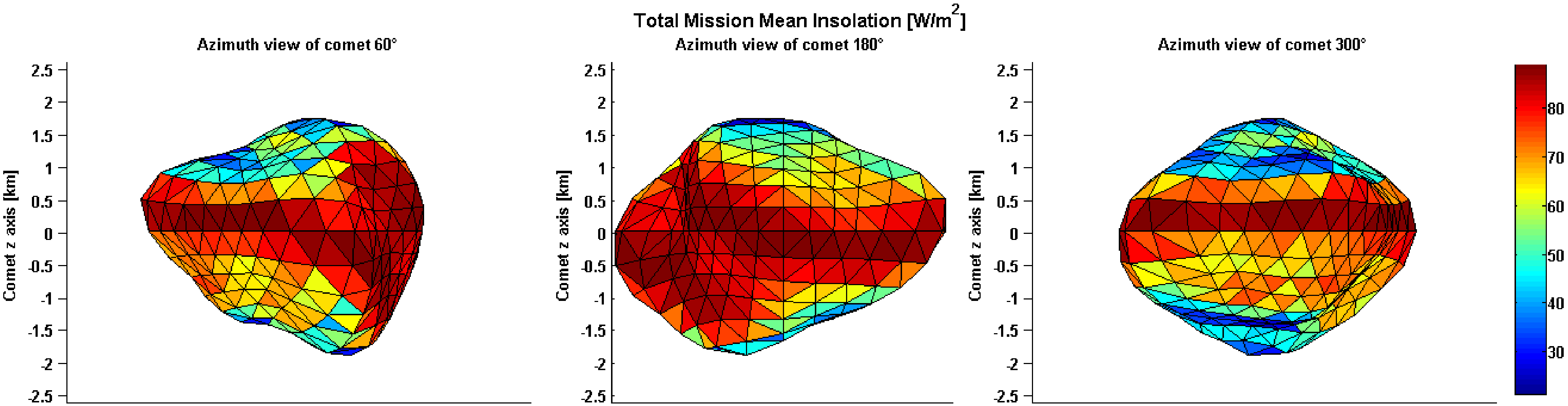

Figure 99 : Total Mission Mean Insolation –Argument Ψ -10°

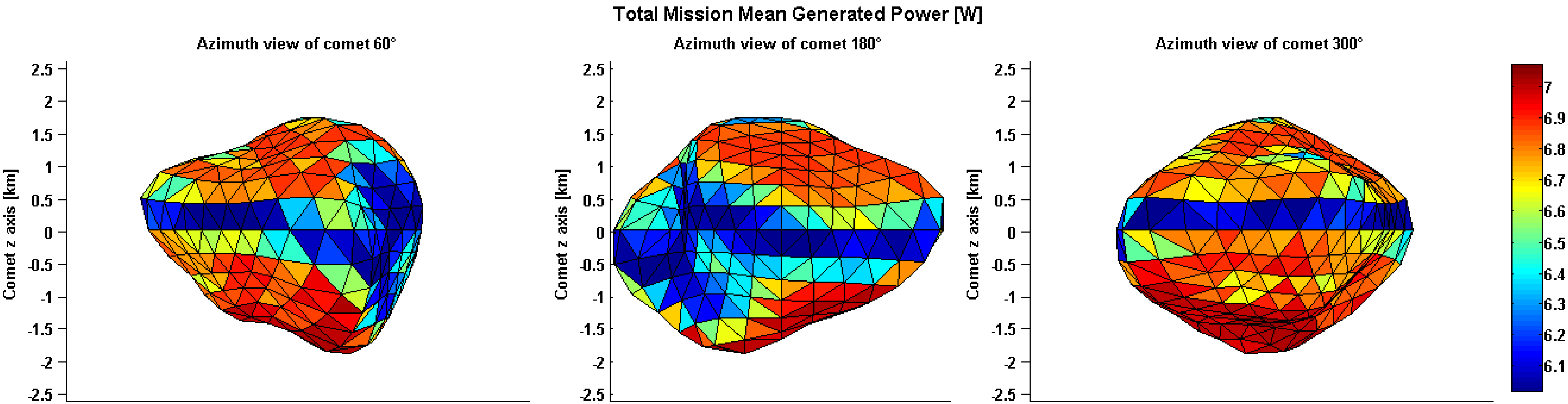

Figure 100 : Total Mission Mean Generated Power –Argument Ψ -10°°

8. Critical Discussion

Philae Landing Site Selection shows results that depend on the performed analysis: depending on the analysis parameters, results evidence different suitable landing sites. This is related to the different requirements deriving from different parameters: e.g. the mission best Mean Generated Power against the Mission Power Minimum Threshold. Consequently **the Landing Site Selection must be a compromise choice** between a wide number of aspects that frequently show cometary locations that are not in accordance.

Due to the indetermination of both mission and environmental parameters, the results presented on this thesis can only be considered indicative, and do not constitute definitive indications for the most suitable landing site. However a number of relevant conclusions can be stated and they are outlined below. Thus interpretation of results, obtained with the "nominal" conditions of parameters adopted in the analysis, is done in order to outline Philae mission scenario in a general sense.

There are three cometary sites in particular that permit to respect most of constraints as evidenced in [Generated Power] results section, their characteristics are resumed in [Table 28].

- **High Latitudes one Orientation Manoeuvre plates**: related to plates that show best Total Mission Mean Generated power and are identified by the map of plates that have Philae initial orientation for $\theta = \alpha_{rot} = -\frac{\pi}{2}$ as presented in [Philae Orientation Operations on the plate], these plates show very similar normal inclinations with respect to the comet equator, ranging from 46.4° to 59.2°.
- **North Pole 6.11W Threshold plates:** is related to North Pole plates that respect for the entire mission the 6.11W Daily Minimum Power Threshold and in particular show the best power generation for Season1 and Season2.
- **Middle Latitudes Northern Hemisphere 6.11W Threshold plates**: are Northern Hemisphere that respect for the entire mission the 6.11W Daily Minimum Power Threshold.

From the features reported in [Table 28], clashing between better performances is evident even between the categories of the most suitable location in the comet. The choice of the definitive landing site is thus a compromise, e.g it can be preferred to optimize power generation at mission beginning to best guarantee the earliest operations, or it can be preferred to ensure the most power generation during the entire mission, or low latitudes can be preferred to reduce risks related to the SDL phase (as seen in [Separation-Descending-Landing] equatorial and/or subsolar point are preferable).

	High Latitudes one Orientation Manoeuvre plates	North Pole 6.11W Threshold plates	Middle Latitudes Northern Hemisphere 6.11W Threshold plates
Total Mission Generated Power	8.84-9.81W (highest)	~8.5W	~8.0W
Daily Minimum Power Threshold	>4.11W <5.11W	>6.11W (highest) <7.11W	>6.11W (highest) <7.11W
Power during Season1	5.0-5.5W	7.6W (highest)	6.2W
Overheating (Preliminary Result)	Avoided	Avoided	Avoided
Total Mission Mean Insolation (Related to comet activity)	55-65W	40-50W (lowest in North. Hemisph.)	~50W
Orography	hill/hump	hill/hump (North Pole Top)	hill/hump
Latitudes	10-80°	50-90°	25-50°

Table 28: Summary of most performing plate categories

As reported in [Philae Orientation on the Plate] given a cometary site is possible to predict **Philae optimal orientation** for power production for the entire mission duration. The maximum number of necessary manoeuvres to provide optimal orientation is minimal (two), thus the orientation manoeuvre has no impact on the lander overall power balance. This permits also minimum necessity of lander orientation control and operations. Results are only close to optimum for shaded plates, but the most suitable landing sites evidenced in [Generated Power] are mainly located in hills/jumps, that are independent from this approximation.

Insolation maps show high **insolation values for location on the comet that do not coincide with the optimal power production locations**. This is related to Philae geometry, 5 out of 6 solar panels are oriented orthogonally with respect to the surface normal. This feature is considered an advantage for the mission, both in thermal control terms, as long as the Warm Compartment temperature is driven by Insolation (mostly due to the fact that Solar Absorbers are parallel to the comet surface), and in surface erosion terms as long as it is mainly driven by insolation as well. Air mass effect and light scattering was neglected in the analysis, their effect is typically most noticeable for low Sun elevation angles over the horizon (where the air mass is more elevate), thus the convenience of illumination conditions that present low Sun elevation angles may be reduced if these aspect were considered. It is to be noticed however that the air mass effect is more elevate for low Sun elevation angles at Earth, where the atmosphere distribution is almost spherical. Comet 67P C-G may have an atmosphere distribution far from spherical and mainly characterized by localized jets and fans. In conclusion the effects of air mass and scattering should be subjected to a dedicated study, in particular to evidence whether their contribution can be neglected. For instance as seen the comet Albedo can be easily neglected, differently from the shadowing effects.

The Mean Generated Power that is guaranteed by the three most suitable cometary sites as evidenced in [Generated Power] permit to produce power values that **guarantee the Long Term Science phase operations**. Minimum operations of the lander in particular are guaranteed, but power excess is shortly above this threshold, thus power consumption must be optimized at best for cometary operations in order to permit to perform science and operate instruments during this phase.

In general terms in the analysis was evidenced that the results related to a plate are mainly driven by its **normal inclination** with respect to the comet equator and to the **facility of the site to be shadowed**. Comet 67P C-G irregular shape do not permit to characterize results depending on the plate latitude alone. In addition shadowing effects are not noticeable in the same way for the entire mission duration. As seen in [Generated Power], the most suitable plates in terms of Mission Mean Generated Power are plates that do not suffer of shadowing during Season 4 and Season 5 from plates that are located in lower latitudes: this is related to the fact that in these seasons the comet is illuminated from a light source that is located almost in the equatorial plane, this means that no shadowing can occur for those plates from plates that are located for instance in the North Pole. Thus in each plate reference frame shadowing can have different effects depending on the position of the shading plates and on the direction of the subsolar point (thus to the season).

Thermal analysis results evidence suitable landing site locations that are in accordance with the generated power results. This is a great advantage for the mission, but it is to be reminded once again that Thermal results are preliminary and more detailed analysis may lead to different considerations. It is to be remarked however that Philae thermal subsystem is designed to permit to the lander to resist until 2AU before overheating. The cometary sites that do not present overheating conditions are located in an area that show scarce insolation when at about 2AU distance from the Sun, this supports that these results may be confirmed in further analysis. The strongest assumption related to the Thermal Model is the lack of accurate modelling of the heat transfer through MLI. In particular the chosen value of Qsink, as discussed in [Philae Thermal Model], permits to simulate the heat dissipation through MLI. Increasing or decreasing the maximum value of Qsink the mission duration can uniformly be extended or shortened, respectively. Thus only the relative behaviour between plates can be analyzed. Modelling of the MLI heat dissipation is fundamental to obtain the correct value of overheating day.

Another general aspect that emerged in the analysis is the **dependency of results on the modelling assumptions**. This aspect is evident for Philae Thermal Model, but also the Solar Array Simulator is affected by simplifications. In particular the Solar Panels temperature was assumed constant, thus the Solar Array efficiency is constant as well. No shadowing of single cells/strings is also modelled. This proves that the best accuracy is required for the models to guarantee realistic results that can permit to predict Philae behaviour on comet 67P C-G for the entire mission duration.

The obtained results showed in general the importance of the determination of the problem parameters in order to produce a realistic modelling, thus to permit to simulate a realistic mission scenario.

Dependency of results is related also to **environment modelling and assumptions**. Air mass and scattering effects have been outlined already, however two other comet features can influence strongly the mission scenario.

The comet shape primarily demonstrate that the most suitable landing sites are not located in wide areas of the comet, rather to restricted position showing contemporarily diverse favourable conditions. The shape requirements of a suitable landing site, taking into account all the performed analysis, require a plate that is located in the Northern Hemisphere, has normal inclination included in the range of few tens of degrees and is not liable of shadowing from plates located in lower latitudes during Season 4 and Season 5. These characteristics are likely to be found also in a comet whose shape is different from the one adopted in this work.

On the other hand favourable or adverse condition can result, depending on the variation of both to the Inclination I and to the Argument ψ of the Spin Axis Orientation. Inclination determines the amplitude of seasonal variation, while Argument the period in the orbit where the season occurs. In general terms both these features of the comet are an advantage for the landing site selection, as long as they permit to select landing sites that show different conditions during the mission and can permit and extended Long Term Science phase: the evidenced suitable landing sites are located in the Northern Hemisphere where is summer in a condition of relatively low solar constant, thus power production in these locations is best at mission beginning, while Thermal constraints are not yet a threat. When the comet is approaching perihelion the Solar Constant increases but the season changes in the comet, leading to an autumn-like condition: overheating is avoided in the Northern Hemisphere as long as Insolation maximum values are located at the equator, while power production in this locations is still elevate. At mission end the Solar Constant is so elevate that mean generated power is high for the whole comet surface, at this period Thermal constraint are a serious threat for the mission, Northern Hemisphere plates move in a winter-like condition and overheating is likely to be avoided. Seasonal variation is guaranteed during the mission for any possible Spin Axis Orientation (except if I ~0° that would produce no seasonal variation) as long as its driven by the angular movement of the comet in its orbit: although the mission duration is only 6 months against the 6.7 orbital period, the proximity to perihelion produce elevate orbital angular velocity. Thus for any orientation

of the spin axis seasonal variation effect can be exploited, but as proved in [Spin Axis Parametric Orientation] favourable or adverse conditions may result from the variation from the nominal orientation.
Below the dependency of different aspects on the Spin Axis Orientation is outlined:

- Season, the magnitude of seasonal variation is affected by Inclination I, the location on the orbit where season occurs is affected by Argument ψ.
- Shadowing: different shadowing effects are created depending on the direction of the illumination source, that is dependent on the Spin Axis orientation.
- Initial orientation of Philae
- Manoeuvre of Philae: spin axis orientation determines both the necessity to perform manoeuvres in a given cometary site and the day at which the manoeuvre occurs.
- Overheating day and lander temperatures profile in general
- Insolation
- Generated Power

Finally the **constraints imposed to the LSSel Concept are discussed** below in the same order of presentation of [Objectives and constraints]:

1. **Thermal Ranges** in this preliminary analysis Thermal Ranges are respected for the chosen suitable landing sitesA as seen in particular almost all the Northern Hemisphere sites are not affected by overheating due to seasonal effects.
2. **Daily Power Threshold**: is respected only for few plates for the entire mission duration. Plates that show the highest values of Mission Mean Generated Power are not included in the 5.11W threshold as long as for the first days of the mission the constraint is not respected. If the constraint is relaxed for the first days of the mission, these plates can be included.
3. **Landing Site Area Robustness**: as seen the foreseen landing accuracy is estimated to be 22m with a standard deviation of 12m. In these estimations some perturbations were neglected however. Taking into account that, in the Tessellated Triangular Shape, plates have sides dimensions of about 300-400m, the magnitude of one plate is considered enough to comply with the landing accuracy.
4. **Landing Site Orography**: as seen different analysis tend to converge to the selection of a landing site that is located in hills/humps for considerations related to shadowing in particular. This is in accordance with communication windows that are best guaranteed for hills/humps.
5. **Landing Site Activity**: due to Philae orientation of Solar Arrays is possible to guarantee that the most suitable landing sites are located where illumination conditions show low Sun elevation angles, this creates Insolation conditions that are not maximal and permit to avoid the most insolated areas that are likely to suffer the most severe erosion. Determination of surface composition before landing may help to prevent to chose a landing site liable to severe erosion, as seen dust crust is preferable to exposed ice.

6. **Instrument Exposure**: Philae optimal orientation on the plate is guaranteed when Wall3 is oriented towards the Sun Culmination direction, thus the Balcony where instruments are located is in shade. In some location close to the North Pole at mission beginning the Sun can be present in the sky for the entire cometary day, in this condition Philae best orientation is with theWall3 facing the opposite to the Sun culmination direction, thus the Balcony is towards the Sun Culmination direction. It is to be remarked that the best exposition for a panel that is vertical with respect to the comet surface is towards the opposite to the Sun culmination direction: i.e. Wall3 is more insolated than the Balcony in this condition. In addition this condition occurs when the value of Solar Constant is low thus it can be accepted.
7. **Comet Data Consistency**: in particular the comet shape, spin axis orientation, air mass and scattering effects are to be further constrained and can lead to results that differ from those exposed in this thesis work. Also determination of surface composition of the chosen landing site may be determinant, to estimate both the surface strength and the possibility of major sublimation activation of that area.

8.1 Further Developments

The purposed further development of this Master in Science thesis work are all related to the enhancement of modelling of both Philae subsystems and the environment.

Regarding the **cometary environment**, the Rosetta mission phase of approach to the comet is fundamental to obtain direct observation and assess the undetermined features of the problem: this will permit to chose with least indetermination the definitive landing site. In particular will be possible to obtain more accurate information on the shape and spin axis orientation. Probably few can be assessed in this phase about air mass and scattering effects as long as the comet is considered to be almost inactive in this phase. Regarding comet erosion instead, the determination of the surface composition may be determinant to assess whether a landing site is liable to activate. Surface mapping and analysis in addition may permit to obtain evidences on the location of fans and jets related to the previous perihelion comet passages. However only when direct observations of Rosetta are performed it will be possible to chose the definitive landing site.

Regarding the **modelling of Philae** subsystems in particular the Thermal Model and Power model are to be refined:

- Philae Power Model: the assumptions related to it regard the solar panels temperature assumed constant and the lack of modelling of single cell/strings damages and shadowing. Also batteries charge/discharge efficiencies are not considered and will likely reduce the available power for the lander.
- Philae Thermal Model: as discussed this is a preliminary model that can currently give only preliminary indications on the thermal conditions that Philae will have to sustain during its mission. More detailed data is fundamental to determine the correct mission scenario.
- Scientific Return: the selection of the landing site can not be independent from science objectives and from the capability of a site to permit scientific return. This thesis work allows to indicate sites that are efficient in terms of Philae subsystems performances, whereas a suitable landing site must be also scientifically relevant to guarantee an optimal Long Term Science phase. As a consequence, scientific constraints shall be applied also.

Appendix 1

In this appendix the coordinate transformation between (RA,DEC) expressed in EME2000 and the angles of Spin Axis orientation (I,Ψ) is presented. RA is the terrestrial right ascension and DEC the declination expressed in EME2000, thus referred to Earth Mean Equator at 12:00hr of January 1st 2000. To permit this transformation orbital parameters of Earth and 67P Churyumov-Gerasimenko reported below are expressed in EME2000. Inclination of the Spin Axis is I, while Ψ is the Argument as defined in [Equatorial Reference Frame - ERF]. This transformation is necessary as long as the Spin Axis orientation is reported in literature in (RA,DEC) coordinates, whereas in the LSSel Concept is expressed in (I,Ψ) coordinates to have a clearer physical understanding of the Spin Axis orientation with respect to the orbital reference frame.

The transformation comes in two steps and exploits as intermediate passage the Ecliptic Frame (EF), whose reference plane is the Ecliptic and reference direction the Vernal Point in EME2000.

<u>EME2000 → EF Transformation</u>

Given (RA, DEC) in EME2000 the equivalent direction of a versor expressed in Ecliptic Frame can be written using the coordinates (x,y,z) using [Eq.(60) [Eq.(61)][Eq. (62)]; where x points the Vernal point, z is orthogonal to the Ecliptic plane and y complete the dextrorotatory tern.

$$z = sin(DEC) * cos(\varepsilon) - cos(DEC) * sin(\varepsilon) * sin(RA) \tag{60}$$

$$x = cos(DEC) * cos(RA) \tag{61}$$

$$y = sin(DEC) * sin(\varepsilon) + cos(DEC) * cos(\varepsilon) * sin(RA) \tag{62}$$

where ε is Earth inclination expressed in EME2000.

<u>EF → ORF Transformation</u>

Once the versor in Ecliptic Frame is obtained the transformation to Orbital Reference Frame coordinates Frame (as defined in [Orbital Reference Frame - ORF]) is possible exploiting the composition of the following rotation matrices that involve 67P Churyumov-Gerasimenko orbital parameters, [Eq.(63)] [Eq. (64)] [Eq. (65)]

$$R1 = \begin{bmatrix} \cos(\mathrm{RAAN}) & \sin(\mathrm{RAAN}) & 0 \\ -\sin(RAAN) & \cos(RAAN) & 0 \\ 0 & 0 & 1 \end{bmatrix} \qquad (63)$$

$$R2 = \begin{bmatrix} 1 & 0 & 0 \\ 0 & \cos i & \sin i \\ 0 & -\sin i & \cos i \end{bmatrix} \qquad (64)$$

$$R3 = \begin{bmatrix} \cos\ \omega & \sin \omega & 0 \\ -\sin \omega & \cos \omega & 0 \\ 0 & 0 & 1 \end{bmatrix} \qquad (65)$$

where RAAN, i, ω are the right ascension of the ascending node, the inclination and the pericentre argument expressed in EME2000 as described in [Orbit modelling]. Interconnecting the above defined rotations, the coordinates of the Spin Axis Orientation is obtained in Orbital Reference Frame using [Eq.(66)]

$$\begin{bmatrix} R \\ T \\ N \end{bmatrix} = R3 * R2 * R1 \begin{bmatrix} x \\ y \\ z \end{bmatrix} \qquad (66)$$

<u>ORF → (I,Ψ) Transformation</u>

From the versor in ORF coordinates, the angles (I,Ψ) can be obtained exploiting the definition of the angles as reported in [Equatorial Reference Frame - ERF], through [Eq.(67)], [Eq. (68)]

$$I = \mathrm{acos}\ (N) \qquad (67)$$

$$\Psi = \frac{\pi}{2} - (atan\left(\frac{T}{R}\right) - \ \pi) \qquad (68)$$

In [Eq. (68)] arctangent discontinuity and domain must be considered.

-

Appendix 2

Due to direct request from the DLR of Köln, Mean Generated Power values are reported for the first 101 days of the mission, five different plots are reported at 20 days of separation each. These results permit to study the most suitable landing sites for the first days of the mission.

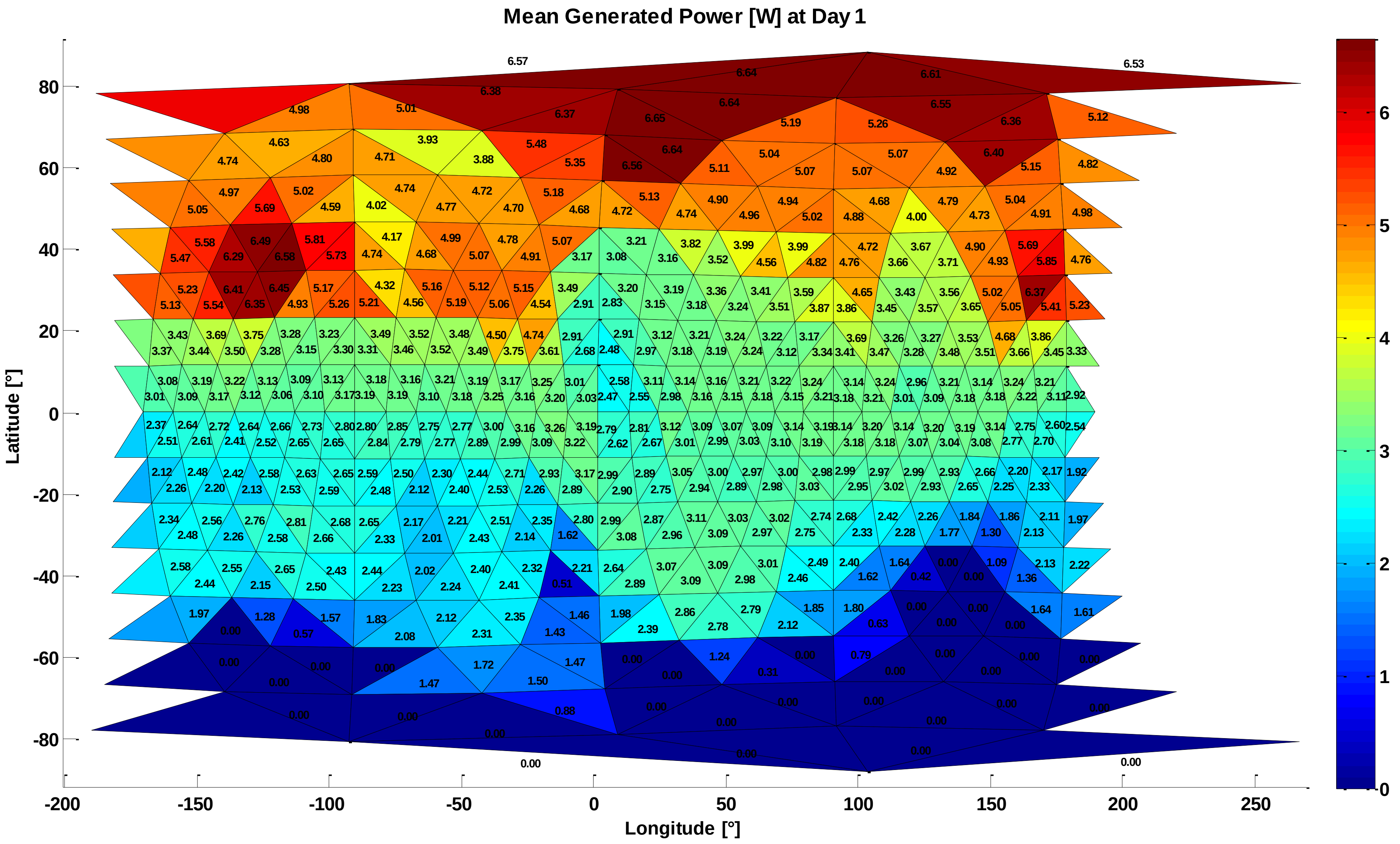

Figure 101 : Mean Generated Power at Day 1

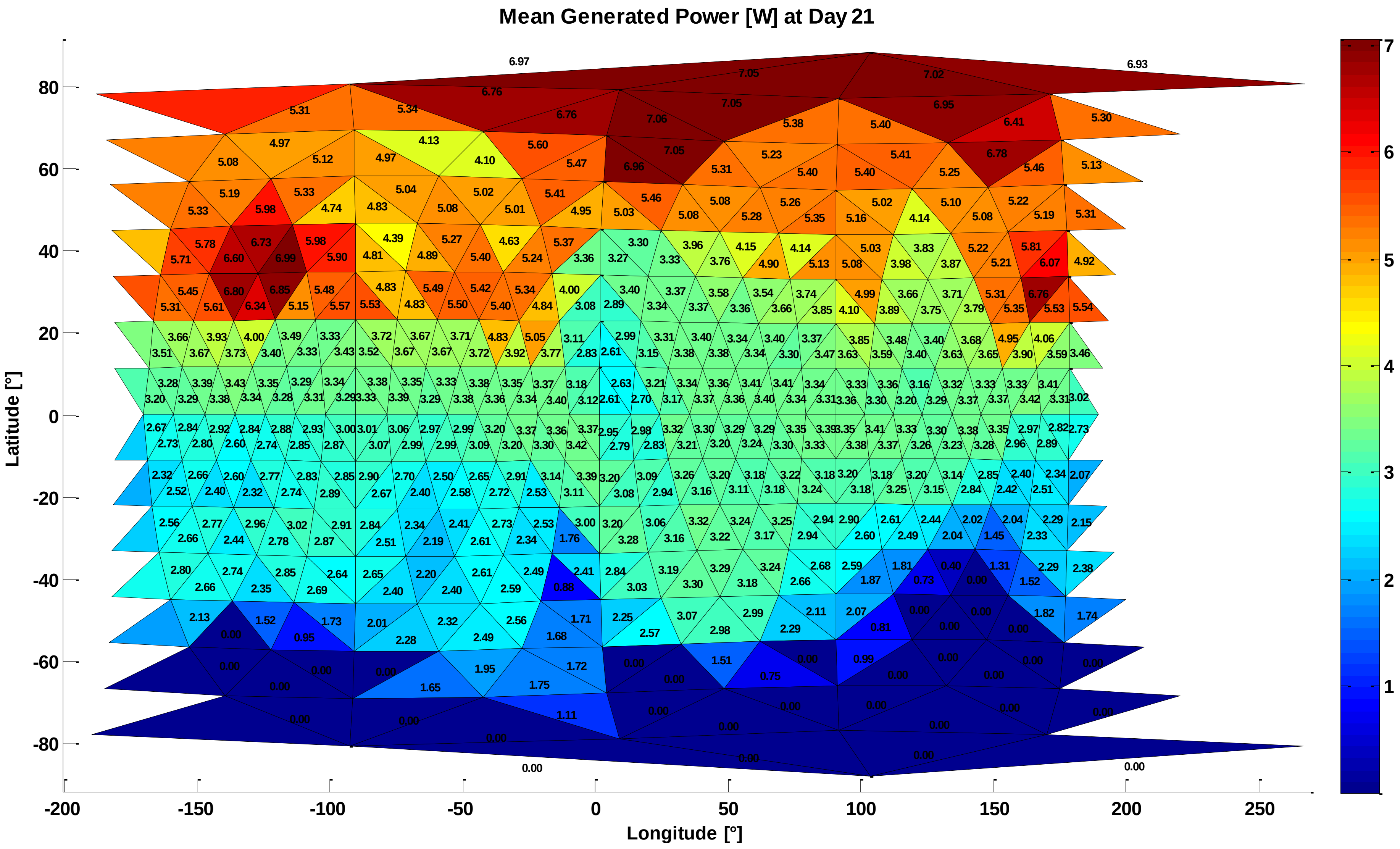

Figure 102 : Mean Generated Power at Day 21

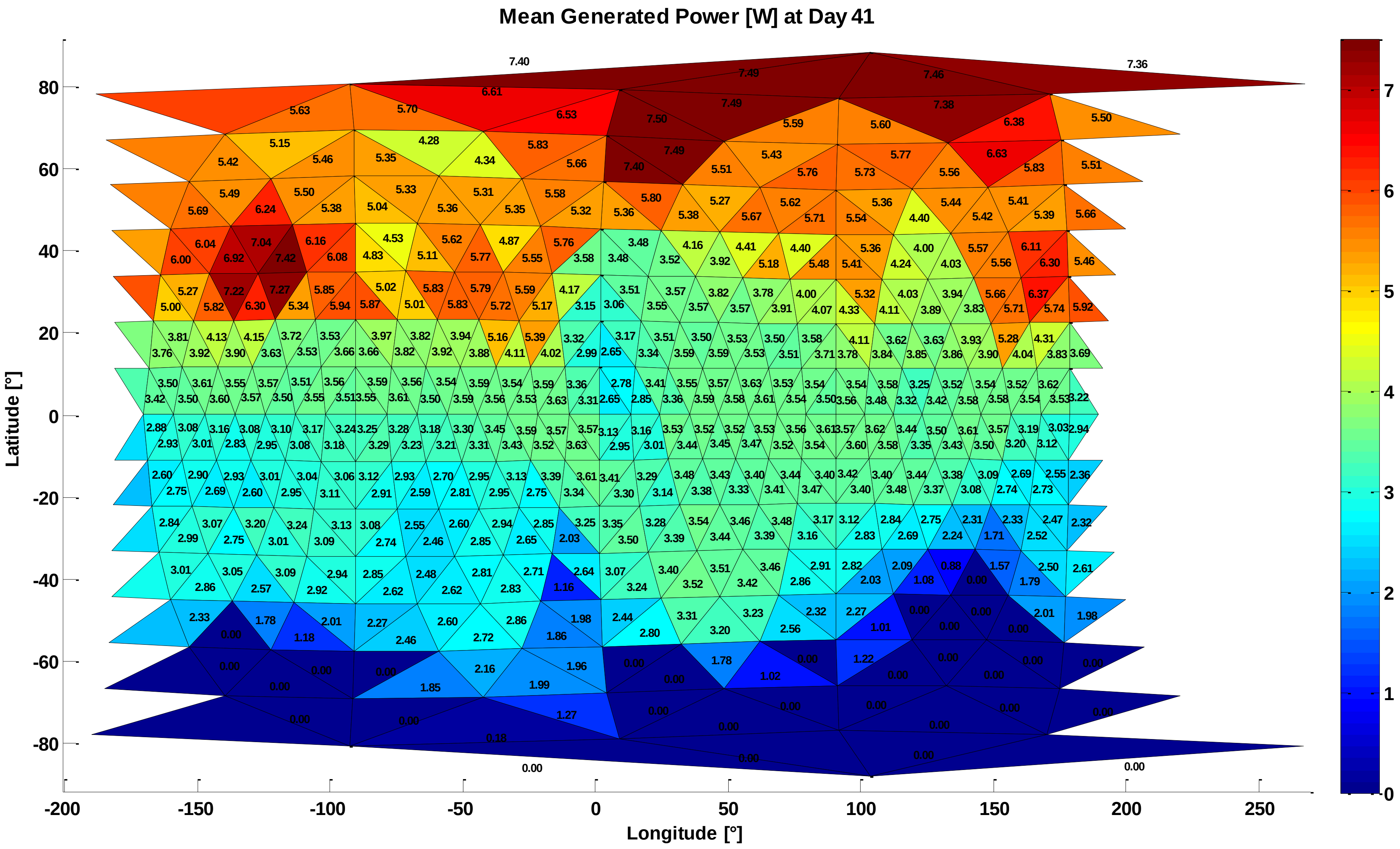

Figure 103 : Mean Generated Power at Day 41

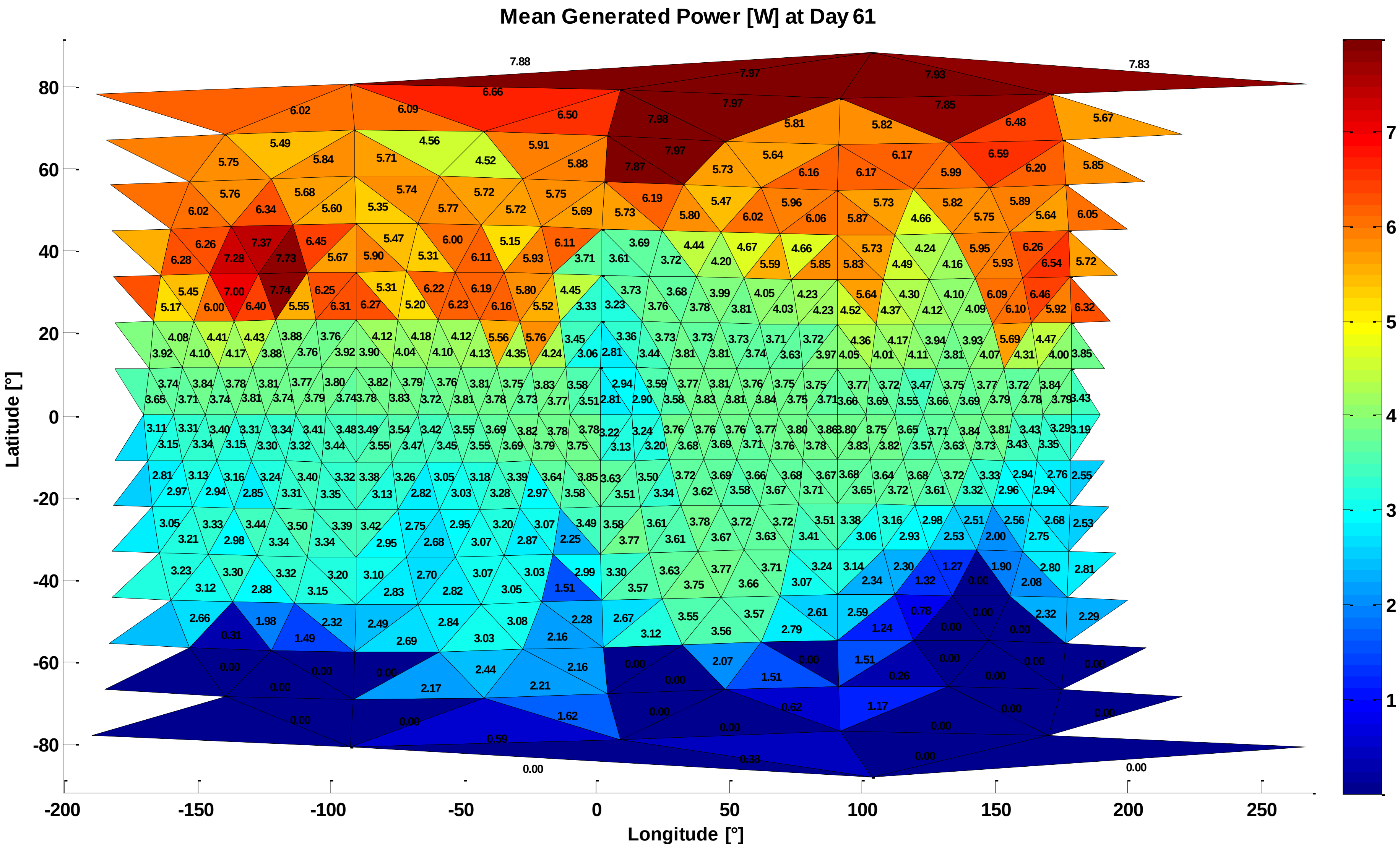

Figure 104 : Mean Generated Power at Day 61

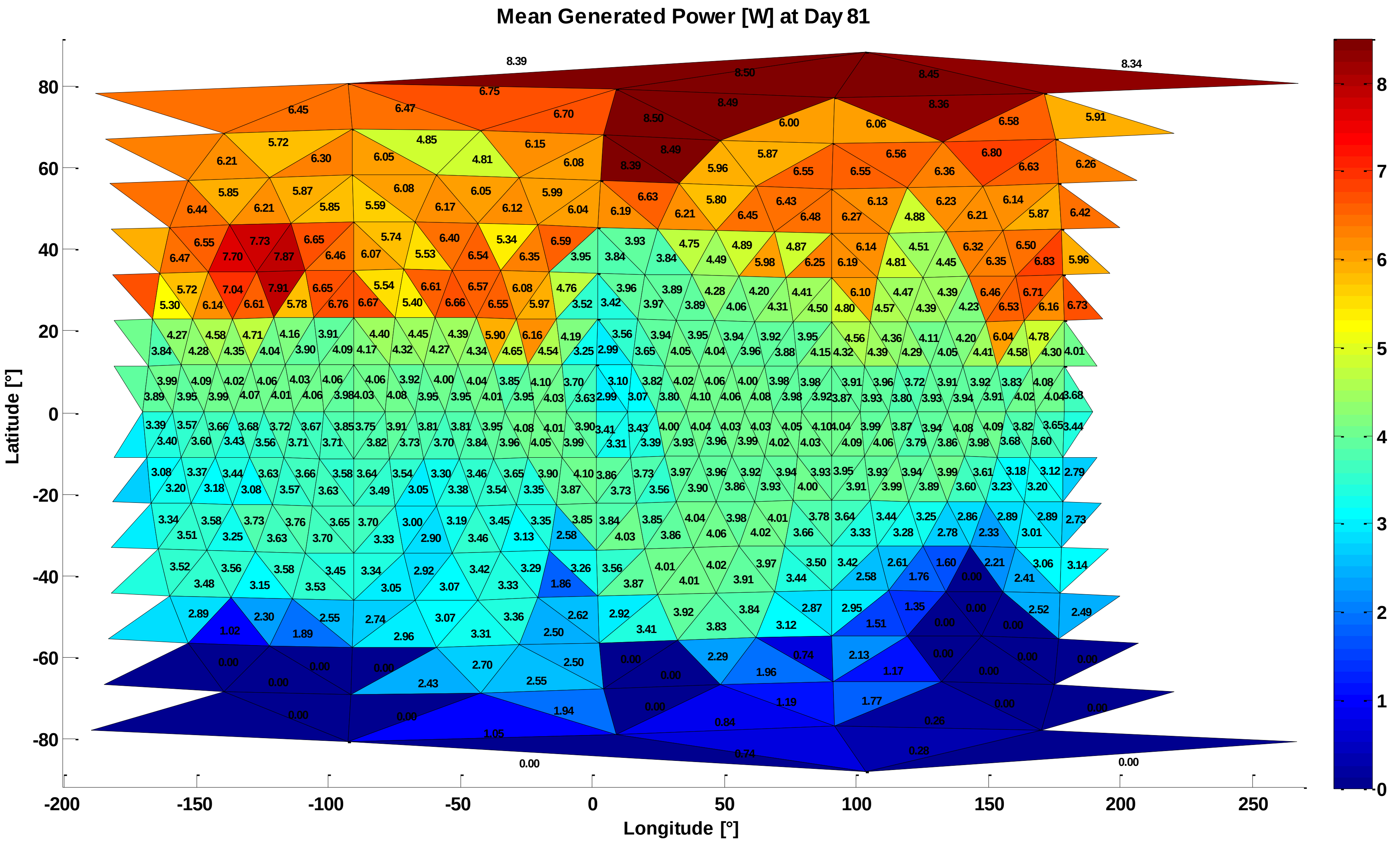

Figure 105 : Mean Generated Power at Day 81

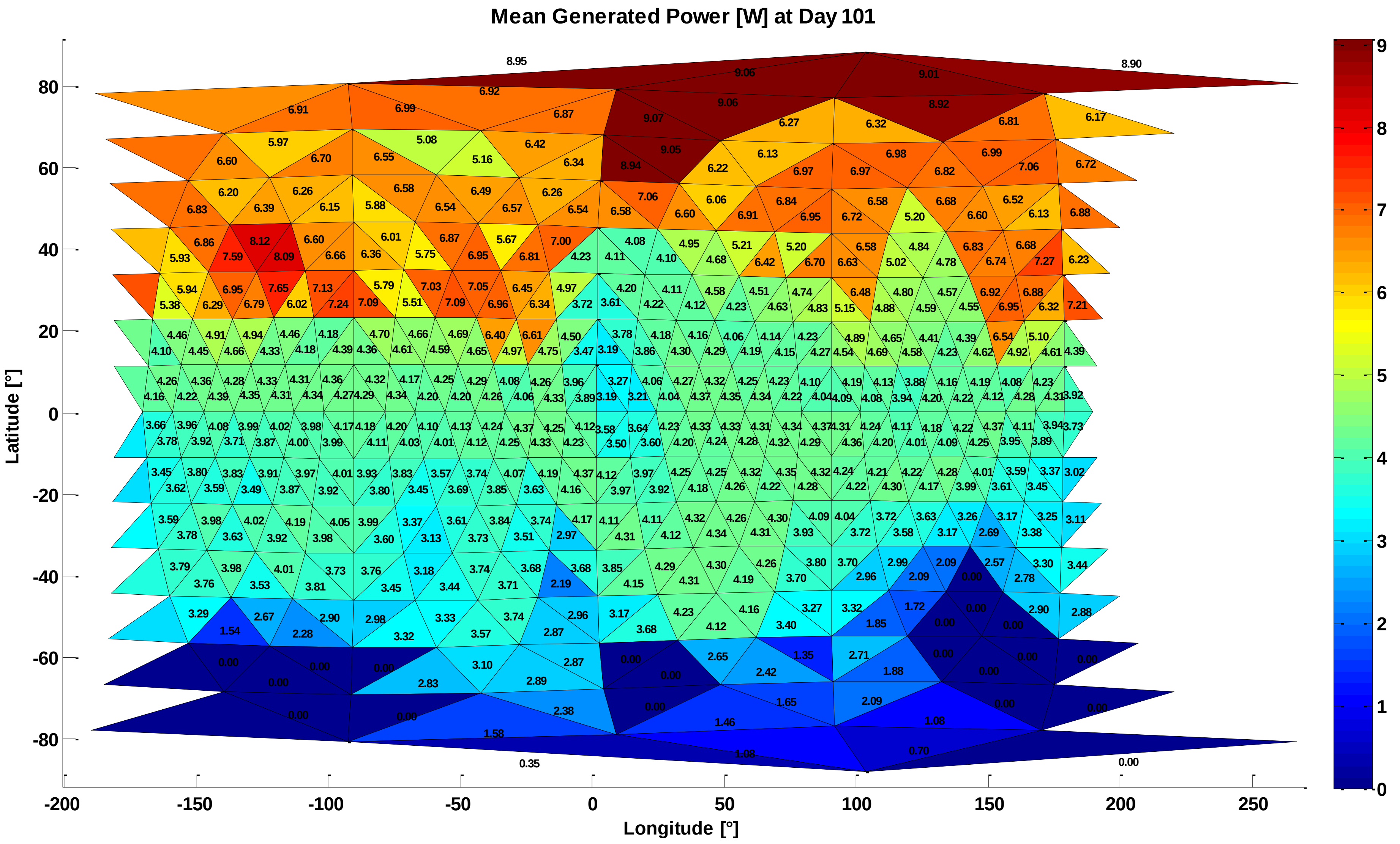

Figure 106 : Mean Generated Power at Day 101

References

[1] R. Schultz, "Rosetta - One Comet Rendezvous and two Asteroids Fly-Bys," *Solar System Research,* vol. 43, no. 4, pp. 343-352, 2009.

[2] S. Ulamec, A. Balazs, J. Biele, S. .. Espinasse and C. Fantinati, "Rosetta Lander - System Status fater Five Years in Space," *Aerotecnica Missili e Spazio,* vol. 88, no. 4, pp. 121-128, 2009.

[3] J. Biele and S. Ulamec, "Capabilities of Philae, the Rosetta Lander," *Space Science Review,* vol. 138, pp. 275-289, 2008.

[4] M. Pesco and A. E. Finzi, "Rosetta Space Mission - The Solar Array Photovoltaic Assembly," in *XIX CONGRESSO NAZIONALE AIDAA,* Forlì - Italy, 2007.

[5] P. Lamy, I. Toth, B. Davidsson, O. Groussin, P. Gutierrez and L. Jorda, "A Portrait of the Nucleus of Comet 67P/Churyumov-Gerasimenko," *Space Science Reviews,* no. 128, pp. 23-66, 2006.

[6] P. Lamy, I. Toth, H. Weaver, L. Jorda, M. Kaasalainen and P. Gutierrez, "Hubble Space Telescope Observtaions of the Nucleus and Inner Coma of the Comet 67P/Churyumov Gerasimenko," *Astronomy and Astrophysics,* no. 458, pp. 669-678, 2006.

[7] B. Davidsson and P. Gutierrez, "Nucleus properties of Comet 67P/Churyumov–Gerasimenko estimated from non-gravitational force modeling," *Icarus,* no. 176, pp. 453-477, 2005.

[8] P. L. Lamy, T. I., O. Groussin, L. Jorda and M. S. Kelley, "Spitzer Space Telescope observations of the nucleus of comet 67P/Churyumov-Gerasimenko," *Astronomy and Astrophysics,* no. 489, pp. 777-785, 2008.

[9] S. Lowry, F. A., P. Lamy and P. Weissman, "Kuiper Belt Objects in the Planetary Region: The Jupiter-family Comets," *The Solar System Beyond Neptune, University of Arizona Press,* pp. 397-410, 2008.

[10] J. Vincent and H. Böhnhardt, "Dust Jet Activity of the Comet 67P/Churyumov-Gerasimenko from 2003 to 2015," *Asteroids Comets Meteors,* no. 6284, 2012.

[11] M. Królikowska, "67P/Churyumov-Gerasimenko – Potential Target for the Rosetta Mission," *Acta Astronomica,* no. 53, pp. 195-209, 2003.

[12] Z. Sekanina, "Rotation and Precession of Cometary Nuclei," 1981.

[13] S. Chesley, *Bulletin of American Astronomical Sociecty,* vol. 36, no. 1118, 2004.

[14] D. G. Schleicher, "Compositional and physical results for Rosetta's new target Comet 67P/Churyumov–Gerasimenko from narrowband photometry and imaging," *Icarus,* no. 181, pp. 442-457, 2006.

[15] P. J. Gutierrez, L. Jorda, N. H. Samarasinha and P. Lamy, "Outgassing-induced effects in the rotational state of comet 67P/Churyumov-Gerasimenko during the Rosetta mission," *Planetary and Space*

Science, vol. 53, pp. 1135-1145, 2004.

[16] L. Jorda and P. Gutierrez, “Rotational Properties of cometari nuclei,” *Earth Moon Planets*, vol. 89, pp. 135-160, 2002.

[17] P. Lamy, L. Jorda, I. Toth, H. Weaver and D. Cruikshank, in *35th COSPAR Scientific Assembly*, Paris, 15-18 July 2004.

[18] M. Wieczorek, “The gravity and topography of the terrestrial planets,” *Treatise on Geophysics*, 2006.

[19] M. D. Sanctis, J. Lasue, M. Capria and G. Magni, “Shape and obliquity effects on the thermal evolution of the Rosetta target 67P/Churyumov–Gerasimenko cometary nucleus,” *Icarus*, vol. 207, pp. 341-358, 2010.

[20] P. Udrea and B. Anderson, “Validation of a Finite Sphere Gravitational Model with Applications to Comet 67P/Churyumov-Gerasimenko,” *American Astronautical Society*, vol. 142, no. 11, 2011.

[21] J. Biele, U. S, L. Richter, J. Knollenberg and E. Kührt, “The putative mechanical strength of comet surface material applied to landing on a comet,” *Acta Astronautica*, vol. 65, pp. 1168-1178, 2009.

[22] J. Biele, R. Willnecker, J. Bibring and H. Rosenbauer, “Philae (Rosetta Lander): Experiment status after commissioning,” *Advance in Space Research*, vol. 38, no. 2025-2030, 2006.

[23] J. Biele and S. Ulamec, “Surface elements and landing strategies for small bodies missions - Philae and beyond,” *Advances in Space Reserach*, vol. 44, pp. 847-858, 2009.

[24] R. Bertrand, T. Ceolin and P. Gaudon, “Rosetta Lander Descending Phase on the Comet 67P Churyumov-Gerasimenko,” in *18th International Symposium on Space Flight Dynamics (ESA SP-548)*, Munich, Germany, 11-15 October 2004.

[25] F. Topputo, F. Bernelli-Zazzera and A. Ercoli-Finzi, “Power Production for Small Body Laders: Post-Launch Activities on Philae's Power Subsystem,” in *62nd International Astronautical Congress*, Cape Town, South Africa, 2010.

[26] S. Brambillasca, F. Topputo, A. Finzi and R. Campesato, “LILT Measurements on Silicon Solar Cells of Rosetta Lander Philae,” in *XX AIDAA Congress*, Milano, Italy, June 29 - July 3 2009.

[27] RO-LAN-UM-3100-TCS, “Lander User Manual - 2.2-12 TCS,” April 2012.

[28] N. DSK, “67P Churyumov-Gerasimenko,” 10 September 2012. [Online]. Available: http://naif.jpl.nasa.gov/pub/naif/generic_kernels/dsk/churyumov-gerasimenko/.

[29] JPL NASA, “JPL Small-Body Database Browser,” 2 May 2012. [Online]. Available: http://ssd.jpl.nasa.gov/sbdb.cgi?sstr=67P;orb=0;cov=0;log=0;cad=0#orb.

[30] A. International, “Standard Solar Constant and Zero Air Mass Solar Spectral Irradiance Tables,” West Conshohocken, PA 19428-2959 United States, 2006.

[31] T. Moller and B. Trumbore, “Fast, Minimum Storage Ray/Triangle Intersection,” *Journal of Graphics Tools*, no. 2, pp. 21-28, 1997.

[32] F. Topputo, F. Bernelli and A. Finzi, “Philae Solar Array Simulator 1.02 User's ManualL,” 2011.

[33] SONC Flight Dynamics Team , “Reference Frames, Models and Conventions for Rosetta Lander Ground Segment,” 2012.

[34] F. Topputo, A. Finzi and F. Bernelli-Zazzera, “LTS Phase: The Power Production Standpoint,” in *30 March - 1 April 2012,* Venice, Italy.